INFORMATION TO USERS

While the most advanced technology has been used to photograph and reproduce this manuscript, the quality of the reproduction is heavily dependent upon the quality of the material submitted. For example:

- Manuscript pages may have indistinct print. In such cases, the best available copy has been filmed.

- Manuscripts may not always be complete. In such cases, a note will indicate that it is not possible to obtain missing pages.

- Copyrighted material may have been removed from the manuscript. In such cases, a note will indicate the deletion.

Oversize materials (e.g., maps, drawings, and charts) are photographed by sectioning the original, beginning at the upper left-hand corner and continuing from left to right in equal sections with small overlaps. Each oversize page is also filmed as one exposure and is available, for an additional charge, as a standard 35mm slide or as a 17"x 23" black and white photographic print.

Most photographs reproduce acceptably on positive microfilm or microfiche but lack the clarity on xerographic copies made from the microfilm. For an additional charge, 35mm slides of 6"x 9" black and white photographic prints are available for any photographs or illustrations that cannot be reproduced satisfactorily by xerography.

Order Number 8722066

Geochemistry and mineralogy of the Molango manganese orebody, Hidalgo State, Mexico

Okita, Patrick Masao, Ph.D.

University of Cincinnati, 1987

U·M·I
300 N. Zeeb Rd.
Ann Arbor, MI 48106

PLEASE NOTE:

In all cases this material has been filmed in the best possible way from the available copy. Problems encountered with this document have been identified here with a check mark ✓.

1. Glossy photographs or pages ✓
2. Colored illustrations, paper or print _____
3. Photographs with dark background _____
4. Illustrations are poor copy _____
5. Pages with black marks, not original copy ✓
6. Print shows through as there is text on both sides of page _____
7. Indistinct, broken or small print on several pages ✓
8. Print exceeds margin requirements _____
9. Tightly bound copy with print lost in spine _____
10. Computer printout pages with indistinct print _____
11. Page(s) _____ lacking when material received, and not available from school or author.
12. Page(s) _____ seem to be missing in numbering only as text follows.
13. Two pages numbered _____. Text follows.
14. Curling and wrinkled pages _____
15. Dissertation contains pages with print at a slant, filmed as received _____
16. Other _____

_____

_____

University
Microfilms
International

GEOCHEMISTRY AND MINERALOGY OF THE MOLANGO MANGANESE OREBODY, HIDALGO STATE, MEXICO

A dissertation submitted to the

Division of Graduate Studies and Research
of the University of Cincinnati

in partial fulfillment of the
requirements for the degree of

DOCTOR OF PHILOSOPHY

in the Department of Geology
of the College of Arts and Sciences

1987

by

Patrick Masao Okita

B.S., University of Rochester, 1980

M.S., Louisiana State University, 1984

UNIVERSITY OF CINCINNATI

May 19 19 87

I hereby recommend that the thesis prepared under my supervision by Patrick M. Okita

entitled Geochemistry and Mineralogy of the Molango Manganese Orebody, Hidalgo State, Mexico

be accepted as fulfilling this part of the requirements for the degree of Doctor of Philosophy

Approved by:

ABSTRACT

The Molango manganese deposit is the only known large Mn deposit in North America. Mineralization involves Mn-carbonate exclusively in a finely laminated bed about 10 meters thick with a strike length greater than 50 kilometers. The ore bed is the basal unit of the Chipoco facies (Taman Fm., Kimmeridgian) and is underlain by laminated black shales of the "Santiago" formation (Oxfordian).

Thin-section observation reveals the ore to be very fine-grained carbonate in laminae and clots with disseminated pyrite and organic matter. Lamination is wavy and shows evidence of soft sediment deformation. The only additional accessory minerals are magnetite and a second magnetic mineral believed to be maghemite. Microprobe analyses show the Mn-carbonate to contain large amounts of Mg (25-50 mole-percent) whereas Ca is very low and invariant (<8 mole-percent). ICP analyses of wholerock pulps from samples in the ore zone indicate enrichments of Co, Ni, and Mg, but low amounts of Ba, Ca, Fe, and Cu. Similar analyses of pyrite separates reveal elevated As and Co concentrations in ore zone pyrite compared to pyrite outside the ore zone; Ni and Zn are low.

Negative ^{13}C (PDB) values correlate with Mn content and range from -16 to -11o/oo in the ore zone. The underlying Santiago and superjacent unmineralized carbonates have $\delta^{13}C$ of 0 to +2^{o}/oo (PDB). Oxygen isotope values for the

subjacent and superjacent carbonates indicate a temperature of precipitation ranging from 40 to 55 ^{o}C. Carbon isotopic data from organic matter, together with vitrinite reflectance and total organic matter, can be interpreted to indicate that the organic matter accumulated in a shallow marine (e.g. <300 meters), stratified basin and that ore mineralization occurred at the peak of a marine transgression. The age of the ore deposit corresponds to the time of a global sea level maximum.

Mineralization can be explained by a variation of the "Bath-tub Ring" model and may have involved diagenetic remobilization of Mn in the sediment. Low Ca content, the trace metal content, and the presence of Fe-oxides are evidence for the possible presence of an oxide (i.e. Mn or Fe) precursor. Particulate Mn-oxide reacted with bicarbonate derived in approximately equal parts from bacterially produced HCO_3^- and seawater HCO_3^- to form negative $\delta^{13}C$ Mn-carbonates. Fe was kept low by oxide formation and possibly by precipitation of FeS_2 elsewhere in the basin.

ACKNOWLEDGEMENTS

It is a great pleasure and privilege to acknowledge the many people and organizations who have aided my research efforts. I owe a great debt to those mentioned below.

My first thanks go to Dr. J. Barry Maynard who served as my chief advisor. I sincerely appreciate his encouragement and guidance in all stages of my doctoral program and research. This work and my growth as a scientist have benefitted greatly from the many hours of discussion with Dr. Maynard. I am also very grateful to Dr. John Grover and Dr. Holly Huyck who made up the rest of my committee. Their interest, constructive criticism, and encouragement are sincerely appreciated.

Dr. Eric Force (United States Geological Survey) brought the Molango deposit to the attention of Dr. Maynard and myself. I also thank him for sharing his thoughts on the deposit.

This study would not have been possible without the very generous gifts of time and resources from Dr. Rafael Alexandri, Jr., Chief Geologist of Compania Minera Autlan. I am especially grateful to Alfonso Martinez-Vera, also of CMA for his hospitality and giving freely of his time to get me oriented in the field and sharing his insights and expertise regarding the geology of the deposit. My fieldwork was also made greatly more productive by the help of Alejandro Medina, Juventino Oñate, Julio Mendez, and Andrés Rocha, all

geologists for Compañia Minera Autlán.

Stable isotope analyses were conducted with the kind permission of Dr. John Hayes at the Biogeochemical Laboratory at Indiana University. Special thanks are extended to Jay Kaufman and Ray Takigiku for their help in training and supervising me during the isotope analyses.

I am very appreciative of the organic carbon data provided courtesy of Dr. Michael Lewan from Amoco Research Company. In addition, Dr. Lewan provided helpful discussions regarding the interpretation of these data.

Induction coupled plasma spectroscopy analyses were conducted by Mr. James Boyle at the Kettering Laboratory of the University of Cinicinnati.

Financial support was provided by the Department of Geology of the University of Cincinnati in the form of tuition, teaching, and research stipends; field costs were deferred by a grant from the Sedimentology Fund of the Department of Geology; laboratory fees were paid for with a grant from the Department of Geology Research Fund; and other laboratory and field expenses were made affordable through grants-in-aid from The American Association of Petroleum Geologists and Sigma Xi - The Research Society.

Special thanks are offered to two fellowship programs: (1) the University Research Council for providing financial support during the summers of 1985 and 1986 and for funding travel to professional meetings, and (2) the Willis G. Meyer

Fellowship for providing tuition and stipend money in 1985 which allowed me to devote my full attention to the important early stages of this research.

I am very thankful for the friendship and help received from Tom Hudson, Kevin Savage, Sally Sutton, and Jeff Grigsby during my stay at Cincinnati. I also thank Randy Mathis and Harley Hopkins for their enduring friendship, and providing avenues for needed diversions in bayou country. Musical inspiration was provided by Jimmy Buffett.

A special thanks is owed to my wife Sarah L. Sheen for her help in preparing the appendices. I am grateful to her and her family for all their encouragement and patience.

Finally, I wish to acknowledge the endless support, both personal and financial, provided by Masao and Joan F. Okita, my parents; and my sister Denise. Their constant interest in my pursuits, untiring patience, and understanding can never be recompensed.

TABLE OF CONTENTS

LIST OF TABLES

LIST OF FIGURES

CHAPTER I. INTRODUCTION AND BACKGROUND

INTRODUCTION

The Molango manganese deposit is a large, stratiform manganese carbonate orebody contained in limestones of marine origin. Its size and some aspects of its origin are similar to those of other large marine sedimentary manganese accumulations (Cannon and Force, 1983). The purpose of this research is to investigate the chemical and mineralogic characteristics of Mn mineralization at Molango, with the goal of understanding the processes responsible for the origin of this deposit.

Economically significant, large accumulations of manganese are found on land (Varentsov and Grasselly, 1980: Roy, 1981), and covering a sizeable portion of the modern ocean floor (Bonatti et al., 1972). Exploitation of the latter deposits is at present hindered by technological and political barriers (Assessment of Manganese Nodule Resources, 1982; Analysis of Exploration and Mining Technology for Manganese Nodules, 1984). Consequently, all manganese production is from land-based deposits which are commonly comprised mainly of Mn-oxides. The original Mn-bearing minerals of these deposits may have been oxides, carbonates, or a mixture of both. Global distribution of the land-based Mn-deposits is shown in Figure 1.

Manganese ore deposits occur in a great diversity of hostrocks (e.g. carbonate, siliciclastic, volcanic,

metamorphic) and range in ages throughout geologic history. Roy (1981) reported over 70 important manganese deposits which have formed from hydrothermal, volcanogenic, sedimentary, and secondary enrichment processes, representing a wide range of physical and chemical conditions in seemingly every conceivable geologic environment.

Owing to the variation of geologic settings in which manganese deposits are found, many classification systems for manganese deposits have been formulated. These schemes variously emphasize lithologic associations, mineral assemblages, or the inferred origin of manganese (see Park, 1956; Varentsov, 1964; and Roy, 1981). Many of these classifications are subjective, and strongly dependent on the presumed origins of the manganese or by the implication of an incorrect vinculum (e.g. the coupling of metamorphosed and supergene enrichment deposits by Rakmanov and Tchaikovsky [see Roy, 1981, p. 240]).

Manganese deposits of economic importance can be grouped into two general categories: (1) Supergene deposits formed by weathering of manganiferous rocks. The deposits of Gabon and Brazil (National Materials Advisory Board, 1981) and those of India (Roy, 1980) are examples of important supergene deposits. (2) Primary deposits, which include volcanogenic and non-volcanogenic sedimentary deposits. By far the most economically important type of primary

FIGURE 1.

Global distribution of major land-based manganese deposits showing their sizes and noting those deposits which are expected to be exhausted by the year 2020 (from DeYoung, et al., 1984).

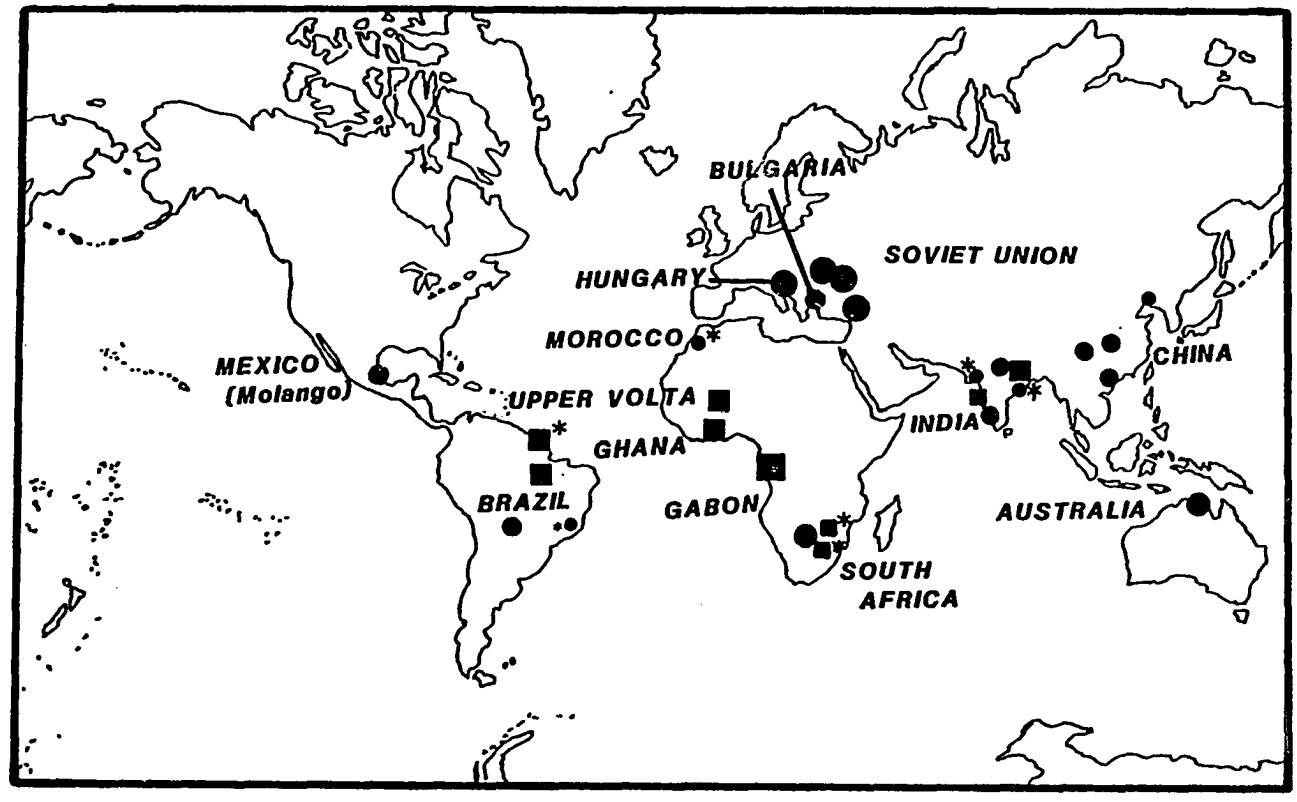

Marine Chemical Sediment

- ● $> 10^8$
- ● $10^7 - 10^8$
- ● $< 10^7$

Resources in metric tons

Secondary Enrichment

- ■ $> 10^8$
- ■ $10^7 - 10^8$
- ■ $< 10^7$

Resources in metric tons

* ***Denotes deposits anticipated to be exhausted by the year 2020.***

deposit is the shallow marine sedimentary deposit (Cannon and Force, 1983). Sedimentary manganese mineralization is the result of syngenetic or diagenetic precipitation of manganese concentrated by sedimentation or by chemical processes. Examples of this type of deposit include Nikopol and Chiatura in the Soviet Union (Gryaznov and Danilov, 1980), Groote Eylandt in Australia (McIntosh, et al., 1975), Kalahari in South Africa (de Villiers, 1971), and the Molango deposit in Mexico (Cannon and Force, 1983; Tavera and Alexandri, 1972), the subject of this study.

A comparison of the geologic features of these sedimentary deposits indicates that, in each case, manganese deposition occurred in a shallow marine depositional environment, under oxygen depleted conditions and at times of sea level transgression. Stable platform conditions were also present in the case of the Russian, Australian and South African deposits. The basin setting appears to be quite different for the Molango area however, compared to these, because the region was actively rifting during the time manganese mineralization occurred.

Recognition of the association between mineralization, oxygen depletion, and peak transgression has lead to the development of a model for mineralization referred to as the "bath-tub ring" model (Cannon and Force, 1983). In this model, manganese, present in the sediment initially as insoluble oxides, is mobilized within the sediment pile

under reducing conditions. If the pore waters are anoxic, divalent manganese is stable in aqueous solution. Chemical gradients are established such that Mn^{2+} travels by diffusion and advection toward the interface between reducing and oxidizing conditions where manganese is precipitated as an oxide. If this redox boundary is at the sediment-water interface, manganese nodules form on the sea floor. If it is in the water column, accumulation of manganese will occur where the oxic/anoxic interface intersects the bottom of the basin on its margins or on some submarine topographic high, hence the name "bath-tub ring".

This model is generally appropriate for explaining many aspects of the large sedimentary deposits, but difficulties exist with its detailed application to Molango and other deposits in which a large part of the primary ore is a carbonate. The model does not explain the abundance of Mn-carbonates, because manganese is held in carbonate phases in the reduced (+2) state. In addition, it is not clear at Molango whether the carbonate phase should be regarded as primary or diagenetic.

An important problem which must be addressed in the development of models for large sedimentary manganese deposits is the source of manganese. This problem has two parts: obtaining the necessary amount of manganese in the system, and concentrating that manganese a sufficiently

high level to constitute an orebody. Manganese can be introduced into the oceans through continental weathering, oceanic volcanism, or hydrothermal activity associated with sea floor spreading. Each of these sources can provide enough manganese to form a large deposit. The concentration of manganese in a depositional environment is limited by the chemical properties of dissolved manganese and stable manganese mineral forms. The chemical properties of manganese are similar to those of iron; therefore, in developing a model for Mn mineralization, it is necessary to include a feasible mechanism to separate Mn from Fe prior to or during the formation of a sedimentary manganese deposit.

BACKGROUND

The Molango manganese district is located in northeastern Hidalgo State; the currently known outcrop area is roughly 25 km (west-east) by 50 km (north-south) in size, encompassing the mines (Figure 2). The center of this district is situated approximately 150 km northeast of Mexico City and about the same distance southwest of Tampico. The deposit was discovered in 1960 and first production began in 1968 (DeYoung, et al., 1984).

The area is mountainous and characterized by very steep to vertical slopes. Vegetation is lush and extremely dense. Access to the district is attained using paved

highway; gravel roads, pack trails, and footpath provide access to individual mine sites and outcrops.

Four mine locations: Acoxcotlan, Naopa, Nonoalco, and Tetzintla, currently exist in the Molango manganese district; the latter two are currently active (Figure 3). The Nonoalco site is being mined for supergene, battery grade oxides and is purported to be the largest such accumulation in the world. The Tetzintla mine is producing primary carbonate ore. The carbonate ore is crushed, roasted, and pelletized at a processing plant located near Otongo to provide a high lime-manganese oxide pellet used as furnace feed for steel mills.

The scattered locations of mines does not reflect the nature of the orebody. In actuality, the mineralization appears as a single stratiform ore zone ranging in thickness from less than 1 meter to approximately 10 meters and having a known strike length in excess of 50 kilometers (Figure 3; Compañia Minera Autlan data).

The significance of the deposit is twofold. First, Molango is the only major manganese deposit known in North America. Proven reserves of the current workings are in excess of 3 million tons, which at current production rates should last about 30 years; district reserves exceed 200 million tons (Martino, 1986, p. 567). The second distinction of Molango is that primary mineralization is in the form of manganese carbonate (i.e. rhodochrosite and

FIGURE 2.

Location map of the Molango district (from Tavera and Alexandri, unpublished). Outlined area denotes the district and is depicted in Figure 3.

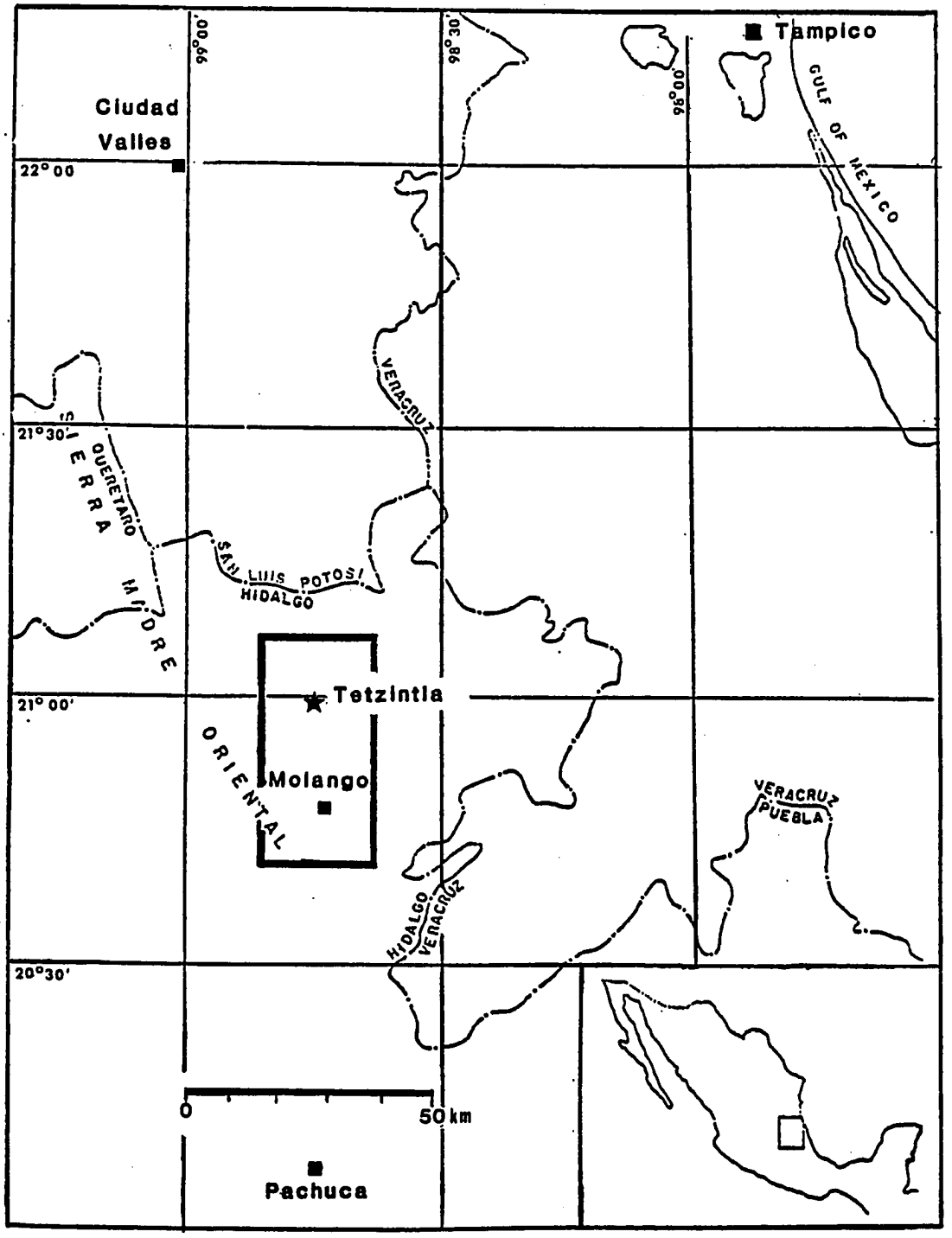

FIGURE 3.

Generalized geologic map of the Molango district showing the four mine locations and the known outcrop of the orebody (simplified from Compañia Minera Autlan data).

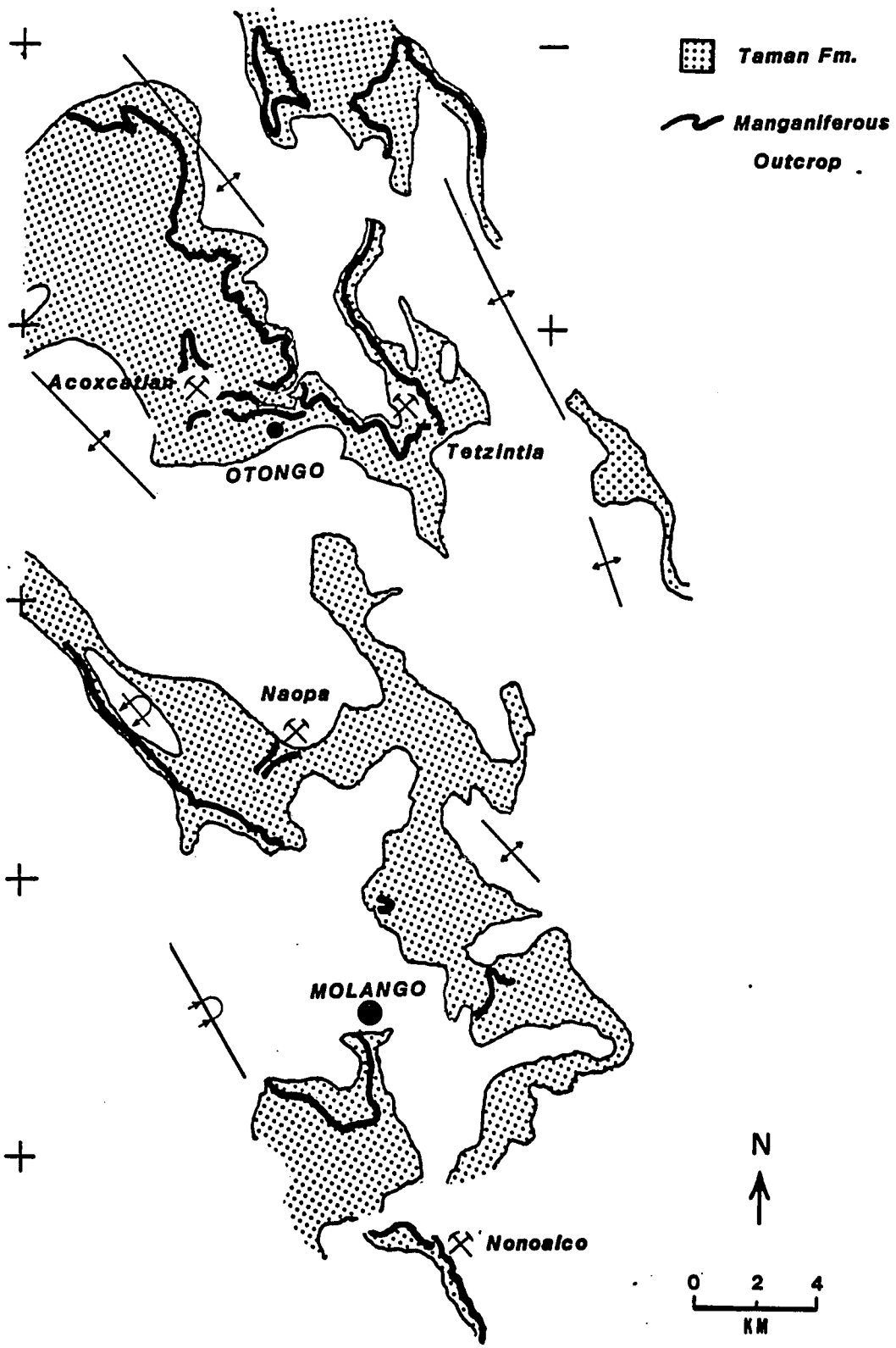

manganoan calcite). Manganese oxide minerals are present and mined at the Nonoalco location, but these deposits are supergene enrichments of the carbonate ores.

ECONOMIC AND SCIENTIFIC MERIT - Research on the Molango deposit is important both economically and scientifically. Economically, the Molango manganese deposit represents a significant resource of this essential industrial metal. Ninety-five percent of the 1981 world manganese production was used in steelmaking processes where it is employed as a "scavenger" of sulfur and oxygen in molten steel (DeYoung, et al., 1984, p. 2). Additional uses of manganese are as an oxidizing agent, catalyst, alloying element, and component in the production of dry-cell batteries. In most applications, no suitable substitute is available. This is particularly true in steelmaking applications.

The Molango manganese deposit is the only major manganese deposit in North America. Although, as Cannon and Force (1983) note, rocks similar to those hosting major manganese deposits elsewhere are known in North America, no other major sedimentary manganese accumulations have been discovered. The manganese mineralization at Molango is unobtrusive, and similar deposits could be easily overlooked. Therefore, a detailed understanding of sedimentary manganese deposits is necessary in order to properly assess the potential for a region to contain such a deposit.

The scientific merits of this study are several. The root of this study is identification of the chemical processes and conditions that allowed concentration and precipitation of manganese in the basin of deposition. Thus, the scientific questions pertinent to this study include the following. How did the Molango manganese deposit form? Why did this deposit form as a carbonate? How do the mineralogic and sedimentologic characteristics of the Molango deposit compare with those of the other giant manganese deposits? Is the timing of mineralization (e.g. precipitation at a peak of transgression) similar to other deposits?

In addition, the occurrence of sedimentary manganese carbonate minerals is of great interest and value to the study of the mineralogy and chemistry of carbonate minerals. The mineral assemblage present at Molango could provide valuable new compositional, isotopic, and mineralogic data.

OBJECTIVES - The objectives of this study are to characterize and quantify, insofar as possible, the isotopic, elemental, and mineralogic properties of the Molango ore deposit for the purposes of: (1) determining the geochemical and depositional conditions which resulted in the formation of a manganese carbonate orebody; (2) refining and modifying the currently favored "Bath-tub Ring" model in order to account for the precipitation

exclusively of carbonate mineral phases of Mn; (3) establishing criteria for identifying future exploration targets in the Molango region; and (4) developing exploration guidelines for assessing the potential for similar deposits elsewhere in North America.

METHODS OF STUDY - A variety of research techniques were employed during the course of this study and include: fieldwork, petrograhic study, x-ray diffraction, electron microprobe, elemental and isotopic analyses. The procedures are described in Appendix A.

CHAPTER II. GENERAL DESCRIPTION OF THE MOLANGO DISTRICT

REGIONAL STRATIGRAPHY

Rocks of the Molango district and vicinity present a discontinuous record of geologic history from Precambrian to Tertiary age (Figure 4). Correlation of formations on a regional and local scale has been hampered by structural complications, lithologic variations within single formations, and similarities between two or more formations. In addition, differences in nomenclature among workers, particularly regarding the Mesozoic rocks, have made matters more confusing. These problems, while significant, are beyond the concern and purpose of this work. The general stratigraphic features and depositional environments of the rocks will be presented as described in the available literature. These rocks can be separated into four general groups: Precambrian Basement, Permian Marine Sequence, Mesozoic Non-marine and Marine Rocks, and Tertiary Igneous Rocks.

Precambrian Basement - The oldest rocks found in the region are middle Proterozoic age metamorphic rocks. As observed in the field and documented in the literature these rocks are quartz-feldspar-biotite gneisses, schists, and metaconglomerates (Carillo-Bravo, 1965; Minera Autlán company documents). The age of this assemblage is reported to be 1,210 ± 140 million years (Fries and Rincon-Orta, 1965).

FIGURE 4.

Generalized stratigraphic column of the rocks found in the Molango district. No stratigraphic thicknesses are implied (after Compañia Minera Autlán).

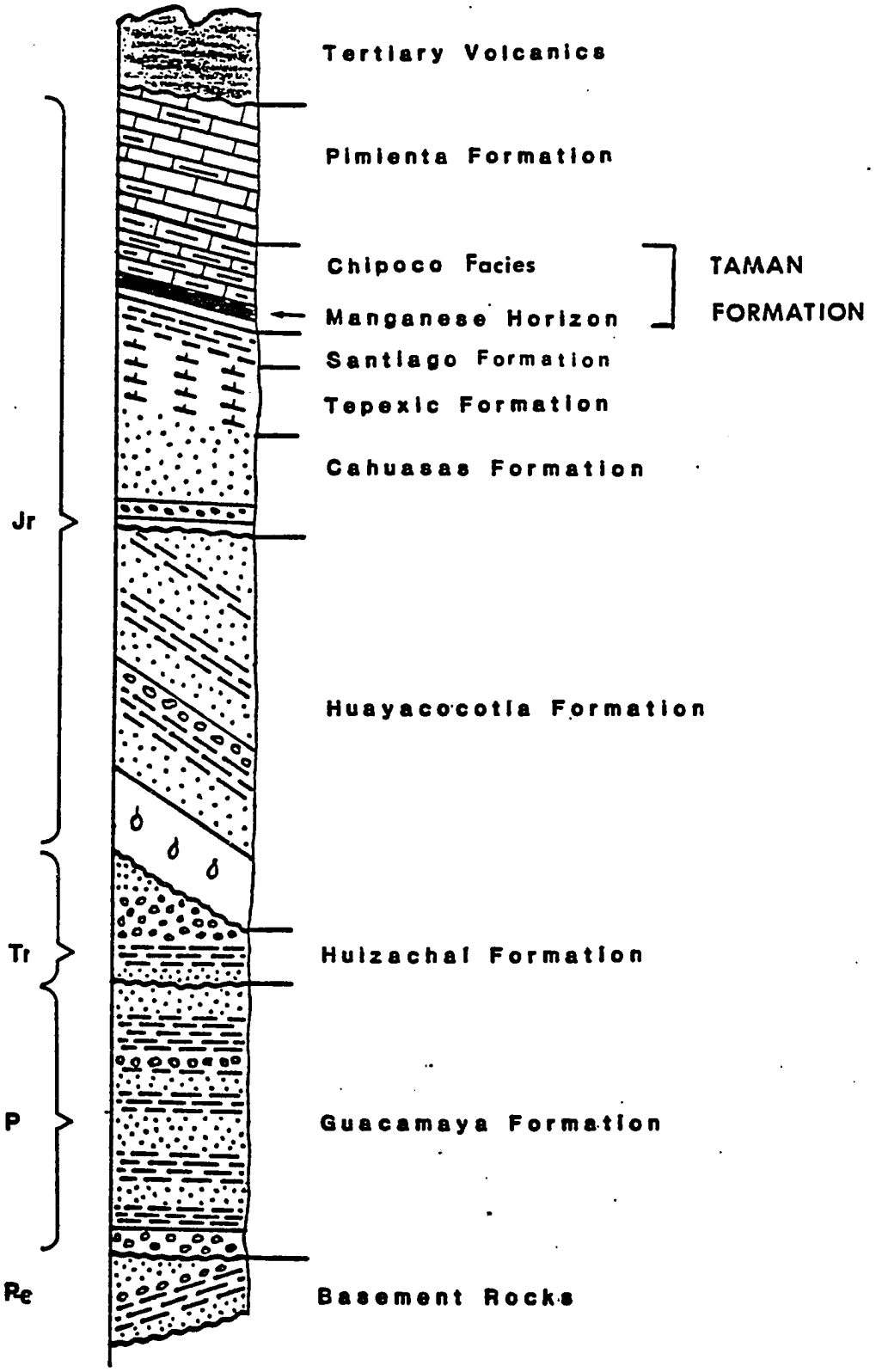

Permian Rocks - The Permian age Guacamaya Formation is the only Paleozoic age sequence found in the area. The formation varies in thickness, but is typically about 200 meters thick. It is composed of alternating black, sandy shales and medium to coarse-grained conglomerate (Carillo-Bravo, 1965). Fossils described from the formation include fusulina, crinoids, corals, brachiopods, pelecypods, some trilobites, and horizons containing abundant, poorly preserved fragments of land plants (Carillo-Bravo, 1965; Minera Autlán company documents).

Mesozoic Rocks - The Mesozoic age strata consist of non-marine fluvial-deltaic sequences overlain by calcareous shales, argillaceous carbonates, and "clean" carbonates. In general, the Mesozoic sequence records a transgressive event, but there is evidence of several regressive phases. The sequential distribution of the several lithologies comprising the Mesozoic rocks is unpredictable and has lead to the establishment of formation status for many of these packages of discontinuous lithologies. As argued below, it may be best to consider such variable and quickly changing lithologies as facies changes, thus referring to such as members or facies within a single formation.

Huizachal Formation - The oldest of the Mesozoic rocks is the Huizachal Formation. It rests upon on the Guacamaya Formation as well as the Precambrian basement and is always marked by an angular unconformity. The Huizachal Fm. is

interpreted to be continental; it is composed of shales, sandy shales, sandstones, and conglomerates. Fossil material is limited to upper Triassic land plants (Rhaetian Stage, Longoria, 1984, p. 67). The thickness of the formation is highly variable and can reach 2000 meters (Carillo-Bravo, 1965).

Huayacocotla Formation - The Huayacocotla Formation, originally named by Imlay (1948) and subsequently redefined by Erben (1956), crops out over a large part of the study area. This formation consists of a basal conglomerate (containing fragments from the Huizachal Fm.) overlain by dark gray to black sandy limestone, and by a black shale that becomes less calcareous upward (Carillo-Bravo, 1965).

The lower third of the formation contains fragments of plant roots whereas the middle and upper thirds contain ammonites and pelecypods (Carillo-Bravo, 1965). The ammonites are reported to indicate a Sinemurian age (i.e. lower Jurassic) for the Huayacocotla Fm. (Carillo-Bravo, 1965; Longoria, 1984). Pedrazzini and Basañez (1978) interpret the Huayacocotla Formation to have been deposited under shallow marine conditions in an intracratonic basin.

Cahausas Formation - The Cahausas Fm. is marked at its base by an angular unconformity. It consists of a sequence of basal conglomerates overlain by siltstones, argillaceous limestones and red to green-gray sandstone. This formation rests on the Huayacocotla Fm. and is considered to be

Middle Jurassic based on its stratigraphic position (Carillo-Bravo, 1965, p. 88).

The rocks of the Cahausas Fm. have been characterized by Pedrazzini and Basañez (1978) as immature litharenites. They are reported to contain mica, alkali feldspar, fragments of Precambrian basement and of the Huizachal Formation, siltstone, shale, limestone and chert. The provenance of the sediments comprising the Cahausas Fm. has not been determined, and the depositional setting is reported only as continental at the base and marine at the top of the formation (see Pedrazzini and Basañez, 1978).

Tepexic Formation - The Tepexic Fm. was observed in outcrop near the study area at the village of Otongo. The rocks at this location were composed of black to dark gray micrites containing steinkerns of gryphea. The basal contact was not exposed. However, the last rocks observed below the Tepexic Fm. were of the Huayacocotla Formation.

The Tepexic Fm. is more commonly reported to overlie the Cahausas Formation and to be composed of bivalve and gastropod packstones and grainstones (Longoria, 1984; Compañia Minera Autlán, pers. comm.). Its thickness varies from less than one meter to a maximum of 50 meters (Longoria, 1984). The Tepexic Fm. is interpreted to include the first marine rocks of the Upper Jurassic transgression (Longoria, 1984).

There is considerable disagreement about the

interpretation and placement of the upper boundary of the Tepexic Fm. The first appearance of calcareous nodules in the black shale facies is taken by some authors (e.g. Longoria, 1984) to indicate the beginning of the superjacent "Santiago" formation of Cantu-Chapa (1971; see discussion below). Suffice it to note that the Tepexic Fm. becomes more shale-rich upward, and that this transition to the superjacent "Santiago" formation can be either abrupt or gradational. Much of the confusion stems from the lateral changes in the lithology coupled with descriptions that appear to reflect the personal biases of those workers who have studied the area. Therefore, the first appearance of calcareous nodules in the black shale facies is taken to indicate the beginning of the superjacent Taman Group (see Longoria, 1984). The transition is reported as abrupt and marked by the occurrence of the ammonite Reineckia. Longoria (1984) interprets the transition as a rapid change in sea level.

"Santiago" formation of Cantu-Chapa - Overlying the Tepexic Formation is a package of black, finely laminated shales which was originally described by Heim (1926) and informally termed the "Santiago Formation" by E. Reyes in 1964 (see Hermoso de la Torre and Martinez-Perez, 1972, p. 51). Cantu-Chapa (1969) formally proposed the name, but, as is pointed out by Hermoso de la Torre and Martinez-Perez (1972, p. 51) the name "Santiago Formation," had previously

been used by C. Fries for the base of the Pachuca Group. The name was published in June, 1962 in the Resumen de la Geologia de la Hoja Pachuca de la Carta Geologica de Mexico serie 1:100,000. As a result, the use of the name "Santiago Formation" for the Oxfordian age package of black shales should not be permitted. Additional discussion regarding this matter can be found in Lopez-Ramos (1979) and Longoria (1984). It is beyond the purpose of this work to set forth a new nomenclature for these and superjacent rocks. However, because so much of the literature uses the name I will employ "Santiago" formation in an informal sense and reiterate the need for a revision of the nomenclature of this and superjacent rock units.

The "Santiago" formation in the study area is also a black, finely laminated shale. It is pyritiferous and becomes more calcareous near the top. Fauna are scarce and occur in locally fossiliferous layers composed of ammonites, bivalves (e.g. Ostrea, Bositra, and Gryphaea), rhynchonellid brachiopods, and bryozoa (Force, pers. comm.). The "Santiago" formation most probably represents deposition in an anoxic, clastic-dominated basin.

Taman Formation - The suite of rocks constituting the Taman Formation also has a great deal of controversy and confusion associated with its lithologic and stratigraphic characteristics and, as a consequence, its nomenclature. The stratigraphic nomenclature employed to denote this

package of calcareous shales and argillaceous limestones is also under criticism by some workers (see Lopez-Ramos, 1979; Longoria, 1984). Attempts have been made to establish the Taman Formation as containing two units; a lower shale package, which is equivalent to the "Santiago Formation" of Cantu-Chapa (1971), and an upper limestone unofficially named the Chipoco Formation by Hermoso de la Torre and Martinez-Perez (1972) and subsequently described in detail by Aguayo (1977; also see Pedrazzini and Basañez, 1978). In older literature no division was made of the Taman Formation; descriptions of the constituent lithologies can be found in Kuegelgen (1958), Carillo-Bravo (1965), and Cantu-Chapa (1971).

The name Taman Group was proposed by Longoria (1984, p. 69) for a collection of lithologies which he summarized as: (1) a lower black shale package containing calcareous nodules and argillaceous black limestone; (2) a middle zone of medium- to thick-bedded black limestone and shale; and (3) an upper, thin to medium-bedded black argillaceous limestone package containing shale and tufaceous layers. Lithology #1 is equivalent to the "Santiago" formation as described above, whereas lithology #2 is the same as the Chipoco Formation (Longoria, pers. comm.). However, a group status for these rocks does not appear acceptable as no formations are named within the group.

The Taman Formation, as described in the literature

before 1969, included, but did not differentiate, the rocks of the so called "Santiago" formation. However, separation of these rocks from the Taman Formation is favored. This is because the "Santiago" formation has been commonly used in the study region, and several workers have noted that the unit is mappable over the whole region and so deserves formation status. For the purpose of this study the name Taman Formation will be used for all rocks above the "Santiago" formation and below the Pimienta Formation. The lower part of the Taman Formation, in the study area, will be denoted as the Chipoco facies. The transition between the "Santiago" formation and the Chipoco facies of the lower Taman Formation is transitional and placed at the first appearance of bedded limestone and shale (Aguilera, 1972; and as inferred from Longoria, 1984). This suite of bedded limestone and shale, together with the upper argillaceous limestone lithologies correspond to the Taman Formation as defined by Heim (1940). Calcarenite beds can be found in the middle part of the Taman Formation and are interpreted to be displaced shallow-water sediments corresponding to the San Andres Member of the Taman Formation (Longoria and Pessagno, Univ. Texas at Dallas, pers. comm.; Maynard, Univ. of Cincinnati, pers. comm.).

The Chipoco facies in the study area consists of argillaceous, laminated mudstones and wackestones. Calcareous shale beds occur in the lower third of the

sections as do up to 3 spiculite horizons. Locally fossiliferous intervals containing radiolarian, sponge spicules, and pelecypods occur at three levels. These features are discussed in the following chapter.

San Andres Member - The San Andres Member is a grey calcarenite containing ooids; pellets; grapestone; lithoclasts; abundant, large (> 1 cm) quartz fragments; feldspars; and non-carbonate rock fragments (Cantu-Chapa, 1971). The depositional environment is considered to have been a shallow-water platform.

Pimienta Formation - Conformably overlying the Taman Fm., and having a contact defined by the first appearance of thinly bedded limestone and chert, is the Pimienta Formation (Carillo-Bravo, 1965; Longoria, 1984). This formation is characterized as containing alternating (rhythmically bedded) black shale and argillaceous limestone. Tuffaceous material in the shale, and small lenses of chert ("pedernal") occur in the limestone and decrease upward. A late Jurassic age has been assigned to the base of the formation, based on fossils present, and the upper Pimienta is considered to be early Cretaceous in age. This formation is interpreted as a deep water accumulation.

Tertiary Igneous Rocks - A large part of the study area is covered by late Tertiary basaltic lava flows and associated pyroclastic material. Andesitic and rhyolitic

rocks have been reported to the south, but are rare (Comp. Minera Autlán; Tavera and Alexandri, in press). Evidence of intrusive activity is limited to scattered dikes and one stock of intermediate composition. These features cross-cut and truncate manganese-rich rocks and ore zones. Their origin is not believed to be related to mineralization.

TECTONIC EVENTS AND PALEOGEOGRAPHIC SETTINGS

The tectonic events affecting the Gulf of Mexico region and the development of a detailed model for the evolution of the region have been topics of extensive research. Summaries and major views regarding the tectonic history of eastern Mexico and the Gulf area can be found in Pindell (1985), Longoria (1984, 1985), Anderson and Schmidt (1983), and Pilger (1978) (see Figure 5). These ideas are summarized below with regard to the study area.

Most workers believe that rifting began during the latest Triassic to early Jurassic periods, producing a block-faulted rift topography (Longoria, 1984). Deposition continued to be dominated by terrigenous sedimentation, as evidenced by the Huizachal, Huayacocotla, and Cahuasas Formations. The first evidence of shallow marine conditions is found in the Callovian age calcarenites of the Tepexic Formation, which has been interpreted to be the result of an east to west transgression (Longoria, 1984). Longoria (1984) suggests that relief produced during Triassic block faulting was present through the middle

FIGURE 5.

Generalized tectonic and paleogeographic setting during the late Jurassic in the Gulf of Mexico region (from Pindell, 1985). CP = Coahuila Platform, TA = Taumaulipas Arch, TMVBL = Trans-Mexican Volcanic Belt.

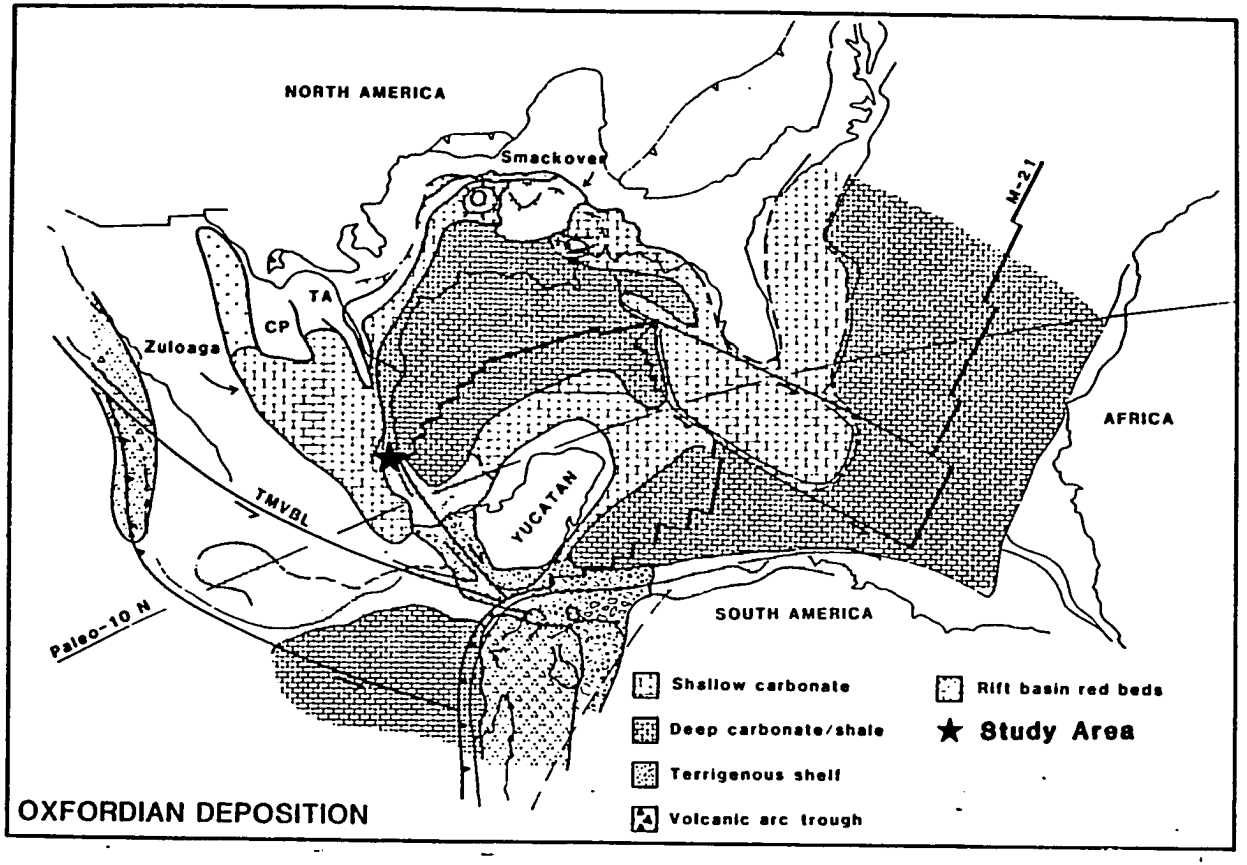

Jurassic and that a second episode of block-faulting may have occurred, reactivating the rift topography. It is possible that multiple episodes of reactivation caused the basin topography to change through time (Longoria, pers. comm.).

Paleogeographic reconstructions for the time and area under consideration have been presented by Aguilera (1972), Lopez-Ramos (1981), Enos (1983), and Pindell (1985). These reconstructions depict the presence of land masses to the west of the study area and two peninsular land masses to the north called the Coahuilla Peninsula and the Tamaulipas Arch (Figure 6). The southward extension of the Tamaulipas Arch was expressed in the form of an archipelago and submerged topographic highs. These topographic features were sites of deposition of shallow marine carbonates, evaporites, and in the case of the islands, erosion or non-deposition.

A complex pattern of marine basins characterized by narrow to irregularly shaped, relatively shallow embayments and narrow, relatively deep channels existed between the topographic highs (Figure 7). Actual water depths are not known but the thickness of the stratigraphic units range from in excess of 500 meters in the deep channelways to as few as 100 meters in the shallow bays (Aguilero, 1972).

FIGURE 6.

Paleogeographic reconstruction of Mexico during the late Jurassic (from Lopez-Ramos, 1981).

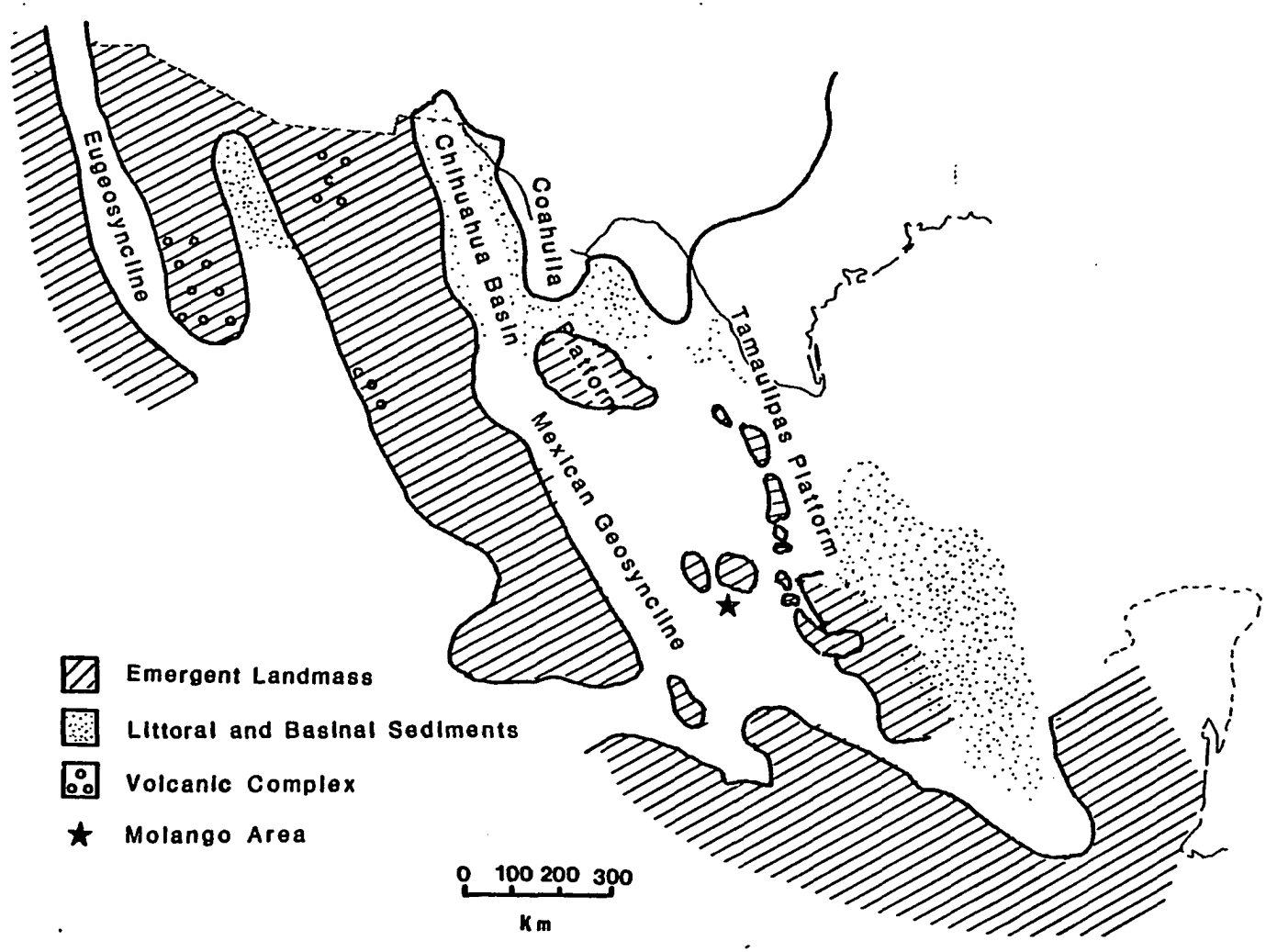

FIGURE 7.

Paleogeographic reconstruction of the study area at the time of mineralization (after Aguilera, 1972; and Hermosa de la Torre and Martinez-Perez, 1972).

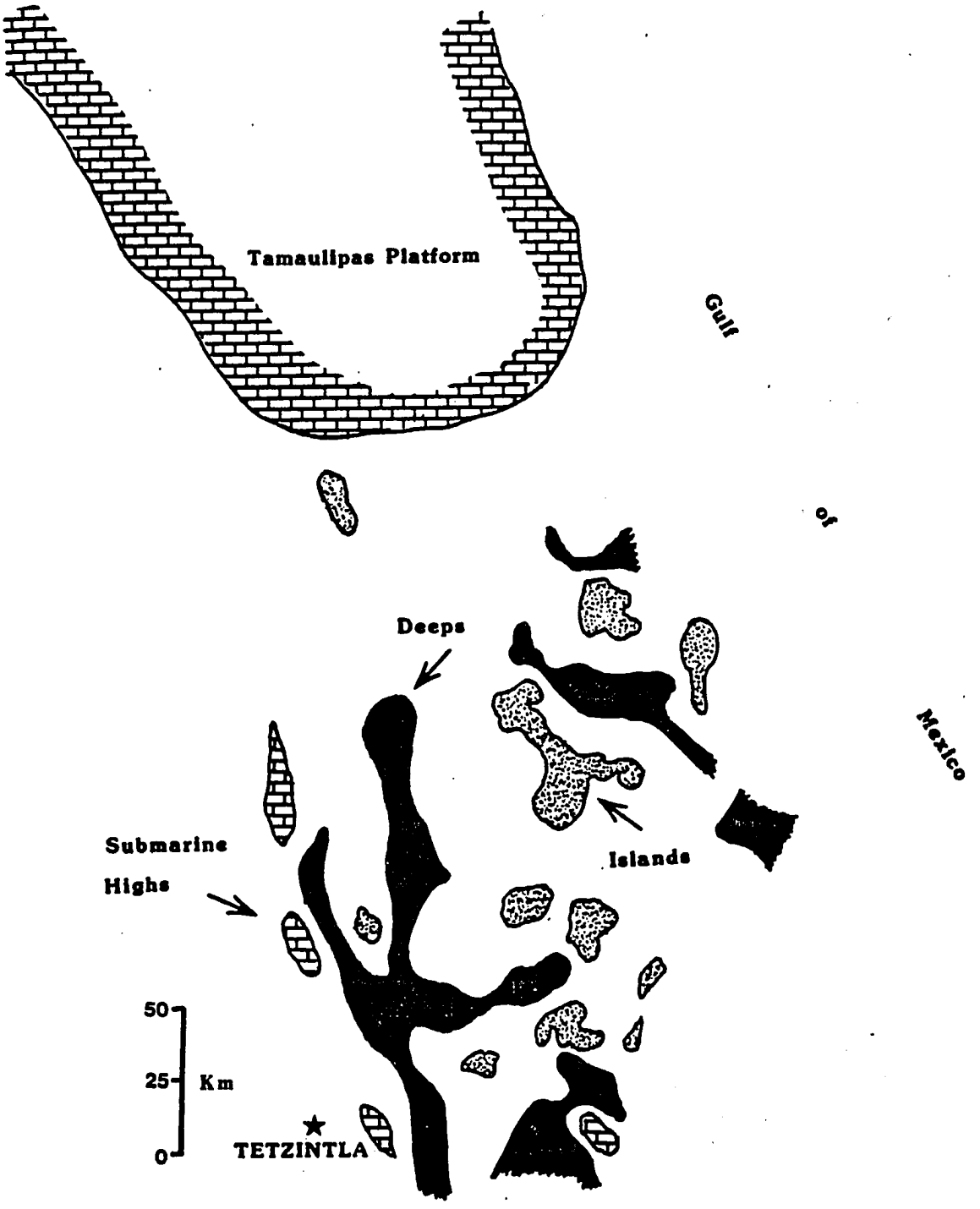

Sea Level Changes - The position of the sea surface can be influenced by eustatic changes and, on a regional or local scale, by tectonic events (i.e. taphrogenesis). During the Jurassic period, the net eustatic change in sea level was toward a high (i.e transgression) which reached its peak during the late Jurassic (Vail, et al., 1984). In addition, a short term maximum transgression and the development of a major condensed section is placed at the Oxfordian-Kimmeridgian boundary (Vail, et al., 1984, p. 350-351).

It is evident that the study area was tectonically active during the Jurassic, and that rifting processes may have lead to relatively rapid vertical movements and consequently in rapid sea level changes. Whether such tectonic movements are responsible for the formation of isolated topographic highs and the islands of the archipelago is unclear but it seems reasonable to infer that such was the case.

LOCAL STRATIGRAPHY

All the stratigraphic units described above can be found in the Molango district. However, those of particular interest are the "Santiago" formation and the Chipoco facies of the Taman Formation. The areal distribution of the Taman Formation, which contains the ore zone in outcrop, and the location of the various mines are shown in figure 3.

Measured sections were obtained at several localities as indicated in Figure 3 and have been generalized in Figures 8, 9, and 10. The most extensive section found is located in the Tetzintla workings and is a combination of measured section from the Frente B adit and of open-pit exposures to the south, along the access road to the service garage (Figures 8 and 11). Details of the stratigraphic sections are given below.

STRUCTURAL GEOLOGY

Information on the structural geology of the study area, and the region in general, has been collected from the literature and through conversation with geologists from Compañia Minera Autlán (Rafael Alexandri, Jr.; Alfonso Martinez-Vera; Juventino Oñate; Alejandro Medina; Andrés Rocha; and Julio Mendez). Personal observations of structural features are limited. Ideas pertaining to the regional tectonics and the implications on the paleogeography of the area are from the literature and conversation with Dr. José Longoria of the University of Texas at Dallas.

Regional Features - The study area has been subjected to compressional forces which have produced a very complex pattern of folds and faults (Chelen-Franulic, 1976) (Figure 3). The region which encompasses the Molango District is part of in a major structural feature referred to as the Huayacocotla Anticlinorium (Erben, 1956). This

FIGURE 8.

The "Frente B" measured section from underground and open-pit mapping. See figure 11 for plan and cross-sectional views of the area.

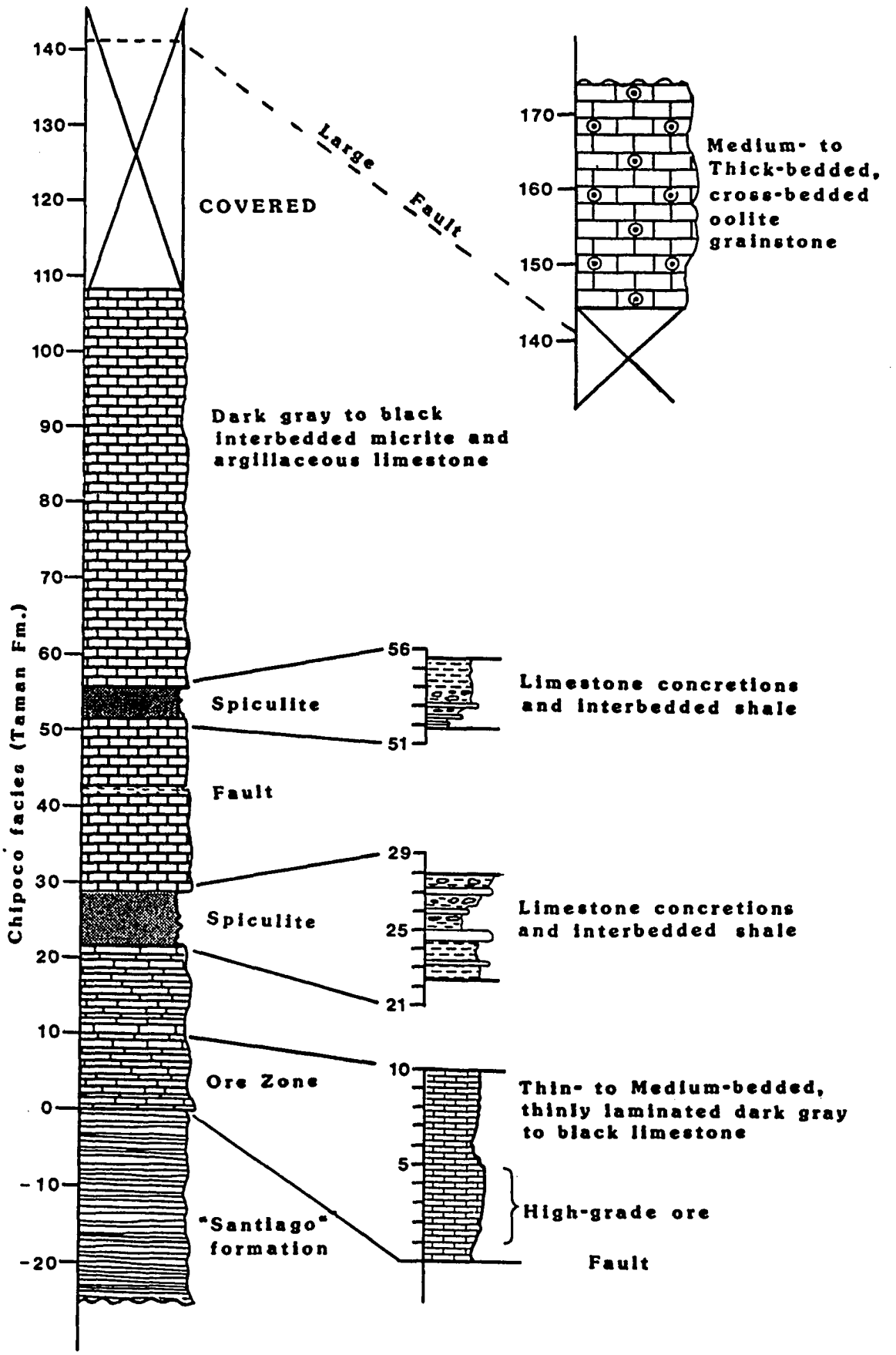

FIGURE 9.

Measured section from level 1052 located approximately 1 km north-northwest of the "Frente B" section.

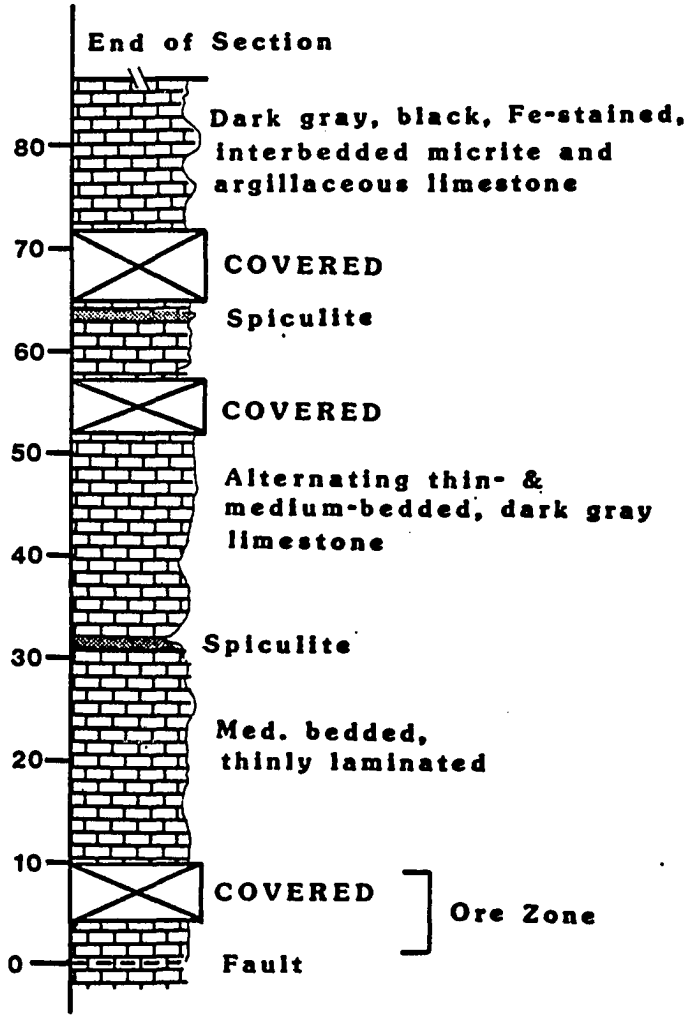

FIGURE 10.

Simplified measured sections from rocks surrounding the Tetzintla open-pit showing the stratigraphic location of the oolite, spiculite beds, ore zone and contact.

Stream Section Below 1000 Level

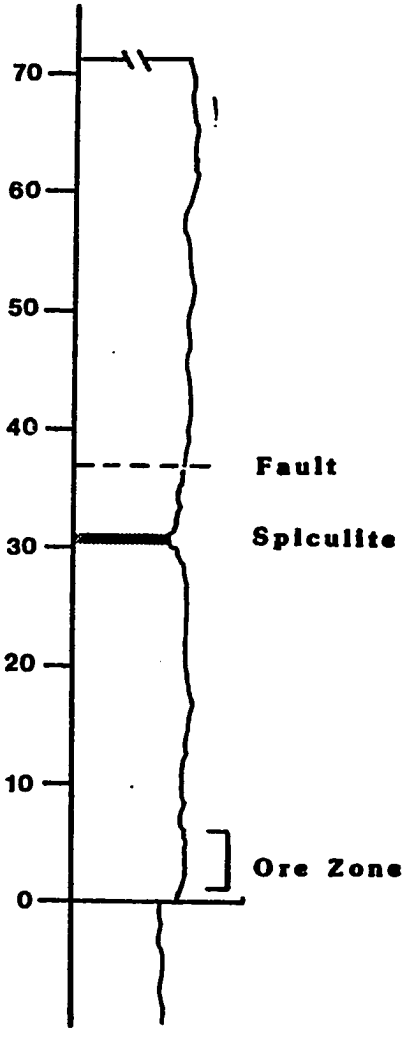

Road-cut North of Acoxcatlan

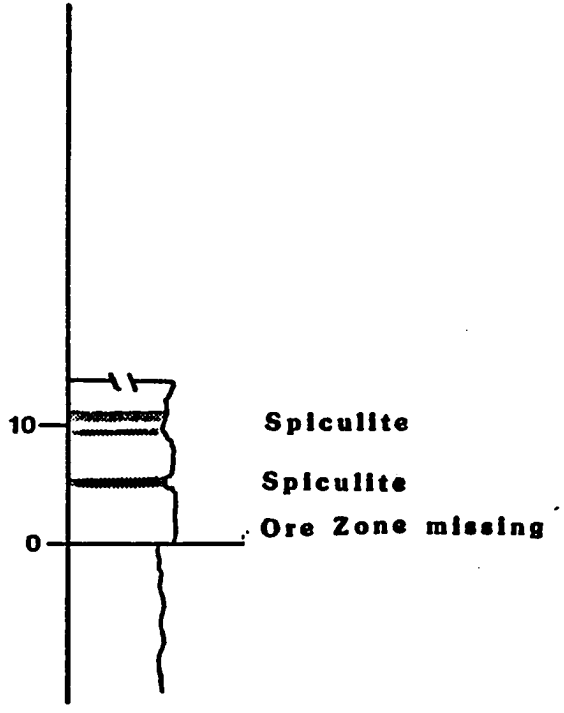

FIGURE 11.

Plan view and cross-sectional view of the "Frente B" adit and outcrop.

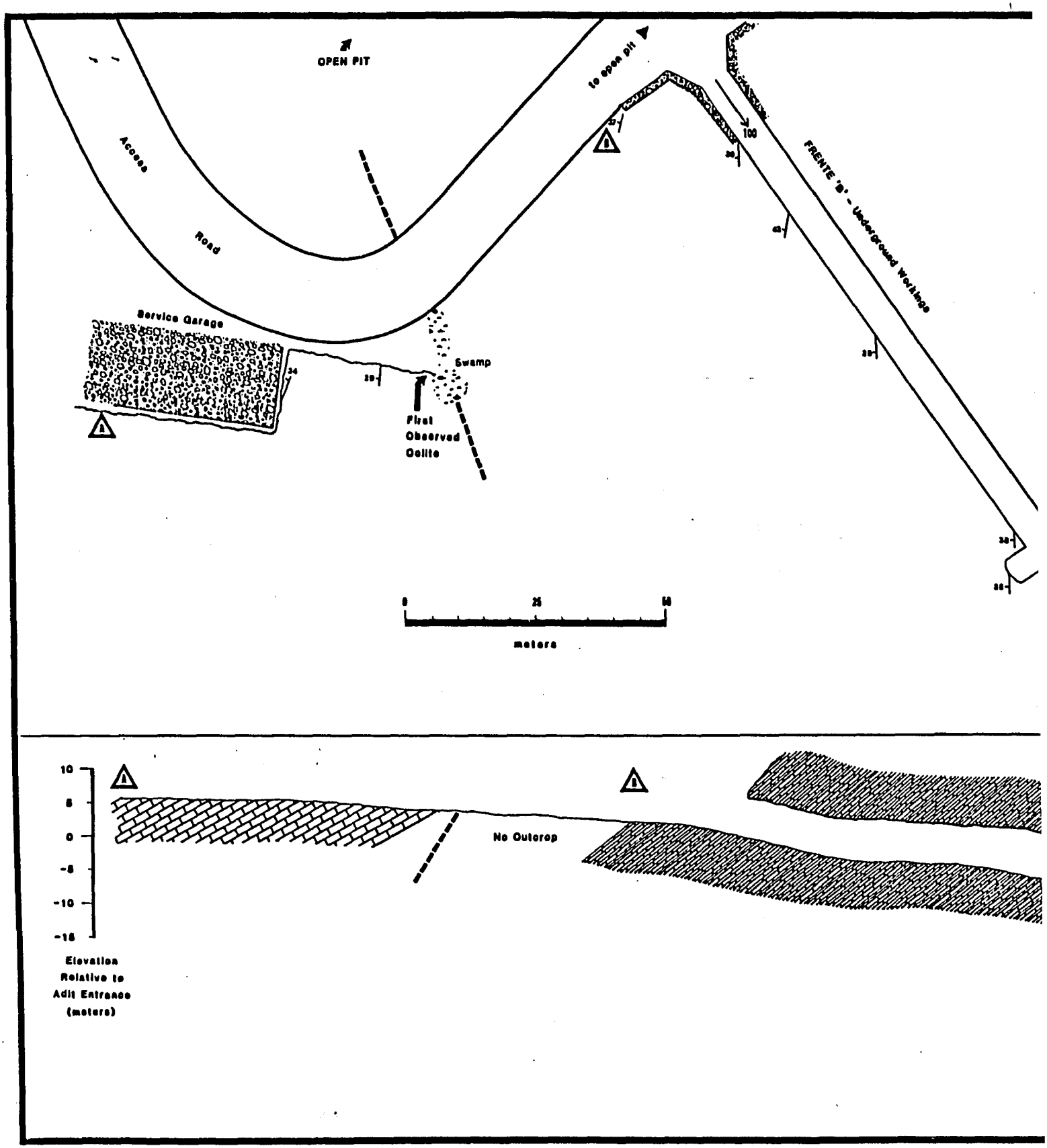

A. Plan View

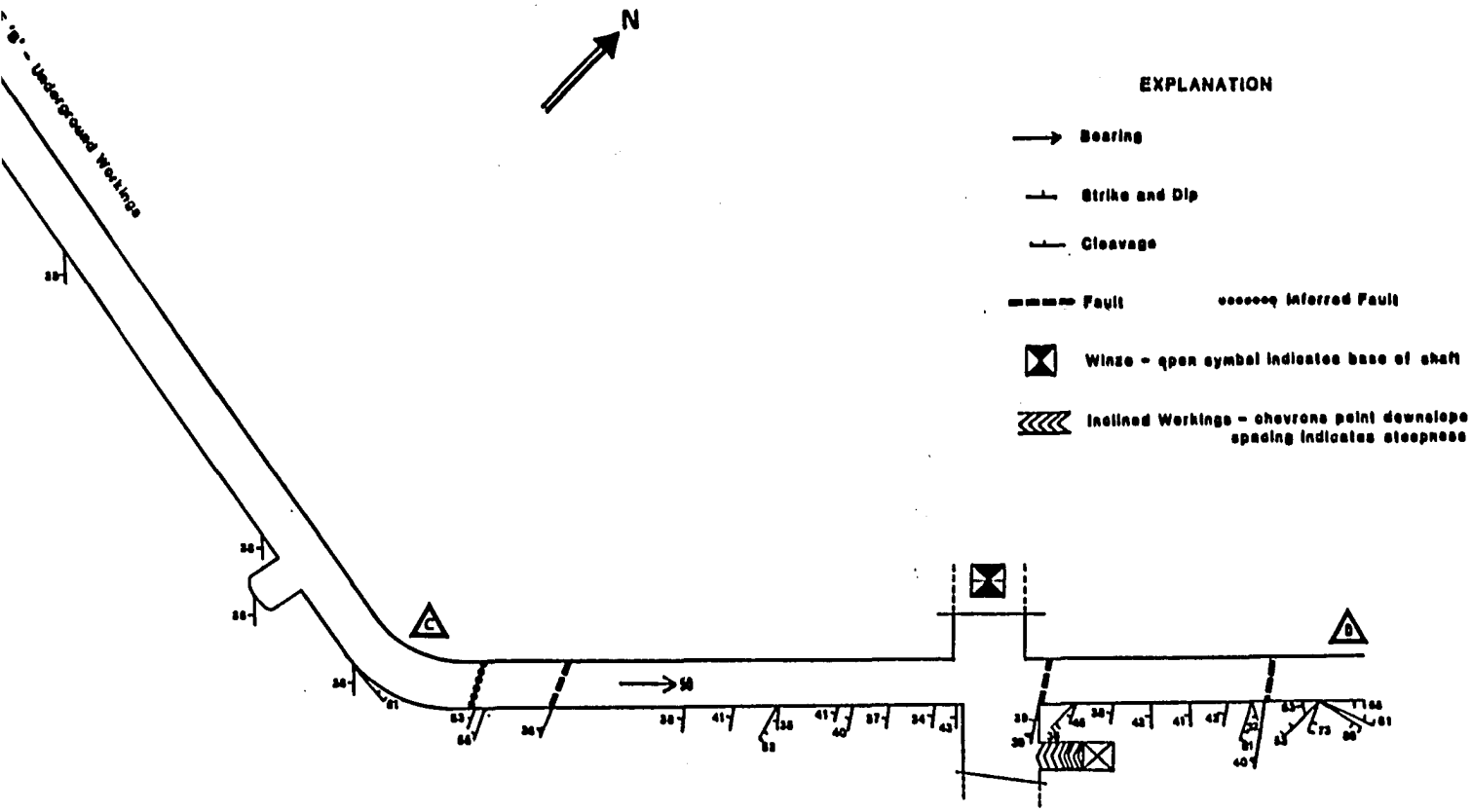

B. Cross-sectional View

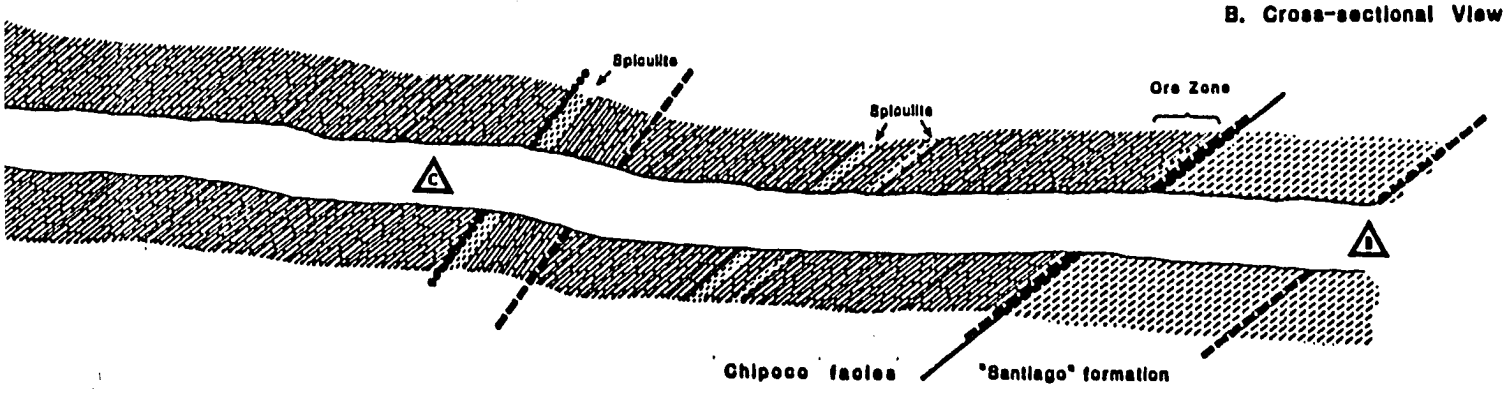

anticlinorium which trends northwest-southeast is in excess of 150 km in length, and has smaller asymmetric folds superimposed on the larger structures (Carillo-Bravo, 1965). This structural feature is part of the tectonostratigraphic domain known as the Huayacocotla Segment (Longoria, 1984).

Local Features - The Tetzintla mine is situated on the southwest flank of an asymmetric anticline. The axial plane of the fold dips 60° southwest and the axis plunges 10° northwest. Cleavage is well developed in places in arillaceous intervals and often obscures bedding. Folds in the mine area are usually asymmetric and range from open in the northwest to tight in the central area. They have been thrusted in the southeast (Cia. Minera Autlán, pers. comm.).

Faults are abundant and occur in a variety of sizes and types. Information regarding the systematics of fault patterns and distribution is incomplete. However, two particular faults important to this study should be noted. In the study area the contact between the Santiago and Chipoco facies is everywhere a fault contact. The fault plane appears planar and occurs at the base of a well-indurated, manganese-rich zone known as the "A-Bed" (Capa A). A second large fault occurs below an upper oolitic grainstone of the upper Chipoco rocks. Rocks below this fault are best described as argillaceous, silty limestones.

This fault is not a bedding plane fault but rather cuts out section from the underlying argillaceous interval. Comparison of measured section from four localities clearly demonstrates the loss of section, moving from south to north, resulting from this fault (Figures 8, 9, and 10).

The amount of section missing as a result of these two faults is unknown. It is possible only to speculate on the significance of the missing material below the "A-Bed". Such suppositions are deferred until appropriate in later discussion.

CHAPTER III. STRATIGRAPHIC AND PETROLOGIC OBSERVATIONS

The following descriptions of the rocks and stratigraphic relationships are based on field observations and study of samples collected. The rocks comprising the upper part of the "Santiago" formation and the Chipoco facies exhibit very little variation in appearance, making identification in the field difficult. Therefore, I shall separate the discussion of features observed at the hand-sample-scale and those seen petrographically in order to emphasize the different lithotypes. Of the localities studied, the Frente B section, measured underground and in outcrop at the Tetzintla workings, provided the most complete section (Figure 8 and 11). This composite stratigraphic section will be described in detail and used as a reference for the description of variations in lithology and stratigraphy of the other locations.

STRATIGRAPHIC OBSERVATIONS

Field observations indicate five general lithologic packages which make useful reference groups for discussion of stratigraphy. These packages are: (1) lower Santiago black shale; (2) the upper Santiago calcareous shale; (3) the lower Chipoco, which includes the "A-Bed" (Capa A) and the ore zone; (4) the middle Chipoco, composed predominantly of argillaceous silty limestone; and (5) the upper Chipoco oolite packstones and grainstones. Several lithotypes, discussed in detail below, exist within the

packages named above.

"Santiago" Formation - The rocks of the "Santiago" formation are divided here into lower and upper parts. The lower Santiago (lithologic package 1) is an black, sooty, laminated, fissile, unfossiliferous, and slightly calcareous shale which easily breaks into small chips. This lithotype was observed to range from its lowest exposed position 300 meters below the base of the Chipoco up to approximately 100 meters below the contact with the Chipoco.

The second lithotype, comprising the upper Santiago (lithologic package 2) is a thinly bedded (i.e. 5 to 10 cm thick), calcareous shale to argillaceous wackestone . The transition between the lower Santiago and this lithotype was not observed. The upper Santiago appears graphitic and, in the uppermost 2 to 5 meters, commonly contains whole ammonites, Gryphea shell beds, and limestone concretions.

Chipoco Facies - The contact between the Santiago and Chipoco appears to be a fault contact everywhere in the vicinity of the study area, and can be characterized as a bedding plane or extremely low angle fault which may represent a décollement. Relative movement and the amount of displacement have not been determined. The occurrence of a fault at this contact may be governed in part by the very evident physical difference between the two units.

The basal Chipoco, which contains the mineralized zone, is significantly harder than the underlying Santiago and superjacent unmineralized zone.

The oldest rocks exposed belonging to the Chipoco facies are found immediately overlying the contact (i.e. the fault). These rocks (lithologic package 3) include a zone of very hard, veined, pyritiferous, manganese carbonate that is effervescent in dilute hydrochloric acid. This is referred to as the "A- Bed".

The "A-Bed" in the underground section at Frente B is about 45 centimeters thick, very hard, and moderately effervescent in the lower two-thirds of the bed. The "A-Bed" has abundant calcite veins, which show no preferential orientation but occur in greater numbers and closer spacings in the lower one-third of the "A-Bed". Pyrite is abundant and occurs in the form of small pods, thin laminae and 2- to 3-centimeter-thick beds. Given the crystal size, habit, and sedimentary features apparent at the upper and lower boundaries of the pyritiferous zone, I interpret these forms of pyrite to be sedimentary and not a product of faulting or metamorphism.

Immediately overlying the "A-Bed", and differentiated by its lack of effervescence, is the base of the high grade ore zone. These rocks have a blocky fracture and contain up to 30 weight-percent manganese (as MnO). They consist of dark gray to black, laminated, non-effervescent,

slightly argillaceous limestone. Soft sediment deformation of the lamination is evident, and a strong magnetic field is present in the rock. Pyrite is noticeably absent in the basal 3 meters of the ore zone but is present in the upper portion of the ore zone.

An upward decrease in manganese content can be detected qualitatively by the return of effervescence of the rock when treated with dilute hydrochloric acid. A lithology similar to that described for the ore zone persists, in Frente B, to a distance 21.6 meters above the contact.

From this point (21.6 meters) upward to the second major fault, which separates the middle Chipoco from the oolitic upper Chipoco, the dominant lithology is a dark gray, thin to medium bedded, argillaceous limestone. Two different minor lithotypes were observed to occur within the argillaceous limestone. The first lithotype is a spiculite interval, and is composed of shaley, silty and concretionary beds. At least three such intervals can be observed in the Frente B adit and can be differentiated on the basis of thickness and the number of concretionary horizons.

The stratigraphically lowest spiculite is also the thinnest. It occurs, in Frente B, from 21.7 to 22.2 meters above the facies contact. This spiculite is composed of 0.5 meters of light gray, iron-stained, friable calcareous shales and has one layer of ellipsoidal calcareous

concretions situated in the middle of the interval. The second spiculite, which begins 4.25 meters above the top of the first spiculite, is 1.4 meters thick and is characterized by regularly spaced horizons of limestone concretions or continuous limestone beds in a light to medium gray shale. The third spiculite is the thickest and begins 51.8 meters above the base of the Chipoco. It varies from 3.5 to 4.0 meters in thickness and is composed of light gray, silty, flatly laminated, non-effervescent shale. Thin limestone beds and ellipsoidal concretions (8 to 10 cm in diameter) occur at regular intervals. The spiculite interval becomes darker in color upward but is much lighter in color than the normal Chipoco argillaceous limestone.

The second minor lithology observed is represented by thin layers containing disarticulated pelecypod shell debris. These beds have been observed at positions 10, 45.3, and 64.9 meters above the Santiago-Chipoco contact.

The final major lithotype observed is represented by the oolitic, pelloidal packstones and grainstones present at several localities in the Tetzintla area and always present above a large fault. The unit has a minimum thickness of about 30 meters (measured at the garage in the Tetzintla open-pit) and is characterized as a light gray, occasionally cross-bedded, poorly sorted but normally graded grainstone. Scoured basal contacts with underlying

fine-grained material have been observed. Field work by Maynard and May (pers. comm.) has revealed that these oolite beds are separated by micstones and invariably have a pronounced normal grading. Allochems range in size from <0.5 to as large as 5 millimeters in maximum dimension. They include ooids, pelloids, clasts of pelloidal aggregates (i.e. grapestones), and red algal fragments. Non-carbonate clasts include large, clear quartz grains, polycrystalline quartz grains, and rock fragments, all up to several millimeters in size.

PETROGRAPHIC OBSERVATIONS

"Santiago" formation - The lower part of the "Santiago" formation shows no petrographic features that are not seen in hand sample. Therefore, description will begin with samples of the upper part of the Santiago.

In thin-section, the upper part of the Santiago (i.e. the last 25 meters) is a dark brown to black, silty, calcareous mudstone. The rock contains local concentrations of pyrite, 10 to 15% by visual estimate, and between 5 and 50% silt-sized (~0.05mm) quartz as equant, angular disseminated grains. Well-developed lamination is absent; however, a sub-parallel orientation of the rock constituents is readily evident.

Closer to the contact with the Chipoco facies, the Santiago is an argillaceous pelletal wackestone (Figure 12). Allochems include abundant platy fragments

FIGURE 12.

A and B. Examples of the typical petrographic characteristics of the upper "Santiago" formation. Photomicrograph A is from 7.2 meters below the upper contact. Photomicrograph B is from 10 centimeters below the upper contact. Note the greater abundance of pelloids and coated grains in B.

C. Sample from 10 centimeters above the "Santiago"-Chipoco contact showing the abundant ooid, coated grain, and pelecypod components. Note that the pelecypod shell is encased in several layers of laminae.

D. Sample from 45 centimeters above the contact, in the middle of the "A-Bed".

E. Sample from 50 centimeters above the contact. Note the laminae and distribution of clotted textures and organic matter.

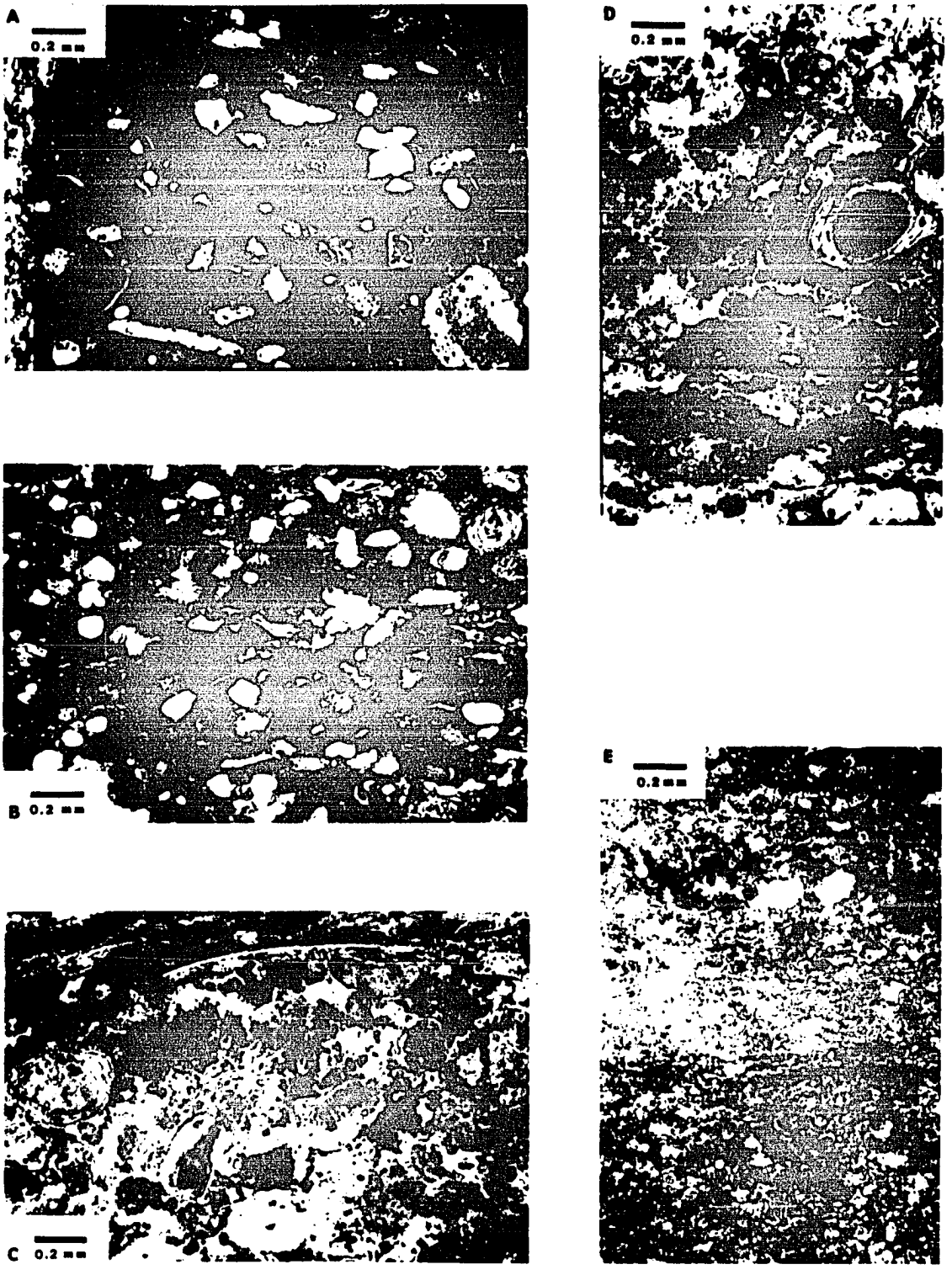

(bivalves); local accumulations of disarticulated, thin-shelled pelecypod valves; and algal pellets, micritized ooids, coated grains, pelloids and an occasional echinoderm fragment. In addition, calcispheres and radiolaria are present.

Ooids and pelloids constitute a large portion of the allochems and appear as structureless, micritic grains light to medium brown in color and averaging about 0.5 millimeters in diameter (Figure 12b). Shell fragments occur sporadically and are typically 2 mm in size (range 0.1 to 5 mm). They sometimes exhibit signs of extensive boring and often possess no internal fabric (i.e. they are extensively recrystallized). Many of the shell fragments are enclosed in a micritic envelope, and pyrite is present at the margins of the shells.

Pyrite is an abundant non-carbonate mineral that occurs as scattered crystals (~5 per cent visual estimate) or as local accumulations comprising up to 50 per cent of the rock. Feldspar grains are scarce, and similar in size and roundness to the quartz grains. Feldspar commonly show some signs of corrosion at the grain margins and is believed to be detrital in origin. Veinlets, which cut across bedding, are filled with calcite spar and small amounts of pyrite. No manganese has been detected in the veins by staining or microprobe analysis.

Chipoco Facies

"A-Bed" ("Capa A") - The first sample collected above the fault contact (T1, +0.10) is a granular carbonate with sub-planar to sub-concavo-convex grain boundaries. The crystal size ranges from 125 to 500 microns, and most crystals are about 375 microns. Scattered, fine silt-sized (0.125 by 0.025 mm) quartz is present and appears to be detrital, typically having irregular boundaries.

The petrographic texture of this carbonate resembles the typical complete diagenetic recrystallization of a primary texture to produce a micrite and a pseudospar, described by Folk (1959, 1963). However, the proximity of this feature to the fault suggests that the observed texture could by the product of strain recrystallization. The arguments for such an origin not only include the proximity to a large fault but also folding of the rocks in general. Strong evidence against a strain origin of the texture however is the non-uniform crystal size, a general lack of twinning, the absence of straight crystal boundaries, and the small grain size (Spry, 1979).

Thin-section observations of samples from the A-Bed reveal the presence of 0.25 to 1.0 cm-thick, very fine-grained, homogenous pyrite layers. Black- to dark-brown pelloids and coated grains (e.g. ooids, pellets, shells) are common and often contain abundant pyrite, both in their centers and along their margins (Figure 12c and 12d).

Curvature of enclosing sediments around allochems, weakly to moderately developed, planar preferred-orientation, flattening (lateral elongation) of the clotted texture, and concentration of organic matter along discrete horizons may indicate compaction of the sediment pile prior to significant cementation. Dissolution along boundaries of ooids and bioclasts (i.e harder grains) has resulted in both horizontally and vertically oriented solution seams (low amplitude stylolites).

A large part of the rock is made up of brown micrite, which possesses a distinctly crenulated to wavy lamination and contains abundant irregularly shaped clots (Figure 12c, d, and e). This texture is interpreted to be algal in origin. From its petrographic texture the rock can be described as an algal laminite.

Ore Zone - Fine lamination is the most noticeable petrographic trait of the ore zone (Figure 13a). These laminations appear as alternating light and dark, brown to black, parallel laminae, which often show evidence of soft sediment deformation from gravity sliding (Figures 13d and f). No evidence of bioturbation has been observed.

The petrographic textures observed in the ore zone are similar to those in the "A-Bed" and are consistent with those of rocks formed in an algal-dominated environment. The clotted texture, which is best developed at the base and above the high-grade portion of the ore

FIGURE 13. High Grade Ore Zone.

A. and B. 1.5 meters above the "Santiago"-Chipoco contact. Mn-mineralization is uniformly distributed.

C. Example of well-developed lamination for 2.5 meters above the "Santiago"-Chipoco contact. Note the greater degree of compaction in the central third which underlies a lamina of nearly pure rhodochrosite.

D. and E. Two examples of clotted textures showing the lack of laterally continuous laminae. D is located 3.4 meters above "Santiago"-Chipoco contact, E is situated 4.0 meters above the contact.

F. Example of soft-sediment deformation effects on the ore laminae. Sample located 4.0 meters above the "Santiago"-Chipoco contact.

zone, extends upward through approximately 40 meters. Rocks in the high-grade portion of the ore zone (Figures 13 c,d,e,f) have undergone greater compaction, resulting in the loss to varying degrees of the algal textures seen below. In some cases, compaction and slumping have resulted in a chaotic texture (Figure 13f).

Manganese mineralization occurs as microcrystalline rhodochrosite in light brown layers that alternate with intervals of predominantly silty shale. The Mn-carbonate can be in the form of discrete layers (i.e parallel upper and lower boundaries) or in clotted textures (Figure 13c and 13d, respectively). Reflected light petrography reveals no patterns of zonation, lamination, or crystal domains in the ore and host material.

Low-amplitude stylolites are abundant in the ore and, in the basal part of the ore zone usually mark the boundaries between clots. This stylolitization may indicate that the clotted appearance at the base of the ore is in part the result of compaction. In zones where less mineralized material occurs, the clots have the appearance of micro-nodules and laterally discontinous beds. Lamination in the enclosing host rock conforms to the shape of the manganese mineral body, suggesting that the manganese minerals were present prior to significant compaction of the host material.

The magnetic minerals present in the ore zone also

appear to be confined to the matrix, and do not occur within clots. Reflected light microscopy and microprobe analyses indicate that the magnetic minerals occur in the darker brown silty shale layers.

Fossil and siliciclastic material (i.e. quartz, feldspar) have not been observed in the high-grade ore zone. However, coated grains - including ooids and grapestones, rip-up clasts, and bioclasts - are common above the ore zone (Figure 14). Pyrite is present as disseminated grains, as small aggregates locally, and, in a few samples, as thin beds. In contrast, the quantity of pyrite in the high grade ore zone is conspicuously low, given that the environment of deposition appears to have been an oxygen-depleted or anoxic marine setting.

Several shale beds are present in the lithologic package defining the lower Chipoco facies. The calcareous zones within these shale intervals are comprised of what are believed to be sponge spicules (Figure 15). These spicules occur as single, straight to gently curved "needle" shapes and possess the central "tunnel" that is considered diagnostic of sponges and which differentiates the structure from radiolarian spines (Pessagno, pers. comm.;). A large portion of the spicules is now calcite, but some spicules are entirely or partly siliceous. It appears, in some instances, that calcite replaced originally siliceous material.

FIGURE 14. Lower Chipoco facies.

Examples of the typical lower Chipoco facies from the Mn-rich rocks overlying the high-grade ore zone. These pictures show the textures and fossils commonly observed. Note the abundance of coated grains (Figs. A, B, and D).

Sample Positions: A. 15.7 meters
B. 27.8 meters
C. 22.6 meters
D. 28.9 meters
E. and F. 35.4 meters

FIGURE 15.

Photomicrographs of spiculite intervals.

A, B, and C are from the lower spiculite interval situated 22.9 meters above the contact between the "Santiago" formation and Chipoco facies.

D and E are from the limestone intervals between spiculites (approx. 23.6 meters above "Santiago"-Chipoco contact).

F and G are from the upper spiculite located about 52 meters above the contact.

Opaque material is pyrite and organic matter.

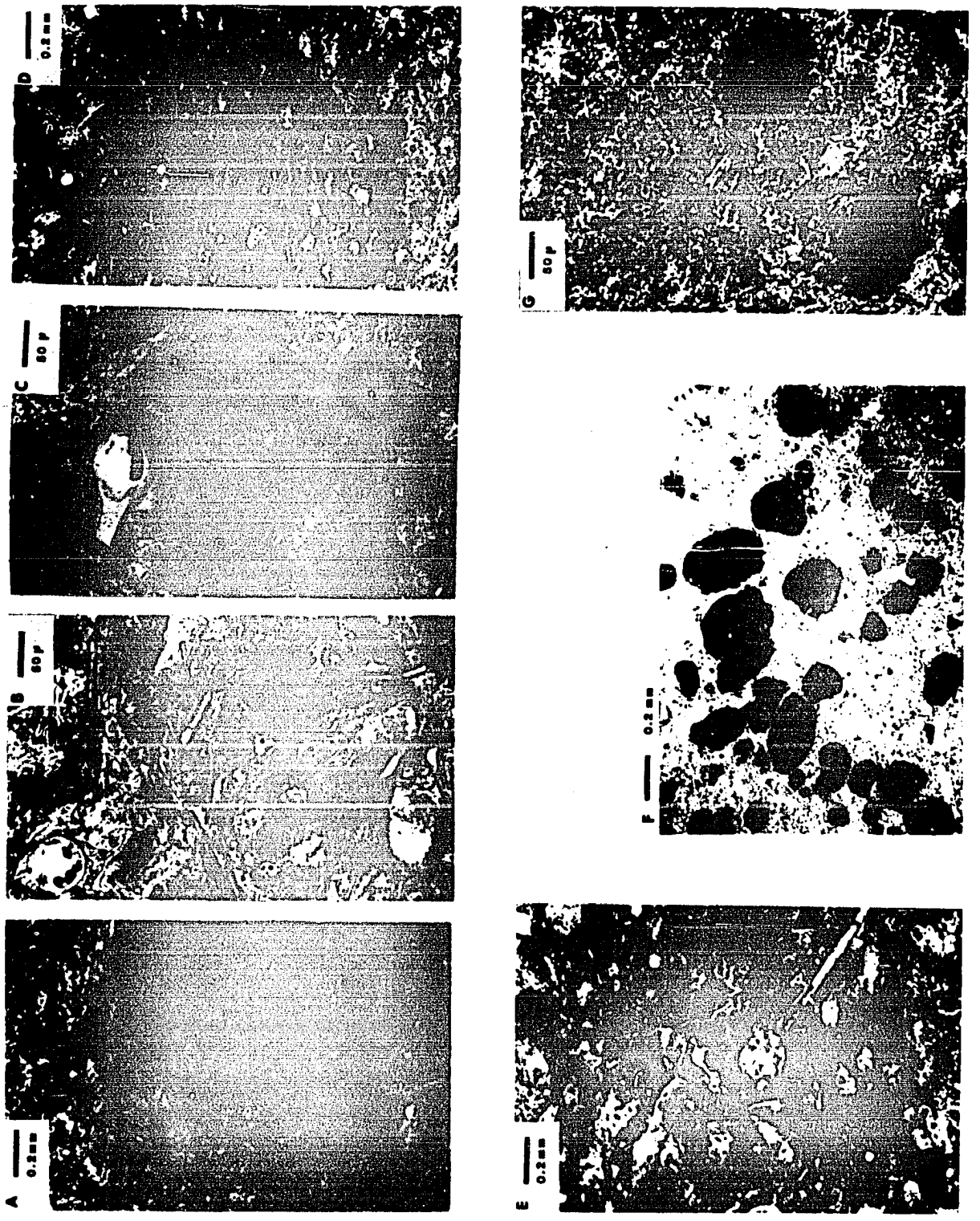

Middle Chipoco Facies - The middle part of the Chipoco facies is a thin- to medium-bedded, argillaceous, silty limestone (Lithologic Package 4). In thin-section the rock exhibits well-developed planar, fine lamination with scattered, fine, silt-sized quartz and irregularly shaped and laterally discontinuous carbonate masses (Figure 16a). This fabric alternates with a less well-compacted and oriented texture that contain abundant calcispheres (possibly recrystallized radiolarian tests) in addition to quartz and carbonate (Figure 16c and d). The presence of sucrosic carbonate texture as calcite microspar is evident in the latter fabric under higher magnification (Figure 16); this indicates that some recrystallization has occurred.

Local accumulations of pelloids and coated grains (ooid, oncolite) occur in the middle part of the Chipoco facies (Figure 16f). In addition, a horizon containing abundant disarticulated peleycpod shells, both broken and intact, was observed from the 45.3 meter level (Figure 16e). This shell hash is similar in appearance to the "filamentous bivalve micrite" commonly reported from Jurassic rocks of the Northern Limestone Alps (Wilson, 1975). Such accumulations are often attributed to the mass mortality of pelagic or nektonic fauna, which produces an accumulation of a large number of shells in an otherwise fine-grained sediment. Alternatively, these accumulations may represent

the effects of storm deposition. A conclusive interpretation is not possible at this time.

Upper Chipoco Facies - The upper part of the Chipoco facies is composed of oolitic packstones and grainstones (Figure 17). The allochems include: fine-, sand-, and gravel-size intraclasts, micritized ooliths, pellets, lumps, algal material and, mollusk, and gastropod fossils. Non-carbonate material is dominated by silt- to coarse-sand size quartz and feldspar grains. Quartz grains are present as single crystals, polycrystalline grains and as the constituents of rock fragments. In any of these occurrences quartz may exhibit unit, sweeping, or undulatory extinction.

All the carbonate allochems have undergone extensive micritization. Intergranular cements include an equant fringing cement and a coarse porefilling, sparry calcite. In some samples recrystallization has resulted in the partial loss of ooliths. However, recrystallization has not affected these rocks to any large degree. Textural integrity, especially of the radial ooid textures, is still present.

Nuclei are present in many of the ooids and are often mono- or polycrystalline quartz grains (Figure 17c and f). Bioclasts are occasionally observed as nuclei, and when identifiable are usually gastropods or single pelecypod valves.

FIGURE 16. Middle Chipoco facies.

A and B. Laminated micrite typical of the bulk of the middle Chipoco (from 58 meters above the contact).

C and D. Calcisphere wackestone. Note echinoderm fragment in C (from 75.2 and 77 meters above the contact, respectively).

E. Pelecypod wackestone (45.3 meters above the contact).

F. Pelloidal wackestone composed of micritized grains, and coated allochems. Note oncolite in lower left corner (from 56 meters above the contact).

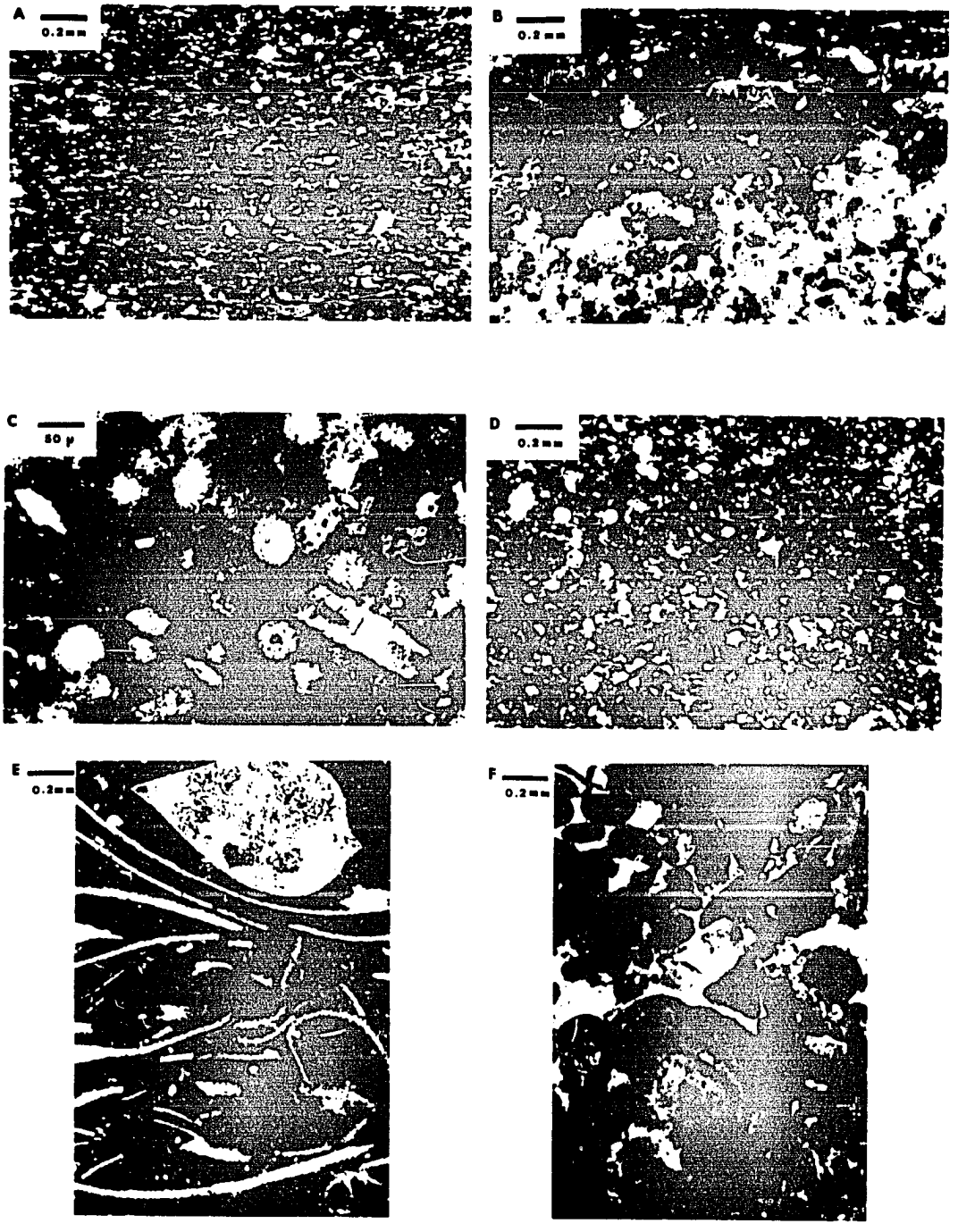

FIGURE 17. Upper Chipoco oolite grainstones. A. and B. Photomicrographs from cross-bedded grainstone unit 154.3 meters above basal contact of the Chipoco facies. Note: (1) the rip-up clast in the upper left corner of A, (2) the large amount of pelletal allochems, (3) micritized ooids, and (4) abundant detrital terrigenous quartz. B shows micritized and pelletal allochems within and surrounding what is probably a gastropod shell.

C. and D. Photomicrographs from cross-bedded grainstone unit 160 meters above basal contact. Note: (1) greater quantity of micritized ooids, (2) pore-filling cements which often show relict structures of allochems (e.g. upper left corner in D), and (3) the lesser degree of compaction as compared to A, B, and E.

E. Photomicrograph from 162.5 meters above basal contact showing the common strongly compacted texture. Note the large amount of large quartz grains, and the absence of ooids.

F. Photomicrograph from 165 meters above the basal contact. Note the well preserved nature of the allochems, suggestive of early cementation.

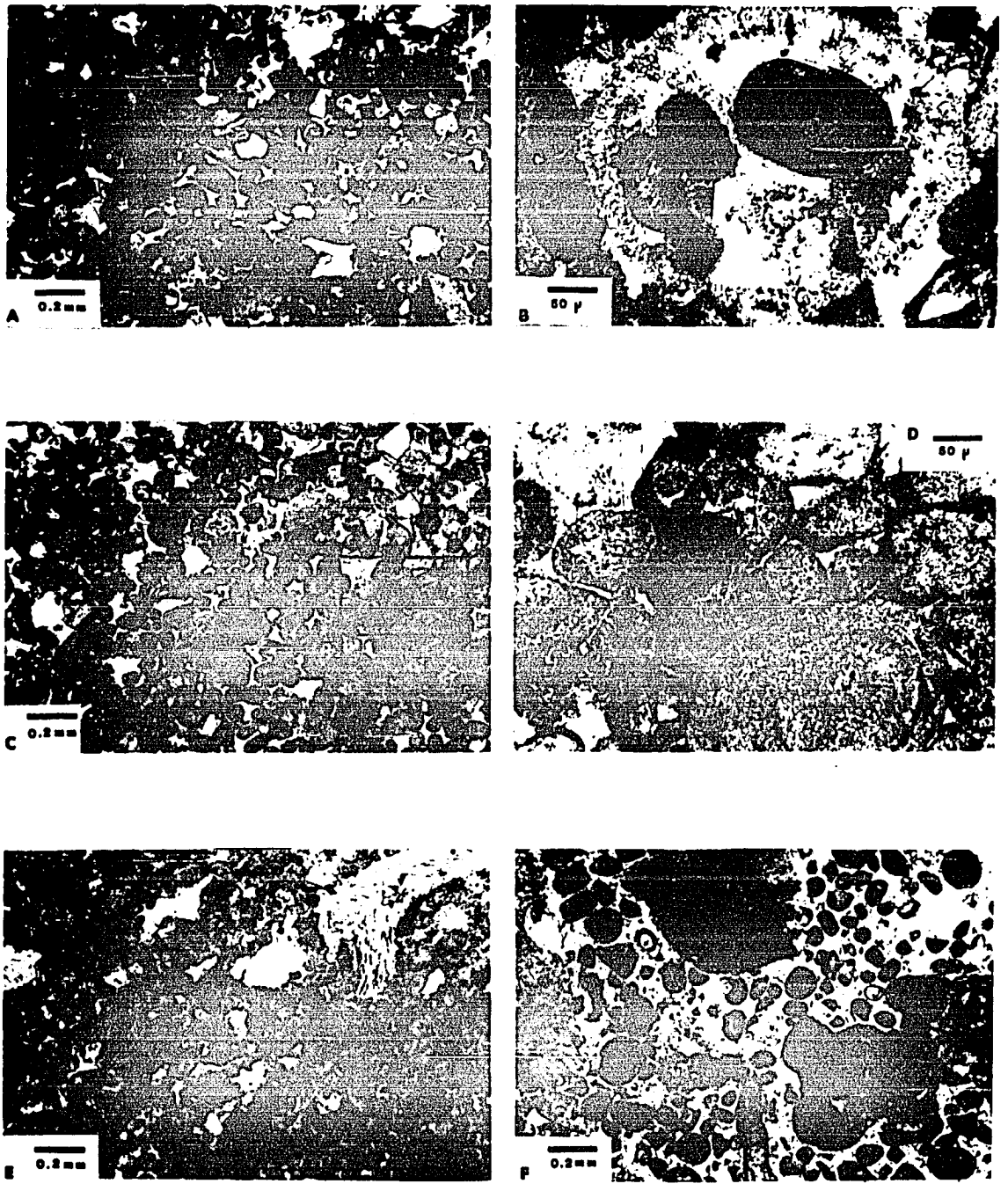

Most ooid nuclei are probably pellets, as indicated by the internal texture and the position of the radial textures (Figure 17). It is not certain whether the pellets are fecal or algal in origin.

Compaction effects vary in a continuous manner from matrix- (cement) supported to an evidently highly compacted, clast-supported texture (Figure 17). In some cases, the degree of compaction has been severe enough to produce a "pseudo" clotted appearance in the rock. This compaction is believed to have been an early event that occurred prior to substantial cementation. Strongly compacted textures are most evident in zones lacking a coated grain component. The abundance of pelletal material in these zones may have lead to the development of such a texture, since these allochems were probably relatively soft and their shape would permit more densely packed accumulations. However, the textures of the ooid grainstones and packstones may ultimately be the result of the greater pore space provided by the more rigid nature of these allochems. Such rigidity would allow some support of other grains. In addition, oosparite textures may have resulted from the diagenetic recrystallization of a wackestone that was originally mud-supported.

DISCUSSION

The "Santiago" formation represents the depositional processes and conditions which existed in the study area prior to mineralization. In addition, these rocks can be considered representative of those processes and conditions downdip of the Chipoco facies.

Given the petrographic and lithologic characteristics, I belived the lower part of the Santiago represents deposition under anoxic conditions. The upper part of the Santiago was also oxygen-depleted, although the abundant pelletal component is suggestive of some biologic activity having been present in or near the area. Abundant clastic (siliceous and carbonate) material is probably allocthonous and derived by transport from shallower waters, although a windblown source for the siliciclastic material cannot be ruled out.

The rocks of the lower Chipoco were also probably deposited under oxygen-depleted conditions. Whether the environment was anoxic is not clear. Bioturbation and in situ fauna are lacking, which, while consistent with oxygen-depleted conditions, is not conclusive evidence for such a condition (High levels of salinity could cause an absence of normal marine fauna). In addition, pyrite is generally very scarce in the lower part of the ore zone, and its occurrence in localized aggregates suggests that sulfate reduction occurred only in micro-reducing

environments. This may indicate that anoxic conditions were not severe enough to initiate sulfate reduction.

Petrographic study of the textures of rocks from the lower part of the Chipoco facies indicates that these sequences are algal in origin. Such an interpretation would imply a shallow marine, low energy environment, situated above the base of the photic zone.

The rocks of the middle Chipoco (i.e. medium-bedded, gray to black, argillaceous silty limestone) were probably also deposited under oxygen-depleted conditions. The characteristics of this interval (medium-bedded, microbioclastic, texturally homogenous) suggest that sedimentation occurred in a more basinal setting than that inferred for the lower Chipoco facies. Middle Chipoco facies rocks in the study area are very similar in appearance to the general petrologic group of pelagic lime mudstones and basinal rocks described by Wilson (1975).

The intervals of shell debris may represent storm deposits derived from shallower-water environments. The occurrence of spiculite-rich beds is also consistent with a basinal setting for the accumulation of the middle Chipoco sediments.

The oolitic wackestones and grainstones of the upper Chipoco are interpreted to be allocthonous accumulations derived from a shallower shelf setting. This interpretation is based on limited field observation but is in agreement

with observed sedimentologic features (basal scour, normal grading, poor sorting) and the opinions of other workers who have studied the unit more carefully (refer to Chapter 2).

CHAPTER IV. MINERALOGY AND MINERAL CHEMISTRY

At least 10 different mineral species are present in the rocks studied (Table I); these can be divided into the carbonates, oxides, sulfides, and silicates. The carbonates are most abundant throughout the Chipoco facies and in the uppermost "Santiago" formation (Figure 18 and Table II) whereas fine-grained silicates (e.g. clays and quartz) dominate the mineral assemblage of the lower "Santiago" formation.

All the mineral phases observed petrographically were also documented by either x-ray diffraction analysis, electron microprobe analysis, or both (Appendices B, C, D, and E). The identification of specific carbonates was made difficult by the presence of several similar carbonate phases in the same sample. Thus XRD identification was difficult and often ambiguous, and the fine-grained nature of the carbonates made visual identification of individual mineral grains impossible during microprobe analysis. Therefore, in some cases, the mineral phases reported were deduced from both types of analyses. The figures presented in the discussion below are representative of the general sample set. The reader is directed to the appendices for specific sample data.

SILICATES

The silicate minerals include predominantly illite and, in some samples, small amounts of chlorite, clay minerals,

TABLE I. MINERAL SPECIES IDENTIFIED FROM THE SANTIAGO AND CHIPOCO ROCKS

SILICATES:

Illite
Chlorite
Quartz
Plagioclase

SULFIDES:

Pyrite

OXIDES:

Magnetite
Maghemite

CARBONATES:

CALCITE - TYPE	DOLOMITE - TYPE
Calcite	Dolomite
Rhodochrosite	Kutnahorite
Manganoan Calcite	Ca-Kutnahorite (?)

TABLE II. RESULTS OF ACID DIGESTION OF SAMPLE MATERIAL FROM SANTIAGO AND CHIPOCO ROCKS.

SAMPLE NUMBER	STRAT. POSITION	INITIAL WEIGHT	TREATED WEIGHT	DIFFERENCE (grams)	WEIGHT % CARBONATE
MOL 1, -350	-350.00	5.00	2.69	2.31	46.20
MOL 1, -210	-210.00	4.00	2.17	1.83	45.75
MOL 1, -100	-100.00	8.00	5.86	2.14	26.75
T1, -24.9 A	-24.90	5.00	2.99	2.01	40.20
T1, -24.9 B	-24.90	5.00	3.00	2.00	40.00
T1, -24.9 C	-24.90	5.00	3.02	1.98	39.60
T1, -24.9 D	-24.90	5.00	3.05	1.95	39.00
T1, -24.9	-24.90	30.00	17.94	12.06	40.20
T1, -19 A	-19.00	5.00	2.07	2.93	58.60
T1, -19 B	-19.00	5.00	2.12	2.88	57.60
T1, -19 C	-19.00	5.00	2.08	2.92	58.40
T1, -19 D	-19.00	5.00	2.02	2.98	59.60
T1, -3.9 A	-3.90	5.00	2.94	2.06	41.20
T1, -3.9 B	-3.90	5.00	2.92	2.08	41.60
T1, -3.9 C	-3.90	5.00	2.90	2.10	42.00
T1, -3.9 D	-3.90	5.00	2.94	2.06	41.20
T1, -0.1 A	-0.10	5.00	1.94	3.06	61.20
T1, -0.1 B	-0.10	5.00	2.96	2.04	40.80
T1, -0.1 C	-0.10	5.00	2.93	2.07	41.40
T1, -0.1 D	-0.10	5.00	2.97	2.03	40.60
T1, +0.1 A	0.10	5.00	0.89	4.11	82.20
T1, +0.1 B	0.10	5.00	0.93	4.07	81.40
T1, +0.1 C	0.10	5.00	0.94	4.06	81.20
T1, +0.5 A	0.50	5.00	1.08	3.92	78.40
T1, +0.5 B	0.50	5.00	1.10	3.90	78.00
T1, +0.5 C	0.50	5.00	0.90	4.10	82.00
T1, +0.5 D	0.50	5.00	1.07	3.93	78.60
T1, +2.0 A	2.00	5.00	1.24	3.76	75.20
T1, +2.0 B	2.00	5.00	1.23	3.77	75.40
T1, +2.0 C	2.00	5.00	1.13	3.87	77.40
T1, +2.5 A BASE	2.50	5.00	1.05	3.95	79.00
T1, +2.5 B BASE	2.50	5.00	1.06	3.94	78.80
T1, +2.5 C BASE	2.50	5.00	1.04	3.96	79.20

TABLE II. (continued) RESULTS OF ACID DIGESTION OF SAMPLE MATERIAL FROM SANTIAGO AND CHIPOCO ROCKS.

SAMPLE NUMBER	STRAT. POSITION	INITIAL WEIGHT	TREATED WEIGHT	DIFFERENCE (grams)	WEIGHT % CARBONATE
5.00	2.55	5.00	1.10	3.90	78.00
T1, +2.5 B TOP	2.55	5.00	1.17	3.83	76.60
T1, +2.5 C TOP	2.55	5.00	1.05	3.95	79.00
T1, +2.5	2.53	30.00	8.86	21.14	70.47
T1, +3.4 A	3.40	5.00	0.85	4.15	83.00
T1, +3.4 B	3.40	5.00	0.91	4.09	81.80
T1, +3.4 C	3.40	5.00	0.79	4.21	84.20
T1, +3.4 D	3.40	5.00	0.80	4.20	84.00
T1, +5.9 A	5.90	5.00	1.00	4.00	80.00
T1, +5.9 B	5.90	5.00	1.00	4.00	80.00
T1, +5.9 C	5.90	5.00	0.96	4.04	80.80
T1, +5.9 D	5.90	5.00	1.00	4.00	80.00
T1, +12.5 A	12.50	5.00	0.98	4.02	80.40
T1, +12.5 B	12.50	5.00	1.01	3.99	79.80
T1, +12.5 C	12.50	5.00	1.06	3.94	78.80
T1, +12.5 D	12.50	5.00	1.06	3.94	78.80
T1, +28.5	28.50	5.00	1.29	3.71	74.20
T1, +32.1	32.10	5.00	0.59	4.41	88.20
T1, +45.3	45.30	5.00	0.58	4.42	88.40
T1, +78.1	78.10	5.00	1.52	3.48	69.60
T1, +110.9	110.90	40.00	16.07	23.93	59.83

FIGURE 18.

Weight-percent carbonate, determined by loss after acidification, for samples from 350 meters below to 111 meters above the "Santiago"-Chipoco contact.

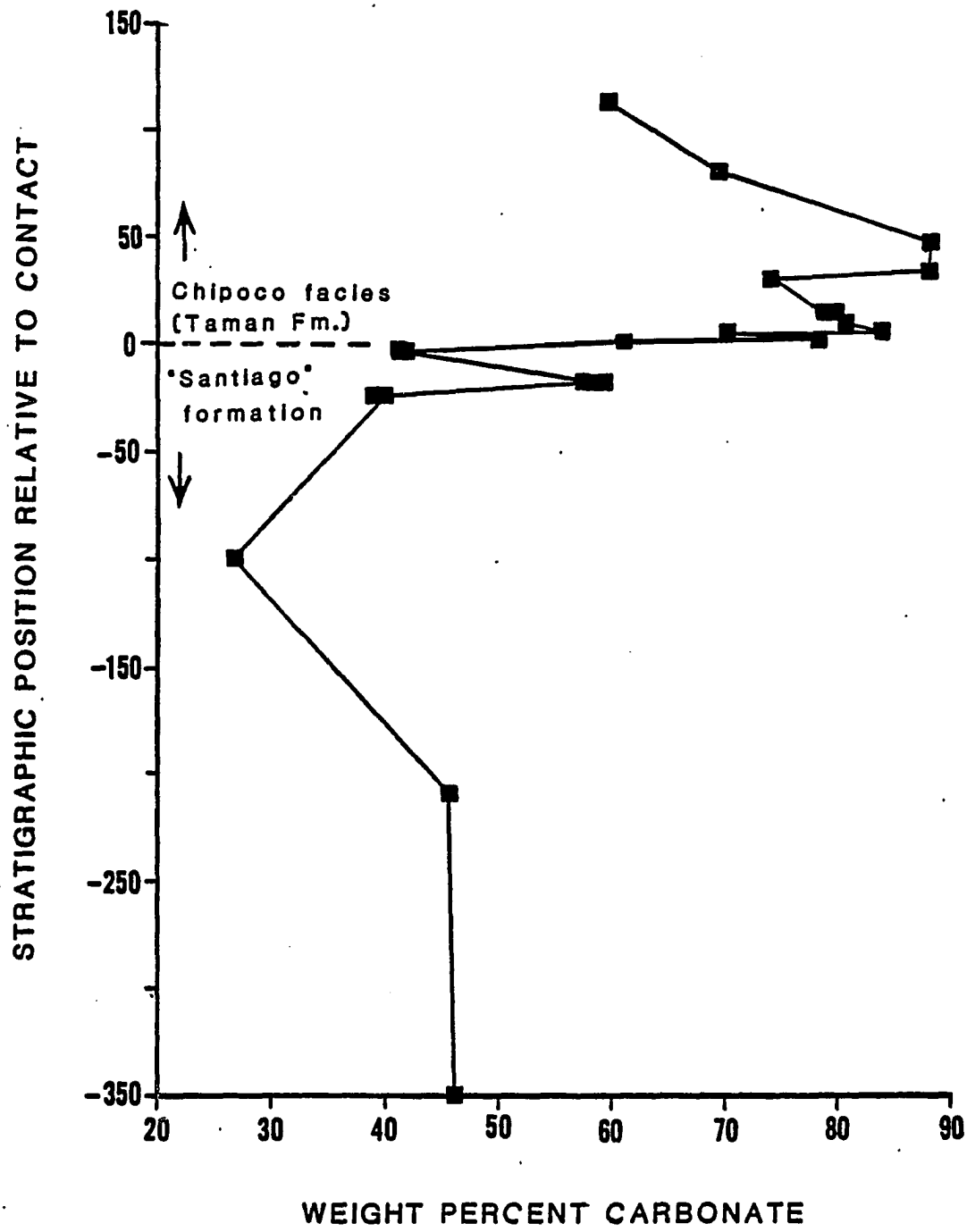

quartz, and plagioclase feldspar. These minerals were identified using x-ray diffraction, but elemental chemical compositions were not determined.

Illite was detected by XRD in all samples, as was quartz, but chlorite was found infrequently and its occurrence followed no stratigraphic pattern or mineral association.

Plagioclase, observed in thin-section at the top of the Santiago and uppermost Chipoco units, was present in quantities great enough to be detected by XRD only in samples from the uppermost Chipoco oolite grainstone.

CARBONATES

X-ray Data - Calcite, rhodochrosite, manganoan calcite, dolomite, kutnahorite, and possibly calcian-kutnahorite are the carbonate minerals identified by x-ray diffraction analysis. The characteristic d-spacings and order reflections for the carbonate minerals considered are listed in Table XXXVI in Appendix C. The manganese carbonate phases are present only in the manganese enriched zone (i.e. the ore zone and superjacent 30 meters or so), whereas dolomite was found in only one sample located at the base of the Chipoco.

Calcite occurs throughout the Santiago and Chipoco rocks, but was only rarely detected in the ore zone, where it occurs typically in secondary veins. The composition of the calcite phase was determined from microprobe analysis

to be nearly pure $CaCO_3$, containing only magnesium as an additional component (i.e. as $MgCO_3$) in quantities from 0 to 5 cation mole percent (e.g. Samples T1, 0 and Misc#4; Figures 20 and 21; and data for these samples in the appendices).

Manganoan calcite was detected in the upper two-thirds of the mineralized zone and in secondary veins in the ore zone (Figure 19). X-ray identification was based on the powder diffraction file for Mn-calcite having a composition intermediate between the rhodochrosite and calcite end-members ($Ca_{0.56}Mn_{0.42}Mg_{0.02}CO_3$) (JCPDS File #2-714). Shifts in the positions of reflections resulting from varying amounts of substitution, were taken to be linear, as demonstrated by Goldsmith and Graf, (1957).

Rhodochrosite is the dominant mineral present in the ore zone and is the exclusive carbonate mineral phase occurring in the basal, high-grade, portion of the ore zone. X-ray diffraction patterns agree closely with the published powder diffraction file for pure rhodochrosite (Figure 20).

Dolomite was detected only at the base of the Chipoco facies 10 centimeters above the contact. This identification, indicated by microprobe data, was confirmed by the presence of the 101, 015, and 021 order reflections (Figure 21) reported to be characteristic of the dolomite crystal structure by Howie and Broadhurst (1958).

FIGURE 19.

Representative x-ray diffraction pattern of sample from upper, lower grade portion of the ore zone.

Abbreviations used:

Q = Quartz
P = Pyrite

K = Kutnahorite
D = Dolomite
R = Rhodochrosite
Mn = Manganoan Calcite
C = Calcite

M = Magnetite
m = Maghemite

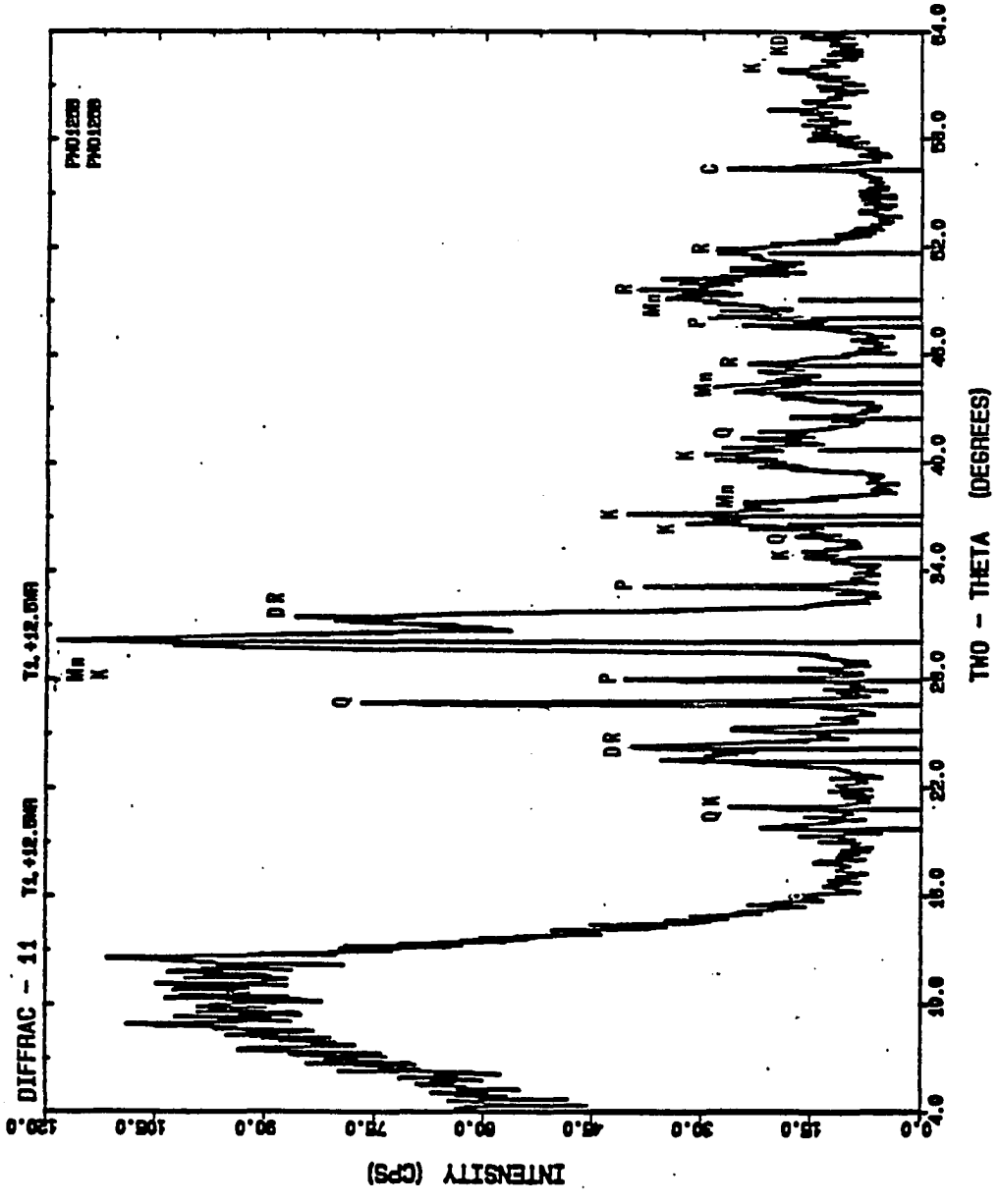

FIGURE 20.

X-ray diffraction pattern from the high grade ore zone. Note sharp peak definition and absence of other mineral phases besides rhodochrosite. Mineral abbreviations are explained in figure 19.

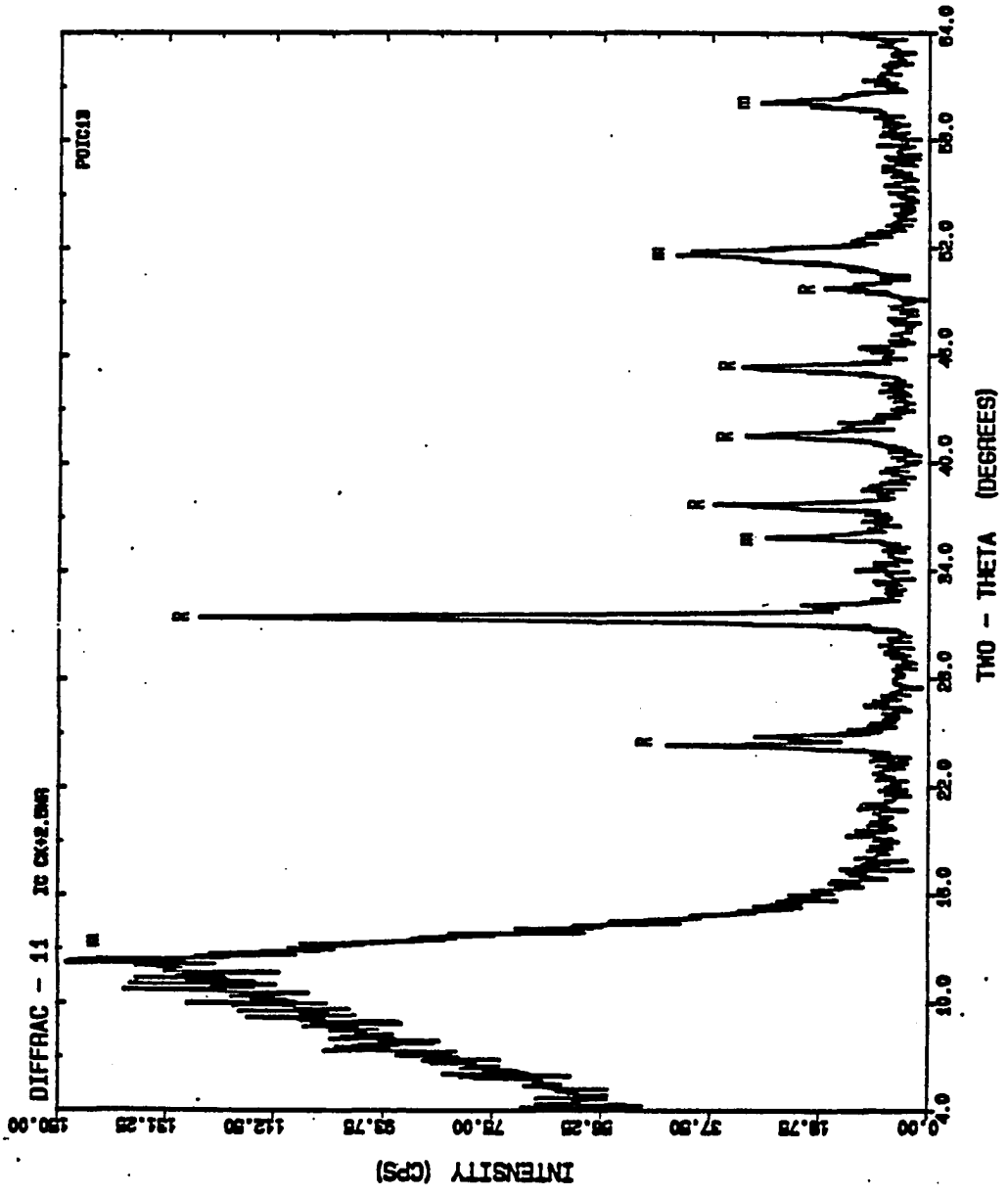

FIGURE 21.

X-ray diffraction pattern from basalmost Chipoco facies showing the presence of quartz and dolomite. * = order reflections for dolomite. Mineral abbreviations are explained in figure 19.

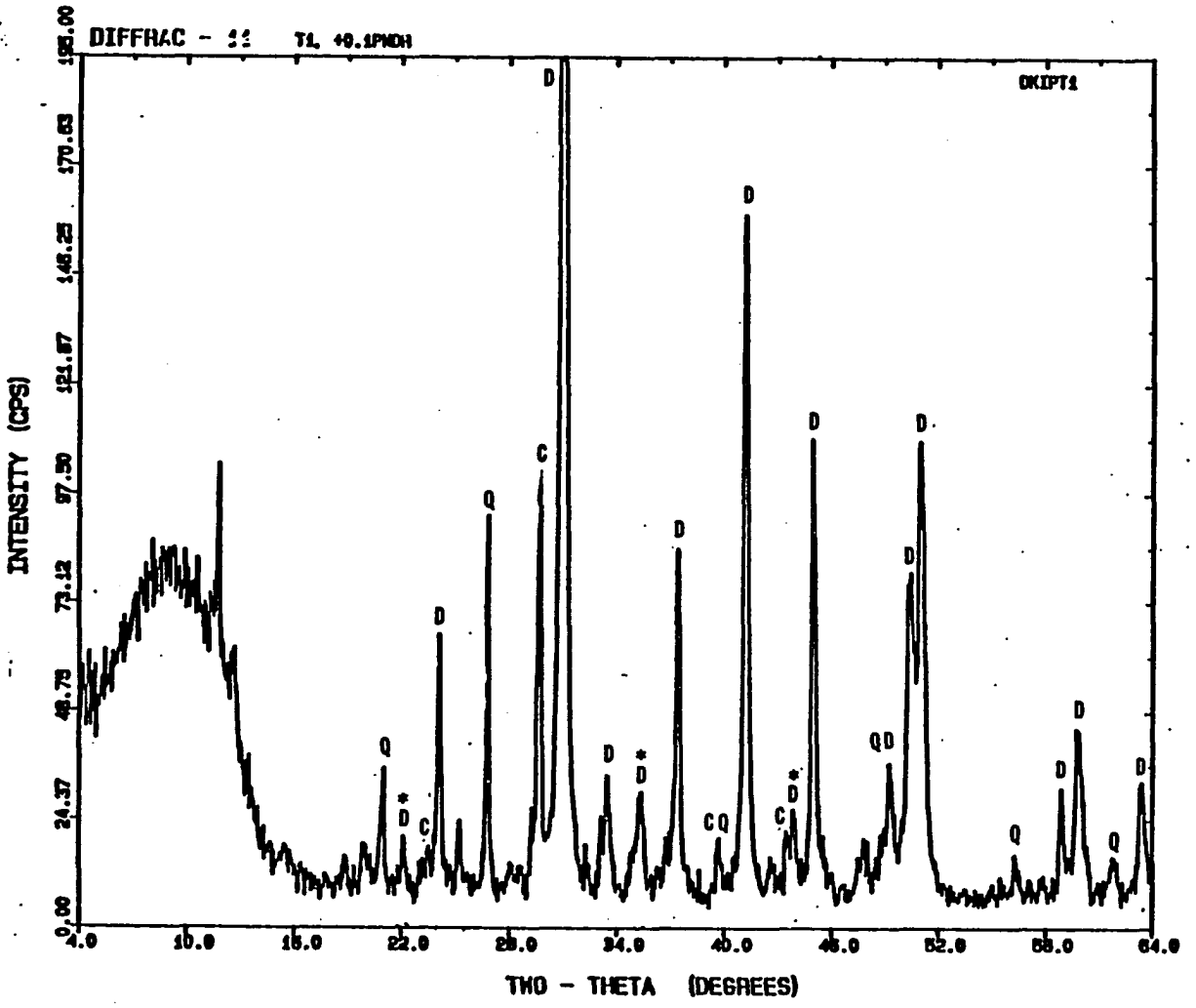

Kutnahorite and calcian-kutnahorite are the dolomite-like (R3) carbonates that contain manganese, calcium and magnesium. These phases were detected using the diffraction criteria established by Frondel and Bauer (1955), Gabrielson and Sundus (1965), and Tsusue (1967). However, the order reflections, characteristic of the dolomite x-ray pattern, are weak for kutnahorite and Ca-kutnahorite and often difficult to detect with certainty (Goldsmith, 1983). Patterns exhibiting the reflections for these phases, including possible order reflections are shown in Appendix C.

Mn-calcite and kutnahorite were found only above the high-grade ore zone. Their appearance was indicated in the x-ray pattern by the change from the sharp, well-defined peaks of rhodochrosite, to wider, rounded peaks and less intense patterns characteristic of phase mixtures. In addition, some of the order reflections for kutnahorite were found. The peaks of all the manganese phases were typically sharp, suggesting well developed crystallinity.

Microprobe Data - The results of electron microprobe analyses of the carbonate minerals are contained in Appendix B. Graphic representation of the composition for each sample is presented in rectangular and triangular plots in Appendices D and E, respectively. Plots of compositional data for probe traverses immediately follow the rectangular plot in Appendix D for certain samples.

These data are summarized in the text below.

High Grade Ore Interval - The compositions of the carbonate minerals in the high grade ore zone (i.e. 0.45 to 2.5 meters) serve to distinguish this interval from the superjacent lower grade ore and unmineralized zone. First, the manganese content ranges continuously from 5 to 95 mole-percent (Figure 22). Second, the high grade ore has a very low and invariant amount of calcium in the carbonate minerals (i.e. not greater than 10 mole-percent, Figure 22). Third, the only significant metal cation, after manganese, is magnesium (Figure 23), although iron can also be abundant in this interval (up to 75 mole-percent). A plot of Fe versus Mn shows a trend that generally follows the pattern of magnesium but with somewhat more scatter (Figure 24).

Analyses were also collected by conducting a traverse across bedding for various samples. The results confirmed petrographic observations that the ore is finely laminated and alternates with weakly mineralized shales. No significant vertical trends were observed. These data are presented graphically in Appendix D.

Low Grade and Non-Ore Zone - Samples 3.4 meters and more above the high grade zone are characterized, not unexpectedly, by lower manganese and higher calcium contents. A plot of Ca versus Mn which includes the samples from this interval shows a well-defined inverse

FIGURE 22.

Plot of Ca and Mn microprobe data for carbonate minerals in the high grade ore zone. For comparison, data are also shown for samples from the contact, 10 cm above the contact (base of "A-bed", and vein filling carbonate.

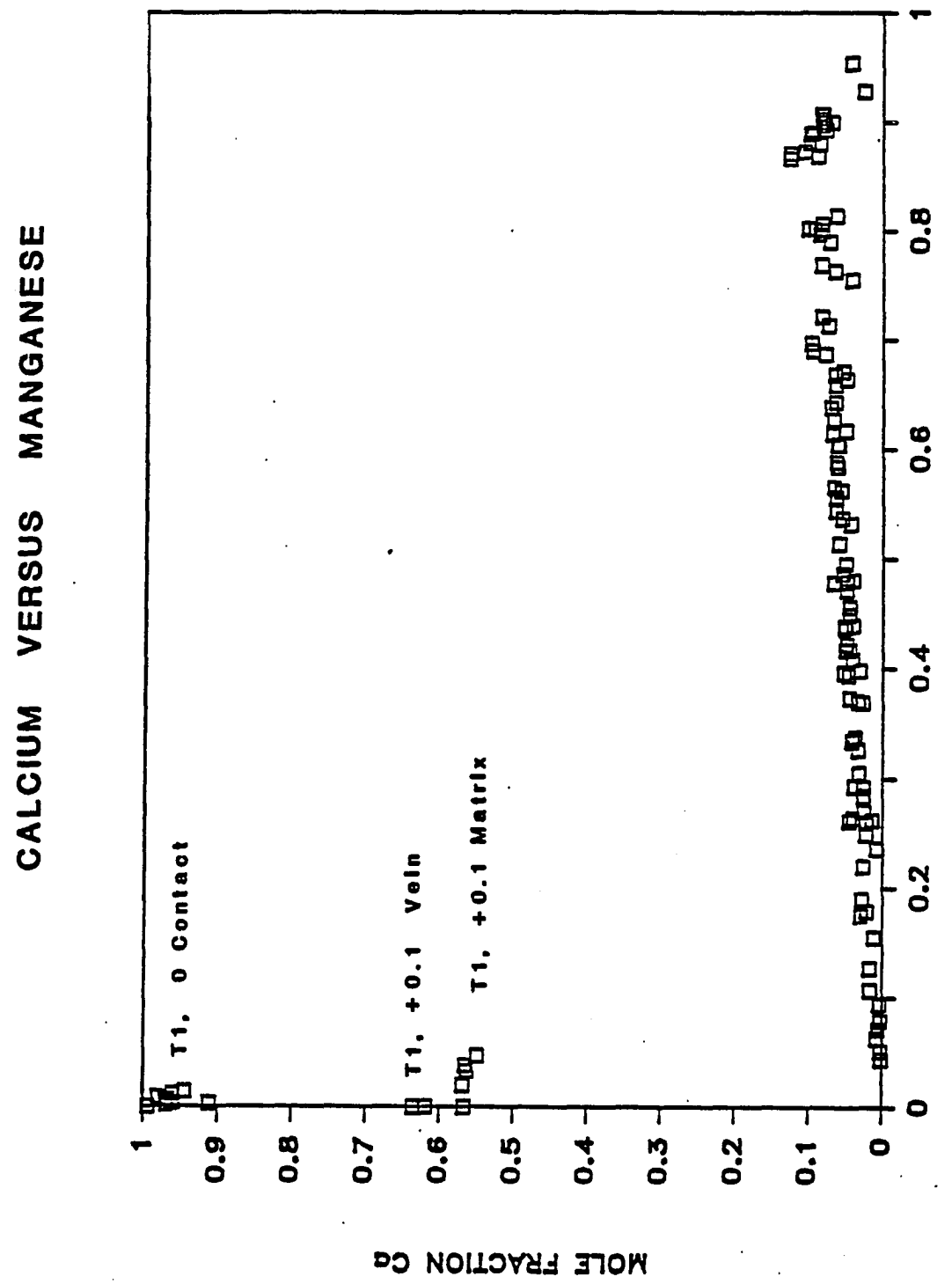

FIGURE 23.

Plot of Mg and Mn microprobe data for carbonate minerals in the high grade ore zone. Comparison to Mn-free samples is made as described in previous figure.

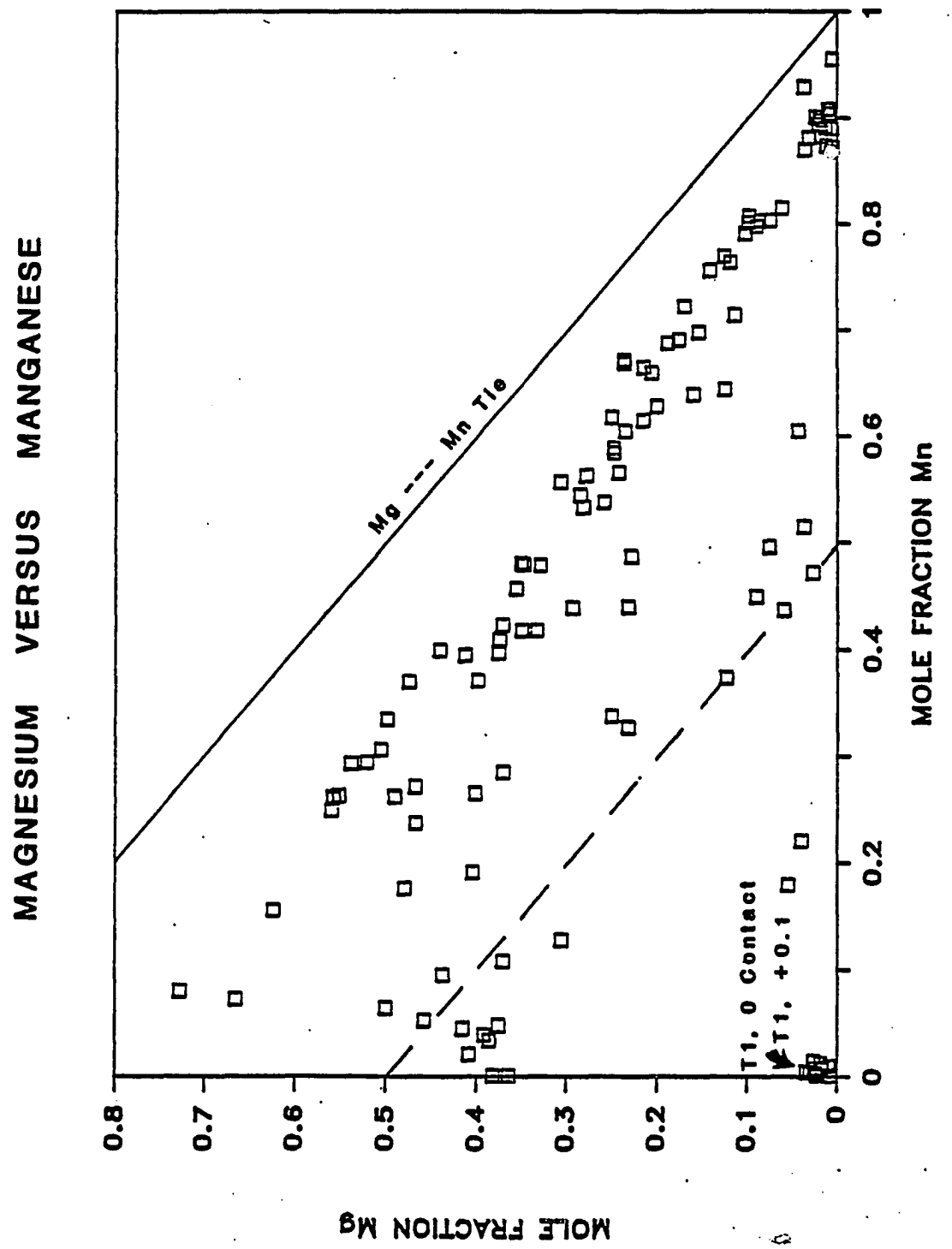

FIGURE 24.

Plot of Fe and Mn microprobe data for carbonate minerals in the high grade ore zone. Comparison to Mn-free samples is made as described in figure 22.

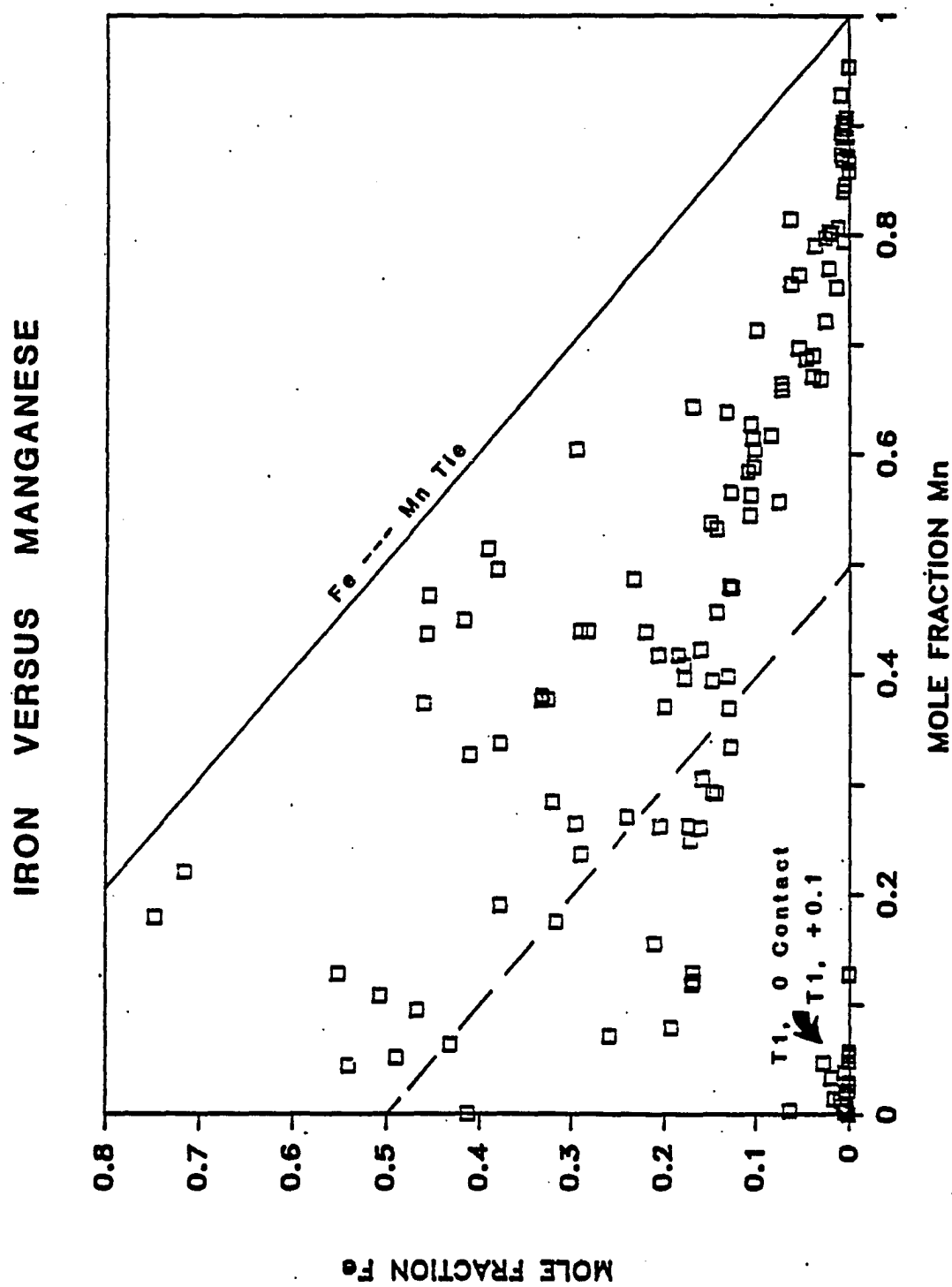

FIGURE 25.

Plot of Ca and Mn microprobe data for all samples analyzed. This plot includes samples from the ore zone (compare to figure 22) in addition to Mn-poor and Mn-free samples. See text for discussion.

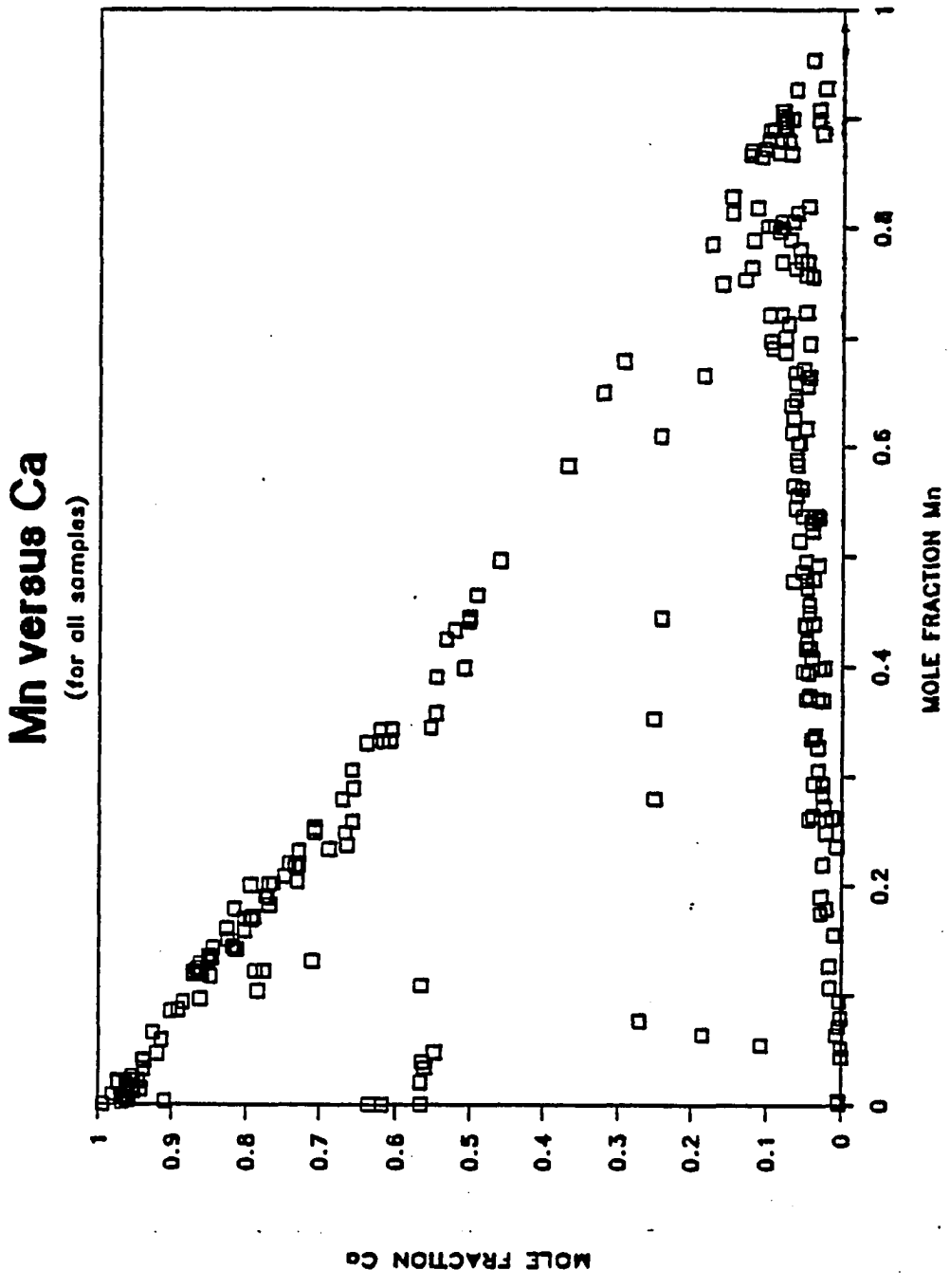

relationship between these two elements (Figure 25). Note that most compositions from low-grade and non-ore carbonates plot below approximately 25 mole-percent manganese. In addition, a gap in calcium compositions is suggested by the scarcity of samples having manganese contents above 50 mole-percent.

The magnesium and iron contents of carbonates in low-grade and non-ore zone are, in general, below 5 mole percent but vary greatly (as is also true for high grade ore minerals) (Figures 26 and 27). In several analyses siderite compositions were measured. No well defined vertical trends in the distribution of either element are evident.

The presence of dolomite-like compositions in the mineralized interval is also indicated by the microprobe analyses for some samples. For example, the raw data (Appendix B) and triangular plots (Appendix E) for T1, +0.45; T1, +8.5; T1, +12.5; and T1, +19.0 have compositions suggestive of a dolomite-like compound. However, most of these samples do not appear to be pure or stoichiometric phases. In almost all cases they are deficient in both calcium and magnesium. It can be seen in Figure 28 that very few of the samples analyzed in this study approach a stoichiometric kutnahorite composition by the substitution of manganese for magnesium. From this observation and the absence of order reflections, I conclude that kutnahorite

FIGURE 26.

Plot of Mg and Mn microprobe data for all samples analyzed as described in figure 25.

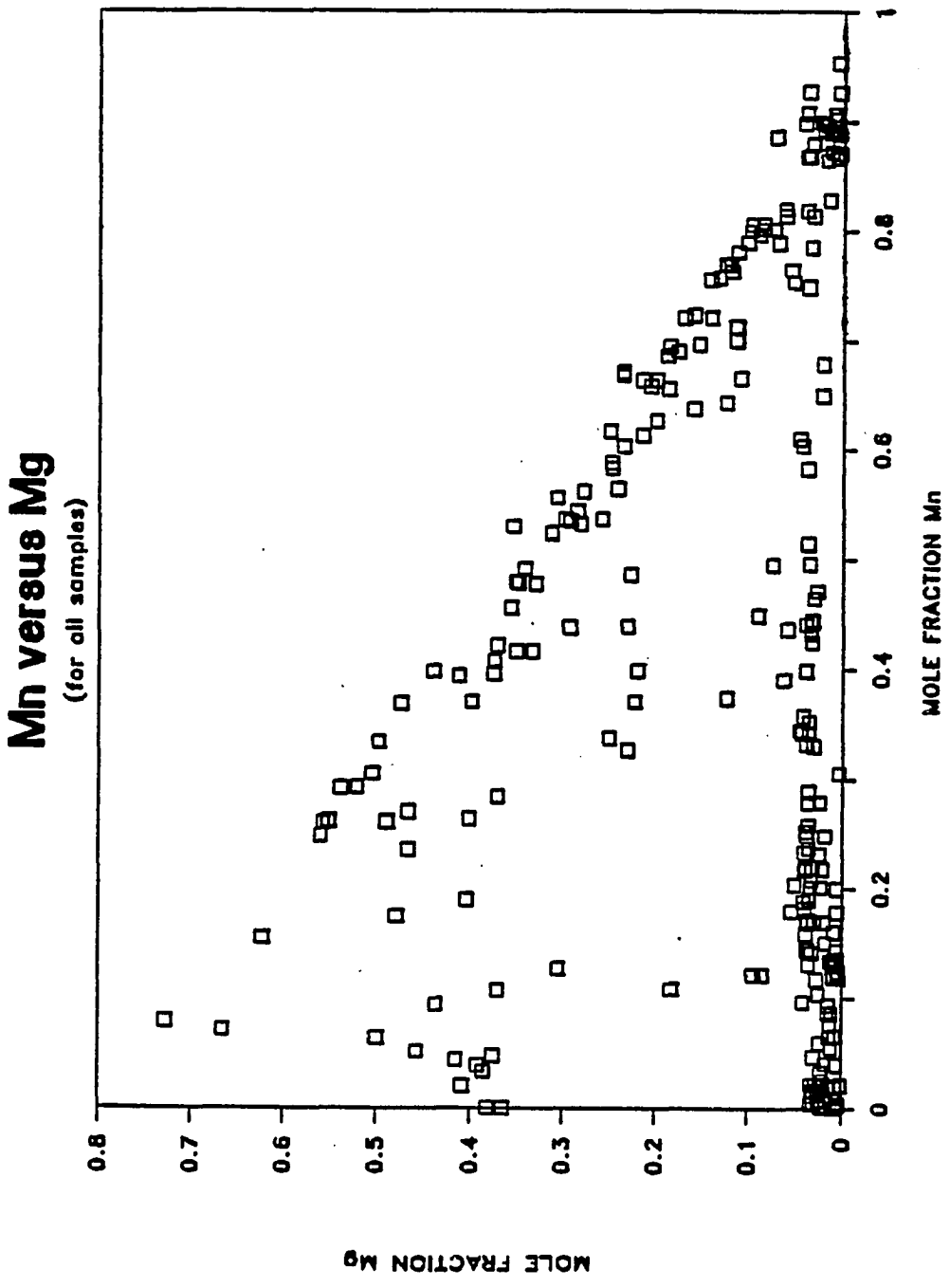

FIGURE 27.

Plot of Fe and Mn microprobe data for all samples analyzed as described in figure 25.

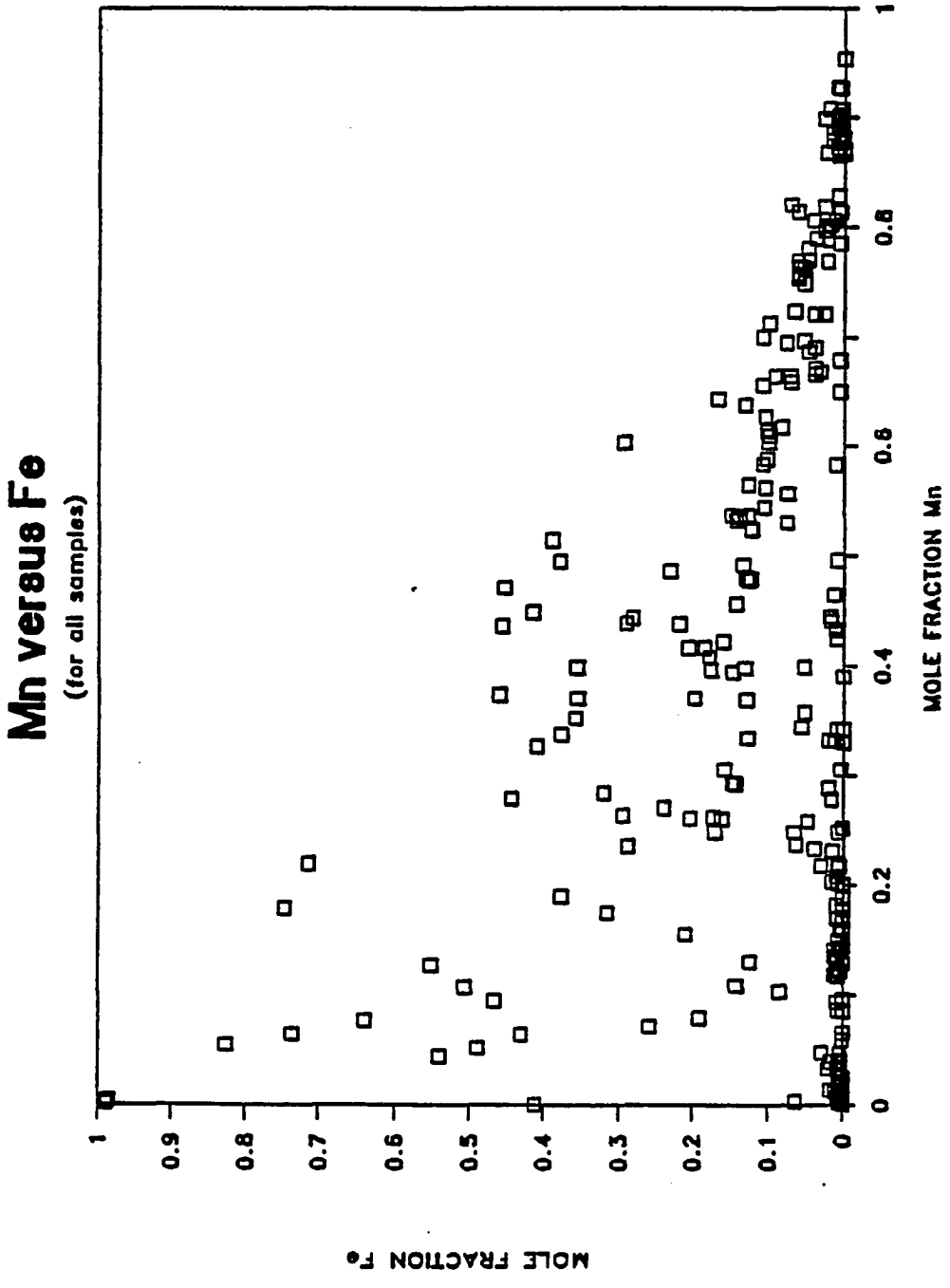

FIGURE 28.

Plot of Mg-ratio versus Mn which would depict any compositions near a dolomite-type carbonate (i.e. kutnahorite) in composition. Nearness to the line is a measure of stoichiometric composition.

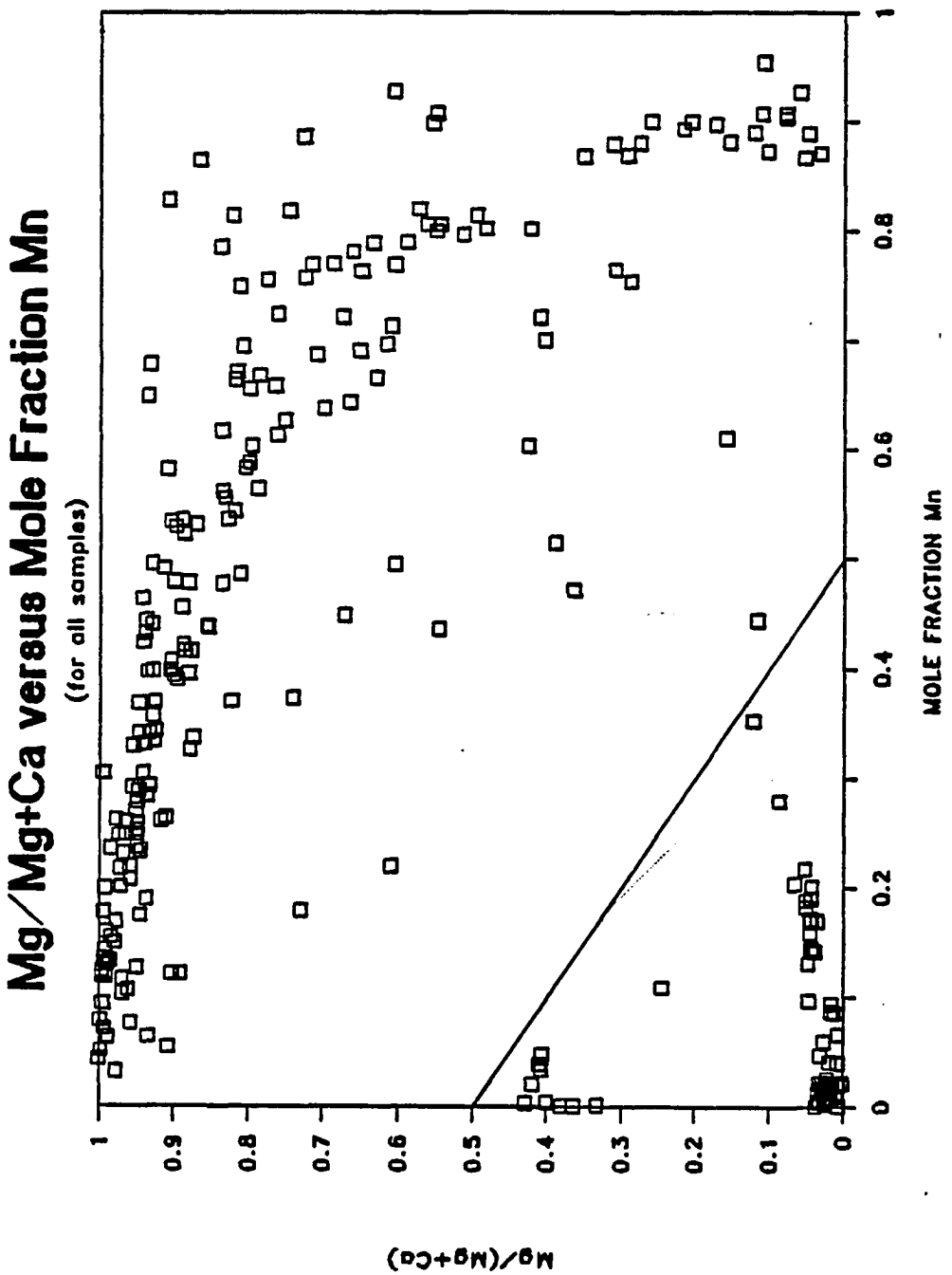

is probably not present, in significant quantities, in the samples studied.

Secondary Features - Carbonate minerals from veins and open fractures in both mineralized and unmineralized rocks were analyzed. These data show near end-member calcite compositions for vein-filling carbonate minerals from the fault breccia at the top of the unmineralized "Santiago" formation. Samples of carbonate minerals from veins and breccia in the ore zone were found to have manganoan calcite and calcian rhodochrosite compositions, respectively (Figure 29).

OXIDES

Two magnetic mineral phases, found during heavy liquid separations, were purified by magnetic separation and identified as magnetite and maghemite using x-ray diffraction (Figure 30). Both of these minerals were analyzed from two samples, T1,+2.5 and T1,+3.4, and identification was based on data from the powder diffraction file (JCPDS Card #'s 4-755, 11-614, and 15-615) and from Schrader and Büttner (1963).

The second sample, T1,+3.4, yielded three sub-samples which varied in their relative magnetic intensity. The most magnetic sub-sample was pulled from the bulk material, using a 25 by 9 millimeter horseshoe-shaped magnet, at a distance of 7 to 10 centimeters above the sample. X-ray powder diffraction patterns for this sub-sample indicate

FIGURE 29.

Plot of Fe, Ca, and Mg content versus Mn content for samples of vein-filling and breccia-cementing carbonate minerals from ore zone and fault breccia at "Santiago"-Chipoco contact.

MISC. SAMPLES

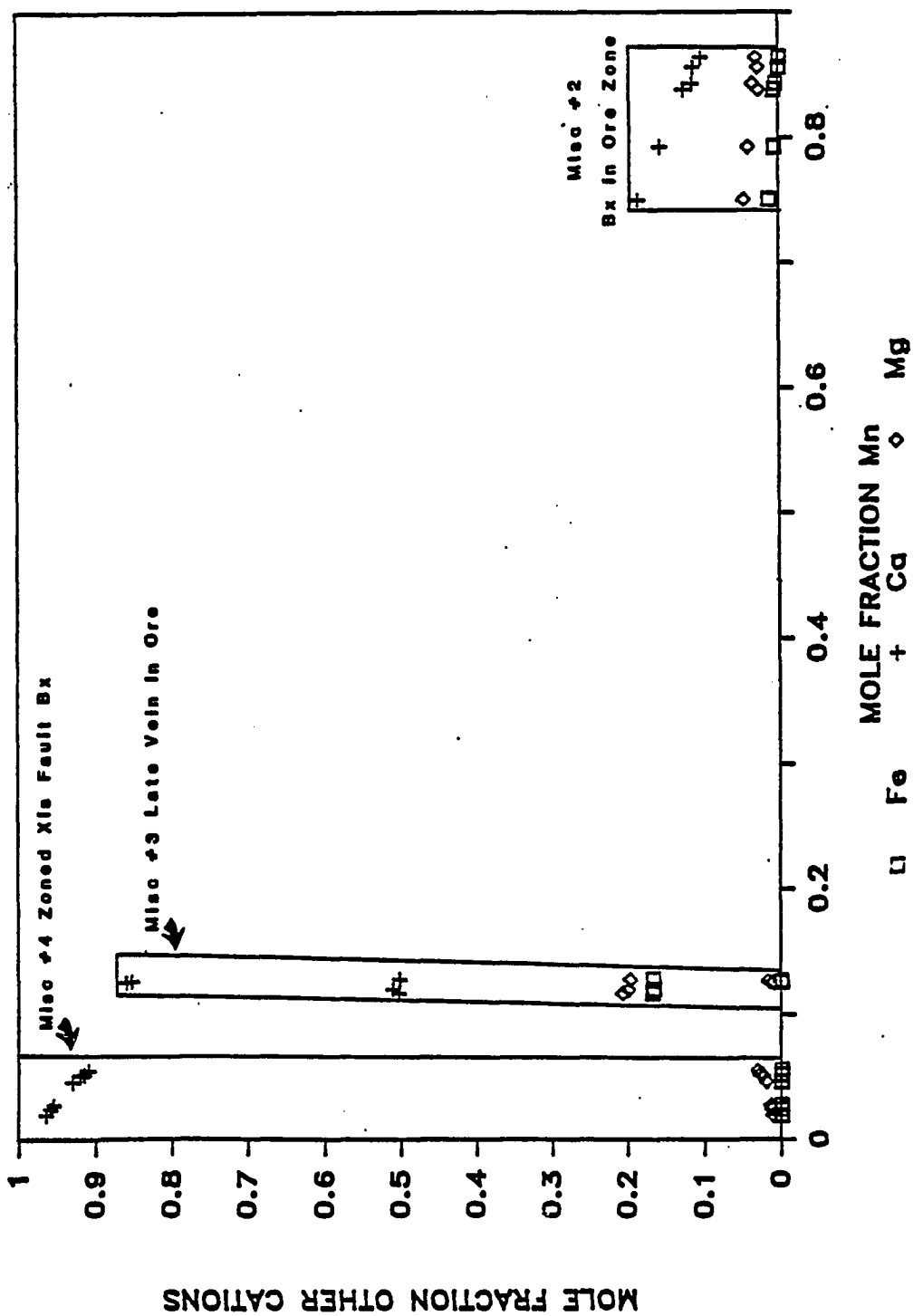

FIGURE 30.

X-ray diffraction pattern for the magnetic separate obtained from sample T1, +2.5. The darker pattern is a magnetite reference standard.

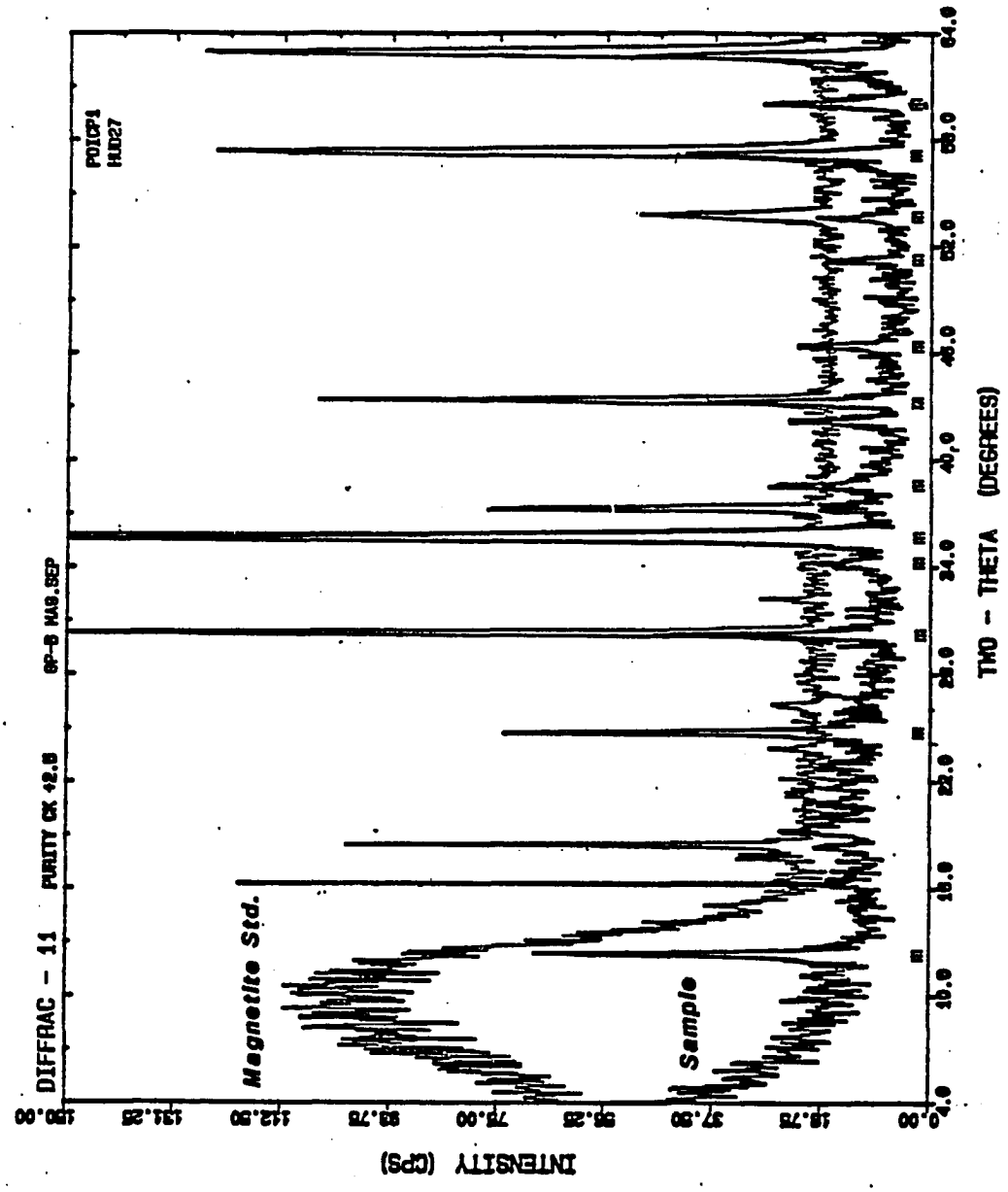

FIGURE 31.

X-ray diffraction pattern for three magnetic separates from sample T1, +3.4. The vertical black lines, starred at the base, indicate the position of magnetite peaks. Note the loss or reduction in intensity of some lines in the more weakly magnetic samples.

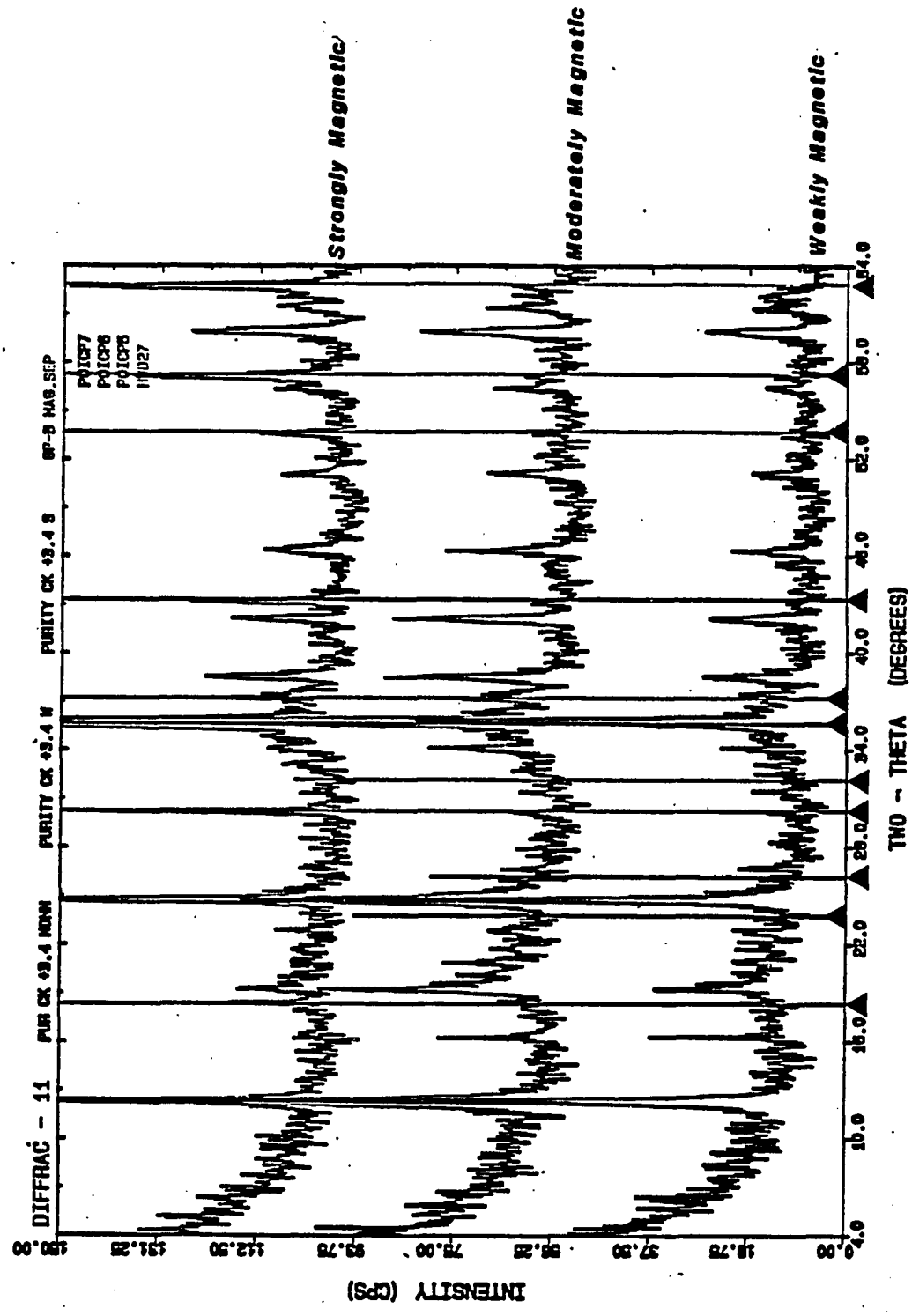

abundant magnetite. The second sub-sample was obtained when the distance between the magnet and sample material was reduced to about 2 to 3 centimeters. Finally, a third sub-sample was very weakly magnetic but could be extracted at distances of 1 to 3 millimeters. X-ray diffraction patterns are similar for the second and third sub-samples, and show an absence of the magnetite peaks that are present in the first, most magnetic, sub-sample (Figure 31). The x-ray patterns for the second and third sub-samples correspond most closely to that of maghemite. Morphologic variations between sub-samples were also seen. The more magnetic fraction contained larger, lathe-shaped grains whereas the grains in the less magnetic fraction were smaller in size and more equant in shape. The significance of these three sub-samples is that two distinct minerals are present.

The identification of maghemite is not without uncertainty. Alternative magnetic mineral phases, such as hausmanite, jacobsite, pyrrhotite, and 7Å manganite, have been ruled out based on the lack of x-ray reflection correlation or magnetic properties. One mineral phase, magnesioferrite ($\{Mg,Fe\}Fe_2O_4$), has not been completely ruled out.

The presence of maghemite may permit insight into the maximum temperatures to which these rocks were exposed. Maghemite is metastable and will convert to hematite upon

heating to temperatures above 350°C (Stacey and Banerjee, 1974; p.30). The transition is a function of grain size, impurities, pressure, and the composition of the ambient atmosphere. The controlling effects of these parameters are not well known, but in general, pressure and temperature are inversely related, whereas increasing amounts of Mg, Mn, and Al all act to raise the temperature of the transition (Stacey and Banerjee, 1974; p. 93). In addition, maghemite can be formed by the low temperature oxidation of magnetite. This temperature is reported to be between 150° and 250°C (Stacey and Banerjee, 1974; p. 30-31). Therefore, if the magnetite mineral phase is primary, and maghemite has been produced from it, then it is possible that the rocks have been heated to a temperature greater that 150-250°C but less than 350°C (as indicated by the absence of hematite). These are reasonable temperature limits given the vitrinite reflectance data (see Chapter 7) and the geologic history of the area.

Finally, it should be noted that both magnetite and maghemite are minerals that are found in association with manganese nodules and in marine sediments (Murray, 1979). The implications that the presence of these minerals may have for the composition of the original sediment pile are discussed on page 124.

SULFIDES

Pyrite is the only sulfide mineral found in the rocks studied. However, no pyrite was recovered by heavy mineral separation of samples from the high grade ore zone, nor was it detected by x-ray diffraction analyses. Trace amounts were recovered from the middle of the ore zone but in insufficient quantities for x-ray or ICP analysis. Amounts of pyrite sufficient for analyses were obtained from the "A Bed" and base of the ore zone (+1.5 meters).

Pyrite separates were also obtained from the upper part of the "Santiago" formation, as well as from the middle and upper part of the Chipoco facies. These samples were analyzed by ICP spectroscopy, and the results are discussed below.

INDUCTION COUPLED PLASMA SPECTROSCOPY (ICP) ANALYSES

ICP analyses were conducted to measure the abundance of 22 elements in a total of 10 samples comsisting of three whole rock samples (Table III), five pyrite separates (Table IV), and two magnetic separates from the ore zone (Table V). The purpose in collecting these data was to compare elemental compositions between the mineralized zone and the sub- and superjacent unmineralized zones. The resulting compositional data were also compared with average elemental compositions for the Earth's crust, seawater, two carbonate rocks, and shale (Table VI).

Wholerock Samples - Concentrations of Ag, As, Au, Cd, Pb, and Se were determined to be below the threshold level for detection in all three wholerock samples. In addition, Cu, K, and Zn were below detectable limits (b.d.l.) in the ore zone sample. Ni was b.d.l. in the two samples outside the ore zone and, Co was b.d.l. in the unmineralized Chipoco sample.

Al, K, Si, and Ti were most probably contained only in the silicate minerals (e.g. quartz, clay minerals, and feldspars). Therefore, a relative measure of the silicate content among the three samples can be made. The Santiago sample appears to contain the greatest silicate content whereas the ore-grade sample has the smallest content of these elements.

Comparison of these data with average values for other rocks reveals that the measured concentrations of the elements in the subjacent Santiago and superjacent unmineralized Chipoco were close to what would "normally" be expected. Significant deviations from the average abundances of the reference data were evident in the whole rock ore zone sample; Ca, Cu, K, S, and Zn were low, and Co, Fe, Mg, Mn, and Ni were elevated. Low values for Ca and K can be explained by the fact that this was a high grade ore sample containing only small amounts of Ca-bearing carbonate and K-bearing silicate. The low S concentration was consistent with the observations from petrography and x-ray diffraction that few or no sulfide minerals were present, and further and further serves to document the overall S-poor character of the high grade ore.

TABLE III. ICP ANALYSES OF WHOLE ROCK SAMPLES.

ELEMENT	SAMPLE WR1, -7.2 NOTE #1	WR2, +2.5 NOTE #2	WR3, +110.9 NOTE #3	COMMENTS NOTE #4
Ag	<50	<50	<50	-----
Al	48000	13000	25000	-----
As	<50	<50	<50	-----
Au	<5	<5	<5	-----
Ba	260	19	150	low in ore
Ca	120000	20000	210000	low in ore
Cd	<10	<10	<10	-----
Co	29	84	<10	high in ore
Cu	44	<5	24	low in ore
Fe	34000	76000	24000	high in ore, and WR3
K	16000	<100	7600	low in ore
Mg	8500	49000	3900	high in ore, low in WR1
Mn	930	250000	1500	high in ore
Mo	<500	<500	<500	-----
Ni	<5	860	<5	high in ore
P	1980	2950	1590	all are high
Pb	<50	<50	<50	-----
S	40000	1200	36000	low but normal in ore zone, high in other two samples
Se	<50	<50	<50	-----
Si	100000	54000	120000	-----
Ti	2900	570	1400	-----
Zn	97	<50	130	-----

Note 1: upper part of "Santiago" formation; calc. shale
Note 2: base of Chipoco facies; high grade ore zone
Note 3: upper part of Chipoco facies; argill. calcarenite
Note 4: values are within expected ranges for the lithology unless otherwise noted. Measurements that are below detectable limits are not compared.

TABLE IV. ICP ANALYSES OF PYRITE SEPARATES (ppm).

ELEMENT	Tl,-7.2 NOTE #1	Tl,-0.1 NOTE #1	Tl,+110.9 NOTE #1	Tl,+0.45 NOTE #2	Tl,+1.5 NOTE #2
Ag	99	<50	64	<50	<50
Al	24000	44000	11000	4100	730
As	<50	<50	<50	72	850
Au	<5	<5	<5	<5	<5
Ba	290	190	9400	1.3	13
Ca	440	1000	1400	530	2000
Cd	<10	<10	180	14	<10
Co	120	40	100	1100	560
Cu	250	250	170	140	190
Fe	270000	150000	290000	380000	390000
K	6900	14000	3400	<500	<500
Mg	3000	4700	1200	14000	2600
Mn	450	440	420	8500	12000
Mo	<500	<500	<500	<500	<500
Ni	66	530	<5	<5	<5
P	<100	<100	<100	<100	<100
Pb	<50	<50	<50	<50	100
S	390000	220000	440000	550000	590000
Se	<50	<50	<50	<50	<50
Si	140000	200000	90000	11000	14000
Ti	5900	3000	7000	230	150
Zn	780	1100	2000	<500	<500

Note 1: Samples from unmineralized zones.
Note 2: Samples from ore zone; Tl,+0.45 from A-Bed, Tl+1.5 from base of high grade ore zone.

TABLE V. ICP ANALYSES OF MAGNETIC SEPARATES FROM HIGH GRADE ORE ZONE (ppm).

ELEMENT	Tl,+2.5	Tl,+3.4
Ag	<50	<50
Al	24000	27000
As	<50	<50
Au	<5	<5
Ba	2	7.2
Ca	130	340
Cd	<10	<10
Co	230	210
Cu	33	100
Fe	190000	230000
K	<100	<100
Mg	95000	99000
Mn	13000	21000
Mo	<500	<500
Ni	<5	<5
P	<100	<100
Pb	<50	<50
S	880	9700
Se	<50	<50
Si	150000	130000
Ti	1600	1400
Zn	<50	<50

Note: Sample Tl,+3.4 contained pyrite visible in hand sample but was believed to have been removed on separation. The fine-grained nature of the pyrite made complete separation impossible.

TABLE VI. ABUNDANCE OF ICP-ANALYZED ELEMENTS IN SELECTED ROCKS, MINERALS AND SEAWATER (ppm).

	A	B	C	D	E	F	G
Ag	0.07	0.00004	0.0X	0.0X	0.07	6	<10
Al	81300	0.002	4200	20000	80000	30981	NR
As	1.7	0.004	1	1	0.3	NR	35-57
Au	0.0043	4 x10-6	0.00X	0.00X	0.00X	0.00248	<0.05
Ba	650	0.002	10	190	580	2012	<300
Ca	29600	411	302300	312400	22100	25348	NR
Cd	0.13	0.00005	0.035	0.0X	0.3	7.9	<20
Co	18	0.00005	0.1	7	19	2987	5-20
Cu	47	0.0005	4	30	45	2561	110-174
Fe	46500	0.002	3800	9000	47200	156080	273000-462000
K	25000	399	2700	2900	26600	6427	<2000-11600
Mg	18700	1290	47000	4000	15000	18234	NR
Mn	1000	0.0002	1100	1000	850	161740	14-46
Mo	1.1	0.010	0.4	3	2.6	412	<5-39
Ni	58	0.0005	20	30	68	4888	34-62
P	930	0.001-0.05	400	350	700	2244	NR
Pb	16	0.00003	9	9	20	867	NR
S	470	(S04) 2710	1200	1300	2400	NR	NR
Se	0.05	0.0002	0.08	0.17	0.6	NR	<10
Si	295000	0.5-10	24000	32000	73000	86240	NR
Ti	4500	0.001	400	770	4600	6424	NR
Zn	83	0.002	20	35	95	710	28-79

A: Earth crust, Vinogradov (1962)
B: Seawater, Drever (1984)
C: Carbonate rocks (undifferentiated by authors), Turekian and Wepepohl (1961)
D: Deep sea carbonate rocks, Turekian and Wedepohl (1961)
E: Shale, Vinogradov (1962)
F: Manganese crusts, Cronan (1976)
G: Sedimentary pyrite, Raiswell and Plant (1980)

zone. The significance of low Cu and Zn values is not clear. These values may not, in fact, be low relative to carbonate rocks in general (i.e. if deep sea carbonate rocks are excluded). Elevated Fe, Mn, and Mg values are consistent with the abundance of (Mn, Mg)-bearing carbonates and the presence of Fe-oxide minerals. High Co and Ni values in the ore zone may bear some relation to the original mineral phases present in the sediment; these are discussed below.

Pyrite Separates - Because of the fine-grained, framboidal textures of the pyrite, the separates analyzed contained some silicate contamination. This was observed with a binocular microscope to be in the form of clear quartz grains and opaque fine-grained material (clays). This contamination will account for the Al, Si, and K detected, and may be responsible for the elevated Ba and Ti concentrations.

Differences observed between ore zone and non-ore zone pyrites include relatively high As, Co, and Mn values, and Ni and Zn values were below detectable limits in pyrite samples from the ore zone. Among samples from outside the ore zone: Co was three times greater in the sample from -7.2 meters than in the sample from -0.1 meters; and the concentration of Ni was one order of magnitude greater in the sample from -0.1 meters, as compared to -7.2 meters sample.

Magnetic Separates - Two samples of the magnetic minerals present in the high grade ore zone had quantities of Ag, As, Au, Cd, K, Mo, Ni, P, Pb, and Zn below detectable limits.

Silicate and sulfide contamination in the magnetic minerals were indicated by the very high Si, Al, and somewhat elevated S concentrations respectively. Titanium and Mg were very high in both samples. It is reasonable to assume that some of the Ti and Mg may be contained in the silicate fraction (i.e. Ti in the quartz, and Ti and Mg in the clay minerals). In addition, both Ti and Mg are common constituents in magnetite and maghemite (Hurlburt and Klein, 1977; Murray, 1979) and may, in these two samples, be present in solid solution. Manganese concentrations were high as well. Given the acid digestion of the original sample material prior to magnetic separation, however, the persistance of a Mn-carbonate was unlikely. Alternatively, a Mn-oxide may have been present or Mn may be substituted the magnetic Fe-oxides. Co concentrations were elevated in the magnetic separates, relative to the reference rocks and non-ore zone pyrites, but were lower than those values measured for ore zone pyrites by as much as a factor of five.

The presence of elevated concentrations of Co and Ni, as determined from wholerock samples, may be evidence for a Mn-oxide precursor. It is known that Ni and Co, among other elements, are strongly enriched in manganese nodules (Burns and Burns, 1979; Maynard, 1983, and references therein). It might then be expected that if these Mn-oxides were converted to Mn-carbonate, the accompanying Co and Ni might be incorporated into sulfide minerals (Leclerc and Weber, 1980).

Evidence in support of Co enrichment can be found in the sulfide separates; however, Ni was below detectable limits in the two ore-zone samples. It is not clear if the high Ni value measured from the pyrite separate 10 cm below the contact of the Santiago and Chipoco (i.e. just below the A-Bed) is significant. Recall that Ni was present in high concentrations from the whole rock sample in the high grade ore zone (i.e. WR2, +2.5) whereas it was b.d.l. in the magnetic separate. The sulfide content of this sample was too low to yield a pyrite separate. This may indicate that Ni is contained in an oxide or silicate mineral.

DISCUSSION

MINERAL CHEMICAL CONSIDERATIONS

Rhodochrosite has been reported from a variety of geologic environments, including sedimentary, hydrothermal and metamorphic. A greater volume of descriptive literature exists for sedimentary manganese carbonates than for the other types, however. Published descriptions of sedimentary manganese-rich carbonates and associated assemblages are generally of diagenetic occurrences (frequently concretions) and usually report both chemical and x-ray diffraction data (e.g. Suess, 1979, Coleman, et al., 1982; Pedersen and Price, 1982; Tassé and Hesse, 1984). Sedimentary carbonates tend to contain a large amount of calcium and are not pure rhodochrosite. Manganese, as a minor or trace element in carbonate minerals, is frequently used to interpret the type and degree of diagenetic processing which has affected a rock, and has been extensively studied by such workers as Brand and Veizer (1980) and Veizer (1978, and 1983). The result is that manganese has been rather well studied as a minor or trace component in carbonates. The behavior of manganese when it is the major cation constituent is less well known however.

Of the four end-member carbonates rhodochrosite, siderite, calcite, and magnesite, rhodochrosite is the carbonate phase predicted on the basis of equilibrium thermodynamic calcuations to be stable in the presence of high

concentrations of dissolved manganese. It follows that the rhodochrosite contained in the high-grade ore zone at Molango reflects a great abundance of divalent manganese (i.e high activity of manganese). The manganese solubility in seawater is limited by the precipitation of rhodochrosite (Li, et al., 1969; Holdren, et al., 1975; Klinkhammer, 1980; Johnson, 1982; Pedersen and Price, 1982), and it follows that the decrease of manganese content in the carbonates stratigraphically upward is the result of decreasing activity of dissolved manganese at the time of ore formation. While the availability of iron may have been limited by redox conditions, there is no reason to believe that a shortage of magnesium or calcium was characteristic of the high grade ore zone. Magnesium was undoubtedly abundant in seawater and Ca-bearing shell material was probably ubiquitous.

The relationships between manganese and the other cations (Mg, Ca, and Fe) discussed above can be explained in terms of the crystal chemistry of the carbonate minerals. High magnesium and Fe contents in rhodochrosite may be expected because complete solid solution is possible along the manganese-magnesium binary owing to the geochemical similarity of Mn^{2+}, Mg^{2+}, and Fe^{2+}.

The low calcium content measured in the rhodochrosite from the high-grade ore-zone may be the result of exclusion from the crystal lattice because of the large difference in ionic radii between calcium and manganese and between calcium and

magnesium. The larger size, of the calcium ion, imparts distortion to the crystal lattice of a predominantly Mn-bearing carbonate producing an instability in the mineral. The $Ca\text{-}Mn^{2+}$, $Ca\text{-}Fe^{2+}$, and $Ca\text{-}Mg^{2+}$ binaries have limited miscibility (Reeder, 1983). Recall that most cabonate minerals in low-grade and non-ore zones contained less than 25 mole-percent manganese, (with some values ranging up to 50 mole-percent) and large amounts of calcium. The amounts of substitution observed at each end of the binary probably reflect the structural limitations imposed on cation substitution that is characteristic of carbonate binaries lacking complete miscibility. Typically, such carbonate binaries exhibit asymmetric solution behavior where the greater solubility is exhibited by the smaller cation substituting into the structure dominated by the larger cation. In the case of calcium and manganese, a greater quantity of manganese can be substituted into calcite than calcium into rhodochrosite. The solid solution relations in the $CaCO_3\text{-}MnCO_3$ system have been studied at elevated temperatures by Goldsmith and Graf (1957) and de Capitani and Peters (1981). At 350°C, up to 40 mole-percent manganese is permitted into calcite whereas a small amount (probably less than 5 mole-percent) of calcium is allowed into rhodochrosite (Figure 32). It is interesting to see that the range in compositions analyzed from Tetzintla samples appear to follow a similar distribution. Unfortunately the 200 - 350°C

portion of the diagram is not known, so the data cannot be used to infer temperature of equilibration.

The significance of these observations and inferences to understanding the origin of mineralization at Molango lies in the interpretation of the chemical environment present during carbonate mineral precipitation. It is evident, from the discussion above, that the low calcium contents in the ore-zone carbonate minerals need not imply an anomalously low Ca^{2+} concentration in seawater at the time of mineralization. Further discussion of the implications of mineral chemistry, with regard to the stratigraphic variations in carbonate compositions, is presented below.

FIGURE 32.

Range of compositions, measured by electron microprobe, of carbonate minerals from this study (shaded area) as compared to the temperature-composition diagram of Goldsmith and Graf (1957).

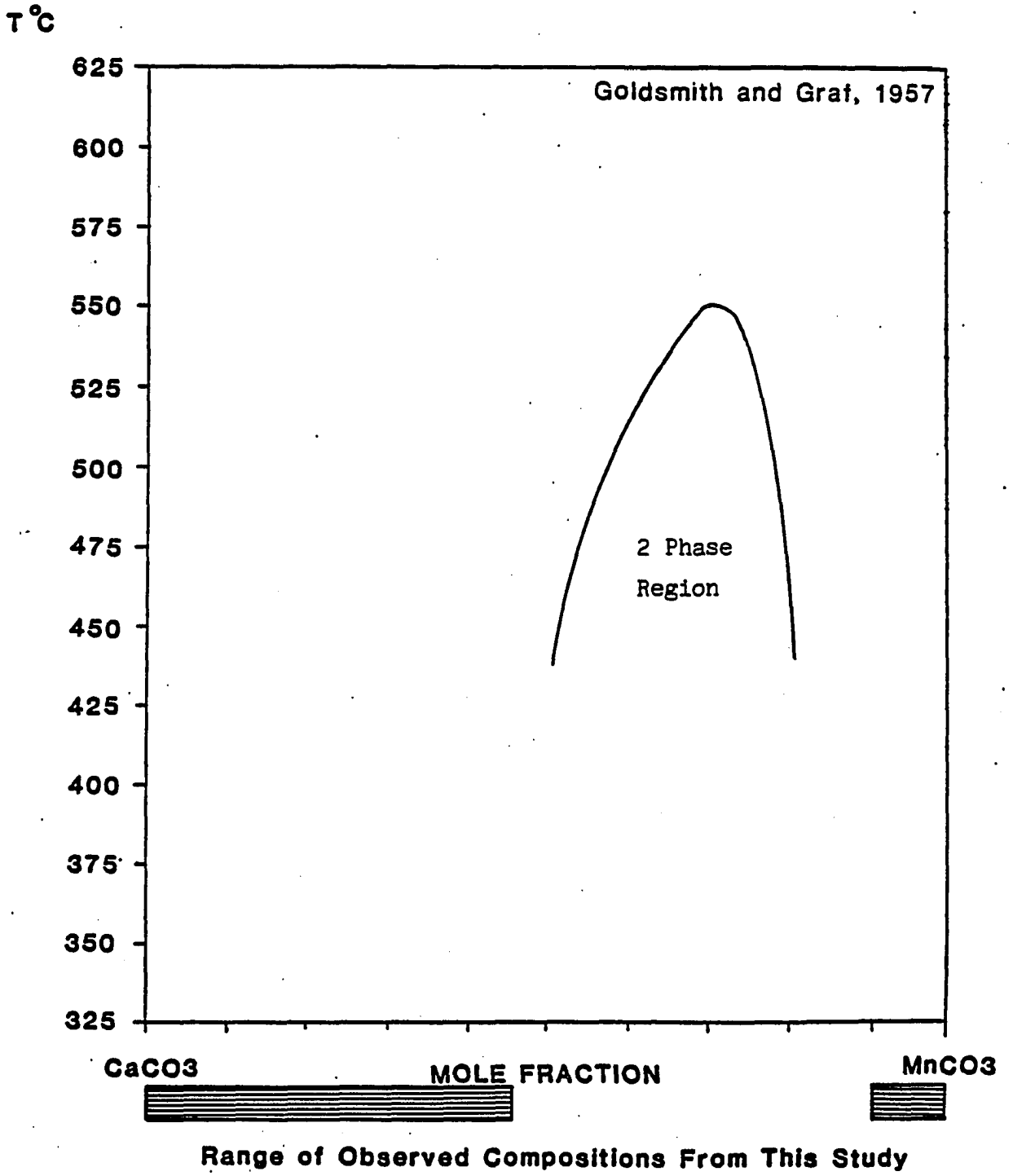

Range of Observed Compositions From This Study

STRATIGRAPHIC CONSIDERATIONS

"Santiago" formation - The mineral assemblage of the "Santiago" formation includes calcite, pyrite, and quartz in a chlorite-illite matrix. Whereas, the lower Santiago lacks pyrite and the detrital quartz content is low, these mineral components are increasingly abundant in the uppermost 25 meters of the unit. This suite of minerals is unremarkable, but so serves to emphasize the ordinary nature of the Santiago, a typical laminated black shale. It is, however, important to note that pyrite is not abundant in the lower Santiago black shale. This absence may imply that deposition of the Santiago mud took place under anoxic, non-sulfidic conditions. Such conditions are thought to arise for one of two reasons: either the oxidation potential was too high for sulfate reduction, or all the available sulfate was reduced while organic matter still remained, leading to methane production (Berner, 1981; Maynard, 1982). In the case where dissolved oxygen is present, the lack of pyrite may mean that sedimentation rates were low enough to result in a slow rate of sulfate reduction (Maynard, 1982). The laminated texture of the Santiago shales probably indicates that the water overlying the sediment was anoxic.

It follows from this reasoning that the pyrite-bearing upper Santiago may have possibly accumulated with lower amounts of organic matter. This is supported by the

observed decrease in organic content of the Santiago near its upper contact. Alternatively, the presence of pyrite may reflect higher sedimentation rates. Sedimentation rate is a difficult parameter to quantify, but the presence of large quantities of detrital quartz silt and bioclastic debris is evidence suggestive of increased sedimentation rates.

Chipoco facies - The mineral assemblage of the Chipoco facies exhibits significant stratigraphic variation. The "A-Bed" contains dolomite and abundant sedimentary pyrite. The restriction of dolomite to this single horizon may imply that the mineral was formed by recrystallization, possibly as the result of fault-related activity and associated fluids. The large quantity of authigenic pyrite indicates that sulfate reduction processes were operating when the sediment was deposited.

The mineral assemblage of the ore zone is dominated by rhodochrosite, which contains reduced manganese and occurs with iron oxide minerals containing both oxidized and reduced iron (i.e. magnetite and maghemite). This assemblage gradually changes vertically to one containing rhodochrosite, manganoan calcite, and possibly kutnahorite. The manganese-bearing phases decrease in abundance upward until low magnesium calcite is the only carbonate phase detected.

The apparent stability of ferric oxides during manganese

carbonate precipitation has important consequences for understanding the geochemical environment of manganese mineralization. This mineral assemblage implies that the redox condition favored manganese reduction but was, in general, too oxidizing for significant quantities of iron to be reduced. However, the presence of magnetite, which contains some ferrous iron, means that redox conditions were occasionally (i.e. temporally or spatially) reducing enough to produce ferrous iron. Lastly, the scarcity of pyrite is in keeping with conditions being somewhat oxidizing because sulfate reduction requires more reducing conditions than ferric iron reduction.

These coexisting minerals serve to constrain the chemical conditions during precipitation of the manganese carbonates. The redox conditions at the sediment-water interface may have been slightly more oxidizing than required for ferric iron reduction but reducing enough for manganese and nitrate reduction.

The high magnesium and low calcium content observed in the ore zone carbonates were unexpected. Two possible explanations come to mind. Perhaps the magnesium levels in the water became greatly increased as a consequence of increased ammonia levels, produced during nitrate reduction, which could result in the expulsion of Mg^{2+} from clay minerals (e.g. smectite). This interaction has been used to explain increased concentrations of Mg^{2+} observed

in modern oceanic conditions by Hesse and Harrison (1981). Alternatively, high magnesium levels in the carbonates may be a function of the greater ease in substituting magnesium for manganese, as opposed to calcium, into the rhodochrosite lattice. In this latter explanation, magnesium is contributed from seawater and no abnormal magnesium levels need be postulated. Experimental evidence of Goldsmith and Graf (1960) and more recent summaries by Reeder (1983) and Goldsmith (1983) indicate that because of the difference in ionic radii between Ca^{2+} and Mg^{2+} the manganese-magnesium binary is complete, whereas the manganese-calcium binary has only limited miscibility.

The observed phase separation reported above (Fig. 32) can be interpreted in terms of the activities of aqueous species to help explain the observed stratigraphic variation in the manganese-bearing phases. Graphic representation of the average carbonate compositions, determined by microprobe analyses and plotted according to stratigraphic position, reveals an abrupt shift from very low calcium (i.e. the rhodochrosite zone) to very high calcium (i.e. the calcite zone) above the ore zone (Figures 33A and 33B). If a representative composition of $Mn_{0.9}Ca_{0.1}CO_3$ is chosen for the most Ca-rich phase in the rhodochrosite zone, and a composition of $Mn_{0.4}Ca_{0.6}CO_3$ is assigned to the most Mn-rich phase in the manganoan calcite zone, then the relationship between these two phases can be

FIGURE 33.

Plot of the average carbonate composition, as determined by electron microprobe, according to stratigraphic position. The ore zone is the basal 10 meters.

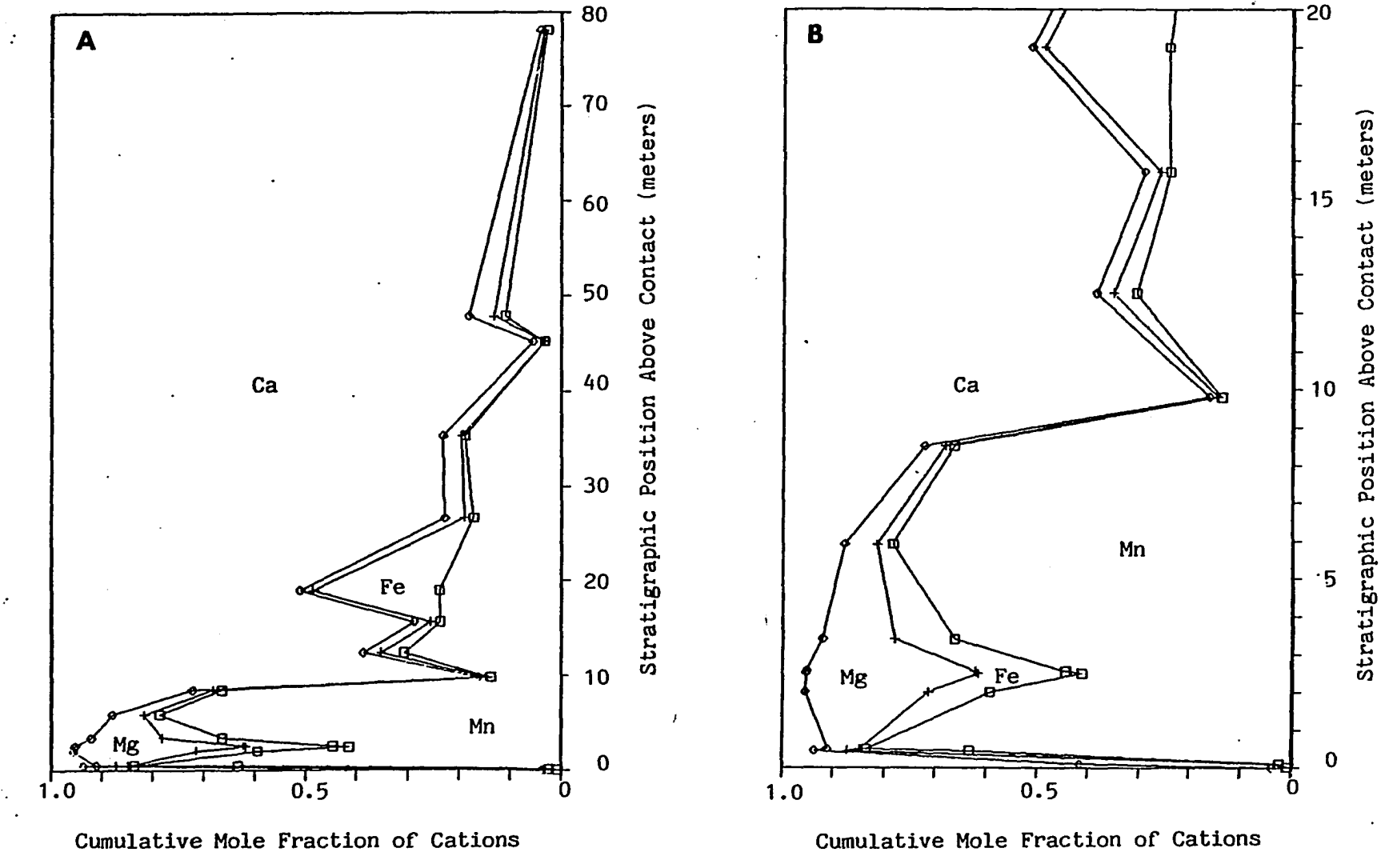

represented by the following reaction:

$$Mn_{0.9}Ca_{0.1}CO_3 + 0.5Ca^{2+} \text{-----} > Mn_{0.4}Ca_{0.6}CO_3 + 0.5Mn^{2+}.$$

The stoichiometries shown are not meant to imply any strict mineral chemical compositions, but rather reasonable values for the most substituted mineral phases, as inferred from the work of Goldsmith and Graf (1957).

Assuming for the moment that there are two solid phases of fixed composition with no substitution of Mn^{2+} and Ca^{2+}, the implications of this reaction are that the equilibrium constant for the reaction is defined only by the activities of Mn^{2+} and Ca^{2+} in seawater. If the activity of Ca^{2+} in seawater in the basin is relatively constant, we find that the direction of the reaction is governed by the activity of Mn^{2+}. Thus, there will be a certain value for the activity of Mn^{2+}, given a fixed activity of calcium, below which only manganoan calcite will form and above which only rhodochrosite will form (Figure 34a).

This reasoning has important repercussions for the distribution of mineral phases and hence ore grade. Given a starting point (T_o) at which the concentration of Mn^{2+} increases in response to the onset of reducing conditions (suggested by the abrupt appearance of manganese at the

base of the Chipoco), the Mn^{2+} concentration can be modelled as decreasing steadily with time (Figure 34b). At time T_1 the activity of Mn^{2+} will have decreased to the critical value which initiates the precipitation of manganoan calcite. At this point rhodochrosite will no longer be the dominant mineral phase precipitated, and abundant calcium can enter the solid phase. The result of the changeover from rhodochrosite to manganoan calcite precipitation will also be expressed stratigraphically (Figure 34c). The expected stratigraphic profile should be a basal rhodochrosite zone overlain by a manganoan calcite zone. The transition between these two zones, when defined with compositional data of individual phases, would be expected to be abrupt and well defined as seen in Figure 33b. Because of averaging this transition may appear more gradational if whole rock data are utilized.

For bulk compositions lying within the two-phase gap on figure 32, this model of fixed compositions is probably reasonable. However, for the large one-phase region on the left-hand or Ca-rich side of the diagram, the equilibrium will be between a variable solid solution and a variable aqueous solution. The equilibrium constant (K) would be:

$$\frac{a_{Mn^{2+}}}{a_{Ca^{2+}}} = \frac{\lambda_{MnCO_3} X_{MnCO_3} K_{Rhod.}}{\lambda_{CaCO_3} X_{CaCO_3} K_{Calcite}}$$

If the activity coefficients in this solid (λ) are constant, this relationship becomes:

$$\frac{a_{Mn^{2+}}}{a_{Ca^{2+}}} = \frac{K' X_{MnCO_3}}{(1 - X_{CaCO_3})}$$

and we see that the composition of the solid will vary continuously as a function of $a_{Mn^{2+}}$ (again holding $a_{Ca^{2+}}$ constant). Figure 32 shows just such behavior for carbonate compositions above the ore zone.

FIGURE 34.

Generalized representation of the aqueous activity and solid phase relationship for Ca and Mn (fig. 34A) and the possible consequence for precipitation of a high-grade Mn ore bed (Rhodochrosite Zone) overlain by a Mn-calcite zone. See the text for detailed discussion.

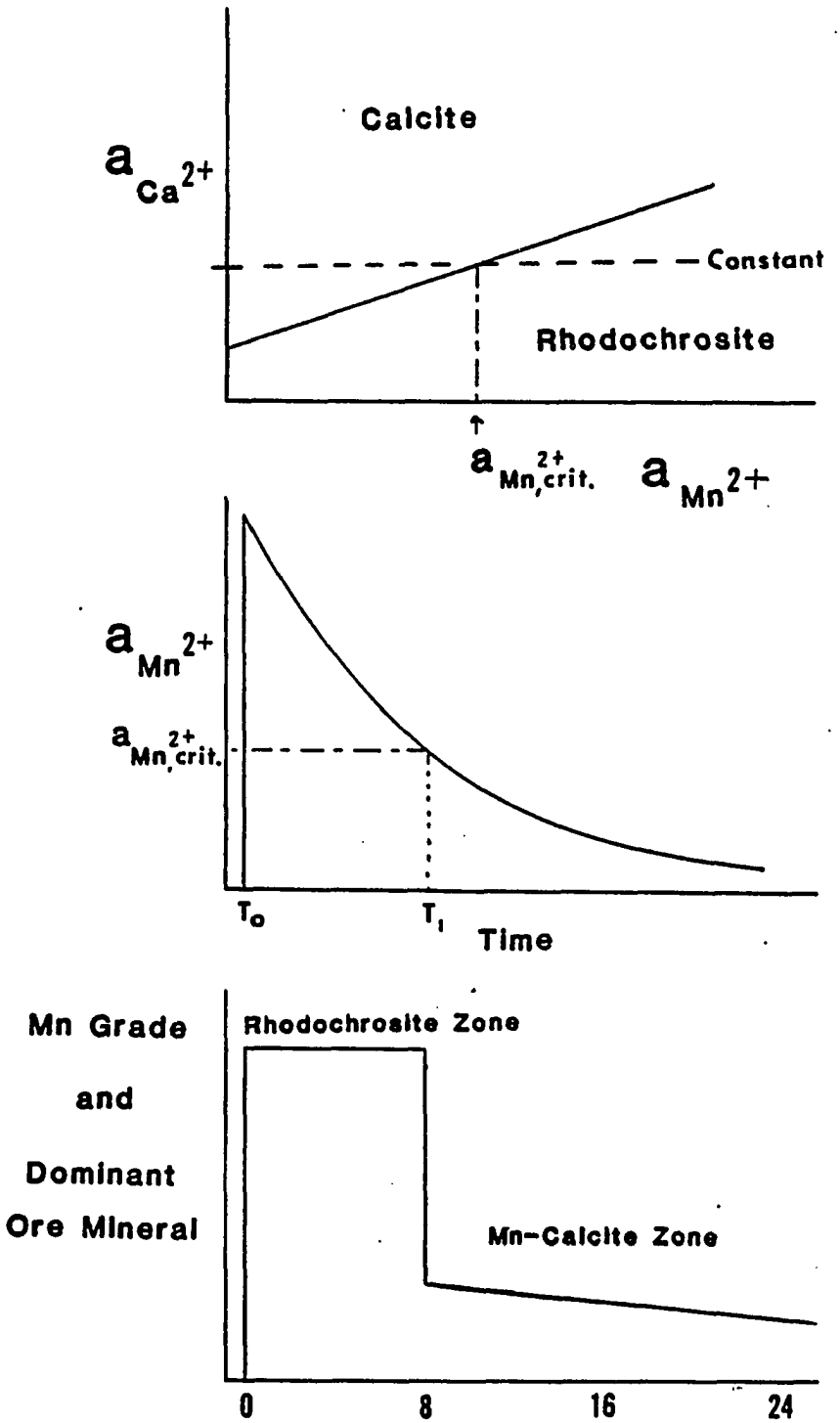

CHAPTER V. STABLE ISOTOPIC ANALYSES OF CARBONATE MINERALS

INTRODUCTION

The stable-isotopic ratios of carbon and oxygen have been analyzed from the carbonate mineral fraction for a total of 49 whole rock samples from the "Santiago" formation and from the Chipoco facies (Table VII). Material was chosen from samples collected in the underground workings known as 'Frente B' at the Tetzintla mine site so that lithologic, textural, and ore grade changes were represented. Every sample collected in the adit from 4 meters below the Santiago - Chipoco contact to about 20 meters above the contact was analyzed, with the exception of T1, +0.45 which is composed massive sulfide. In addition, selected samples above and below this interval, several vein filling carbonates, mineral separates, and miscellaneous other samples were analyzed (Table VIII).

RESULTS

Carbon Isotopes - Measured $\delta^{13}C$ values for carbon range from +5.4°/oo to -19.4°/oo. The data show distinct variations with stratigraphic position relative to the ore zone (Figure 35). Samples from the underlying "Santiago" formation and upper Chipoco facies (i.e. > 70 m) are characterized by $\delta^{13}C$ values of about +1.0 °/oo; the stratigraphically highest samples (> 150 m) possess $\delta^{13}C$

TABLE VII. CARBON AND OXYGEN ISOTOPE DATA FROM CARBONATE MINERALS (WHOLEROCK ANALYSES) AND TEMPERATURE ESTIMATES BASED ON OXYGEN GEOTHERMOMETERY.

SAMPLE ID	NOTES	STRAT. POSITION (meters)	13C/12C PDB	STAND. DEV.	STAND. ERR.
T1,-24.9		-24.9	1.190	0.045	0.015
T1,-20.3		-20.3	1.028	0.048	0.017
T1,-19.0		-19.0	0.840	0.070	0.024
T1,-3.9		-3.9	0.122	0.026	0.010
T1,-0.1		-0.1	-3.898	0.044	0.015
T1,0	CONTACT	0.0	0.920	0.090	N.M.
T1,+0.1DUP	A-BED	0.1	5.432	0.061	0.021
T1,+0.5	ORE	0.5	-11.670	0.034	0.012
T1,+2.0	ORE	2.0	-15.628	0.022	0.007
T1,+2.5B	ORE	2.5	-15.433	0.026	0.009
T1,+3.0	ORE	3.0	-12.557	0.026	0.009
T1,+3.4DUP	ORE	3.4	-13.078	0.030	0.010
T1,+4.0	ORE	4.0	-11.582	0.060	0.021
T1,+4.5DUP	ORE	4.5	-16.340	0.048	0.017
T1,+5.9	ORE	5.9	-7.934	0.059	0.020
T1,+8.5	ORE	8.5	0.522	0.041	0.014
T1,+12.5		12.5	-5.558	0.039	0.014
T1,+19.0		19.0	-4.133	0.041	0.014
T1,+21.95		22.0	-5.201	0.035	0.012
T1,+22.3		22.3	-2.109	0.046	0.017
T1,+25.6	SPICULITE	25.6	-1.930	0.036	0.013
T1,+26.5	SPICULITE	26.5	-7.086	0.052	0.018
T1,+26.7	SPICULITE	26.7	-0.679	0.030	0.011
T1,+26.95	SPICULITE	27.0	-13.659	0.037	0.013
T1,+27.8	SPICULITE	27.8	-0.349	0.090	0.034
T1,+28.5	SPICULITE	28.5	0.058	0.079	0.028
T1,+32.1		32.1	-1.035	0.031	0.011
T1,+35.4		35.4	-1.217	0.060	0.021
T1,+45.3	SHELL BED	45.3	-19.444	0.076	0.027
T1,+47.9		47.9	1.705	0.082	0.029
T1,47.9B		47.9	-0.865	0.022	0.007

TABLE VII. CONTINUED (page 2 of 6).

SAMPLE ID	NOTES	STRAT. POSITION (meters)	13C/12C PDB	STAND. DEV.	STAND. ERR.
T1,+51.8A	SPICULITE	51.8	-1.290	0.080	N.M.
T1,+51.8B	SPICULITE	51.8	-1.226	0.054	0.020
T1,+55.1	SPICULITE	55.1	-1.520	0.070	N.M.
T1,+58.4		58.4	-0.197	0.056	0.019
T1,+64.9		64.9	0.773	0.061	0.021
T1,+71.5		71.5	1.193	0.077	0.027
T1,+78.1		78.1	0.753	0.068	0.024
T1,+87.9		87.9	1.010	0.021	0.007
T1,+94.5		94.5	1.001	0.092	0.035
T1,+110.9		110.9	1.170	0.061	0.021
T1,+120.7		120.7	2.397	0.042	0.016
T1,+133.8		133.8	1.069	0.047	0.016
T1,+140.6		140.6	2.348	0.023	0.008
T1,+140.9		140.9	2.364	0.045	0.016
T1,+152.8		152.8	2.543	0.001	0.028
T1,+162.5		162.5	2.441	0.049	0.017
T1,+165B		165.0	2.302	0.034	0.012
T1,+165.5		165.5	-1.086	0.043	0.015

TABLE VII. CONTINUED (page 3 of 6).

SAMPLE ID	NOTES	STRAT. POSITION (meters)	18O/16O SMOW	STAND. DEV.	STAND ERR.
T1,-24.9		-24.9	33.651	0.070	0.024
T1,-20.3		-20.3	33.445	0.095	0.033
T1,-19.0		-19.0	33.959	0.055	0.020
T1,-3.9		-3.9	32.745	0.079	0.028
T1,-0.1		-0.1	34.223	0.061	0.021
T1,0	CONTACT	0.0	33.950	0.060	N.M.
T1,+0.1DUP	A-BED	0.1	40.655	0.053	0.019
T1,+0.5	ORE	0.5	37.047	0.045	0.016
T1,+2.0	ORE	2.0	37.025	0.053	0.018
T1,+2.5B	ORE	2.5	36.928	0.047	0.016
T1,+3.0	ORE	3.0	37.426	0.023	0.008
T1,+3.4DUP	ORE	3.4	36.106	0.031	0.011
T1,+4.0	ORE	4.0	35.901	0.048	0.016
T1,+4.5DUP	ORE	4.5	37.255	0.099	0.035
T1,+5.9	ORE	5.9	35.150	0.124	0.043
T1,+8.5	ORE	8.5	32.924	0.048	0.017
T1,+12.5		12.5	36.663	0.051	0.018
T1,+19.0		19.0	39.897	0.182	0.064
T1,+21.95		22.0	34.635	0.044	0.015
T1,+22.3		22.3	35.664	0.084	0.029
T1,+25.6	SPICULITE	25.6	35.309	0.041	0.014
T1,+26.5	SPICULITE	26.5	35.038	0.030	0.011
T1,+26.7	SPICULITE	26.7	34.645	0.064	0.022
T1,+26.95	SPICULITE	27.0	34.768	0.028	0.010
T1,+27.8	SPICULITE	27.8	36.318	0.218	0.770
T1,+28.5	SPICULITE	28.5	37.377	0.090	0.032
T1,+32.1		32.1	34.854	0.032	0.011
T1,+35.4		35.4	34.887	0.087	0.031
T1,+45.3	SHELL BED	45.3	35.457	0.073	0.027
T1,+47.9		47.9	42.487	0.051	0.018
T1,47.9B		47.9	34.584	0.023	0.008

TABLE VII. CONTINUED (page 4 of 6).

SAMPLE ID	NOTES	STRAT. POSITION (meters)	18O/16O SMOW	STAND. DEV.	STAND ERR.
T1,+51.8A	SPICULITE	51.8	32.490	0.180	N.M.
T1,+51.8B	SPICULITE	51.8	34.373	0.070	0.026
T1,+55.1	SPICULITE	55.1	33.670	0.140	N.M.
T1,+58.4		58.4	33.427	0.097	0.034
T1,+64.9		64.9	33.503	0.049	0.017
T1,+71.5		71.5	34.300	0.278	0.098
T1,+78.1		78.1	33.464	0.048	0.018
T1,+87.9		87.9	33.583	0.027	0.009
T1,+94.5		94.5	34.024	0.070	0.026
T1,+110.9		110.9	33.811	0.113	0.040
T1,+120.7		120.7	46.528	0.172	0.060
T1,+133.8		133.8	34.167	0.076	0.027
T1,+140.6		140.6	35.022	0.052	0.018
T1,+140.9		140.9	35.387	0.024	0.009
T1,+152.8		152.8	42.612	0.627	0.221
T1,+162.5		162.5	35.723	0.050	0.017
T1,+165B		165.0	36.133	0.040	0.015
T1,+165.5		165.5	35.559	0.058	0.020

TABLE VII. CONTINUED (page 5 of 6).

SAMPLE ID	18O/16O SMOW corrected see note	18O/16O PDB	PALEOTEMPERATURE ESTIMATE (oC) FOR SEAWATER ISOTOPIC VALUES= -5 PDB	AND	0 PDB
T1,-24.9	24.401	-6.266	22.4		48.3
T1,-20.3	24.195	-6.465	23.3		49.5
T1,-19.0	24.709	-5.967	21.1		46.6
T1,-3.9	23.495	-7.145	26.5		53.5
T1,-0.1	24.973	-5.711	20.0		45.1
T1,0	24.700	-5.976	21.1		46.6
T1,+0.1DUP	31.405	0.529	-2.3		14.7
T1,+0.5	27.797	-2.971	8.9		30.5
T1,+2.0	27.775	-2.993	9.0		30.6
T1,+2.5B	27.678	-3.087	9.3		31.1
T1,+3.0	28.176	-2.604	7.6		28.7
T1,+3.4DUP	26.856	-3.884	12.4		35.2
T1,+4.0	26.651	-4.083	13.2		36.2
T1,+4.5DUP	28.005	-2.770	8.2		29.5
T1,+5.9	25.900	-4.812	16.1		40.1
T1,+8.5	23.674	-6.971	25.7		52.5
T1,+12.5	27.413	-3.344	10.3		32.4
T1,+19.0	30.647	-0.207	-0.2		17.8
T1,+21.95	25.385	-5.311	18.2		42.9
T1,+22.3	26.414	-4.313	14.1		37.4
T1,+25.6	26.059	-4.657	15.5		39.3
T1,+26.5	25.788	-4.920	16.6		40.7
T1,+26.7	25.395	-5.301	18.2		42.8
T1,+26.95	25.518	-5.182	17.7		42.2
T1,+27.8	27.068	-3.678	11.6		34.1
T1,+28.5	28.127	-2.651	7.8		28.9
T1,+32.1	25.604	-5.099	17.3		41.7
T1,+35.4	25.637	-5.067	17.2		41.5
T1,+45.3	26.207	-4.514	14.9		38.5
T1,+47.9	33.237	2.306	-6.8		7.9

TABLE VII. CONTINUED (page 6 of 6).

SAMPLE ID	18O/16O SMOW corrected see note	18O/16O PDB	PALEOTEMPERATURE ESTIMATE (oC) FOR SEAWATER ISOTOPIC VALUES= -5 PDB	AND	0 PDB
T1,47.9B	25.334	-5.361	18.4		43.2
T1,+51.8A	23.240	-7.392	27.7		55.0
T1,+51.8B	25.123	-5.565	19.3		44.3
T1,+55.1	24.420	-6.247	22.3		48.2
T1,+58.4	24.177	-6.483	23.4		49.6
T1,+64.9	24.253	-6.409	23.1		49.2
T1,+71.5	25.050	-5.636	19.6		44.7
T1,+78.1	24.214	-6.447	23.2		49.4
T1,+87.9	24.333	-6.332	22.7		48.7
T1,+94.5	24.774	-5.904	20.8		46.2
T1,+110.9	24.561	-6.110	21.7		47.4
T1,+120.7	37.278	6.226	-13.9		-4.2
T1,+133.8	24.917	-5.765	20.2		45.4
T1,+140.6	25.772	-4.936	16.6		40.8
T1,+140.9	26.137	-4.582	15.2		38.9
T1,+152.8	33.362	2.427	-7.1		7.5
T1,+162.5	26.473	-4.256	13.8		37.1
T1,+165B	26.883	-3.858	12.3		35.0
T1,+165.5	26.309	-4.415	14.5		38.0

TABLE VIII. CARBON AND OXYGEN ISOTOPE DATA FROM CARBONATE MINERALS SEPARATED FROM VEIN, BRECCIA, AND FOSSIL MATERIAL.

SAMPLE ID	NOTES	STRAT. POSITION (meters)	13C/12C PDB	STAND. DEV.	STAND. ERR.
T1,+0.1	VEIN	0.1	1.861	0.051	0.018
T1,+9.8	VEIN	9.8	-3.218	0.055	0.019
T1,+15.7	VEIN	15.7	-2.989	0.035	0.012
MISC 2	BRECCIA		-8.375	0.020	0.007
MISC 3	VEIN IN ORE		-3.588	0.042	0.015
MISC 4	XLS IN FAULT		-4.496	0.017	0.006
MISC 5	BRECCIA		-5.358	0.031	0.011
MISC 6	AMMONITE FILL		-19.323	0.064	0.022

			18O/16O SMOW	STAND. DEV.	STAND. ERR.
T1,+0.1	VEIN	0.1	36.197	0.067	0.023
T1,+9.8	VEIN	9.8	32.869	0.083	0.029
T1,+15.7	VEIN	15.7	33.692	0.036	0.012
MISC 2	BRECCIA		33.146	0.034	0.012
MISC 3	VEIN IN ORE		31.006	0.062	0.022
MISC 4	XLS IN FAULT		33.883	0.031	0.011
MISC 5	BRECCIA		32.973	0.052	0.108
MISC 6	AMMONITE FILL		38.534	0.083	0.029

	18O/16O SMOW corrected see note	18O/16O PDB	PALEOTEMPERATURE ESTIMATE (oC) FOR SEAWATER ISOTOPIC VALUES = -5 PDB	AND	0 PDB
T1,+0.1	26.947	-3.796	12.0		34.7
T1,+9.8	23.619	-7.024	25.9		52.8
T1,+15.7	24.442	-6.226	22.2		48.1
MISC 2	23.896	-6.756	24.7		51.2
MISC 3	21.756	-8.831	34.9		64.1
MISC 4	24.633	-6.041	21.4		47.0
MISC 5	23.723	-6.923	25.5		52.2
MISC 6	29.284	-1.529	3.9		23.6

FIGURE 35.

Carbon and oxygen isotopic ratio plotted according to stratigraphic position.

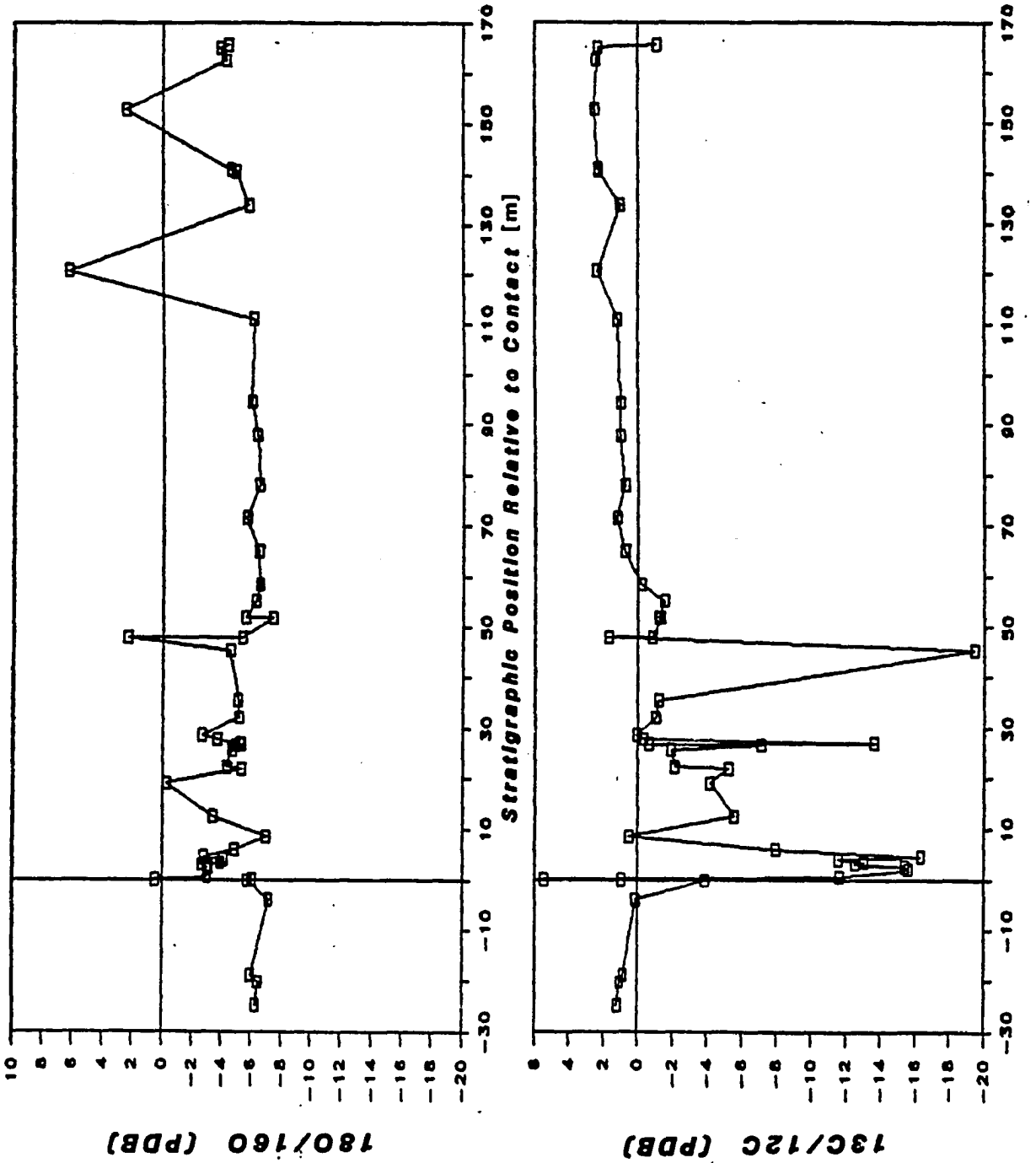

values ranging from +2.0 to +3.0 °/oo.

Anomalously high amounts of manganese were observed in the lower 50 to 60 meters of the Chipoco facies at this location; the ore zone is currently considered to comprise the basal 6 to 10 meters. Samples from the ore zone have very negative $\delta^{13}C$ isotopic values, ranging from approximately -8.0 to -16.34 °/oo. The base of the ore zone is marked by a sharp deflection to negative values (Figure 36), whereas the upper part of the ore interval is characterized by an overall gradual increase in $\delta^{13}C$ towards a value near 0°/oo. Negative carbon isotopic values correlate well with whole rock manganese content, as shown in Figures 37 and 38. The data on Mn content are from Compañia Minera Autlan files, and were collected from the same stratigraphic section, but independently of this study.

Several samples deviate significantly from the overall trend. The first notable sample occurs at the base of the A Bed, 10 cm above the contact. This sample (T1, +0.1), situated immediately above the fault in an extensively veined and brecciated lithology, has a $\delta^{13}C$ value of +5.4 °/oo. This may result from alteration by processes related to faulting (e.g. metamorphism, fluid migration). Samples from the middle of the Chipoco, 'T1,+26.95' and 'T1,+45.3', have extremely negative $^{13}C/^{12}C$ values of -13.6 and -19.4 °/oo respectively. These two samples are from two

FIGURE 36.

Detail of the variation of isotopic composition in the ore zone and immediately above and below.

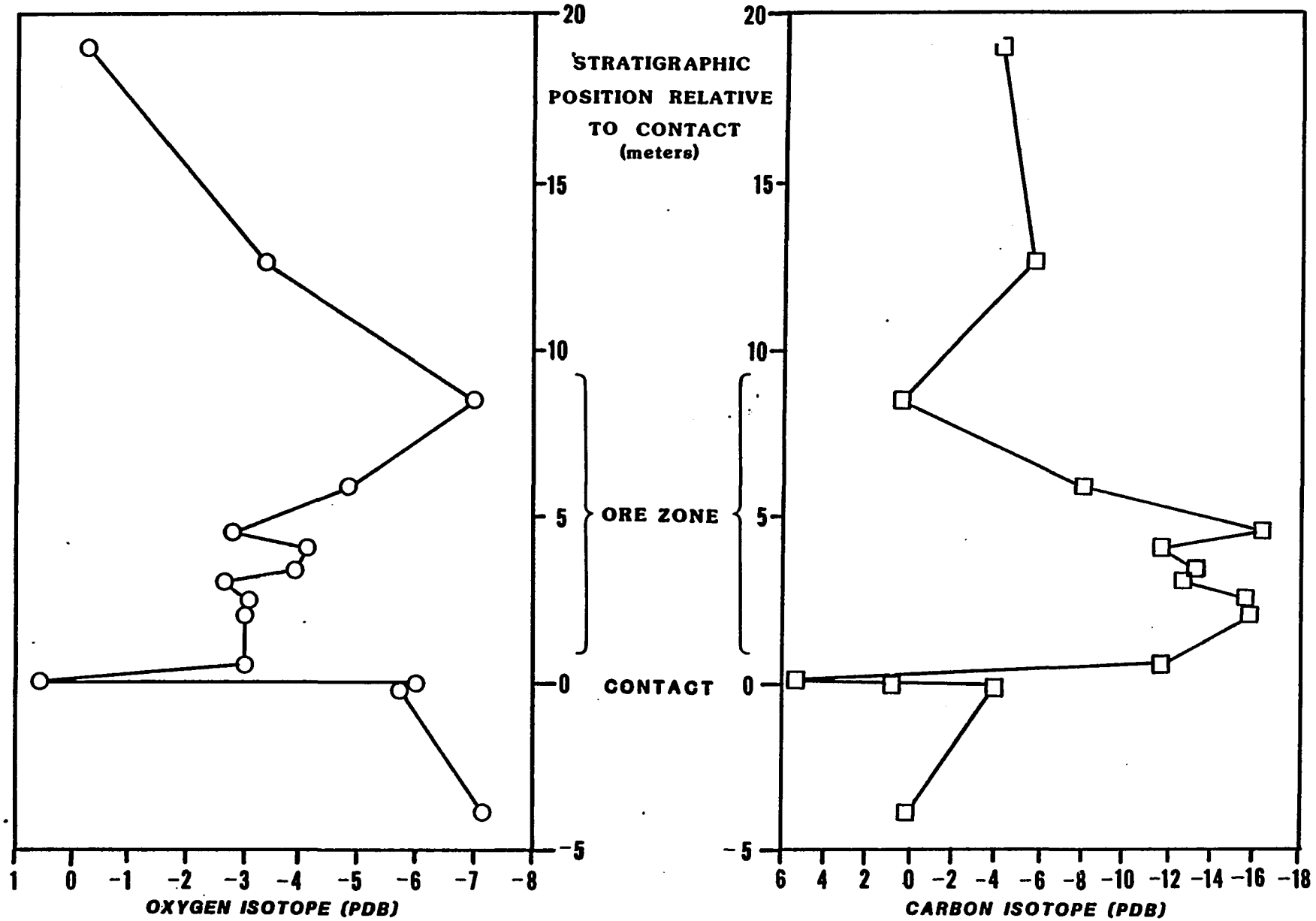

FIGURE 37.

Comparison of carbon isotopic composition and weight percent manganese for the upper part of the Santiago and the lower part of the Chipoco. The data for manganese content are from Compania Minera Autlan and are from the same section.

TETZINTLA ADIT SECTION

CARBON ISOTOPE VS MANGANESE CONTENT

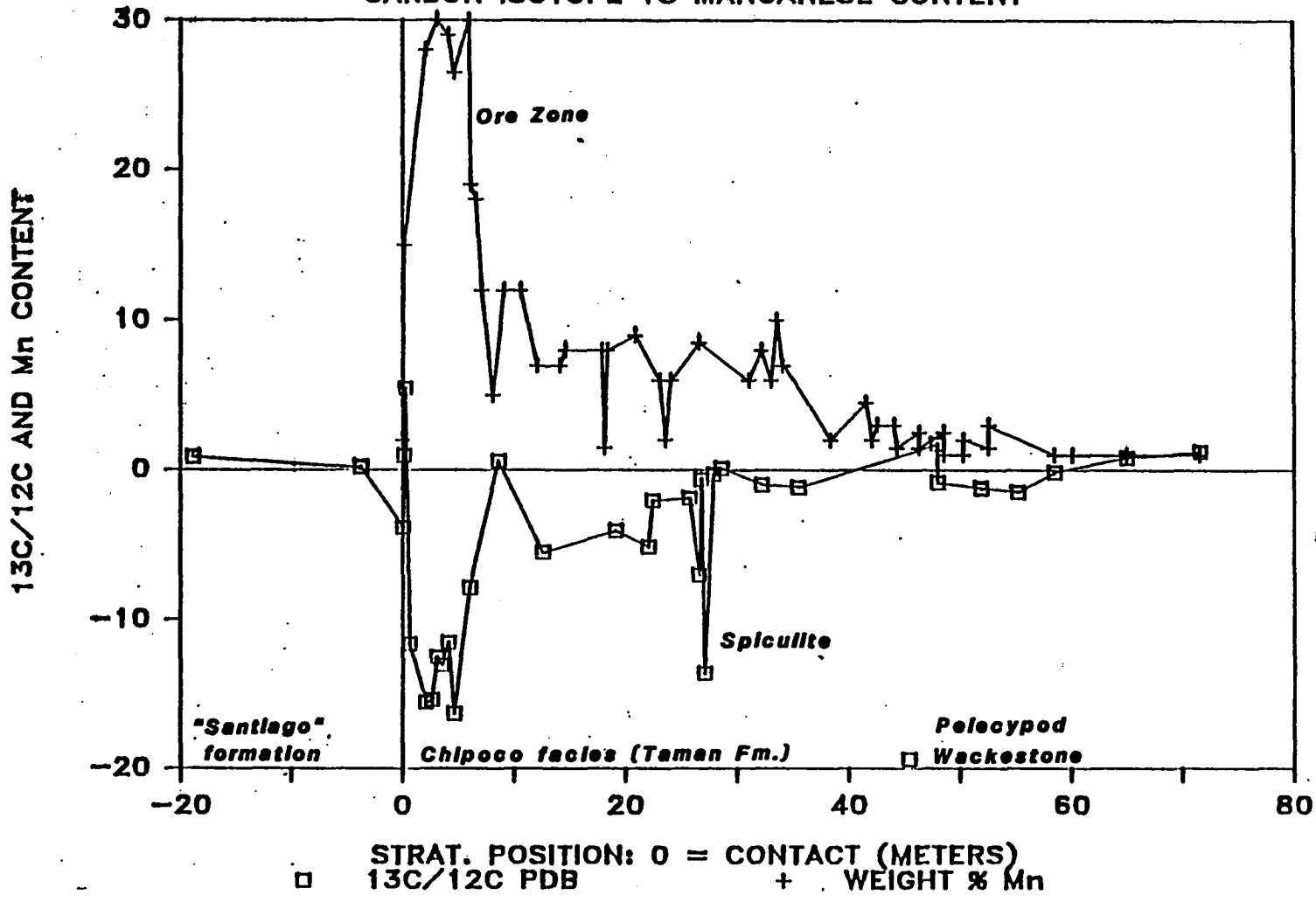

FIGURE 38.

Plot of carbon and oxygen isotopic composition versus manganese content. The data for weight percent Mn are courtesy of Compania Minera Autlan.

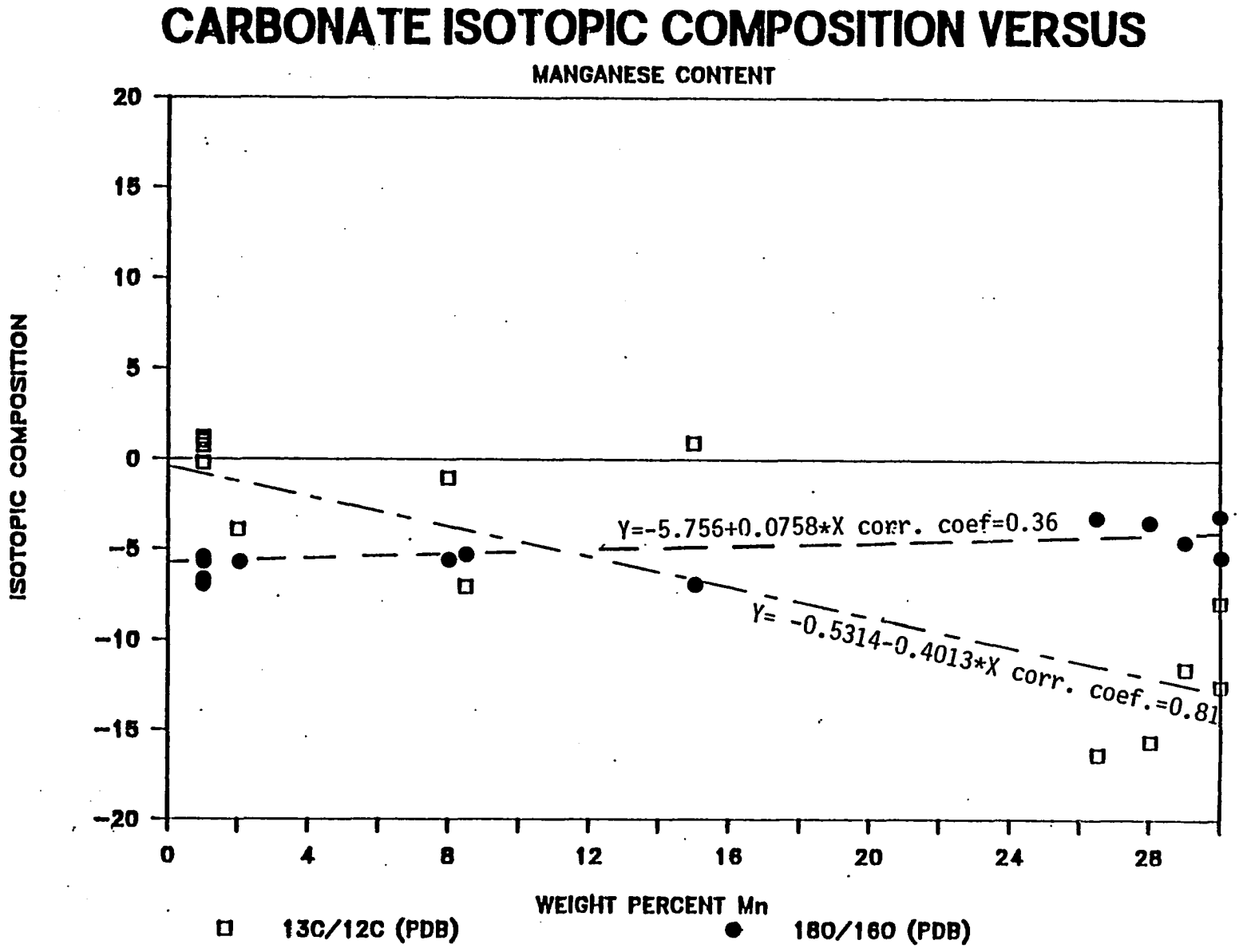

lithologies which differ from the normal Chipoco lithology. The first sample (T1, +26.95) is from a spiculite that was determined petrographically to have formed by calcareous replacement of originally siliceous spicules. Furthermore, samples from +26.5 m and +21.95 m, also from this spiculite interval, have $\delta^{13}C$ values more negative than the typical Chipoco immediately below and above. Sample 'T1, +45.3' is from a bioclastic (pelecypod) wackestone that contains a high density of disarticulated shell debris.

Oxygen Isotopes - Oxygen isotopic ratios vary from -7.39 to +6.23 °/oo relative to PDB. In the plot of $^{18}O/^{16}O$ values against stratigraphic position (Figure 35) no clear patterns are evident, although several samples deviate significantly from a roughly straight baseline which can be drawn through the data at a value of about -6.5 °/oo. Comparison of these oxygen data with the carbon data reveals that for samples from the ore zone and superjacent Mn-rich interval (i.e. from the Santiago-Chipoco contact up to and including the sample from +19.0 meters) the data exhibit an inverse relationship between $\delta^{13}C$ and $\delta^{18}O$; the oxygen values are more positive. The few samples from the upper part of the Santiago and the remainder of samples above +19.0 meters exhibit a normal pattern in which the deflection of both isotopic ratios is in the same direction (i.e. heavier or lighter). These relationships are depicted in a plot of $\delta^{18}O$ versus $\delta^{13}C$ which reveals an

apparent negative correlation between the positive $^{18}O/^{16}O$ and negative $^{13}C/^{12}C$ values (i.e. the ore zone samples and superjacent Mn-rich zone) (Figure 39). This correlative relationship seems to reverse for unmineralized and Mn-poor samples (i.e. $\delta^{13}C$ values near $0^{o}/oo$). However, statistical analysis does not indicate a significant correlation between oxygen and carbon values.

DISCUSSION

Carbon Isotopes - Carbon in carbonates can originate from seawater bicarbonate, from bicarbonate produced by the diagenetic degradation of organic matter in the sediment pile, from the dissolution of primary marine carbonates (e.g. biogenic material, ooids, pelagic precipitates) or from any combination of these three. The reactions and processes which occur successively during burial have been studied by Coleman (1985), Curtis et al., (1985), Maynard (1982), and Berner (1981) and are summarized here in Figure 40. Characterization of the isotopic compositions resulting from the above processes has produced an extensive literature (Hudson, 1977; Irwin et al., 1977; Pisciotto and Mahoney, 1981; and many others). The most important distinction to be made in isotopic compositions is that primary marine carbonates (e.g. shell material, ooids, cements and other carbonate precipitated from seawater) will have $^{o}\delta^{13}C$ values of near $0^{o}/oo$ with respect to PDB, whereas carbonates precipitated from purely

FIGURE 39.

Plot of oxygen versus carbon isotopic composition. Statistical analysis does not support any correlation between oxygen and carbon for the entire sample population. Furthermore, the apparent negative correlation between oxygen and carbon, for negative 13C/12C ratios, is not statistically significant.

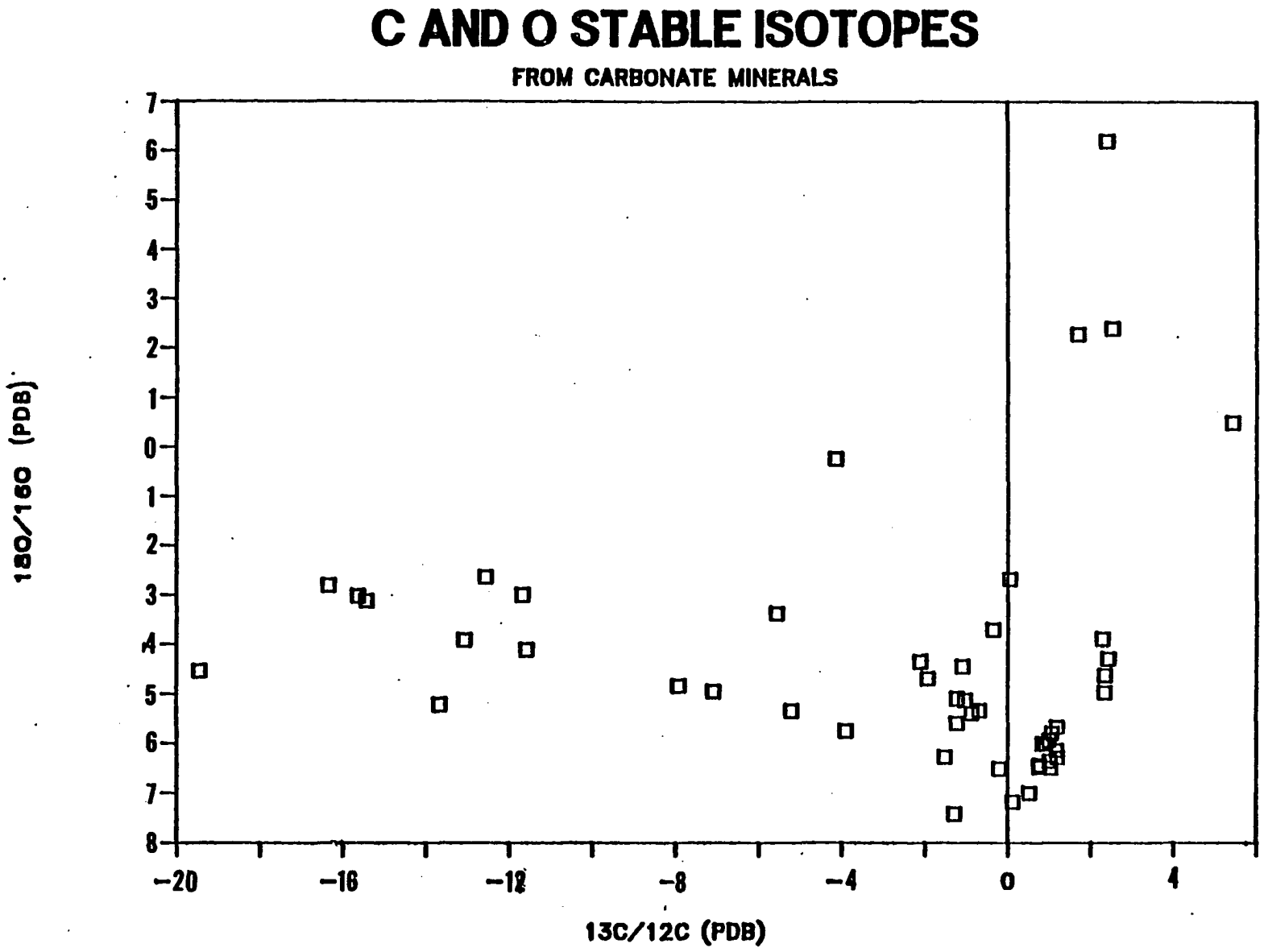

FIGURE 40.

Variation in carbon and oxygen isotopic composition for carbonate sediments and cements from various environments and the factors affecting the compositions (from Hudson, 1977).

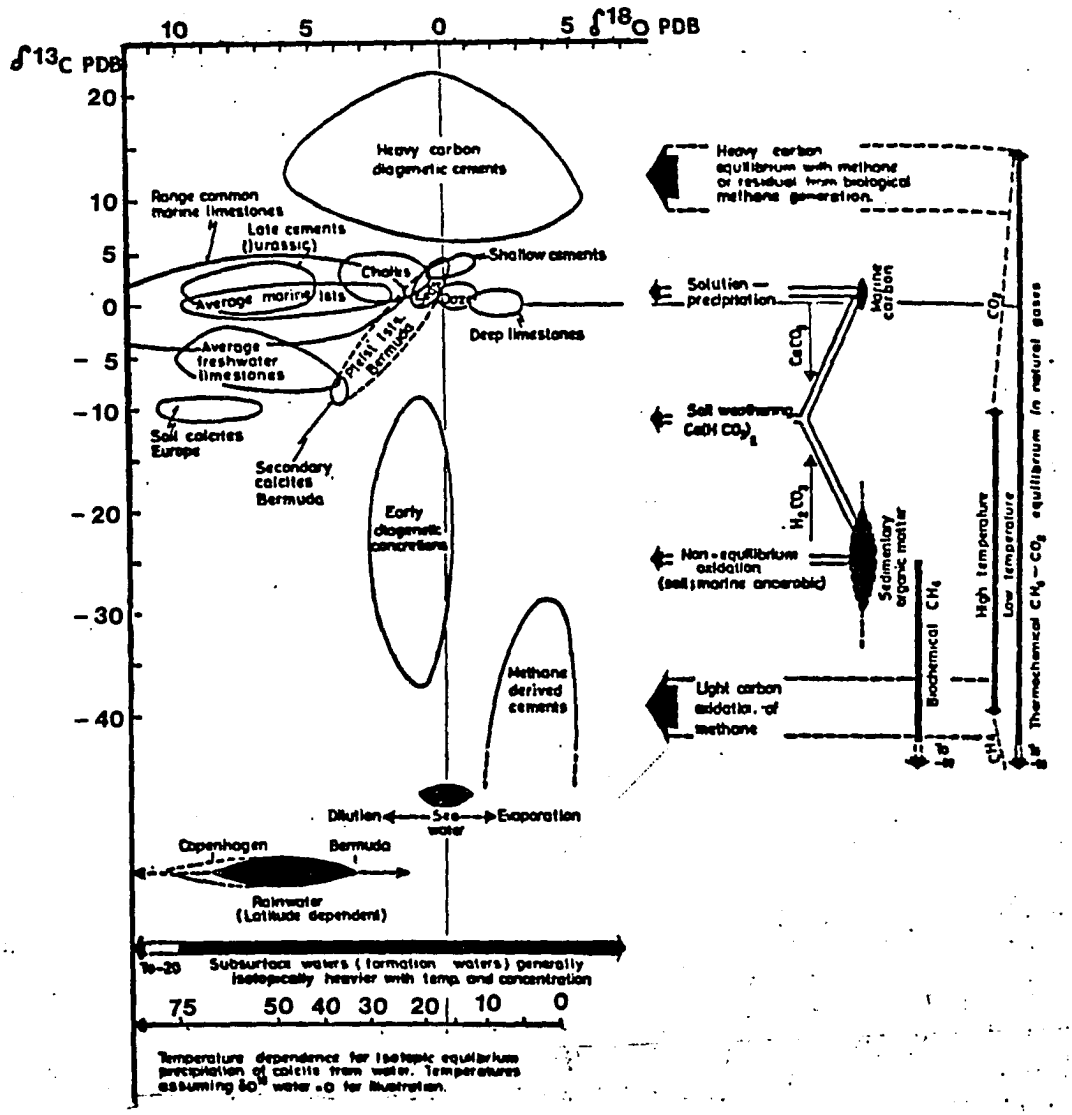

organic-derived bicarbonate may have values as light as -20 to -30 °/oo (Hudson, 1977). In addition, sulfate reduction produces dissolved bicarbonate which can give rise to a carbonate mineral having a $\delta^{13}C$ value of about -15°/oo (Coleman and Raiswell, 1981). Dilution of purely organic-derived bicarbonate with marine bicarbonate, derived presumably either from seawater or from the dissolution of primary marine carbonates, may produce values similar to those of sulfate reduction (Coleman et al., 1982, p. 483).

The isotopic compositions reported in this study for carbonates from the "Santiago formation and the upper part of the Chipoco facies indicate precipitation of primary marine carbonates from seawater having a $\delta^{13}C$ composition near 0°/oo. Such a value is consistent with what is known about Jurassic seawater composition. Veizer and Hoefs (1976) have concluded that there were no significant changes in the carbon isotopic composition of carbonates through the late Mesozoic. However, their data show a shift in the frequency of occurrence toward slightly positive $\delta^{13}C$ values (e.g. +3°/oo PDB) during the Jurassic. These so called "positive excursions" have been documented by other workers (e.g. Jenkyns and Clayton, 1986, and references therein) and are interpreted to reflect the incorporation into sediments of significant quantities of a very light (-30°/oo) organic carbon fraction, thereby leaving the oceans relatively enriched in ^{13}C. Carbon

isotopic values are not sufficiently different from 0°/oo to necessitate invoking additional controls on the carbon reservoir.

The isotopic signature of the ore zone and manganese-enriched interval has a range of values significantly lighter than that for primary marine carbonates, but heavier than the value associated with purely organogenetic carbonates. The isotopic composition of Mn-carbonates may be the product of sulfate reduction or the result of mixing in some ratic of the various carbon reservoirs (i.e. organogenetic, primary marine precipitated material, and seawater bicarbonate). It is generally believed that sulfate reduction results in the precipitation of carbonate minerals which have a $\delta^{13}C$ value about -15°/oo (Coleman and Raiswell, 1981). Invocation of this process to explain the precipitation of the manganese minerals would only be applicable to the ore zone and cannot explain the upper, isotopically heavier portion of the manganese-enriched interval. The noted absence of pyrite, an expected by-product of sulfate reduction, is further evidence against this process having been important in controlling the carbon isotopic composition of the carbonate minerals in the high grade ore zone.

The most plausible explanation is that the carbon isotopic ratios observed from the mineralized zone are the product of mixing isotopically light, organically-derived

(e.g. -20 to -30 °/oo) carbon with near 0°/oo carbon introduced either by downward diffusion of seawater bicarbonate or by the dissolution of primary, marine-precipitated carbonate. Since the $\delta^{13}C$ ratio is essentially the same for these last two sources of heavy carbon they cannot be distinguished; and both sources are sufficiently likely to occur in this type of depositional environment. The average $\delta^{13}C$ value observed in the ore zone is compatible with a 1:1 mixture of organic and seawater carbon.

The increasingly heavy isotopic ratio observed vertically probably reflects a decreasing contribution of organically-derived carbon. Abundant bioclastic material and good communication with seawater are characteristic throughout the section. The decrease in manganese content that accompanies the shift to heavier carbon suggests that conditions became more oxidizing up section, resulting in less organically-derived carbon being incorporated into the carbonate reservoir.

Diagenesis of manganese and of organic matter can be related by considering the sequence of reactions encountered during diagenesis. Beginning with the work of Curtis (1977), later modified by Froelich et al. (1979), and Coleman (1985), seven diagenetic zones have been recognized which are based on the predominant chemical reaction responsible for the oxidation of organic matter.

These zones occur in a sequence which reflects the energy released by the reaction per mole of organic carbon (Tables IX and X).

It is possible from petrographic and mineralogic observations to infer the diagenetic zone in which manganese mineralization occurred. The absence of sulfides and the presence of primary mineral phases containing ferric iron (e.g. magnetite, maghemite) are evidence against both sulfate reduction and extensive ferric iron reduction having occurred. The presence of reduced manganese mineral phases constrains the chemical conditions still further, and is interpreted to imply that manganese reduction was an important reaction resulting in the oxidation of organic carbon. Furthermore, nitrate reduction may have occurred concurrently with manganese reduction, as suggested by the overlapping range in values for the energy released by the two reactions (Table IX). It is not clear from the literature whether manganese reduction or nitrate reduction is favored thermodynamically or kinetically (at 25°C), and therefore which occurs first. Data presented by Coleman (1985) suggest that both reactions may proceed concurrently, whereas Berner (1980) states that nitrate reduction precedes manganese reduction.

TABLE IX. FREE ENERGY YIELD OF DIAGENETIC REACTIONS FOR THE OXIDATION OF ORGANIC MATTER IN SEDIMENTS

DIAGENETIC REACTION	ΔG^{o} (kJ per mol organic C)	
	Berner[1]	Coleman[2]
AEROBIC OXIDATION	-475	-530
MANGANESE REDUCTION	-349	-480-515
NITRATE REDUCTION	-448	-460-505
FERRIC IRON REDUCTION	-114	-220-235
SULPHATE REDUCTION	-77	-65
METHANOGENESIS	-58	-60
DECARBOXYLATION	N.R.	-60

1. Berner, 1980, p. 83.
2. Coleman, 1985, p. 40.

TABLE X. REACTANTS AND PRODUCTS FOR THE DIAGENETIC REACTIONS IN TABLE IX.

1) Aerobic Oxidation:

$$CH_2O + O_2 \longrightarrow HCO_3^- + H^+$$

2) Manganese Reduction:

$$CH_2O + 3CO_2 + H_2O + 2MnO_2 \longrightarrow 2Mn^{++} + 4HCO_3^-$$

3) Nitrate Reduction:

[a] $$5CH_2O + 4NO_3^- \longrightarrow 2N_2 + 4HCO_3^- + CO_2 + 3H_2O$$

OR

[b] $$CH_2O + NO^- + 2H_2O \longrightarrow NH_4^+ + OH^- + HCO_3^-$$

4) Ferric Iron Reduction:

$$CH_2O + 7CO_2 + 4Fe(OH)_3 \longrightarrow 4Fe^{++} + 8HCO_3^- + 3H_2O$$

5) Sulphate Reduction:

$$2CH_2O + SO_4^{--} \longrightarrow H_2S + 2HCO_3^-$$

6) Methanogensis:

$$2CH_2O \longrightarrow CH_4 + CO_2$$

Regardless of the exact order, it is probable that as the dissolved oxygen content decreases, manganese and nitrate reduction will either proceed together, or that one reaction will occur soon after the other. Both workers' data indicate that aerobic oxidation and ferric iron reduction have relatively large differences in the energy of reaction, respectively well above and well below the manganese- and nitrate- reduction level. This further implies that manganese and nitrate reduction may proceed to produce a distinct chemical facies and mineral product with relatively little influence and contribution of products from the other diagenetic reactions (i.e. aerobic oxidation and ferric iron reduction).

The significance of these constraints is that manganese mineralization quite probably occurred in the sub-oxic (dysaerobic or oxygen minimum) zone. The trend toward heavier isotopic compositions with decreasing manganese content may indicate a change to more oxidizing conditions. Specifically, it might be expected that under oxidizing conditions more organic matter would be oxidized and contribute to the bicarbonate reservoir to produce a more negative $\delta^{13}C$ value. Although oxidation of organic matter does generate large amounts of carbon dioxide in the aerobic zone, this gaseous/volatile contribution is generally lost from the sediment pile (Gautier, 1985, p.15). In order for a relatively greater amount of

organically derived carbon to remain in the porewaters as bicarbonate and carbonate ions it is necessary that the pH of the waters be increased above the normal seawater values of 7.5 to 8.4. The by-products of nitrate reduction are very effective in increasing the alkalinity of the porewater (Eqn. 3b, Table X). Thus the end-product of more reducing basinal conditions associated with Mn-carbonate mineralization may be an increase in pH. Furthermore, greater alkalinity (i.e. higher pH) would retard dissolution of any carbonate minerals and favor the downward diffusion of seawater bicarbonate as the dominant source of inorganic-derived carbon.

TOWARD A GEOCHEMICAL MODEL

The interpretation of chemical conditions responsible for the vertical trend toward decreasingly negative carbon isotopic ratios can be combined with observed stratigraphic relationships to produce a chemical facies model for mineralization at Molango. Consideration must first be given to the mass balance for carbon in the system, however. It seems possible that in an oxygen-poor environment a sufficiently large mass of organic carbon was present to provide for the approximately 1:1 ratio of organic-carbon (~-30°/oo) and seawater-derived (~0°/oo) bicarbonate that would be required in the ore zone. For example, the high grade ore zone contains about 30 weight percent MnO, which is equivalent to 4.23 moles or

approximately 0.5 kg of Mn-carbonate ($MnCO_3$) per kilogram of rock. This would require that 4.23 moles or about 5 weight percent of carbon also be present per kilogram of rock. If one-half or 2.5 weight percent carbon present in the manganese ore were derived from organic matter then the total organic carbon content of the original sediment pile, determined by adding the TOC content presently in the rock to the amount of carbon calculated above, must have been at least 3.25 weight percent. Such an amount is not unreasonable for the early diagenetic stage of many sediments (Gautier, 1985).

The vertical section analyzed in this study should represent a sequence of facies that would have existed side by side at any particular time, for example, the time of mineralization (Walther's Law). Thus, the ore zone may be considered to represent a position laterally adjacent to the weakly mineralized superjacent interval. For a regressive sequence, the ore would lie on the basinward side. Generalized facies tracts can be formulated from the stratigraphic and thin-section data (Figure 41). Parallel to these lithofacies, there would have existed geochemical facies tracts defined by parameters such as dissolved oxygen, dissolved reduced manganese, and isotopic composition. It should be noted here that portions of the stratigraphic section may be missing as a result of faulting at the base of the ore zone. The fault is low

FIGURE 41.

Schematic representation of the chemical and sedimentary facies at Molango at the time of maximum transgression.

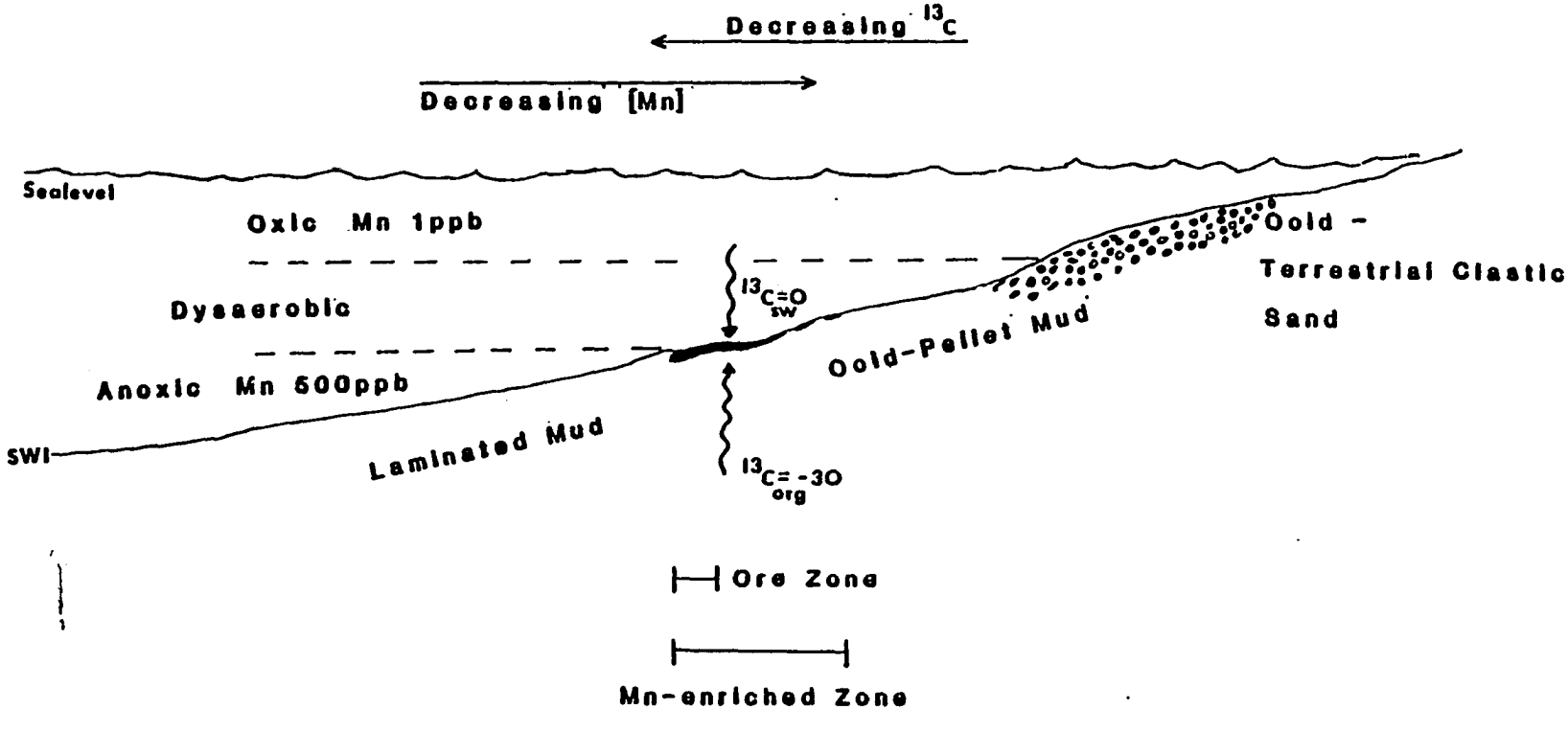

angle, and probably parallel to bedding in many or all locations, and I have assumed that relatively little section has been lost. Furthermore, in light of the depositional facies represented in the section and the chemical and isotopic results from samples collected at close spacing throughout the section it has been concluded that the missing section probably represents the final stage of a regressive event in the upper Santiago followed by onset of the next transgression. More oxidizing conditions would be expected to have affected the upper, weakly mineralized zone if it lay proximal to, but still below, the anoxic/oxic boundary. A higher oxidation state should lead to diminished incorporation of organic matter into the sediment and, subsequently, a higher ratio of inorganic-derived to organic-derived carbon in the carbonate minerals. Thus, the carbon isotopes of the carbonate minerals should become heavier if less light, organically derived bicarbonate were mixed with the heavy bicarbonate supplied by downward diffusion from the overlying seawater. The occurrence of isotopically heavier carbonates stratigraphically higher in the zone of manganese enrichment in the section measured at Tetzintla is consistent with the basinward movement of the oxic boundary in response to the subsequent regression.

The exact nature of carbon sources cannot be determined without further stratigraphic control and additional

information about the depth of burial at the time of mineralization. Information on the depth of precipitation may typically come from oxygen isotopic data. However, the available $\delta^{18}O$ data cannot be used to determine depth of precipitation because of uncertainties about the temperature - fractionation behavior of oxygen during rhodochrosite precipitation. Oxygen isotopic data are discussed below.

Oxygen Isotopes - The oxygen isotopic composition of carbonate minerals is a function of the isotopic composition of the water from which the mineral precipitated and the temperature of precipitation. The temperature-dependent fractionation that occurs between the fluid and the solid has been the subject of extensive study, focused primarily on calcite and dolomite (e.g. O'Neil et al., 1969; Sharma and Clayton, 1965; and many others). The temperature-dependance of oxygen isotopic fractionation in Mn-carbonates has not been calibrated at low temperature, although it can be expected that relative changes in isotopic composition should be similar to those exhibited by calcite. That is, at higher temperatures the carbonate $^{18}O/^{16}O$ ratio becomes lighter for a given ^{18}O content in the water. It is accepted that during burial $\delta^{18}O$ in diagenetic carbonates becomes more negative, reflecting higher temperatures at depth. Lawrence et al. (1975) state that diagenetic reactions may result in a

porewater up to 3 °/oo lighter. Finally, late alteration of isotopic composition may be caused by exchange with deep formation fluids and metamorphic fluids. Oxygen isotopes are readily exchanged between carbonate minerals and these fluids.

The carbonates analyzed in this study have, in most cases, uniformly light isotopic ratios that are slightly lighter than values commonly encountered for marine precipitates (i.e. Jurassic seawater of 0 to -5°/oo PDB; see Veizer and Hoefs, 1976) but are similar to values associated with burial diagenesis (e.g. -8 to -4 °/oo PDB; see Dickson and Coleman, 1980; Moore, 1985; Prezbindowski, 1985: and Fig. 40). Secular variations of the oxygen isotopic ratio are not well known for the pre-Tertiary ocean although it is documented that the $\delta^{18}O$ composition of limestones and cherts increases with decreasing geologic age (Veizer and Hoefs, 1976; Knauth and Epstein, 1976; Knauth and Lowe, 1978; Perry, 1967; Perry and Tan, 1972). Several hypotheses have been suggested to explain these observations: (1) post-depositional exchange with warm and isotopically light meteoric water; (2) decrease in ocean temperature has decreased throughout geologic time; and (3) increase in the $\delta^{18}O$ composition of the ocean throughout geologic time (see Anderson and Arthur, 1983, p.1-60).

Use of the data from calcite phases, that is Santiago and upper Chipoco samples, would imply low temperatures

FIGURE 42.

Relationship between the temperature of precipitation and the oxygen isotopic composition for calcite precipitated from a water of specific composition. The shaded area reflects the range of oxygen values measured for calcites in this study.

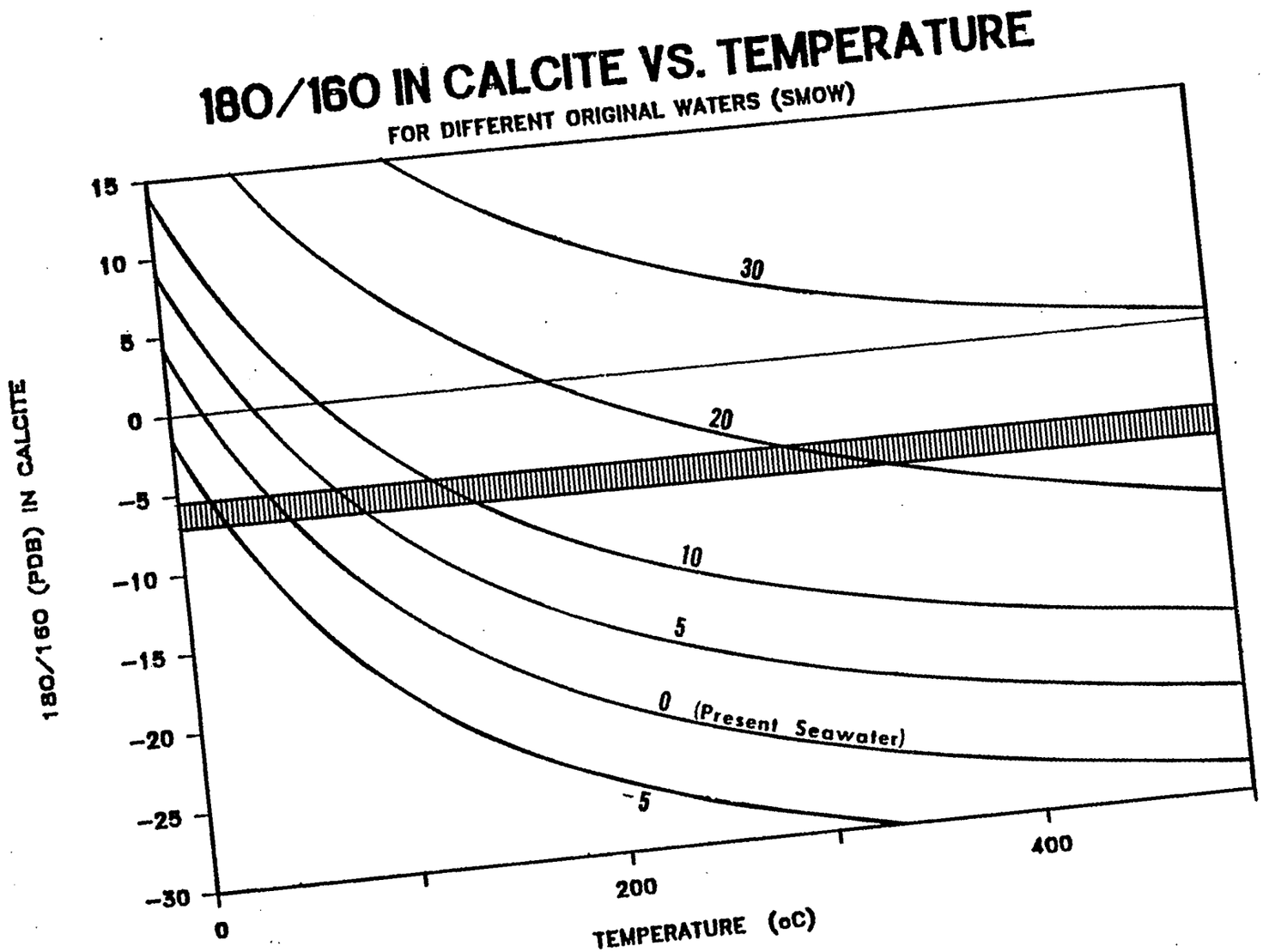

(e.g. 10 to 25 ^{o}C) if treated as Jurassic marine precipitates from a -5^{o}/oo water (Table VII and Figure 42). However, if the seawater were approximately 0^{o}/oo PDB, and the calcite phases were unaltered by post-depositional alteration, then a temperature of precipitation ranging from about 40 to 50 ^{o}C is indicated (Table VII and Figure 42). Interaction of these rocks with post-depositional fluids (e.g. groundwaters, metamorphic waters) cannot be ruled out, and a very low-grade metamorphic overprint is suspected, given the graphitic nature of the rocks. The $\delta^{18}O$ value of metamorphic waters is not well documented.

A case for re-equilibration of the original isotopic signature of the minerals by a particular fluid is difficult to make without a firm constraint on the oxygen isotopic composition of Upper Jurassic seawater. Some variability in the oxygen values from these rocks suggests that exchange did not occur or was at least incomplete. If an assumption of no exchange is made, and an additional assumption is made that the Mn mineralization took place under conditions similar to those present during precipitation of Santiago and upper Chipoco carbonates, then a low temperature origin of the manganese deposit is indicated. This temperature is probably too warm for a marine precipitate but may rule out a hydrothermal or deep burial replacement origin of mineralization.

Some samples have per mil values several units heavier

than those determined for the majority of the analyses. The significance of this heavier oxygen is not apparent, although these samples do contain large amounts of bioclastic debris. It is also noteworthy that the ore zone and much of the mineralized interval is isotopically heavier than the subjacent and superjacent calcium carbonates (Figure 43). This could be caused by differing fractionation factors for the precipitation of rhodochrosite and calcite. Clayton (1961) and Hodgson (1966, p. 1228) report that the equilibrium fractionation factor between calcite-rhodochrosite is smaller and opposite in direction from than that of calcite-dolomite. At room temperature this would result in calcite being isotopically heavier (<1°/oo) than rhodochrosite. O'Neil et al. (1969, p. 5550-5551) state that at higher temperatures the fractionation of oxygen isotopes between rhodochrosite and water is greater than that of calcite. This would mean that rhodochrosite should be heavier than calcite for a given water composition.

Construction of a temperature-fractionation curve for rhodochrosite is not possible. At this time only one value, that of O'Neil et al. (1969), has been determined for the fractionation on precipitation of rhodochrosite. The construction of a curve parallel to the calcite curve to pass through the one value for rhodochrosite is not justified. The argument against this approach is based on

FIGURE 43.

Detail of the del^{18}O values for the stratigraphic section. Note the separation of values between Mn-carbonates and calcite. Filled symbols denote samples of calcite composition, whereas open symbols represent Mn-rich carbonates.

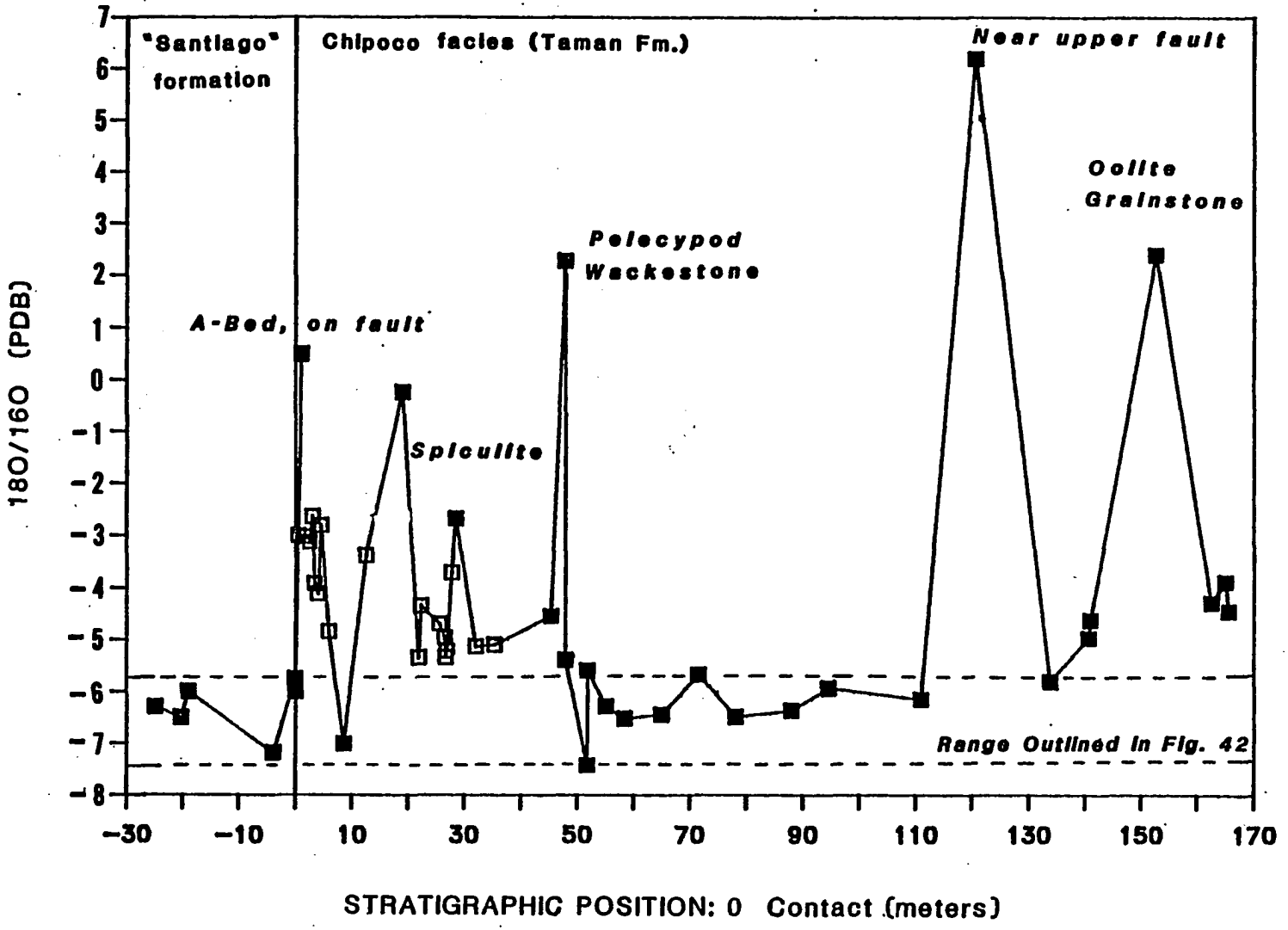

the observation that the curves for other carbonates (i.e. dolomite, witherite, strontianite) are not parallel to that for calcite. The temperature-fractionation equations have the form:

$$10^3 \ln \alpha = A(10^6 T^{-2}) - B.$$

The creation of a parallel curve passing through a different point simply requires changing the intercept value B. This is hardly reasonable in view of the widely varying values reported for A. Furthermore, the vibrational properties of the cation in the carbonates play a large role in isotopic fractionation. The effects of transition metal cations in carbonates are not well known and thus the assumption that fractionation behavior during rhodochrosite precipitation will be similar in character to calcite is groundless.

No additional inferences or conclusions can be extracted from the oxygen data in this study. It is hoped that with further work a geothermometer can be applied to determine the temperature of formation of mixed carbonates or the compositions of post-depositional fluids with which the carbonates have exchanged. This temperature scale may be based on the isotopic analyses of a coexisting mineral phase such as magnetite.

CHAPTER VI. CHARACTERIZATION AND ISOTOPIC ANALYSES OF THE ORGANIC CARBON COMPONENT

INTRODUCTION

Thirteen (13) samples from four stratigraphic levels of the "Santiago" formation and the Chipoco facies of the Taman Formation were analyzed to determine (1) the $\delta^{13}C$ composition of the kerogen component, (2) total organic carbon content, (3) vitrinite reflectance, and (4) pyrolysis characteristics by the Rock-Eval method (Table XI). These analyses were performed at the Amoco Production Company Research Center, courtesy of Dr. Michael D. Lewan.

The objectives in collecting these data were to identify (1) the source(s) and type(s) of organic matter (OM) present; (2) any changes in the amount and type of OM through the stratigraphic section; and (3) the degree of organic metamorphism. Additionally, this data set was studied in an effort to further the understanding of the depositional environment, identify possible changes in sea level, to reveal any differences between mineralized and unmineralized rocks, and to constrain the maximum temperature affecting these rocks. The raw data are presented in Tables XII and XIII and Figure 44.

TOTAL ORGANIC CARBON

Total organic carbon (TOC) values range from 0.32 to 2.88 weight percent (Table XII). In the Santiago, TOC increases from a value of 1.14 wt-% at -350 meters through

TABLE XI.
LIST OF SAMPLES ANALYZED FOR PYROLYSIS CHARACTERISTICS, VITRINITE REFLECTANCE, TOTAL ORGANIC CARBON, AND $^{13}C/^{12}C$ COMPOSITION OF ORGANIC MATTER.
(GROUPED INTO STRATIGRAPHIC LEVELS)

GROUP A - Lower "Santiago" formation

MOL1, - 350
MOL1, - 210
MOL1, - 100

GROUP B - Upper "Santiago" formation

T1, - 24.9
T1, - 7.2

GROUP C - Lower Chipoco Facies

T1, 0 (contact)
T1, + 0.50
T1, + 2.50
T1, + 4.50
T1, + 28.50

GROUP D - Upper Chipoco Facies

T1, + 45.3
T1, +110.9

Note: The numeric part of the sample numbers indicates the position of the sample relative to the "Santiago" - Chipoco contact (i.e. 0 meters).

TABLE XII. RESULTS OF CARBON ISOTOPE, ORGANIC CARBON ANALYSIS, AND ROCK-EVAL PYROLYSIS

SAMPLE	STRAT. POSIT.	TOC wt.-%	S1 mg/g	S2 mg/g	S3 mg/g	TMAX (oC)	S2/S3	VITR. REFL. %	$\delta^{13}C$ PDB	ORGANIC
T1,+110.9	110.9	1.49	<0.10	<0.10	0.16			3.36	-26.6	-26.7
T1,+ 45.3	45.3	0.55	<0.10	<0.10	0.13			2.82	-27.5	
T1,+ 28.5	28.5	0.32	<0.10	<0.10	0.17			0	-26.7	-26.5
T1,+ 4.5	4.5	0.91	<0.10	<0.10	0.9			2.65	-26.4	-26.5
T1,+ 3.4	3.4	0.64	<0.10	0.1	1.05		0.1	2.5	-27.2	
T1,+ 2.5	2.5	0.75	<0.10	0.1	0.9		0.11	2.45	-27.2	
T1,+ 0.5	0.5	0.95	<0.10	<0.10	0.61	522		2.8	-27.6	-27.6
T1, 0	0	1.77	<0.10	<0.10	0.2			2.3	-27.6	
T1,- 7.2	-7.2	1.75	<0.10	<0.10	0.18			2.01	-27.5	-27.5
T1,- 24.9	-24.9	1.32	<0.10	<0.10	0.14			1.78	-27	
T1,-100	-100	2.88	<0.10	<0.10	0.56			3.93	-26.8	-27.1
T1,-210	-210	2.2	<0.10	<0.10	0.37			3.99	-26.9	
T1,-350	-350	1.14	<0.10	<0.10	0.36			3.93	-26.9	

TABLE XIII. ORGANIC CARBON STABLE ISOTOPE ANALYSIS.

SAMPLE NUMBER	del $^{13}C_{PDB}$
MOL1, -350	-26.9
MOL1, -210	-26.9
MOL1, -100	-26.8,-27.1
T1, -24.9	-27.0
T1, - 7.2	-27.5,-27.5
T1, - 0	-27.6
T1, + 0.5	-27.6,-27.6
T1, + 2.5	-27.2
T1, + 3.4	-27.2
T1, + 4.5	-26.4,-26.5
T1, +28.5	-26.7,-26.5
T1, +45.3	-27.5
T1, +110.9	-26.6,-26.7

FIGURE 44.

Stratigraphic profile of isotopic composition, TOC, and $\%R_o$ data. Recall that the ore zone occurs immediately overlying the "Santiago" - Chipoco contact (i.e. 0 meters). Negative values are meters below the contact. Positive values are meters above the contact.

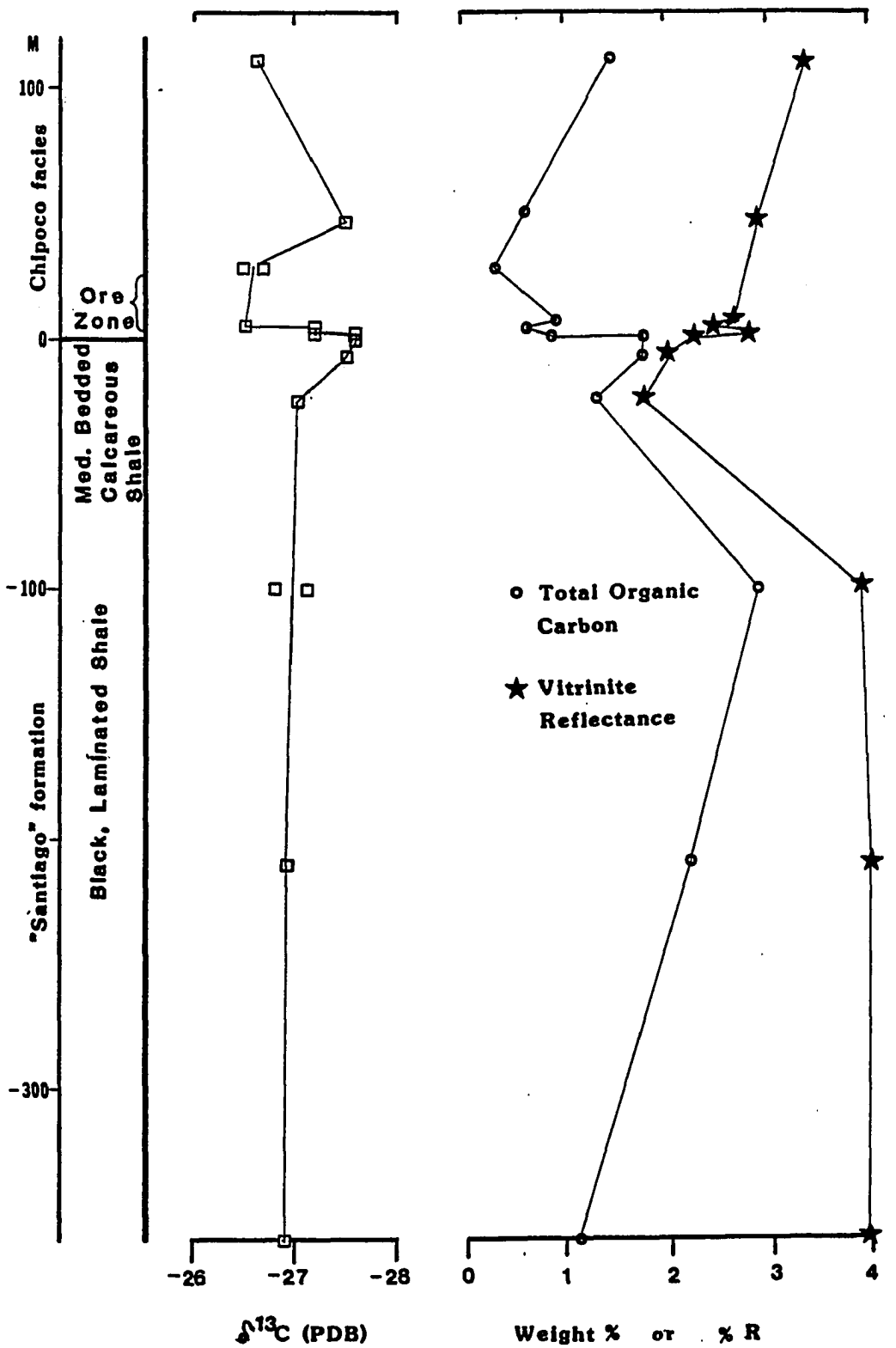

a maximum value of 2.88 wt-% at -100 meters before decreasing (Figure 44). A second, smaller increase is observed from -24.9 meters to the contact between the Santiago and Chipoco facies.

The lower part of the Chipoco (0 to +28.5 meters) is marked by a sharp decrease in TOC at the contact and, while variable, TOC stays in the lowest observed values up to +28.5 meters before beginning to increase. It should be noted here that the sharp decrease at the contact corresponds with the base of the mineralized zone.

PYROLYSIS DATA

Rock-Eval pyrolysis data are unremarkable but reveal that no free or adsorbed hydrocarbons (S1 <0.110 mg/g) were present (Table XII). Two samples produced a minimum detectable level of hydrocarbons (S2 = 0.10 mg/g) whereas all other samples were below detectable levels. S3 values are variable and range from 0.13 to 1.05 mg/g, reflecting variable amounts of CO_2 and water produced in the samples. It appears that these rocks have passed through all the stages of hydrocarbon generation.

VITRINITE REFLECTANCE ANALYSIS

The samples analyzed for vitrinite reflectance (VR) fall into two categories. The first has average values ranging between 3.36 and 3.99 $\%R_o$ whereas the measurements for the second group vary from 1.78 to 2.82 $\%R_o$ (Figure 45a - 45d).

FIGURE 45a.

Histograms of vitrinite reflectance data.

VITRINITE REFLECTANCE ANALYSIS

MOLANGO MANGANESE DEPOSIT

LOCALITY 1717 TECH SVC NO. 86-1717

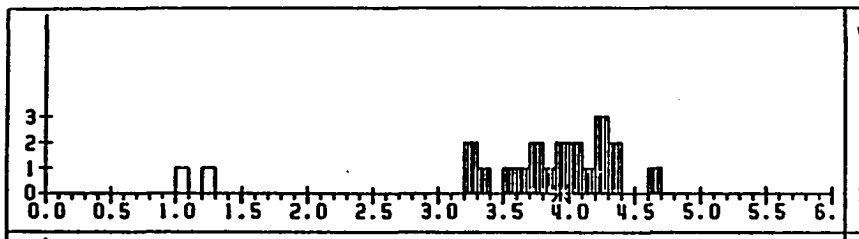

V-5549 RL

4-28-86

KERO=AMOR

	AVG.%RO	MEDIAN	S.DEV.	POINTS
1) *	3.93	3.95	0.380	19

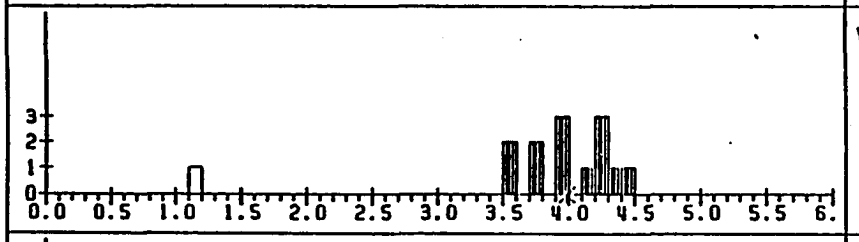

V-5550 RL

4-28-86

KERO=AMOR

	AVG.%RO	MEDIAN	S.DEV.	POINTS
1) *	3.99	3.97	0.297	13

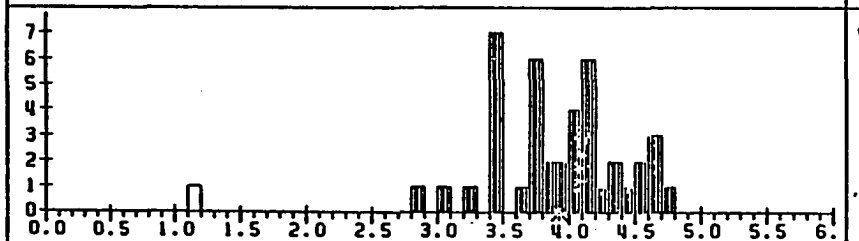

V-5551 RL

4-28-86

KERO=AMOR

	AVG.%RO	MEDIAN	S.DEV.	POINTS
1) *	3.93	3.95	0.448	41

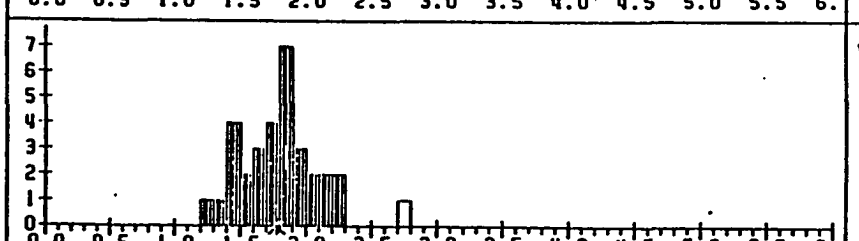

V-5552 RL

4-28-86

KERO=AMOR

	AVG.%RO	MEDIAN	S.DEV.	POINTS
1) *	1.78	1.80	0.265	31

FIGURE 45b.

Histograms of vitrinite reflectance data.

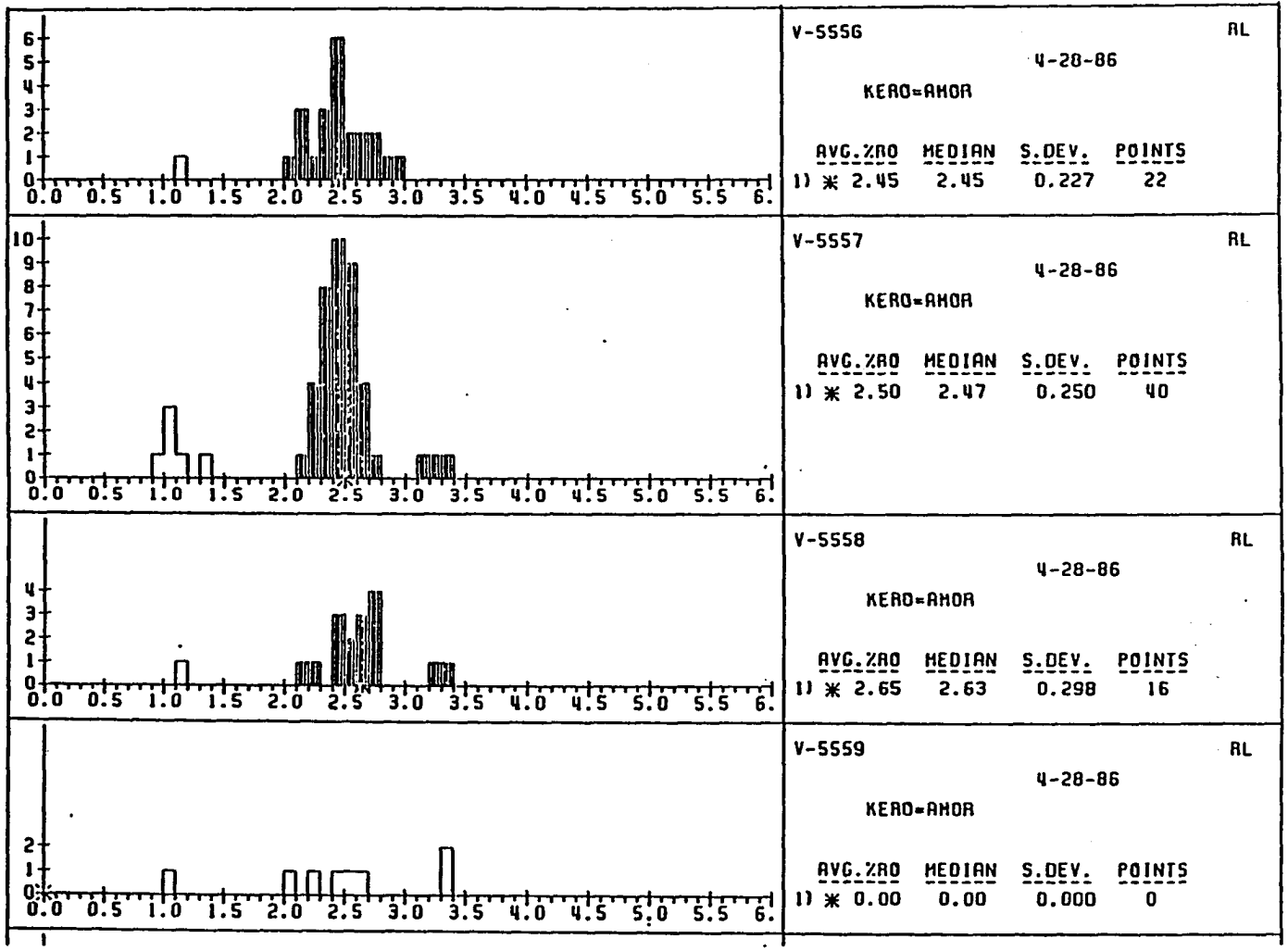

FIGURE 45c.

Histograms of vitrinite reflectance data.

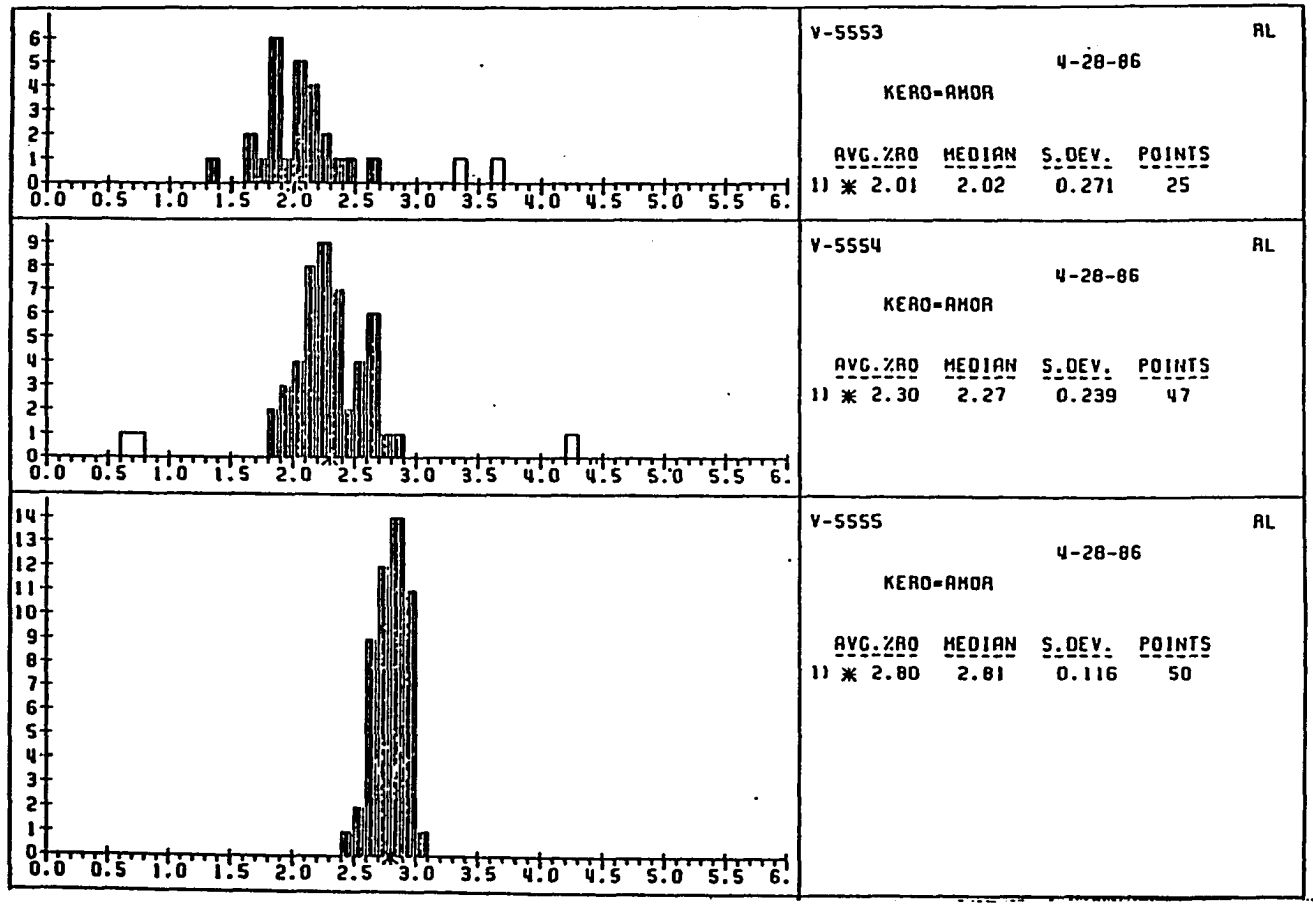

FIGURE 45d.

Histograms of vitrinite reflectance data.

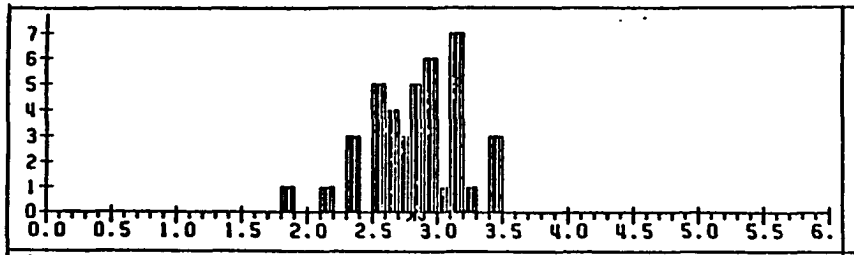

V-5560 AL

4-28-86

KERO-MIX

	AVG.%RO	MEDIAN	S.DEV.	POINTS
1) *	2.82	2.86	0.349	40

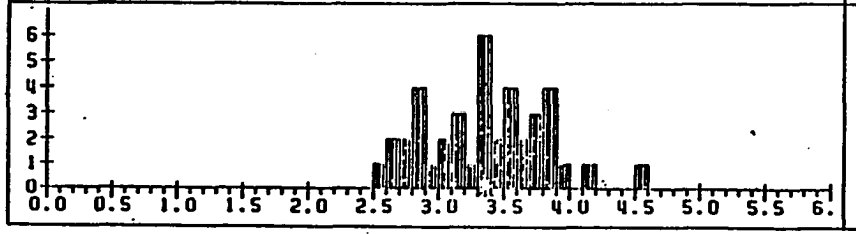

V-5561 AL

4-28-86

KERO-MIX

	AVG.%RO	MEDIAN	S.DEV.	POINTS
1) *	3.36	3.37	0.447	40

X-AXIS = PERCENT REFLECTANCE OF VITRINITE (%RO)

Y-AXIS = FREQUENCY

AVERAGE %RO FOR POP.1 = 2.65

One sample did not yield a value. The kerogen in eleven samples is characterized as amorphous and in the remaining two as mixed.

The samples in the first category ($3.36 < \%R_o < 3.99$) have a wide spread in $\%R_o$ values. In addition, within a single sample reflectance values may show a wide spread or more than one population of values. The practice employed in interpreting these histograms is to assume that the lowest $\%R_o$ values are produced by autochthonous organic material (Tissot and Welte, 1984, p. 516). The higher reflective component is the result of the incorporation of reworked vitrinite.

Such an assumption leads to the interpretation that the OM of the lower part of the Santiago (-100 m and below) is comprised of a relatively large fraction of reworked vitrinite. This reworked component decreases upward to a minimum (-24.9 m) before increasing again at the Santiago-Chipoco contact. A further increase in VR is observed in the ore zone. Above the ore zone the trend appears to be towards increasing VR levels.

An alternative interpretation of $\%R_o$ values of about 4.00 is that the OM has been subjected to near or incipient metamorphic (i.e. greenschist, T ~400°C) conditions. If this were true it would be expected that all the samples would show some effect. This is not the case, and metamorphism does not appear to have severely affected the OM.

THERMAL HISTORY

It was not possible to extract information regarding the maximum temperature to which these rocks have been exposed. Correlations of vitrinite reflectance data to maximum paleotemperature do not usually extend to $\%R_o$ values greater than about 2.5 (Kinghorn, 1983, p. 330). In addition, such a comparison does not take time of exposure into account.

The rocks in this area are undoubtedly graphitic. An attempt to utilize the Wada and Suzuki (1983) calcite-graphite geothermometer was made for the unmineralized rocks of the Santiago and the upper part of the Chipoco facies. This required two assumptions: first, that the isotopic composition of the kerogen was representative of the graphite, and second that the lower temperature end of the geothermometer is linear. The latter is a poor assumption; the first assumption may be permissable for the samples of the deep Santiago which have $\%R_o$ near 4.0. The value of $\%R_o = 4.0$ corresponds with the change from metagenesis to greenschist grade metamorphism. The stage during the alteration of OM (i.e. metagenesis to metamorphism) at which graphite becomes a significant component is unclear.

Temperatures obtained from these calculations ranged from 157 to 167 ^oC. The temperature range for greenschist metamorphic conditions is 375 to 425 ^oC (Mason, 1978, p.

198). Further work should be done to see if another avenue can be pursued to obtain the maximum temperature associated with burial.

$\delta^{13}C$ ANALYSIS OF KEROGEN

Measurements of the carbon isotope composition of kerogen from the 13 samples are shown in Table XIII. The average value for all samples is -27.0 ± 0.407°/oo PDB. The carbon isotope content of kerogen from rocks of the "Santiago" formation averages -27.1 ± 0.267°/oo PDB. Kerogen from the basal 4.5 m of the Chipoco facies (i.e. Capa A and Ore Zone) averaged -27.2 ± 0.478°/oo whereas three samples from the middle and upper part of the Chipoco had an average value of -26.8 ± 0.358°/oo. These data are within the range of values which delimit the L-amorphous kerogen variety of Lewan (1986). Such isotopic compositions have been found to be a characteristic of restricted basins overlain by stratified shallow water (<200 m) where the prevailing source of carbon in the photic zone is organically derived CO_2 (Lewan, 1986; and pers. comm.).

While at first glance there does not appear to be significant isotopic difference among the samples, a plot of $\delta^{13}C$ versus stratigraphic position shows some variation which, when considered with the sensitivity of these measurements (roughly ±0.0X °/oo), indicates significant deviations (Figure 44). Rocks in the upper part of the

Santiago have a more negative isotopic signature reaching a peak at the contact. The Ore Zone is marked by a sharp decrease in the lighter isotope (heavier $\delta^{13}C$ values) resulting in a +1°/oo shift. The isotopic composition returns to a more negative value in the middle Chipoco, then becomes heavier again in the upper Chipoco.

One goal of isotopic studies is to interpret the C isotopes in terms of the sources of the organic matter. Comparison of the data from this study with typical $\delta^{13}C$ composition of natural materials (Table XIV) suggests that the organic material may have been be derived from a mixture of land plants (-22 to -26 °/oo PDB) and marine lipids (-30°/oo PDB). Jurassic marine organic matter has $\delta^{13}C$ values in the range of -28.8 to -34 °/oo (Jenkyns and Clayton, 1986). These data are from abyssal depositional environments and may represent an extreme (i.e., representing little terrestrial input); thus, they may provide an accurate sample of marine organic matter in the Jurassic.

One plausible interpretation is that throughout the stratigraphic column in this area the isotopic values reflect a mixing of both terrestrial and marine organic matter. It follows that the observed stratigraphic variation results from variation in the amount of each component. These variations may in turn be linked to sea

TABLE XIV. TYPICAL CARBON ISOTOPE COMPOSITIONS OF NATURAL MATERIALS.

A)

Material	$\delta^{13}C_{PDB}$
Peedee belemnite (PDB)	0
Typical limestone	+5
Plankton lipids	-30
Marine plants	-10 to -18
Freshwater plants	-22
Land plants	-22 to -26
Crude oils	-20 to -32
Biogenic gas	-55 to -85
Thermogenic gas	-25 to -60

B)

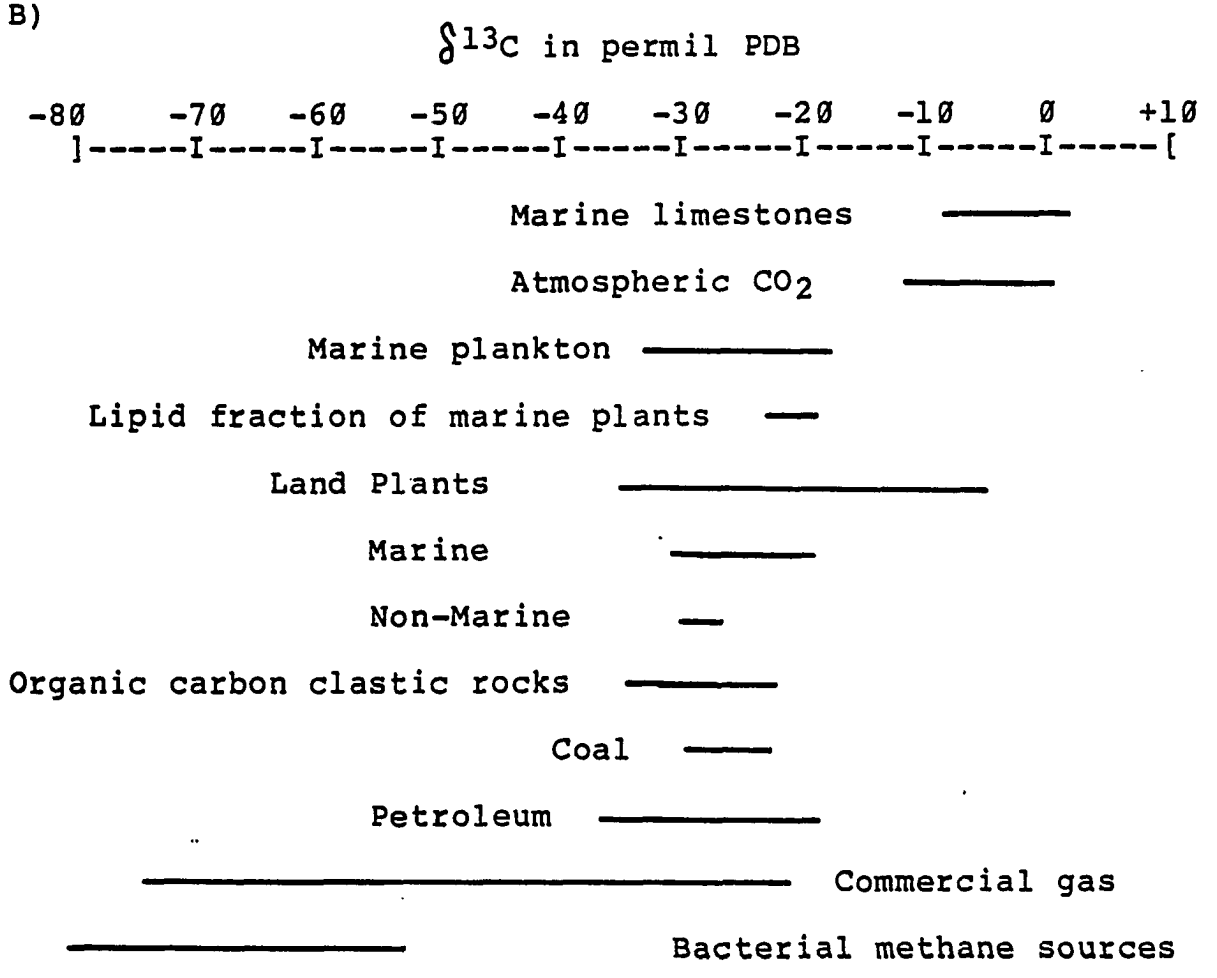

Data modified from Kinghorn, 1983.

level changes. The lower part of the Santiago contains "some mix" of terrestrial and marine OM. Near the top of the Santiago an increasingly negative $\delta^{13}C$ value is seen which, if the result of a larger contribution of marine organic matter, may depict a transgressive event. Sea level rise would be expected to decrease the terrestrial OM component in the sediment pile. Similarly, the sharp change to heavier values higher in the section may be the result of a relative increase in the terrestrial component, in this case, from a sea level fall.

A possible alternative to the above interpretation might be the presence of crude oils or thermogenic gas in the sample. However, this possibility is ruled out on the basis of the Rock-Eval and vitrinite reflectance data discussed above. Another argument to explain the light isotopic signature, if terrestrial OM is the dominant component, is bacterial reworking of the OM. Jenkyns and Clayton (1986, p. 99) note that bacterial reworking under reduced oxygen levels in bottom waters selectively removes heavy organic components and contributes bacterial cell matter to the sediment pile. This process would shift $\delta^{13}C$ compositions to lighter values.

DISCUSSION

Plots of $\delta^{13}C$ versus TOC and vitrinite reflectance versus TOC show no systematic relationships. This shows that neither $\delta^{13}C_{org}$ nor VR values are artifacts of organic

FIGURE 46.

$\delta^{13}C$ vs. TOC - showing no correlation between these two parameters.

ISOTOPIC COMPOSITION OF ORGANIC CARBON

VS. TOTAL ORGANIC CARBON CONTENT

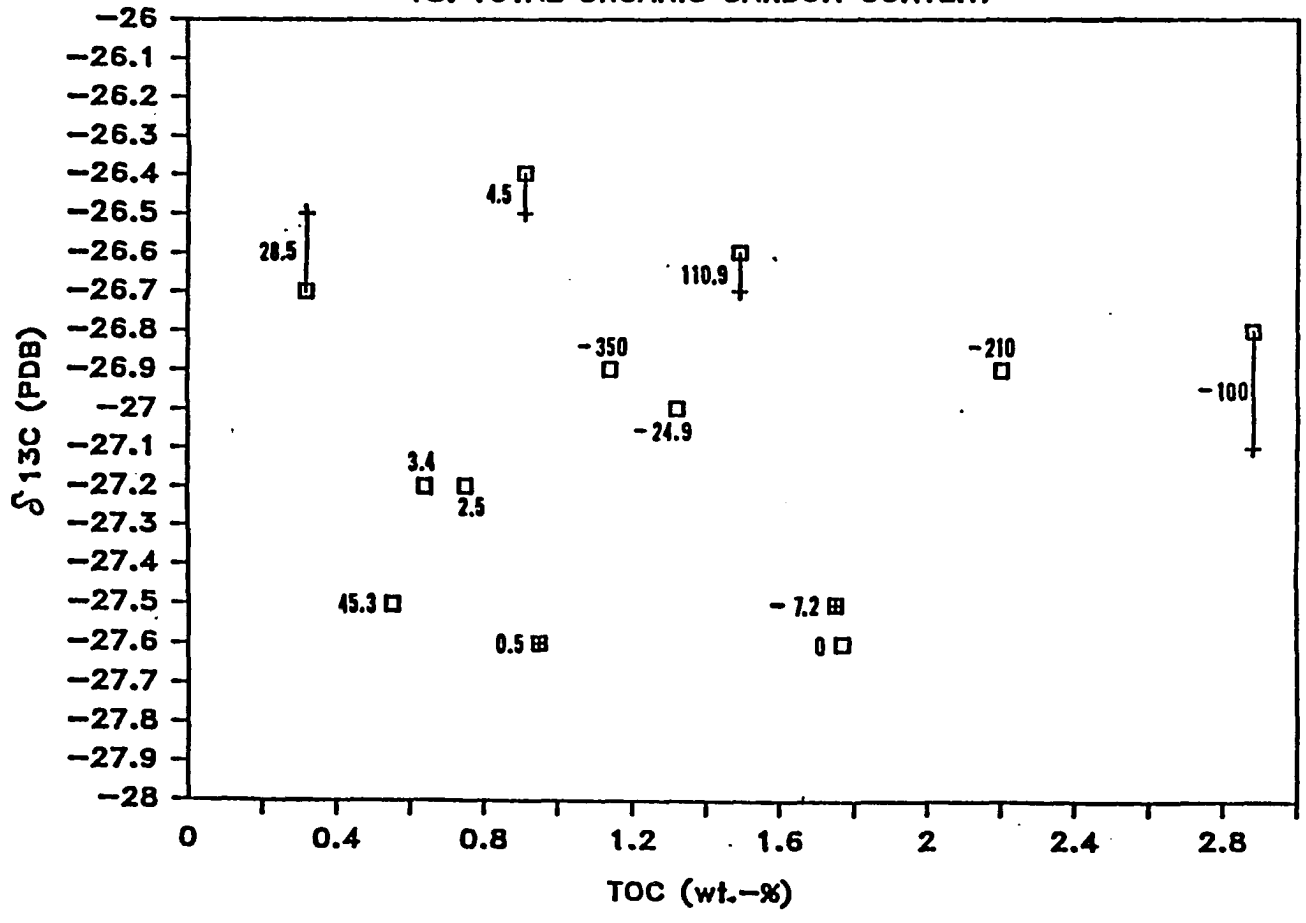

FIGURE 47.

Vitrinite reflectance vs. TOC - also showing no correlation between these two parameters.

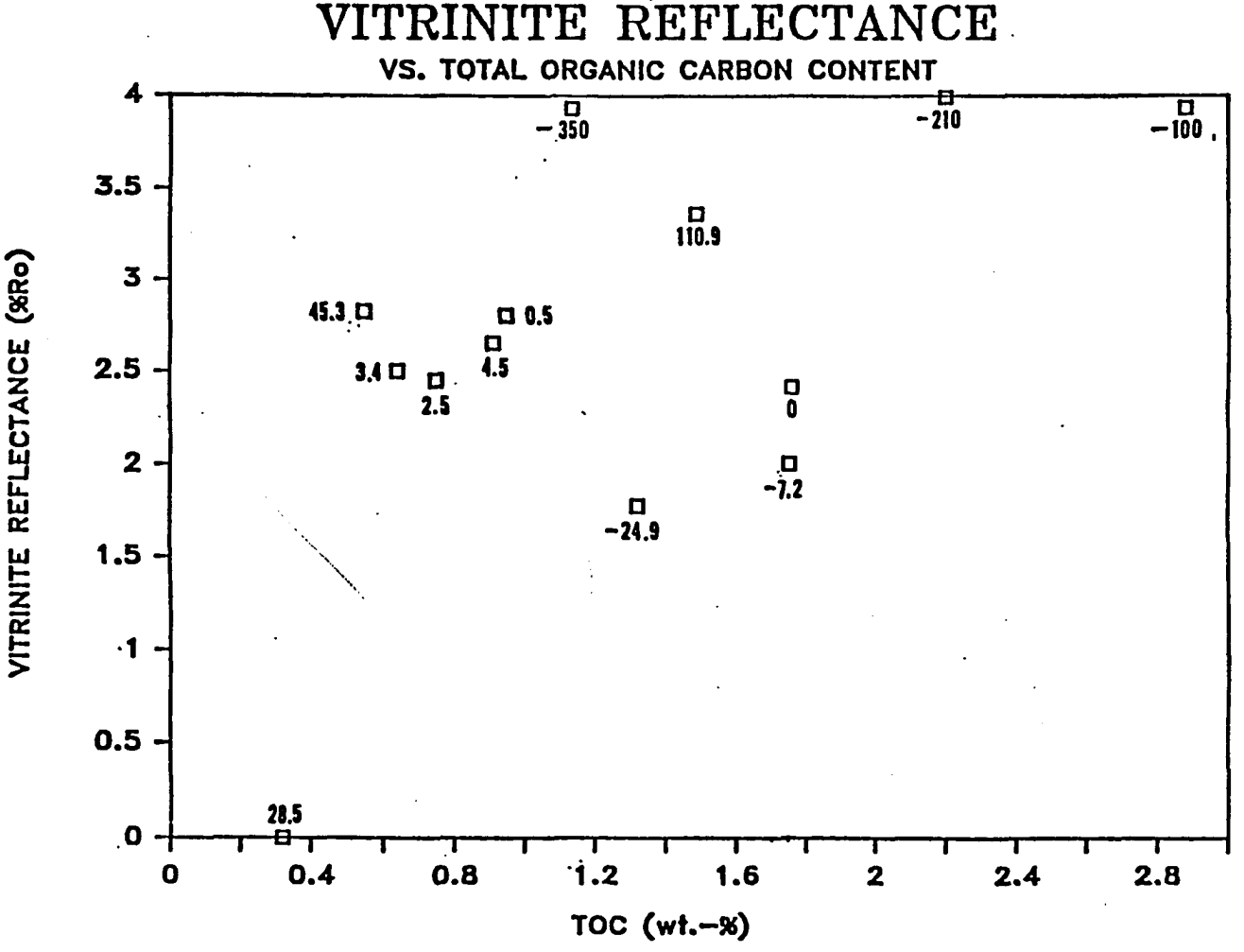

carbon levels (Figures 46 and 47). Isotopic values for organic carbon, plotted against VR, illustrate the changes from relatively heavy isotope and high $\%R_o$, in the lower part of the Santiago, to lighter isotope compositions having lower $\%R_o$ values in the upper part of the Santiago and in the ore zone. Reflectivity measurements for the upper part of the Chipoco have values similar to those in the lower part of the Santiago (Figure 48). The data obtained from these analyses can all be explained in terms of either (1) the variation in the source of organic material (terrestrial versus marine OM component) or (2) in the nature of the depositional environment, which would change the degree of bacterial reworking. In either case, it is possible to postulate a relation between the OM character and the relative sea level changes affecting the depositional area.

Source of OM as the Control - In this interpretation, high VR values are considered to be the result of the presence of reworked vitrinite, and the overall character of the organic matter is considered to be a function of the relative contribution of marine and terrestrial organic matter. It follows that the lower part of the Santiago, taken in this discussion to represent a background level in depositional and environmental conditions, contains abundant reworked vitrinite. In addition, the earliest sediments possibly contained a larger fraction of

FIGURE 48.

Plot of del^{13}C versus vitrinite reflectance showing the trend in samples according to their stratigraphic position. Note the position of the contact (labelled 0) and the ore zone (labelled 2.5, and 3.4). "+" symbols are duplicate analyses and are connected to their corresponding analysis by a straight line. The transgressive - regressive labels refer to the source - control model of organic matter properties.

ISOTOPIC COMPOSITION OF ORGANIC CARBON

VS. VITRINITE REFLECTANCE

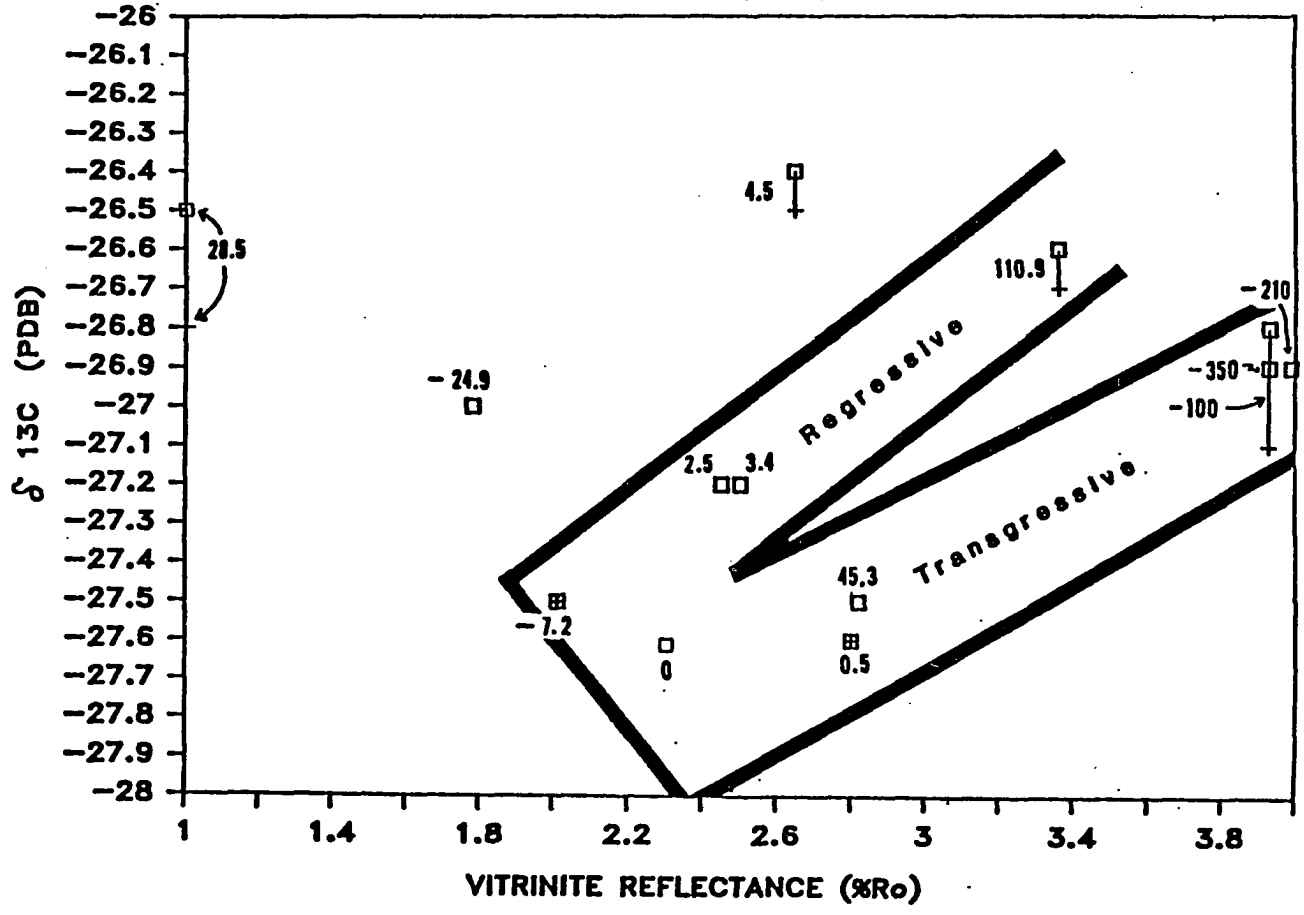

terrestrial OM relative to marine OM. This inference, which is based on the isotopic composition, is reasonable given the high component of reworked vitrinite.

The upper part of the Santiago, from -24.9 m to the contact with the superjacent Chipoco facies, could be interpreted as the result of a transgressive event. The more negative isotopic composition reflects a decrease in the heavier terrestrial OM, which would have been restricted to inland bays and estuaries during times of rising sea level. In addition, a high sea level favors increased surface productivity. Accompanied by anoxic conditions in the underlying water, this may lead to increased TOC levels marked by an absolute or relative decrease in the reworked component (i.e. a lower $\%R_o$) and a more negative carbon isotope ratio.

The data from the ore zone and the middle of the Chipoco facies would indicate a regressive episode. This is suggested by an increase in $\delta^{13}C$, which signals a decrease in the marine OM component, and corresponding decreases in TOC. No vitrinite was found in the sample from +28.5 meters.

The arguments given above might also lead to the support a second transgressive event at the base of the upper part of the Chipoco facies (+45.3 m). However, this sample is from a pelecypod shell hash, and its isotopic composition should be expected to contain a greater marine OM

contribution. Therefore this shift to a lighter isotope ratio is not signalling a sea level rise. Note that a regressive event may be indicated by both TOC and VR increases. Addition of reworked terrestrial OM, released from inland reservoirs with falling sea level, should cause both TOC and VR to increase. Regression in this interval is consistent with the character of the rocks overlying the Chipoco facies (i.e. calcarenites and evaporites of the San Andres Member).

It is interesting to speculate on the significance of isotopic variations that might be caused by biologic processes. The contribution of bacterial OM to a decrease in the isotopic ratio would be greater in dysaerobic to anoxic conditions. The entire known Santiago and the lower two-thirds of the Chipoco facies appear to have been subjected to dysaerobic or anoxic conditions. That being the case, the Santiago may be considered to be a baseline representing the near maximum contribution of bacterial processes to the organic carbon reservoir. Thus, further negative deviations must reflect marine OM introduced to the sediment pile from the water column. This concept may be supported by the sample from +45.3 meters, which consists of an articulated and disarticulated pelecypod shell hash. The contribution of the anomalous quantity of marine OM may have resulted in the nearly $-1^{o}/oo$ deviation in the $\delta^{13}C$ composition observed.

Depositional Environment as the Control - Toxopeus (1983) reported that two types of vitrinite may be distinguished by their differing reflectivity: "vitrinite-1" has a higher reflectivity than "vitrinite-2". Vitrinite-1 is characterized as being the least oxidized form and as having escaped microbial attack during sedimentation. Vitrinite-2 is considered to be allocthonous (i.e. redeposited) landplant matter which has undergone partial alteration by bacterial activity and is therefore more oxidized. These two types of vitrinite react differently under identical thermal stress. Vitrinite-1 reacts most quickly and therefore acquires a higher VR, relative to the more refractory vitrinite-2, for a given period of time (Lewan, 1985 and pers. comm.; Toxopeus, 1983, p. 302; Antia, 1986).

These characteristics provide a basis for an alternative interpretation of the VR profile documented in this study. Laminated black shales often contain a predominance of vitrinite-1 whereas mudrocks may contain more of the vitrinite-2 matter (Lewan, pers. comm.) It is possible that the lower part of the "Santiago" formation, a laminated black shale, may contain more of an unoxidized vitrinite-1 component than the upper, more poorly laminated, pelletal Santiago. Such an assumption would be consistent with the expectation that vitrinite accumulating under anoxic conditions (i.e. Santiago black shale) should

be less oxidized than vitrinite deposited in association with rocks showing evidence of higher oxygen levels (e.g. pelletal textures). The resulting VR values measured are thus a function of the relative amount of each vitrinite-type present, but may in this interpretation also indicate the nature of the depositional conditions under which the OM accumulated. High VR values from the upper Chipoco facies, which is considered to have accumulated under relatively higher oxygen levels than the subjacent rocks, may be the result of a larger quantity of vitrinite-1 (i.e. unaltered organic matter) contained in the oolite fraction. The preservation of unweathered organic matter within ooids has been documented by Ferguson and Ibe (1981) and Ferguson et al. (1984), and ooids are a significant component in this part of the section.

The interpretation of the VR values in light of possible variations in the proportions of vitrinite-1 and vitrinite-2 results in an interpretation of the type of OM present that differs from the source interpretation. For example, the OM of the lower Santiago might not be reworked as was inferred from the likely source of organic matter. In addition, the upper Santiago might contain a greater amount of partially oxidized OM, as indicated by the lower VR values. Vitrinite in the ore zone has a slightly higher reflectivity which may mean a decrease in the quantity of oxidized OM (i.e. of vitrinite-2).

This interpretation of the vitrinite pattern focuses on the oxygen levels in the basin. It is obvious from the lithology of the lower part of the "Santiago" formation that anoxic conditions prevailed. The VR profile may indicate that the basin became slightly more oxidizing during accumulation of the upper part of the Santiago, consistent with its lithology. Furthermore, the VR values from the ore zone may signify a return to more anoxic conditions (i.e. a transgression).

It is more difficult to make a case for relative sealevel changes based on the VR values using this interpretation. However, has been noted by many workers that transgressive events can be accompanied by the establishment or enhancement of anoxic conditions in the water body (Schlanger and Jenkyns, 1976; Fischer and Arthur, 1977). Assuming, in general, that a transgressive event leads to anoxia, a trend towards high VR would indicate transgression, towards low VR regression. The VR data could be suggesting a regressive event in the upper part of the Santiago followed by a transgressive event at the base of the Chipoco facies (i.e. the ore zone). No additional inferences with regard to superjacent rocks are possible because the vitrinite component in the upper part of the Chipoco is contained in the allochems of the rock. Note this is the opposite of the conclusion of the source model.

Obviously, the apparent cycles are averages of many smaller events not depicted because of the sample spacing. It would be beneficial to have additional analyses in order to refine the stratigraphic profiles. Nevertheless, the carbon isotope values can be interpreted to indicate a sea level transgression in the upper "Santiago" formation. The vitrinite reflectance data is probably best interpreted in the context of the recent work characterizing the kinetic properties of reflectance, because this approach takes into account the source, environment of deposition, and post-depositional effects on the vitrinte. Thus, the interpretation of the data, currently favored, is that the top 100 meters of the "Santiago" formation is dominated by a regressive event, which was followed by a transgression in the top 10 meters that continued into the Chipoco facies.

The inference of sea level changes, whichever model is followed, is tenuous given the limited number of data. More data are required to establish any firm trends. It is important to note that if an oxidizing event (regardless of sea level change) occurs below the ore zone, it is a potentially important part of any model based on an oxide precursor for the Mn carbonates. That is, the oxidizing event may act to concentrate large quantities of manganese in the sediment pile.

It is important that manganese mineralization occurred

near the peak of the supposed transgressive event. This is exactly the same timing of mineralization that has been deduced for other giant manganese deposits such as Chiatura (Cannon and Force, 1983; Bolton and Frakes, 1985) and Groote Eylandt (Cannon and Force, 1983; Frakes and Bolton, 1984). The inferences regarding relative sea level changes permitted by these data are in harmony with the global sea level positions for the late Jurassic as interpreted by Vail et al. (1984). The data from this study would seem to point to a high stand of sea level at the Santiago - Chipoco contact, which is located at the Oxfordian - Kimmeridgian time boundary.

CHAPTER VII. SUMMARY AND CONCLUSION

The data collected from this study provide insight and constraints on the conditions and processes that led to manganese mineralization at Molango. However, these data do not define a single scenario for manganese precipitation; rather several possibilities remain, which cannot be excluded without additional study.

SALIENT ASPECTS OF THE DATA

Lithologic, petrographic, and paleontologic characteristics of the rocks studied indicate that the "Santiago" formation and Taman Formations formed from sediments deposited in a marine environment. The unfossiliferous, laminated, pyritic nature of the lower part of the Santiago exposure is consistent with deposition under euxinic conditions. Sediments of the upper part of the Santiago may have accumulated under similar conditions but apparently received a larger amount of carbonate and non-carbonate clastic material, suggesting that the source area was nearer or more active during that time. Movement of the clastic source area toward the basin could be the result of progradation, or of sea level fall. Enhanced carbonate productivity (e.g. widening of the zone inhabitable by organisms) made possible by more oxidizing conditions is another explanation, but it cannot account for the increase in terrigenous clastic material.

The presence of shell beds in the lower part of the

Chipoco facies and the likely algal origin of the sediments would necessitate more oxidizing conditions for the lower part of the Chipoco. Low energy levels and the paucity of fauna imply that deposition took place below storm wave base and under conditions too hostile chemically to support a normal marine benthic fauna. Whether or not the water column contained a normal fauna is not clear. A schematic summary of the depositional paleo-environments is presented in Figure 49.

Petrographic observations, such as the fine-grained crystal size of the ore minerals and the deformation of mineralized laminae by soft-sediment slumping, suggest that manganese mineralization was very early and not the result of replacement upon recrystallization. The very low concentration of Ca, and the lack of Ca-rich zones (especially in the center of clots and laminae), are also believed to argue against the replacement of any precursor carbonate.

Stable isotopic ratios for carbon from whole rock samples in the mineralized zone are interpreted to reflect the relative contribution of two carbon reservoirs. I propose that both organically derived and seawater-derived bicarbonate contributed to the measured $\delta^{13}C$ ratio. The most feasible interpretation of the carbon isotopic evidence is that the very light values of the ore zone represent predominantly organic-derived carbonate produced

Figure 49.

Schematic summary of the inferred depositional paleo-environments, at the time of mineralization, based upon literature review and the observation made in this study.

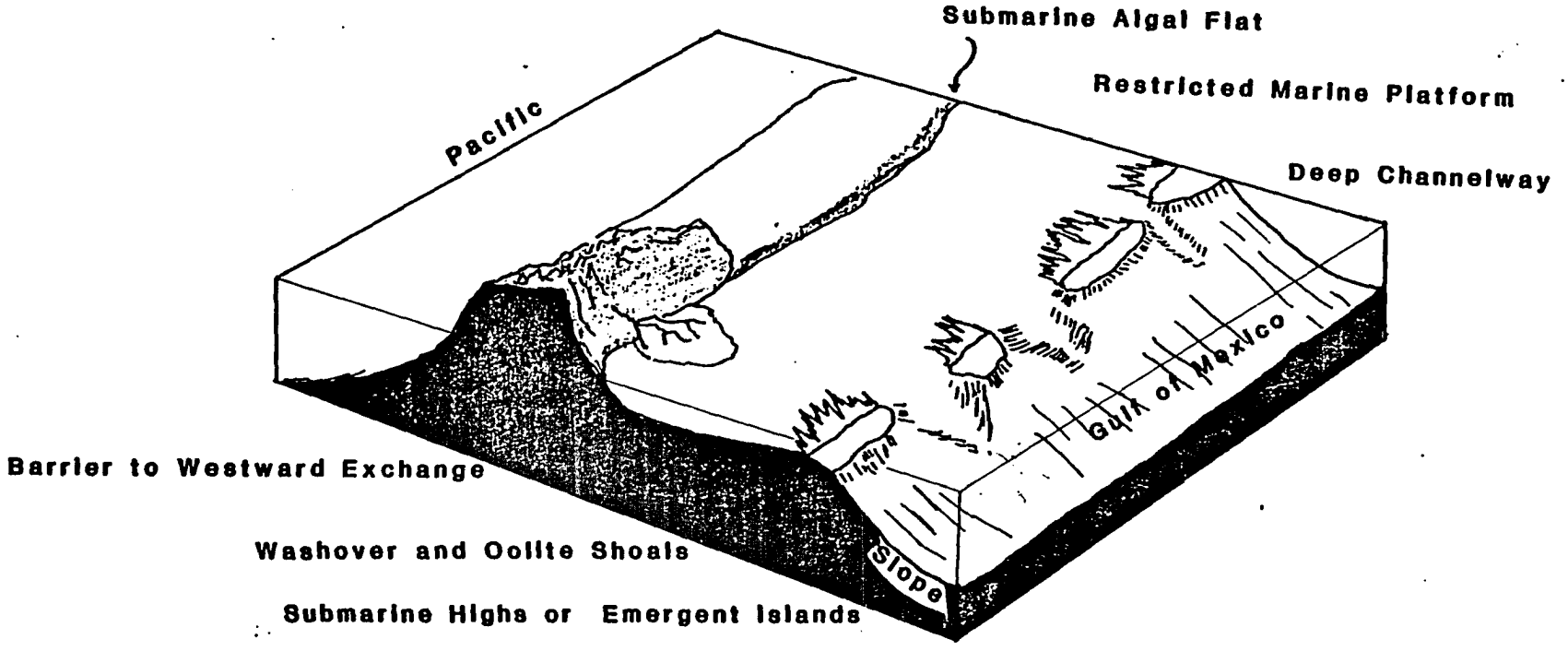

by manganese and nitrate reduction rather than by sulfate reduction. This is suggested by the lack of sulfide in the high-grade ore zone. The heavier values of $\delta^{13}C$, found in the carbonate minerals overlying the high grade ore zone, reflect a decreasing contribution of organically derived bicarbonate, probably resulting from a decrease in pH and increase in oxygen levels in the water.

Organic carbon characteristics, i.e. vitrinite reflectance and isotopic ratios, are compatible with an anoxic depositional environment for the lower part of the Santiago and a relatively more oxidizing environment in the upper part of the Santiago. The uppermost Santiago and the lower Chipoco facies are more ambiguous. The data could support either a transgression or a continuation of regression. Howver, manganese mineralization is believed to have occurred at a sea level highstand based on the data of Vail, et al. (1984) on global sea level changes, which favors the transgressive interpretation of the organic geochemical data for the ore zone.

MODELS FOR MINERALIZATION

The general model that is most reasonable for the origin of mineralization at Molango is the so called "Bath-tub" ring model of Cannon and Force (1983). The applicability of this model is indicated by the lack of volcanic or hydrothermal activity in the vicinity of the deposit, mineralization having occurred during a time of high sea

level and near the intersection of the redoxcline on the basin margin. However, three variants of the model are possible: (I) a Direct Precipitation model, (II) a Static, Diagenetic model, and (III) a Transgressive Diagenetic model.

Direct Precipitation - In this variation of the general model (Figure 50a), manganese mineralization occurs by the precipitation of divalent manganese from seawater or porewaters as a carbonate. The carbonate precipitated from seawater would probably have an isotopic signature near 0 per mil (PDB), whereas precipitation from porewater could produce a very negative $\delta^{13}C$ ratio. It does not seem feasible that seawater could develop such a negative $^{13}C/^{12}C$ ratio as observed for the high grade ore zone, because no restricted basins are known with such light bicarbonate.

Static Diagenetic - In this model, the oxic-anoxic interface remains essentially immobile throughout the time of mineralization (Figure 50b). Dissolved divalent manganese in the anoxic layer diffuses to the oxic boundary, where it is converted to an oxidized solid (e.g. oxide, hydroxide, oxyhydroxide) and sinks to the sea floor. On the sea floor the manganese oxides undergo reduction and react with the bicarbonate released the from degradation of organic matter to produce a manganese carbonate. This process would be characterized by a carbon isotope value

depleted in the ^{13}C atom (i.e. isotopically light). The magnitude of the isotopic ratio would be a function of the relative contributions of the seawater and organic bicarbonate sources.

Transgressive Diagenetic - The transgressive diagenetic model embodies a mobile oxic-anoxic interface (Figure 50c). In this model the primary manganese phase is also an oxide. As the anoxic boundary advances landward the establishment of reducing conditions allows the oxide to be reduced and to interact with bicarbonate ions derived from the processes of dysaerobic or anaerobic respiration. The resulting carbonate would be isotopically identical to carbonate in the Static Diagenetic model.

All these models would probably produce a very fine-grained precipitate as a result of crystallization from supersaturated solutions; thus, they might not be distinguishable by petrographic observations. Chemical differences between Direct Precipitation (Model I) and the other Models II and III may exist because in the latter two cases a Mn-oxide is involved which may contain or have adsorbed heavy metals. Enrichment of these metals, as observed in the whole rock sample and accessory minerals (i.e. pyrite, Fe-oxides) of the high grade ore zone, may indicate that a Mn-oxide form was a precursor to the Mn-carbonate. Whether or not such an Mn-oxide was present in the form of an oxide bed on the sea floor, as in the

Figure 50a.

Direct Precipitation Model for the origin of manganese mineralization. See text for discussion.

Figure 50b.

Static Diagenetic Model for the origin of manganese mineralization. Note that carbon is contributed from the water column and from organic matter in the sediment pile.

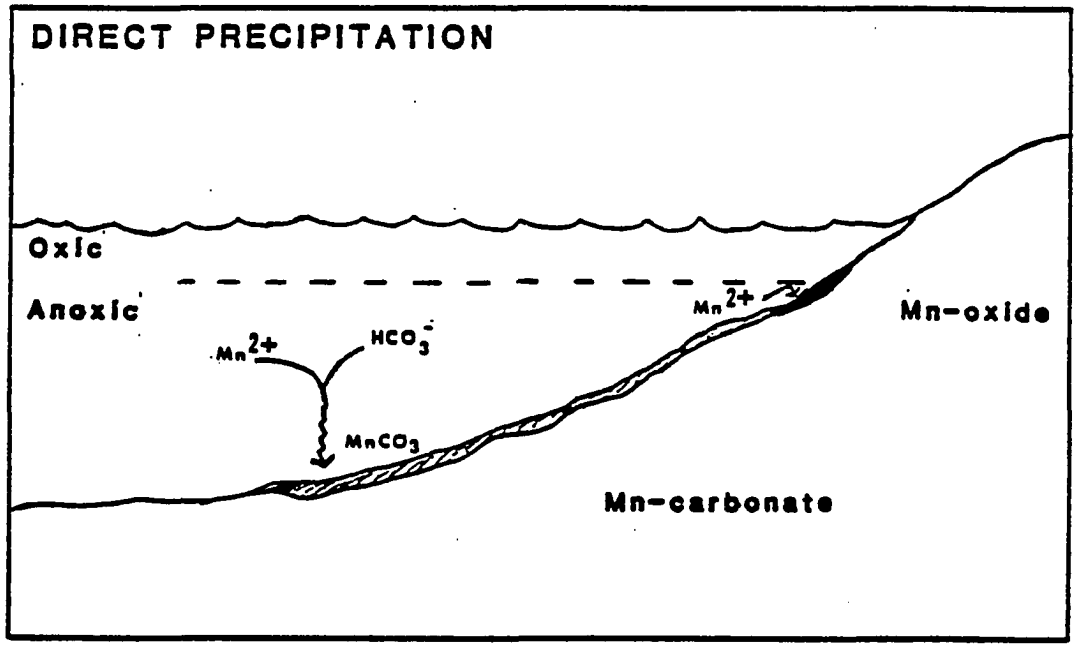

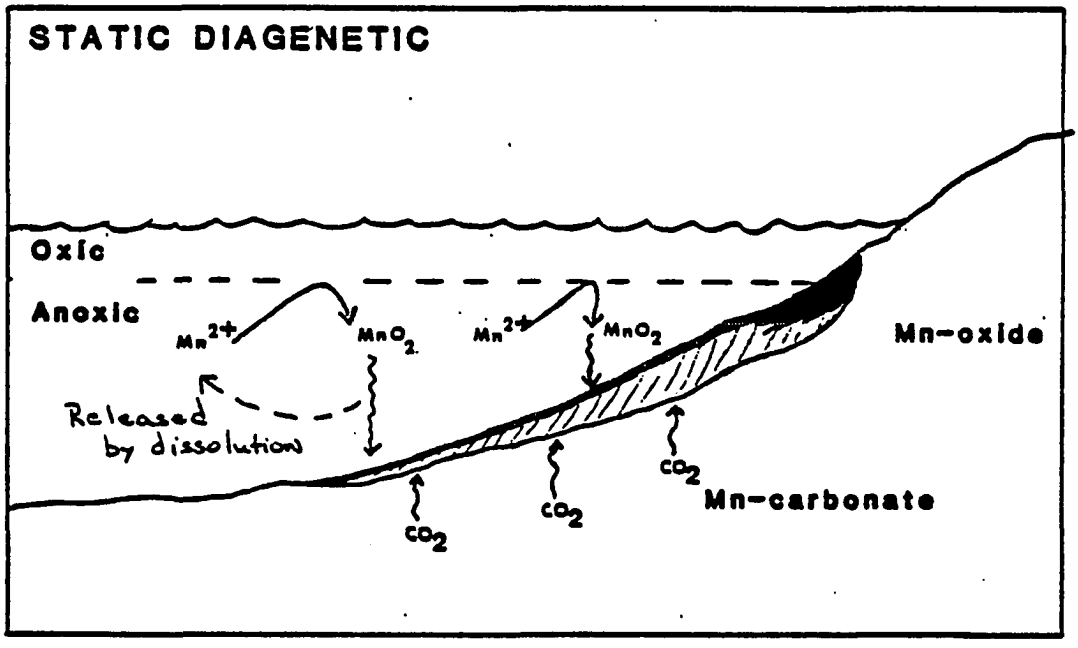

Figure 50c.

Trangressive Diagenetic Model for the origin of manganese mineralization. Depicted is an "initial" state (T=0) that is followed in time by a trangression of the anoxic/oxic boundary (T=1). This may result in the conversion of the Mn-oxide, formed at T=0, to a carbonate thereby increasing the size of the carbonate orebody. The processes of precipitation and sources of carbon are the same as shown in Figure 50b.

TRANSGRESSIVE DIAGENETIC

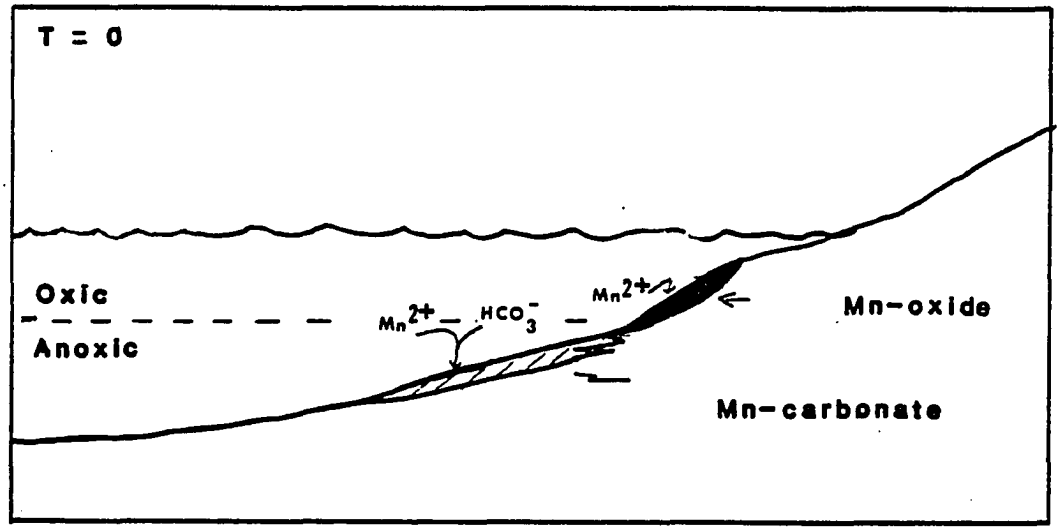

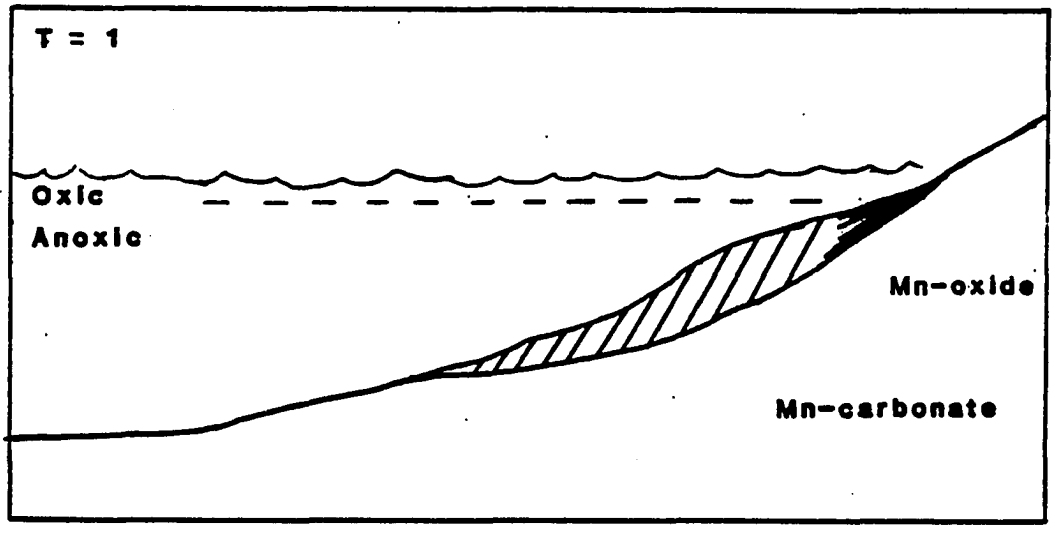

Transgressive Diagenetic Model (Model III), or was only transiently present as pelagic particles, as in the Static Diagenetic Model (Model II), is uncertain and thus Models II and III are chemically indistinguishable. An argument against an oxide bed as a precursor is the absence of any remnant manganese oxide in the ore zone, although iron oxides are present. The importance of this constraint depends on the rate of transgression and the thickness of the oxide bed. If reducing conditions can be maintained for a sufficiently long time then perhaps all the Mn-oxide could be reduced and converted to carbonate. Indeed, it is necessary to consider whether the time required to precipitate a deposit such as Molango is reasonable for the Static Diagenetic Model. This model is somewhat more appealing in explaining the absence of any residual Mn-oxides because conversion could easily take place at a rate faster than accumulation.

Given the results of this study, it is impossible to champion only one of the variations. Isotopic data appear to rule out a syngenetic seawater precipitation mechanism for the origin of the Molango manganese deposit. Given the data from this study I favor a diagenetic origin for the Mn-carbonates and believe them to have been derived from a precursor Mn-oxide. The grain size and physical distribution (e.g. dispersed particulates, bedded accumulation) of the oxide minerals are uncertain at this time.

APPLICATION OF MODELS AT MOLANGO

The "Bath-tub Ring" model can be envisioned to take three possible forms given the general paleogeographic characteristics of the region (Figures 5, 6, 7, 49, and 51). The result of the various configurations would be the precipitation of a landward oxide and basinward carbonate deposit, or the development of only a carbonate deposit. This is important in view of the absence, to date, of any documentation of a primary Mn-oxide deposit at Molango. I do not mean to imply that a primary oxide did not develop landward of the carbonate orebody; it may have done and subsequently been removed by erosion. However, the total loss of what would probably be a mineralized zone larger than the presently known carbonate orebody seems unlikely.

The paleogeographic position of the mineralized site may be either landward or seaward of the archipelago. The depositional environment was probably in a restricted, shallow marine environment, below storm wave base but shallower than 300 meters, and in a region dominated by algae. This would mean that mineralization could have taken place in a back barrier environment or around one of the topographic highs (e.g. islands) present during the time.

Figure 51.

Three possible configurations for mineralization as a function of the extent of ocean anoxic conditions and the nature of the pathways and barriers to water masses (and hence Mn-transport). These drawings are intended to represent possible conditions based on the inferred paleogeography of the study area (e.g. topographic highs/emergent areas, channels between highs).

"BATH-TUB RING" MODEL

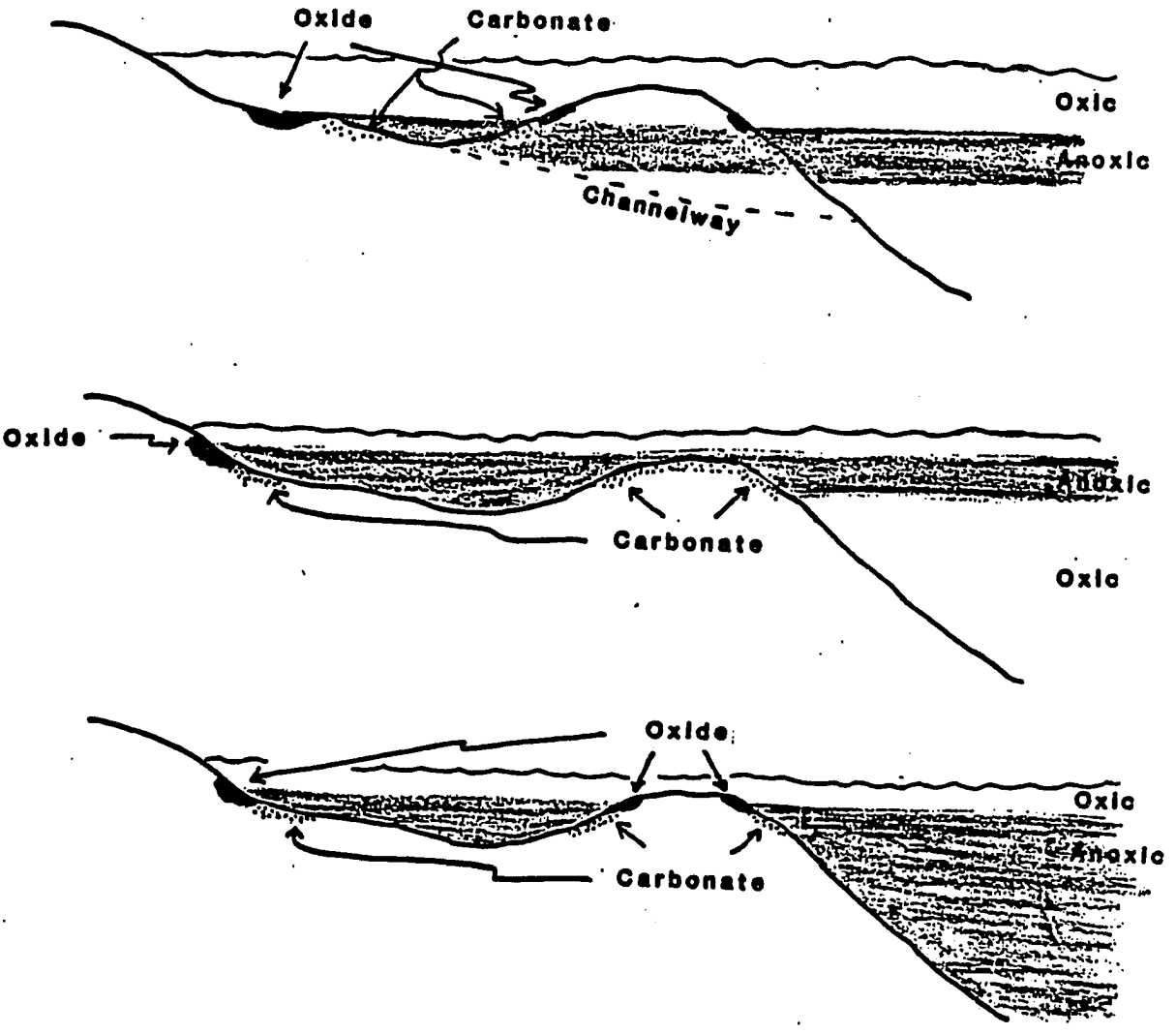

RECOMMENDATIONS FOR FURTHER WORK

Investigation of other localities (e.g. Acoxcotlan, Naopa, and others) is required to determine if the ore zone is confined to a single type of lithology or if it cross-cuts several lithologies. In addition, further study of the "Santiago" formation and the units of the Taman Formation (Chipoco, San Andres) for the purposes of correlation and further understanding of depositional environments and paleogeography is very important.

A comparison of the mineralogy in the ore zone between the Tetzintla location and others would improve the understanding of chemical characteristics of the mineralizing fluid and possibly lead to refinement of the factors controlling mineralization. Further chemical analyses of the trace metal composition in whole-rock pulps and in accessory minerals may provide insight into the chracter of oxide precursors (is any). The analysis of sulfur isotopes from sedimentary pyrite would be useful in understanding changes in basin circulation and hence in delineating the spatial distribution of anoxic conditions. Similarly, additional data on the organic carbon component would clarify the ambiguities in the current interpretation of source and sea level change.

Finally, understanding (a) the fractionation factor for oxygen in rhodochrosite, (b) the kinetics associated with Mn oxidation-reduction, and (c) the partitioning of

divalent cations into Mn-rich carbonate minerals would certainly allow a more informed interpretation of the data collected from this study.

REFERENCES CITED

Aguayo-Camargo, J.E., 1977, Sedimentacion y diagenesis de la Formacion "Chipoco" (Jurasico Superior) en afloramientos, Estados de Hidalgo y San Luis Potosi, Revista del Instituto Mexico del Petroleo, v. 9, p. 11-37.

Aguilera H., E., 1972, Ambientes de deposito de las formaciones del Jurasico Superior en la region Tampico-Tuxpan, Boletin de la Asociacion Mexicana de Geologios Petroleos, v. 24,p. 129-163.

Analysis of Exploration and Mining Technology for Manganese Nodules, 1984, United Nations, Ocean Economics and Technology Branch, Seabed Mineral Series, v. 2, Graham and Trotman in co-operation with the U.N., 140p.

Anderson, T. F., and Arthur, M. A., 1983, Stable isotopes of oxygen and carbon and their application to sedimentologic and paleoenvironmental problems, in Stable Isotopes in Sedimentary Geology, Soc. Econ. Paleontolog. and Mineralog. Short Course Notes No. 10, p. 1-1 -- 1-151.

Anderson, T. H., and Schmidt, V. A., 1983, The evolution of Middle America and the Gulf of Mexico-Caribbean Sea region during Mesozoic time, Geol. Soc. Amer. Bull., v. 94,p. 941-966.

Antia, D. D. J., 1986, Kinetic method for modeling vitrintie reflectance, Geology, v. 14, p. 606-608.

Assessment of Manganese Nodule Resources, 1982, United Nations, Ocean Economics and Technology Branch, Seabed Mineral Series, v. 2, Graham and Trotman in co-operation with the U.N., 79p.

Berner, R. A., 1980, Early Diagenesis - A Theoretical Approach, Princeton Univ. Press, Princeton, 241p.

_____, 1981, A new geochemical classification of sedimentary environments, J. Sed. Pet., v. 51, p.359-365.

Bolton, B. R., and Frakes, L. A., 1985, Geology and genesis of manganese oolite, Chiatura, Georgia, U.S.S.R., Geol. Soc. of Amer. Bull., v. 96, p. 87-102.

Bonatti, E., Kraemer, T., and Rydell, H. S., 1972, Classification and genesis of submarine iron-manganese deposits, in, D.R. Horn, Ed., Ferromanganese Deposits on

the Ocean Floor, National Science Foundation, Washington, p. 159-166.

Brand, U. and Veizer, J., 1980, Chemical diagenesis of a multicomponent carbonate system. 1. Trace elements, J. Sed. Petrol., v. 50, p. 1219-1236.

Burns, R. G., and Burns, V. M., 1979, Manganese oxides, in R. G. Burns, Ed., Marine Minerals, Mineralogical Soc. Amer. Short Course Notes, Rev. in Mineralogy, v. 6, p. 1-46.

Cannon, W. F.,and Force, E. R., 1983, Potential for high-grade shallow-marine manganese deposits in North America in: Unconventional Mineral Deposits, W. C. Shanks, ed. American Institute of Mining, Metallurgical, and Petroleum Engineers, New York, p. 175-190.

Cantu-Chapa, A., 1969, Estratigrafia del Jurasico Medio-Superior del Subsuelo de Poza Rica, Ver. (Area de Soledad-Miquetla), Rev. del Inst. Mex. del Petr., v. 1, p. 3-9.

_____, 1971, La serie Huasteca (Jurasico Medio-Superior) del centro este de Mexico, Rev. del Inst. Mex. del Petr., v. 3, p. 17-40.

Carrillo-Bravo., J., 1965, Estudio geológico de una Parle de Anticlinorio de Huayacocotla, Boletin de la Asociacion, p. 73-96.

Chelen-Franulic, J. D., 1976, Analisis estructural del yacimiento manganesifero de Tetzintla, Hidalgo, Mexico, Congreso Latinoamericano de Geol. Resumenes, v. 3, p. 34.

Clayton, R. N., 1961, Oxygen isotope fractionation between calcium carbonate and water, J. Chem. Phys., v. 34, p. 724-857.

Coleman, M. L., 1985, Geochemistry of diagenetic non-silicate minerals: kinetic considerations, Phil. Trans. Roy. Soc. Lond., A, v. 315, p. 39-56.

Coleman, M. L., Fleet, A., and Donson, P., 1982, Preliminary studies of manganese-rich carbonate nodules from Leg 68, Site 503, eastern equatorial Pacific, Init. Rep. of the Deep Sea Drilling Proj., v. 68, p. 481-489.

Coleman, M. L., and Raiswell, R., 1981, Carbon, oxygen, and sulphur isotope variations in concretions from the Upper Lias of N.E. England, Geochim. et Cosmochim. Acta, v.

45, p. 133-149.

Cronan, D. S., 1976, Manganese nodules and other ferro-manganese oxide deposits, in J. P. Riley and R. Chester, Eds., Chemical Oceanography Volume 5, 2nd Ed., Academic Press, London, p. 217-263.

Curtis, C. D., 1977, Sedimentary geochemistry, environments and processes dominated by involvement of an aqueous phase, Phil. Trans. Royal Soc. London, v. A286, p. 353-372.

_____, Coleman, M. L., and Love, L. G., 1985, Detailed history of burial diagenesis of a Westphalian coal measures sequence, from isotopic and mineral chemistry of siderite, dolomite and calcite concretions, Geochim. et Cosmochim. Acta, preprint from authors.

deCapitani, C., and Peters, T., 1981, The solvus in the system $MnCO_3$-$CaCO_3$, Contrib. Mineral. Petrol., v. 76, p. 394-400.

DeYoung, J. H., Jr., Sutphin, D. M., and Cannon, W.F., 1984, International strategic minerals inventory summary report - manganese, U. S. Geol. Surv., Circ. 930-A, 22p.

Dickson, J. A. D., and Coleman, M. L., 1980, Changes in carbon and ox;ygen isotope compositions during limestone diagenesis, Sedimentology, v. 27, p. 1-12.

Drever, J. I., 1984, The Geochemistry of Natural Waters, Prentice-Hall, New Jersey, 388p.

Enos, P., 1983, Late Mesozoic paleogeography of Mexico, in M.W. Reynolds and E.D. Dolly, Eds., Mesozoic Paleogeography of West-Central United States, Rocky Mountain Section - Soc. Econ. Paleontolog. Mineralog., P. 133-157.

Erben, H. K., 1956, Estratigrafia y Paleontologia del Jurasico Inferior y Medio Marino de la region Central de la Sierra Madre Oriental, XX Intl. Geol. Cong. Field Excursion C-8, p. 9-30.

Ferguson, J., and Ibe, A. C., 1981, Origin of light hydrocarbons in carbonate oolites, J. Petrol. Geol., v. 4, p. 103-107.

_____, Bush, P. R., and Clarke, B. A., 1984, The role of organic matter in the early diagenesis of carbonate ooids - An experimental study, J. Petrol. Geol., v. 7, p. 245-266.

Fischer, A. G., and Arthur, M. A., 1977, Secular variations in the pelagic realm, Soc. Econ. Pal. Min. Spec. Pub. 25, p. 19-25.

Folk, R. L., 1959, Practical petrographic classification of limestones, Amer. Assoc. Petrol. Geol.,Mem. 1, p. 62-84.

_____, 1965, Some aspects of recrystallization in ancient limestones, in, L.C. Prayand R.C. Murray, Eds., Dolomitization and Limestone Diagenesis: a Symposium, Soc. Econ. Paleontolog. Mineralog., Spec. Publ., v. 13, p. 14-48.

Frakes, L. A., and Bolton, B. R., 1984, Origin of manganese giants: sea level change and anoxic-oxic history, Geology, v. 12, p. 83-86.

Fries, Jr., C., and Rincon-Orta, C., 1965, Nuevas aprotaciones geocronologicas y tecnicas empleadas en el alboratorio de geocronometria, Univ. Nal. Autonoma Mexico, Inst. Geol., Bol. 73, p. 57-133.

Froelich, P. N., Klinkhammer, G. P., Bender, M. L., Luedtke, N. A., Heath, G. R., Cullen, D., Dauphin, P., Hammond, D., Hartman, B., and Maynard, V., 1979, Early oxidation of organic matter in pelagic sediments of the eastern equatorial Atlantic: suboxic diagenesis, Geochim. et Cosmochim. Acta, v. 43, p. 1075-1090.

Frondel, C., and Bauer, L. H., 1955, Kutnahorite: a manganese dolomite, $CaMn(CO_3)_2$, Amer. Mineral., v. 40, p. 748-760.

Gabrielson, O., and Sundus, N., 1965, Ca-rich kutnahorite from L ngban, Sweden, Arkiv Mineral. Geol., v. 4, p. 287-289.

Gautier, D. L., 1985, Interpretation of early diagenesis in ancient marine sediments, in Relationship of Organic Matter and Mineral Diagenesis, Soc. Econ. Mineralog. Paleontolog. Short Course Notes No. 17, p. 6-78.

Goldsmith, J. R., 1983, Phase relationsof rhombohedral carbonates, in R.J. Reeder, Ed., Carbonates: Mineralogy and Chemistry, Mineralogical Society of America, Reviews in Mineralogy, v. 11, p. 310-334.

_____, and Graf, D. L., 1957, The system CaO-MnO-CO_2: solid solution and decomposition relations, Geochim. et Cosmochim. Acta, v. 11, p. 310-334.

_____, and Graf, D. L., 1960, Subsolidus phase relations in

the system $CaCO_3$-$MgCO_3$-$MnCO_3$, J. Geol., v. 68, p. 324-335.

Graf, D.L., 1961, Crystallographic tables for the rhombohedral carbonates, Amer. Mineral., v. 46,p. 1283-1316.

Gryaznov, V. I., and Danilov, I. S., 1980, Oxidized manganese ores of the Nikopol deposits, Ukranian SSR in Geology and Geochemistry of Manganese, I.M. Varentsov and Gy. Grassely, Eds., Schweizerbart'sche Verlagsuchhandlung, Stuttgart, v. 2, p. 403-416.

Heim, A., 1926, Notes on the Jurassic of Tamanzunchale (Sierra Madre Oriental, Mexico), Ecl. Geol. Helvetiae, v. 20, p. 84-87.

_____, 1940, Geologie de la Sierra Madre, Ecl. Geol. Helvetiae, v. 33, p. 313-360.

Hermoso de la Torre, C. and Martinez-Perez, J., 1972, Medicion detallada de formaciones del Jurasico Superior en el frente de la Sierra Madre Oriental, Boletin de la Asociacion Mexicana de Geologios Petroleos, v. 24, p. 45-63.

Hesse, R., and Harrison, W. I., 1981, Gas hydrates (clathrates) causing pore-water freshening and oxygen isotope fractionation in deep-water sedimentary sections of terrigenous continental margins, Earth Planet. Sci. Lett., v. 55, p. 453-462.

Hodgson, W. A., 1966, Carbon and oxygen isotope ratios in diagenetic carbonates from marine sediments, Geochim. et Cosmochim. Acta, v. 30, p. 1223-1233.

Holdren, G. R., Bricker, O. P., and Matisoff, G., 1975, A model for the control of dissolved manganese in the interstitial waters of Chesapeake Bay, in T. M. Church, Ed., Marine Chemistry in the Coastal Environment, Amer. Chem. Soc., p. 364-381.

Howie, R. A., and Broadhurst, F. M., 1958, X-ray data for dolomite and ankerite, Amer. Mineral., v. 43, p. 1210-1214.

Hudson, J. D., 1977, Stable isotopes and limestone lithification, J. Geol. Soc. London, v. 133, p. 637-660.

Hurlburt and Klein, 1977, Manual of Mineralogy, 19th Ed., Wiley and Sons, New York, 532p.

Imlay, R. W., 1948, Characteristic marine Jurassic fossils from the western interior of the United States, U. S. Geol. Survey, Prof. Pap. 214-B, p. 13-33.

Irwin, H. C., Curtis, C. D., and Coleman, M. L., 1977, Isotopic evidence for source of diagenetic carbonates formed during burial of organic-rich sediments, Nature, v. 269, p. 209-213.

Jenkyns, H. C., and Clayton, C. J., 1986, Black shales and carbon isotopes in pelagic sediments from the Tethyan Lower Jurassic, Sedimentology, v. 33, p. 87-106.

Johnson, K. S., 1982, Solubility of rhodochrosite ($MnCO_3$) in water and seawater, Geochim. et Cosmochim. Acta, v. 46, p. 1805-1809.

Kinghorn, R. R. F., 1983, An Introduction to the Physics and Chemistrky of Petroleum, Wiley and Sons, New York, 420p.

Klinkhammer, G. P., 1980, Early diagenesis in sediments from the Eastern Equatorial Pacific: II. Trace metal results, Earth Planet Sci. Lett., v. 49, p. 81-101.

Knauth, L. P., and Epstein, S., 1976, Hydrogen and oxygen isotope ratios in nodular and bedded cherts, Geochim. et Cosmocim. Acta, v. 40, 1095-1108.

_____, and Lowe, D. L., 1978, Oxygen isotope geochemistry of cherts from the Onverwacht group (3.4 billion years), Transvaal, South Africa, with implications for secular variations in the isotopic composition of chert, Earth Planet. Sci. Lett., v. 41, p. 209-222.

Kuegelgen, H. V., 1958, Der Aufbau der zentralen Sierra Madre Oriental, Mexico, Zeitschrift der Deutschen Geologischen Gesellshaft, Band 110, Teil 1, p. 117-142.

Lawrence, J. R., Gieskes, J. M., and Broecker, W. S., 1975, Oxygen isotope and cation composition of DSDP pore waters and the alteration of Layer II basalts, Earth Planet. Sci. Let., v. 27, p. 1-10.

Leclerc, J., and Weber, F., 1980, Geology and genesis of the Moanda manganese deposits, Republic of Gabon, in Geology and Geochemistry of Manganese, v. 2, I.M. Varentsov and Gy. Graselly, Eds., Schweiszerbartsche Verlagsbuchhandlung, Stuttgart, p. 89-109.

Lewan, M. D., 1985, Evaluation of petroleum by hydrous pyrolysis experimentation, Phil. Trans. R. Soc. Lond.

Part A, v. 315, p. 123-134.

_____, 1986, Stable carbon isotopes of amorphous kerogens from Phanerozoic sedimentary rocks, Geochim. et Cosmochim. Acta, v. 50, p. 1583-1591.

Li, Y. H., Bischoff, J., and Mathieu, G., 1969, The migration of manganese in the Arctic Basin sediment, Earth Planet Sci. Lett., v. 49, p. 265-270.

Longoria, J. F., 1984, Mesozoic tectostratigraphic domains in east-central Mexico, in G.E.G. Westermann, Ed., Jurassic-Cretaceous biochronology and paleogeography of North America, Geol. Assoc. Canada Spec. Pap. 27, p. 65-76.

_____, 1985, Tectonic transpression in the Sierra Madre Oriental, northeastern Mexico: An alternative model, Geology, v. 13, p. 453-456.

Lopez-Ramos, E., 1979, Geologia general y de Mexico: Mexico, D.F., part 3, Edicion escolar, 445p.

Lopez-Ramos, 1981, Paleogeografia y tectonica del Mesozoico en Mexico, Univ. Nal. Auton. Mexico, Inst. Geologia, Revista, v. 5., p. 158-177.

Martino, O., 1986, The minerals industry of Mexico, in Minerals Yearbook 1984, v. 3 Area Reports: International, p. 553-573.

Mason, R., 1978, Petrology of the Metamorphic Rocks, Allen and Unwin, London, 254p.

Maynard, J. B., 1982, Extensions of Berner's "New geochemical classification of sedimentary environments" to ancient sediments, J. Sedim. Petrol., v. 52, p. 1325-1331.

_____, 1983, Geochemistry of Sedimentary Ore Deposits, Springer-Verlag, New York, 305p.

McIntosh, J. L., Farag, J. S., and Slee, K. J., 1975, Groote Eylandt manganese deposits, in C.L. Knight, Ed., Economic geology of Australia and Papua New Guinea, v. 1, Metals, Austral. Inst. of Mining and Metall., Monograph 5, p. 815-821.

Moore, C. H., 1985, Upper Jurassic subsurface cements: a case history, in N. Schneidermann and P.M. Harris, Eds., Carbonate Cements, Soc. Econ. Paleontolog. Mineralog. Spec. Publ. No. 36, p. 291-308.

Murray, J. W., 1979, Iron Oxides, in R. G. Burns, Ed., Marine Minerals, Mineralogical Soc. Amer. Short Course Notes, Rev. in Mineralogy, v. 6, p. 1-46.

National Materials Advisory Board, 1981, Manganese reserves and resources of the world and their industrial implications, Natl. Mater. Advis. Board Publication NMAB-374, 334p.

O'Neil, J. R., Clayton, R. N., and Mayeda, T.K., 1969, Oxygen isotope fractionation in divalent metal carbonates, J. Chem. Phys., v. 51, p. 5547-5548.

Park, C. F., 1956, On the origin of manganese, 20th Intl. Geol. Cong., Symposium on Manganese, v. 1, p. 75-78.

Pederson, T. F., and Price, N. B., 1982, The geochemistry of manganese carbonate in Panama Basin sediments, Geochim. et Cosmochim. Acta, v. 46,p. 59-68.

Pedrazzini, C., and Basañez, M. A., 1978, Sedimentation del Jurassico Medio-superior en el anticlinoria de Huayacocotla-Cuenca de Chicontepec, Estados de Hidalgo y Veracruz, Mexico, Revista del Instituto Mexicano del Petroleo, v. 10, p. 6-19.

Perry, E. A., 1967, The oxygen isotope chemistry of ancient cherts, Earth Planet. Sci. Lett., v. 3, p. 62-66.

_____, and Tan, F. C., 1972, Significance of oxygen and carbon isotope variations in early Precambrian cherts and carbonate rocks of southern Africa, Geol. Soc. America Bull., v. 83, p. 647-664.

Pilger, R. H., Jr., 1978, A closed Gulf of Mexico, pre-Atlantic ocean plate reconstruction and the early rift history of the Gulf and North Atlantic, Trans. Gulf Coast Assoc. Geol. Soc., v. 28, p. 385-393.

Pindell, J. L., 1985, Alleghenian reconstruction and subsequent evolution of the Gulf of Mexico, Bahamas, and proto-Caribbean, Tectonics,v. 4, p. 1-39.

Pisciotto, K. A., and Mahoney, J. J., 1981, Isotopic survey of diagenetic carbonates, Init. Rep. of the Deep Sea Drilling Proj., v. 63, p. 595-609.

Prezbindowski, D. R., 1985, Burial cementation - is it important? A case study, Stuart City trend, south central Texas, in N. Schneidermann and P.M. Harris, Eds., Carbonate Cements, Soc. Econ. Paleontolog.

Mineralog. Spec. Publ. No. 36, p. 241-264.

Raiswell, R. and Plant, J., 1980, The incorporation of trace elements into pyrite during diagenesis of black shales, Yorkshire, England, Econ. Geol., v. 75 p. 684-699.

Reeder, R. J., 1983, Crystal chemistry of the rhombohedral carbonates, in R.J. Reeder, Ed., Carbonates: Mineralogy and Chemistry, Mineralogical Society of America, Reviews in Mineralogy, v. 11, p. 1-47.

Roy, 1980, Manganese ore deposits of India, in Geology and Geochemistry of Manganese, v. 2, I.M. Varentsov and Gy. Graselly, Eds., Schweiszerbartsche Verlagsbuchhandlung, Stuttgart, p. 237-263.

_____, 1981, Manganese Deposits, Academic Press, New York, 458p.

Schrader, R., and Buttner, G., 1963, Untersuchungen uber - Eisen(III)-oxid, Zeitschrift fur anorganische und allgemeine Chemie, v. 320, p. 205-216.

Schlanger, S. O., and Jenkyns, H. C., 1976, Cretaceous oceanic anoxic sediments: causes and consequences, Geologie en Mijnbouw, v. 55, p. 179-184.

Sharma, T., and Clayton, R. N., 1965, Measurement of O^{18}/O^{16} ratios of total oxygen of carbonates, Geochim. et Cosmochim. Acta, v. 29, p. 1347-1353.

Stacey, F. D., and Banerjee, S. K., 1974, The Physical Principles of Rock Magnetism, Elsevier, Amsterdam, 195p.

Suess, E., 1979, Mineral phases formed in anoxic sediments by microbial decomposition of organic matter, Geochim. et Cosmochim. Acta, v. 43, p. 339-352.

Tasse, N., and Hesse, R., 1984, Origin and significance of complex authigenic carbonates in Cretaceous black shales of the western Alps, J. Sedim. Petrol., v. 54, p. 1012-1027.

Tavera, E. and Alexandri, R., 1972, Molango manganese deposits, Hidalgo, Mexico, Acta Mineralogica Petrographica, v. 20, p. 387-388.

_____, in press, The manganese deposits of the Molango area Hidalgo, Mexico, Econ. Geol.

Tissot, B. P., and Welte, D. H., 1984, Petroleum Formation

and Occurence, 2nd Ed., Springer-Verlay, New York, 699p.

Toxopeus, J. M. A. Buiskool, 1983, Selection criteria for the use of vitrinite reflectance as a maturity tool, Geol. Soc. London Spec. Publ. no. 12, p. 245-307.

Tsusue, A., 1967, Magnesian kutnahorite from Ryujiima mine, Japan, Amer. Mineral., v. 52,p. 1751-1761.

Turekian, K. K., and Wedepohl, K. H., 1961, Distribution of the elements in some major units of the earth's crust, Geol. Soc. Amer. Bull., v. 72, p. 175-192.

Vail, P. R., Hardenbol, J., and Todd, R. G., 1984, Jurassic unconformities, chronostratigraphy and sea-level changes from seismic stratigraphy and biostratigraphy, in J. S. Schlee, Ed., Interregional Unconformities and Hydrocarbon Accumulation, Amer. Assoc. Petrol. Geologists Memoir No. 36, p. 347-364.

Varentsov, 1964, Sedimentary Manganese Ores, Elsevier, New York, 119p.

_____, I. M., and Grasselly, Gy., 1980, Geology and Geochemistry of Manganese, E. Schweizerbart'sche Verlagsbuchhandlung, Stuttgar, 433p..

Veizer, J., 1978, Secular variations in the composition of sedimentary carbonate rocks - II: Iron, manganese, calcium, magnesium, silica and minor constituents, Precambrian Research, v. 6, p. 381-413.

_____, 1983, Chemical diagenesis of carbonates: theory and application of trace element technique, in M.A. Arthur, et al., Eds., Stable Isotopes in Sedimentary Geology, Soc. Econ. Paleont. and Mineral. Short Course Notes No. 10, p. 3-1 -- 3-100.

_____, and Hoefs, J., 1976, The nature of O^{18}/O^{16} and C^{13}/C^{12} secular trends in sedimentary carbonate rocks, Geochim. et Cosmochim. Acta, v. 40, p. 1387-1395.

Vinogradov, A. P., 1962, Average contents of chemical elements in the principal types of igneous rocks of the earth's crust, Geokhimya, p. 555-571.

Wada, H., and Suzuki, K., 1983, Carbon isotopic thermometry calibrated by dolomite-calcite solvus temperatures, Geochim. et Cosmochim. Acta, v. 47, p. 697-706.

Wilson, J. L., 1975, Carbonate Facies in Geologic History, Springer-Verlag, New York, 471p.

APPENDIX A

METHODS OF STUDY

METHODS OF STUDY

FIELDWORK

Field study of the Molango manganese district, conducted over a two week period (March 10 to 24, 1985), involved a reconnaissance excursion throughout the entire stratigraphic section (Precambrian to Tertiary) and the active and inactive mine workings to determine the most productive approach for collecting data.

Tetzintla Mine - A detailed composite measured section and samples were obtained from the Tetzintla underground and open pit workings. The majority of the stratigraphic section was measured in an adit known as "Frente B" and began 245 meters into the drift. The bearing of the workings was perpendicular to bedding and exposed the most continuous section available.

Rocks observed in outcrop at the entrance to the adit were able to be traced into a faulted and covered interval. The next lithology above the fault was found to be exposed in a cut along a road which runs from Frente B to the service garage. This outcrop makes up the uppermost portion of the stratigraphic section.

Data were collected by first measuring the adit marking off 5 meter intervals along a horizontal line projected on the wall. Strike and dip measurements were collected every 10 to 15 meters or where obvious changes and faults were observed. In addition, strike and dip was determined for

every sample collected. Sample material was collected every 5 meters or where lithologic changes merited. The ore zone was sampled with a closer spacing.

An additional stratigraphic section was measured from the bench at Level 1052. This section provided information from the top of the Santiago, exposed as a bedding plane surface in the open-pit, through the second spiculite.

The third stratigraphic section was measured in a stream at the northern limits of the Tetzintla workings. This section provided information regarding a major fault which is the same feature observed at the break in the Frente B section.

Lastly, several measured sections were obtained from localities outside the immediate vicinity of the Tetzintla workings. These sections, were sought primarily for information about the thickness of units and to seek out other lithologies not seen in Tetzintla.

PETROGRAPHY

Petrographic observations were made primarily through standard transmitted light microscopy, and were supplemented with reflected light and cathodoluminescent techniques. These methods utilized using thin-sections prepared using conventional techniques. Sections were polished in four steps and usually finished with 3 micron diamond paste.

X-RAY DIFFRACTION

Identification of mineral phases was accomplished through

x-ray diffraction study conducted with a Siemans-Allis D500. Data were collected using copper radiation generated at 40 kilovolts with a current of 30 milliamp. Goniometer speeds (i.e stepsizes and the duration of counting) were varied as needed for resolution.

Samples were analyzed as unoriented powder mounts, oriented clay smears, and mineral separates. Powder mounts were prepared by crushing several to 10 grams of sample in an agate mortar and pestle until the material was less than 125 microns (120 mesh). The powder was pressed into a plastic carrier and analyzed.

Clay sized material was obtained from samples after removal of the carbonate fraction using 15% cold HCl followed by washing and suspension in distilled water. The suspended clay fraction was then centrifuged, the supernatant decanted, and the material spread onto a welled glass slide to dry. If glycolation of the sample was necessary this was carried out by placing the sample in a bell jar containing a reservoir of ethylene glycol and heated to 50^{o}C for a time not less than 12 hours.

Vein filling material and samples intended to be analyzed by plasma spectroscopy (ICP) were mineral separates analyzed by XRD. In the case of vein filling and minerals cementing breccias the purpose was for identification and were done as powder mounts. Those samples being analyzed by ICP were obtained following acid digestion and heavy liquid separation

(described below) and were analyzed by XRD to judge the purity of the separation.

MICROPROBE

Microprobe chemical compositions were determined from thin-section and mineral separates. Sample material was prepared by mounting the sample on a glass slide or in the case of mineral separates, in a brass tube. The specimen was polished in five steps to a 1 micron finish. The polish was checked using a reflected light microscope.

Each sample was analyzed for Mn, Fe, Ca, and Mg using an ARL-EMX 3 channel microprobe with Krisel correction. Operating parameters for the microprobe were 15 kilovolts accelerating voltage, a specimen current of 1.2 millimicroamps, and a 2000 micro-amp emission current. Standardization was done using dolomite (USNM #10057) for Ca and Mg, and siderite (USNM #R 2460) for Mn and Fe. The standards were analyzed prior to and after each sample was analyzed. Bence-Albee (1968) correction methods were used to convert raw count data to weight-percent oxide and mole percent carbonate.

ISOTOPE DATA

CARBONATE CARBON AND OXYGEN - The stable isotopic ratios of carbon and oxygen have been analyzed from the carbonate mineral fraction for a net number of 56 wholerock samples. The sample set and data are listed in Table VII. Sample material was chosen from the material collected in the

underground workings known as 'Frente B' at the Tetzintla mine site so that lithologic, textural, and ore grade changes were represented. Every sample collected in the adit from 4 meters below the Santiago - Chipoco contact to about 20 meters above the contact was analyzed with the exception of T1, +0.45 which is comprised of massive sulfide, as well as selected additional samples above and below this interval, several vein filling carbonates, mineral separates, and miscellaneous samples were also chosen. The results for these samples are presented in Table VIII.

Sample preparation involved cutting a channel sample perpendicular to bedding. In the case of vein samples, the material was collected across the width of the vein. The sample material was ground to a fine powder in an agate mortar and pestle. All of the powder was transferred to a glass ampule, evacuated, and sealed until ready for phosphorolysis.

The digestion reaction was accomplished by transferring a small amount of sample into one branch of a Y-shaped reaction tube. Carbon dioxide was evolved from the carbonates using "102.4%" phosphoric acid (i.e anhydrous) which was placed in the other branch of the reaction tube. The notation used for the concentration of H_3PO_4 reflects "...the total amount of H_3PO_4 that could be prepared from the solution after hydrolysis of all polymeric species, not the true abundance of H_3PO_4" (Wachter and Hayes, 1985, p. 367).

The reaction tubes were evacuated, sealed, and the phosphorolyses carried out in a convection oven set at a temperature of 50°C for 72 hours. In all cases the reaction appeared, by visual inspection, to have gone to completion by the end of this period. However, the chemical similarities between Mn and Fe indicate the possibility that the reaction of rhodochrosite, by analogy to siderite, does not go to completion in such a short time, thereby resulting in incomplete fractionation of oxygen. On the other hand, work by Hayes and coworkers of the Biogeochemistry Lab at Indiana University has demonstrated that, in the case of siderite, no significant fractionation occurs after about 24 hours (Kaufman and Hayes, pers. comm.). This observation has been assumed to apply in this study to the decomposition of rhodochrosite.

Carbon dioxide was isolated from the reaction tubes by cryogenic distillation. The CO_2 was analyzed using a Finnigan MAT Delta E, 90°, 18 cm, triple collector mass spectrometer.

The carbon isotopic data are expressed relative to the PDB standard. The raw machine values of the oxygen isotopic ratios were adjusted by subtracting 9.25 °/oo in order to correct for reacting the carbonates at 50°C. Data are reported relative to both SMOW and PDB. The correction of SMOW to PDB was accomplished using the equation of Craig (1961):

$$\delta^{18}O(\text{cct vs SMOW}) = 1.03086\ \delta^{18}O(\text{cct vs PDB}) + 30.86\ .$$

The manganoan calcite and rhodochrosite samples were corrected using the above equation also. It should also be noted here that the analytical fractionation for calcite differs from rhodochrosite. The correction for this variation, although simple, was not done because it is insignificant. For example, a pure rhodochrosite would differ from a pure calcite by being only 0.129 °/oo too light as demonstrated below from the data of Sharma and Clayton (1965):

$$\{1000\ln \alpha_{cct} - 1000\ln \alpha_{rho}\} = 0.1287$$

where $\alpha_{cct} = 1.01008$ and $\alpha_{rho} = 1.00995$.
1982, p. 483).

ORGANIC CARBON - Thirteen (13) samples covering four generalized stratigraphic levels of the Santiago and Chipoco facies of the Taman Formation were analyzed to determine the $del^{13}C$ composition of the kerogen component. These analyses were determined courtesy of Dr. Michael D. Lewan of Amoco Production Company Research Center.

Additional Techniques - The thirteen samples submitted for organic carbon isotopic study were also analyzed to determine the total organic content, vitrinite reflectance, and

pyrolysis characteristics by the Rock-Eval method. These analyses were performed at the Amoco Production Company Research Center, again courtesy of Dr. Michael D. Lewan.

INDUCTIVELY COUPLED PLASMA SPECTROSCOPY

Inductively coupled plasma spectroscopy (ICP) analyses were sought for a total of 10 samples from the Santiago and Chipoco facies (Tables III - VI). Five of these samples were pyrite separates, two were samples of the magnetic mineral phases found in the ore zone, and the remaining three were wholerock samples from the upper Santiago, ore zone, and upper Chipoco facies. The purpose in collecting these data was to determine if any anomalous concentrations existed for elements commonly associated with seafloor spreading activity.

Wholerock samples were acquired from channel samples over the thickness of the sample material which were then crushed to a <2mm fragments. Mineral separates were obtained using a modification of the procedures outlined by Raiswell and Plant (1980). Between 30 and 50 grams of sample was crushed to a size <250 micron followed by treatment with 15% cold HCl for a minimum of 24 hours. The acidity of the solution was checked periodically and fresh HCl was replenished as necessary. In addition samples were placed in an ultrasonic bath to aid in disaggregating the material and thus speeding up the digestion process. Following its digestion the sample was allowed to settle out of suspension, the acid was

aspirated as completely as possible with out removing any of the sample. The remaining HCl and any chlorides were removed by centrifugation with distilled-deionized water. Water was driven from the sample by washing with acetone after which the material was spread onto a watch glass and the remaining acetone allowed to evaporate. The dry sample was weighed to allow determination of the percent carbonate that was originally present and then sieved through a 125 micron (120 mesh) screen. Visual observation after this stage revealed the persistance of composite grains of hostrock and pyrite. To further dissagregate the sample dichloromethane (methylene chloride) was added and the sample stirred overnight. The sample was recovered by centrifugation and cleaned with methanol and acetone, followed by drying and sieving through a 75 micron (200 mesh) screen. Pyrite was then separated from this size fraction using tetrabromomethane (Bromoform), washed with acetone and stored in a dessicator. In the case where magnetic minerals were present separation of this phase was accomplished using a large bar magnet. Both the magnetic and non-magnetic mineral separates were purified using heavy liquid techniques. The magnetic minerals produced a light, intermediate, and heavy fraction which was at first thought to be due to the persistance of composite grains. It was later demonstrated, and is discussed in Chapter IV, that these were indeed two mineral phases and that the third fraction may be a mixture of the two.

The purity of the sample was checked first by visual inspection for composite grains and the possible presence of other heavy mineral species. The final check was made by x-ray diffraction which, as was found in one case, was able to detect very small quantities of a mineral phase (Appendix C).

The ICP analyses were conducted by Mr. James Boyle and Dr. Shane Que Hee at the Kettering Laboratory of the Institute of Environmental Health in the University of Cincinnati Medical Center. Sample preparation involved dissolution of the sample in a nitric - perchloric acid solution (10:1 by volume) at 100°C followed by dilution with a hydrochloric - nitric acid solution (1:1 by volume). Measurements were conducted for twenty elements with a lower cut-off in sensitivity of 0.01 micrograms per milliliter.

APPENDIX B

ELECTRON MICROPROBE DATA

TABLE 15. MICROPROBE DATA FOR SAMPLE T1, 0

SAMPLE NUMBER	POSITION	NOTES	STRAT POSIT	Mn	Fe	Ca	Mg	TOTAL	Ca/ Ca+Mg	Mg/ Ca+Mg	Mn/ Fe	Mg/ Ca
T1,+0	NONE	CONTACT	0	0.007	0.007	0.969	0.016	0.999	0.9837	0.0162	1	0.0165
T1,+0	NONE	CONTACT	0	0.004	0.002	0.958	0.034	0.998	0.9657	0.0342	2	0.0354
T1,+0	NONE	CONTACT	0	0.002	0.005	0.968	0.023	0.998	0.9767	0.0232	0.4	0.0237
T1,+0	NONE	CONTACT	0	0.003	0.063	0.91	0.023	0.999	0.9753	0.0246	0.0476	0.0252
T1,+0	NONE	CONTACT	0	0.004	0.003	0.961	0.03	0.998	0.9697	0.0302	1.3333	0.0312
T1,+0	NONE	CONTACT	0	0.014	0.016	0.943	0.026	0.999	0.9731	0.0268	0.875	0.0275
T1,+0	NONE	CONTACT	0	0.007	0.002	0.965	0.025	0.999	0.9747	0.0252	3.5	0.0259
T1,+0	NONE	CONTACT	0	0.012	0.01	0.959	0.018	0.999	0.9815	0.0184	1.2	0.0187
T1,+0	NONE	CONTACT	0	0	0	0.993	0.006	0.999	0.9939	0.0060		0.0060
T1,+0	NONE	CONTACT	0	0.009	0.002	0.979	0.009	0.999	0.9908	0.0091	4.5	0.0091
T1,+0	NONE	CONTACT	0	0	0.412	0.566	0.022	1	0.9625	0.0374	0	0.0388
		AVERAGE:		0.0056	0.0474	0.9246	0.0210	0.9988				
		STD. DEV.:		0.0044	0.1165	0.1151	0.0079					
		AVERAGE:		0.0062	0.011	0.9605	0.021	0.9987				
		STD DEV.:		0.0042	0.0179	0.0210	0.0083					
				WITHOUT	THE	LAST	SAMPLE					

TABLE 16. MICROPROBE DATA FOR SAMPLE T1, +0.1

SAMPLE NUMBER	POSITION	NOTES	STRAT POSIT	Mn	Fe	Ca	Mg	TOTAL	Ca/ Ca+Mg	Mg/ Ca+Mg	Mn/ Fe	Mg/ Ca
T1,+0.1	NONE	MATRIX	0.1	0.047	0.028	0.548	0.375	0.998	0.5937	0.4062	1.6785	0.6843
T1,+0.1	NONE	IN VEIN	0.1	0	0	0.618	0.381	0.999	0.6186	0.3813		0.6165
T1,+0.1	NONE	IN VEIN	0.1	0	0	0.635	0.364	0.999	0.6356	0.3643		0.5732
T1,+0.1	NONE	MATRIX	0.1	0.038	0.005	0.564	0.391	0.998	0.5905	0.4094	7.6	0.6932
T1,+0.1	NONE	AB STY	0.1	0.02	0.004	0.567	0.408	0.999	0.5815	0.4184	5	0.7195
T1,+0.1	NONE	MATRIX	0.1	0.033	0.02	0.561	0.385	0.999	0.5930	0.4069	1.65	0.6862
		AVERAGE:		0.023	0.0095	0.5821	0.384	0.9986				
				0.0181	0.0106	0.0322	0.0136					

TABLE 17. MICROPROBE DATA FOR SAMPLE T1, +0.45

SAMPLE NUMBER	POSITION	NOTES	STRAT POSIT	Mn	Fe	Ca	Mg	TOTAL	Ca/ Ca+Mg	Mg/ Ca+Mg	Mn/ Fe	Mg/ Ca
T1,+0.45	711	TOP	0.45	0.881	0.001	0.099	0.018	0.999	0.8461	0.1538	881	0.1818
T1,+0.45	721		0.45	0.713	0.099	0.073	0.114	0.999	0.3903	0.6096	7.2020	1.5616
T1,+0.45	731		0.45	0.893	0.009	0.076	0.021	0.999	0.7839	0.2164	99.222	0.2763
T1,+0.45	741		0.45	0.721	0.026	0.082	0.17	0.999	0.3253	0.6746	27.730	2.0731
T1,+0.45	751		0.45	0.954	0	0.041	0.005	1	0.8913	0.1086		0.1219
T1,+0.45	761		0.45	0.869	0.007	0.087	0.036	0.999	0.7073	0.2926	124.14	0.4137
T1,+0.45	771		0.45	0.89	0.002	0.094	0.013	0.999	0.8785	0.1214	445	0.1382
T1,+0.45	781		0.45	0.769	0.022	0.082	0.126	0.999	0.3942	0.6057	34.954	1.5365
T1,+0.45	791		0.45	0.802	0.018	0.092	0.086	0.998	0.5168	0.4831	44.555	0.9347
T1,+0.45	801		0.45	0.22	0.715	0.025	0.039	0.999	0.3906	0.6093	0.3076	1.56
T1,+0.45	811		0.45	0.495	0.38	0.049	0.075	0.999	0.3951	0.6048	1.3026	1.5306
T1,+0.45	821		0.45	0.604	0.294	0.058	0.043	0.999	0.5742	0.4257	2.0544	0.7413
T1,+0.45	831		0.45	0.471	0.454	0.047	0.027	0.999	0.6351	0.3648	1.0374	0.5744
T1,+0.45	841		0.45	0.449	0.416	0.044	0.09	0.999	0.3283	0.6716	1.0793	2.0454
T1,+0.45	851		0.45	0.373	0.46	0.043	0.123	0.999	0.2590	0.7409	0.8108	2.8604
T1,+0.45	861		0.45	0.179	0.747	0.02	0.054	1	0.2702	0.7297	0.2396	2.7
T1,+0.45	871		0.45	0.436	0.456	0.049	0.059	1	0.4537	0.5462	0.9561	1.2040
T1,+0.45	881		0.45	0.514	0.39	0.058	0.037	0.999	0.6105	0.3894	1.3179	0.6379
T1,+0.45	891	BASE	0.45	0.797	0.026	0.085	0.09	0.998	0.4857	0.5142	30.653	1.0588
		AVERAGE:		0.6331	0.238	0.0633	0.0645	0.9990				
		STD. DEV.:		0.2316	0.2499	0.0233	0.0442					

TABLE 18. MICROPROBE DATA FOR SAMPLE T1, +0.50

SAMPLE NUMBER	POSITION	NOTES	STRAT POSIT	Mn	Fe	Ca	Mg	TOTAL	Ca/ Ca+Mg	Mg/ Ca+Mg	Mn/ Fe	Mg/ Ca
T1,+0.5	NONE	GRAIN	0.5	0.806	0.012	0.082	0.098	0.998	0.4555	0.5444	67.166	1.1951
T1,+0.5	NONE	LAM	0.5	0.88	0.003	0.084	0.032	0.999	0.7241	0.2758	293.33	0.3809
T1,+0.5	NONE	LAM	0.5	0.867	0	0.125	0.007	0.999	0.9469	0.0530		0.056
T1,+0.5	NONE	TH BED	0.5	0.871	0	0.124	0.004	0.999	0.9687	0.0312		0.0322
T1,+0.5	NONE	TH BED	0.5	0.9	0.006	0.068	0.024	0.998	0.7391	0.2608	150	0.3529
T1,+0.5	NONE	MASSIVE	0.5	0.556	0.075	0.062	0.306	0.999	0.1684	0.8315	7.4133	4.9354
T1,+0.5	NONE	L FRACT	0.5	0.897	0.003	0.081	0.017	0.998	0.8265	0.1734	299	0.2098
T1,+0.5	NONE	HOMOG	0.5	0.9	0.003	0.077	0.02	1	0.7938	0.2061	300	0.2597
		AVERAGE:		0.8346	0.0127	0.0878	0.0635	0.9987				
		STD. DEV.:		0.1091	0.0237	0.0222	0.0957					

TABLE 19. MICROPROBE DATA FOR SAMPLE T1, +2.0

SAMPLE NUMBER	POSITION	NOTES	STRAT POSIT	Mn	Fe	Ca	Mg	TOTAL	Ca/ Ca+Mg	Mg/ Ca+Mg	Mn/ Fe	Mg/ Ca
T1,+2.0	736	BOTTOM	2	0.903	0.007	0.082	0.007	0.999	0.9213	0.0786	129	0.0853
T1,+2.0	746		2	0.763	0.053	0.064	0.119	0.999	0.3497	0.6502	14.396	1.8593
T1,+2.0	756		2	0.27	0.239	0.024	0.467	1	0.0488	0.9511	1.1297	19.458
T1,+2.0	766		2	0.617	0.083	0.049	0.25	0.999	0.1638	0.8361	7.4337	5.1020
T1,+2.0	776		2	0.664	0.072	0.048	0.215	0.999	0.1825	0.8174	9.2222	4.4791
T1,+2.0	786		2	0.044	0.54	0	0.415	0.999	0	1	0.0814	
T1,+2.0	796		2	0.26	0.161	0.021	0.557	0.999	0.0363	0.9636	1.6149	26.523
T1,+2.0	806	IN PYRITE	2	0.928	0.009	0.024	0.037	0.998	0.3934	0.6065	103.11	1.5416
T1,+2.0	816		2	0.755	0.061	0.041	0.142	0.999	0.2240	0.7759	12.377	3.4634
T1,+2.0	826		2	0.907	0.002	0.08	0.01	0.999	0.8888	0.1111	453.5	0.125
T1,+2.0	836		2	0.907	0.003	0.082	0.007	0.999	0.9213	0.0786	302.33	0.0853
T1,+2.0	846		2	0.671	0.039	0.053	0.236	0.999	0.1833	0.8166	17.205	4.4528
T1,+2.0	856		2	0.532	0.143	0.042	0.282	0.999	0.1296	0.8703	3.7202	6.7142
T1,+2.0	866		2	0.262	0.173	0.013	0.551	0.999	0.0230	0.9769	1.5144	42.384
T1,+2.0	876		2	0.79	0.037	0.071	0.102	1	0.4104	0.5895	21.351	1.4366
T1,+2.0	886		2	0.814	0.062	0.062	0.061	0.999	0.5040	0.4959	13.129	0.9838
T1,+2.0	896		2	0.236	0.289	0.007	0.467	0.999	0.0147	0.9852	0.8166	66.714
T1,+2.0	906	TOP	2	0.37	0.199	0.032	0.398	0.999	0.0744	0.9255	1.8592	12.437
		AVERAGE:		0.5940	0.1206	0.0441	0.2401	0.9990				
		STD. DEV.:		0.2755	0.1315	0.0252	0.1880					

TABLE 20. MICROPROBE DATA FOR SAMPLE T1, +2.5A

SAMPLE NUMBER	POSITION	NOTES	STRAT POSIT	Mn	Fe	Ca	Mg	TOTAL	Ca/ Ca+Mg	Mg/ Ca+Mg	Mn/ Fe	Mg/ Ca
T1,+2.5A	563	BOTTOM	2.5	0.69	0.039	0.094	0.176	0.999	0.3481	0.6518	17.692	1.8723
T1,+2.5A	573		2.5	0.293	0.148	0.037	0.521	0.999	0.0663	0.9336	1.9797	14.081
T1,+2.5A	583		2.5	0.537	0.149	0.054	0.259	0.999	0.1725	0.8274	3.6040	4.7962
T1,+2.5A	593		2.5	0.456	0.143	0.044	0.356	0.999	0.11	0.89	3.1888	8.0909
T1,+2.5A	603		2.5	0.584	0.108	0.06	0.247	0.999	0.1954	0.8045	5.4074	4.1166
T1,+2.5A	613		2.5	0.565	0.127	0.065	0.242	0.999	0.2117	0.7882	4.4488	3.7230
T1,+2.5A	623		2.5	0.127	0.551	0.016	0.305	0.999	0.0498	0.9501	0.2304	19.062
T1,+2.5A	633		2.5	0.19	0.377	0.027	0.404	0.998	0.0626	0.9373	0.5039	14.962
T1,+2.5A	643		2.5	0.417	0.206	0.043	0.333	0.999	0.1143	0.8856	2.0242	7.7441
T1,+2.5A	653		2.5	0.668	0.031	0.064	0.236	0.999	0.2133	0.7866	21.548	3.6875
T1,+2.5A	663		2.5	0.337	0.377	0.036	0.25	1	0.1258	0.8741	0.8938	6.9444
T1,+2.5A	673		2.5	0.604	0.101	0.06	0.235	1	0.2033	0.7966	5.9801	3.9166
T1,+2.5A	683		2.5	0.394	0.148	0.045	0.412	0.999	0.0984	0.9015	2.6621	9.1555
T1,+2.5A	693		2.5	0.478	0.127	0.065	0.329	0.999	0.1649	0.8350	3.7637	5.0615
T1,+2.5A	703		2.5	0.408	0.178	0.04	0.374	1	0.0966	0.9033	2.2921	9.35
T1,+2.5A	713		2.5	0.334	0.128	0.04	0.498	1	0.0743	0.9256	2.6093	12.45
T1,+2.5A	711		2.5	0.326	0.41	0.032	0.231	0.999	0.1216	0.8783	0.7951	7.2187
T1,+2.5A	717		2.5	0.107	0.507	0.015	0.37	0.999	0.0389	0.9610	0.2110	24.666
T1,+2.5A	723		2.5	0.292	0.144	0.025	0.538	0.999	0.0444	0.9555	2.0277	21.52
T1,+2.5A	733		2.5	0.544	0.106	0.063	0.285	0.998	0.1810	0.8189	5.1320	4.5238
T1,+2.5A	743		2.5	0.284	0.32	0.025	0.37	0.999	0.0632	0.9367	0.8875	14.8
T1,+2.5A	741		2.5	0.305	0.158	0.031	0.505	0.999	0.0578	0.9421	1.9303	16.290
T1,+2.5A	751	TOP	2.5	0.588	0.102	0.062	0.248	1	0.2	0.8	5.7647	4
			AVERAGE:	0.4142	0.2036	0.0453	0.3358					
			STD. DEV.:	0.1618	0.1417	0.0188	0.1027					

TABLE 21. MICROPROBE DATA FOR SAMPLE T1, +2.5B

SAMPLE NUMBER	POSITION	NOTES	STRAT POSIT	Mn	Fe	Ca	Mg	TOTAL	Ca/ Ca+Mg	Mg/ Ca+Mg	Mn/ Fe	Mg/ Ca
T1,+2.5B	525	TOP	2.55	0.369	0.13	0.026	0.474	0.999	0.052	0.948	2.8384	18.230
T1,+2.5B	535		2.55	0.155	0.21	0.01	0.623	0.998	0.0157	0.9842	0.7380	62.3
T1,+2.5B	545		2.55	0.051	0.489	0.001	0.457	0.998	0.0021	0.9978	0.1042	457
T1,+2.5B	555		2.55	0.697	0.053	0.096	0.154	1	0.384	0.616	13.150	1.6041
T1,+2.5B	565		2.55	0.873	0.009	0.105	0.012	0.999	0.8974	0.1025	97	0.1142
T1,+2.5B	563		2.55	0.802	0.022	0.101	0.074	0.999	0.5771	0.4228	36.454	0.7326
T1,+2.5B	575		2.55	0.071	0.259	0.004	0.665	0.999	0.0059	0.9940	0.2741	166.25
T1,+2.5B	585		2.55	0.261	0.204	0.044	0.49	0.999	0.0823	0.9176	1.2794	11.136
T1,+2.5B	595		2.55	0.396	0.177	0.051	0.375	0.999	0.1197	0.8802	2.2372	7.3529
T1,+2.5B	605		2.55	0.889	0.007	0.098	0.005	0.999	0.9514	0.0485	127	0.0510
T1,+2.5B	615		2.55	0.398	0.131	0.03	0.44	0.999	0.0638	0.9361	3.0381	14.666
T1,+2.5B	625		2.55	0.249	0.171	0.021	0.559	1	0.0362	0.9637	1.4561	26.619
T1,+2.5B	635		2.55	0.479	0.125	0.047	0.348	0.999	0.1189	0.8810	3.832	7.4042
T1,+2.5B	645		2.55	0.486	0.232	0.053	0.228	0.999	0.1886	0.8113	2.0948	4.3018
T1,+2.5B	655		2.55	0.48	0.129	0.039	0.351	0.999	0.1	0.9	3.7209	9
T1,+2.5B	665		2.55	0.175	0.316	0.028	0.479	0.998	0.0552	0.9447	0.5537	17.107
T1,+2.5B	675		2.55	0.063	0.431	0.006	0.5	1	0.0118	0.9881	0.1461	83.333
T1,+2.5B	685		2.55	0.439	0.29	0.039	0.231	0.999	0.1444	0.8555	1.5137	5.9230
T1,+2.5B	695		2.55	0.638	0.132	0.069	0.16	0.999	0.3013	0.6986	4.8333	2.3188
T1,+2.5B	705		2.55	0.8	0.02	0.081	0.099	1	0.45	0.55	40	1.2222
T1,+2.5B	715		2.55	0.094	0.467	0.002	0.437	1	0.0045	0.9954	0.2012	218.5
T1,+2.5B	725		2.55	0.417	0.184	0.049	0.35	1	0.1228	0.8771	2.2663	7.1428
T1,+2.5B	735		2.55	0.687	0.046	0.077	0.188	0.998	0.2905	0.7094	14.934	2.4415
T1,+2.5B	745		2.55	0.643	0.168	0.063	0.125	0.999	0.3351	0.6648	3.8273	1.9841
T1,+2.5B	755		2.55	0.438	0.219	0.05	0.293	1	0.1457	0.8542	2	5.86
T1,+2.5B	753		2.55	0.079	0.192	0.001	0.727	0.999	0.0013	0.9986	0.4114	727
T1,+2.5B	765		2.55	0.614	0.103	0.067	0.215	0.999	0.2375	0.7624	5.9611	3.2089
T1,+2.5B	775		2.55	0.659	0.071	0.063	0.206	0.999	0.2342	0.7657	9.2816	3.2698
T1,+2.5B	785		2.55	0.422	0.16	0.047	0.371	1	0.1124	0.8875	2.6375	7.8936
T1,+2.5B	795		2.55	0.627	0.105	0.066	0.2	0.998	0.2481	0.7518	5.9714	3.0303
T1,+2.5B	805		2.55	0.562	0.105	0.055	0.278	1	0.1651	0.8348	5.3523	5.0545
T1,+2.5B	725	RECHEK	2.55	0.264	0.295	0.039	0.401	0.999	0.0886	0.9113	0.8949	10.282
			AVERAGE:	0.4461	0.1766	0.0477	0.3285					
			STD. DEV.:	0.2455	0.1228	0.0297	0.1830					

TABLE 22. MICROPROBE DATA FOR SAMPLE T1, 2.5 (ALL POINTS)

SAMPLE NUMBER	POSITION	NOTES	STRAT POSIT	Mn	Fe	Ca	Mg	TOTAL	Ca/ Ca+Mg	Mg/ Ca+Mg	Mn/ Fe	Mg/ Ca
T1,+2.5A	563	BOTTOM	2.5	0.69	0.039	0.094	0.176	0.999	0.3481	0.6518	17.692	1.8723
T1,+2.5A	573		2.5	0.293	0.148	0.037	0.521	0.999	0.0663	0.9336	1.9797	14.081
T1,+2.5A	583		2.5	0.537	0.149	0.054	0.259	0.999	0.1725	0.8274	3.6040	4.7962
T1,+2.5A	593		2.5	0.456	0.143	0.044	0.356	0.999	0.11	0.89	3.1888	8.0909
T1,+2.5A	603		2.5	0.584	0.108	0.06	0.247	0.999	0.1954	0.8045	5.4074	4.1166
T1,+2.5A	613		2.5	0.565	0.127	0.065	0.242	0.999	0.2117	0.7882	4.4488	3.7230
T1,+2.5A	623		2.5	0.127	0.551	0.016	0.305	0.999	0.0498	0.9501	0.2304	19.062
T1,+2.5A	633		2.5	0.19	0.377	0.027	0.404	0.998	0.0626	0.9373	0.5039	14.962
T1,+2.5A	643		2.5	0.417	0.206	0.043	0.333	0.999	0.1143	0.8856	2.0242	7.7441
T1,+2.5A	653		2.5	0.668	0.031	0.064	0.236	0.999	0.2133	0.7866	21.548	3.6875
T1,+2.5A	663		2.5	0.337	0.377	0.036	0.25	1	0.1258	0.8741	0.8938	6.9444
T1,+2.5A	673		2.5	0.604	0.101	0.06	0.235	1	0.2033	0.7966	5.9801	3.9166
T1,+2.5A	683		2.5	0.394	0.148	0.045	0.412	0.999	0.0984	0.9015	2.6621	9.1555
T1,+2.5A	693		2.5	0.478	0.127	0.065	0.329	0.999	0.1649	0.8350	3.7637	5.0615
T1,+2.5A	703		2.5	0.408	0.178	0.04	0.374	1	0.0966	0.9033	2.2921	9.35
T1,+2.5A	713		2.5	0.334	0.128	0.04	0.498	1	0.0743	0.9256	2.6093	12.45
T1,+2.5A	711		2.5	0.326	0.41	0.032	0.231	0.999	0.1216	0.8783	0.7951	7.2187
T1,+2.5A	717		2.5	0.107	0.507	0.015	0.37	0.999	0.0389	0.9610	0.2110	24.666
T1,+2.5A	723		2.5	0.292	0.144	0.025	0.538	0.999	0.0444	0.9555	2.0277	21.52
T1,+2.5A	733		2.5	0.544	0.106	0.063	0.285	0.998	0.1810	0.8189	5.1320	4.5238
T1,+2.5A	743		2.5	0.284	0.32	0.025	0.37	0.999	0.0632	0.9367	0.8875	14.8
T1,+2.5A	741		2.5	0.305	0.158	0.031	0.505	0.999	0.0578	0.9421	1.9303	16.290
T1,+2.5A	751	TOP	2.5	0.588	0.102	0.062	0.248	1	0.2	0.8	5.7647	4
T1,+2.5B	525	TOP	2.55	0.369	0.13	0.026	0.474	0.999	0.052	0.948	2.8384	18.230
T1,+2.5B	535		2.55	0.155	0.21	0.01	0.623	0.998	0.0157	0.9842	0.7380	62.3
T1,+2.5B	545		2.55	0.051	0.489	0.001	0.457	0.998	0.0021	0.9978	0.1042	457
T1,+2.5B	555		2.55	0.697	0.053	0.096	0.154	1	0.384	0.616	13.150	1.6041
T1,+2.5B	565		2.55	0.873	0.009	0.105	0.012	0.999	0.8974	0.1025	97	0.1142
T1,+2.5B	563		2.55	0.802	0.022	0.101	0.074	0.999	0.5771	0.4228	36.454	0.7326
T1,+2.5B	575		2.55	0.071	0.259	0.004	0.665	0.999	0.0059	0.9940	0.2741	166.25
T1,+2.5B	585		2.55	0.261	0.204	0.044	0.49	0.999	0.0823	0.9176	1.2794	11.136
T1,+2.5B	595		2.55	0.396	0.177	0.051	0.375	0.999	0.1197	0.8802	2.2372	7.3529
T1,+2.5B	605		2.55	0.889	0.007	0.098	0.005	0.999	0.9514	0.0485	127	0.0510
T1,+2.5B	615		2.55	0.398	0.131	0.03	0.44	0.999	0.0638	0.9361	3.0381	14.666
T1,+2.5B	625		2.55	0.249	0.171	0.021	0.559	1	0.0362	0.9637	1.4561	26.619
T1,+2.5B	635		2.55	0.479	0.125	0.047	0.348	0.999	0.1189	0.8810	3.832	7.4042
T1,+2.5B	645		2.55	0.486	0.232	0.053	0.228	0.999	0.1886	0.8113	2.0948	4.3018
T1,+2.5B	655		2.55	0.48	0.129	0.039	0.351	0.999	0.1	0.9	3.7209	9
T1,+2.5B	665		2.55	0.175	0.316	0.028	0.479	0.998	0.0552	0.9447	0.5537	17.107
T1,+2.5B	675		2.55	0.063	0.431	0.006	0.5	1	0.0118	0.9881	0.1461	83.333
T1,+2.5B	685		2.55	0.439	0.29	0.039	0.231	0.999	0.1444	0.8555	1.5137	5.9230
T1,+2.5B	695		2.55	0.638	0.132	0.069	0.16	0.999	0.3013	0.6986	4.8333	2.3188
T1,+2.5B	705		2.55	0.8	0.02	0.081	0.099	1	0.45	0.55	40	1.2222
T1,+2.5B	715		2.55	0.094	0.467	0.002	0.437	1	0.0045	0.9954	0.2012	218.5
T1,+2.5B	725		2.55	0.417	0.184	0.049	0.35	1	0.1228	0.8771	2.2663	7.1428
T1,+2.5B	735		2.55	0.687	0.046	0.077	0.188	0.998	0.2905	0.7094	14.934	2.4415

T1,+2.5B	745		2.55	0.643	0.168	0.063	0.125	0.999	0.3351	0.6648	3.8273	1.9841
T1,+2.5B	755		2.55	0.438	0.219	0.05	0.293	1	0.1457	0.8542	2	5.86
T1,+2.5B	753		2.55	0.079	0.192	0.001	0.727	0.999	0.0013	0.9986	0.4114	727
T1,+2.5B	765		2.55	0.614	0.103	0.067	0.215	0.999	0.2375	0.7624	5.9611	3.2089
T1,+2.5B	775		2.55	0.659	0.071	0.063	0.206	0.999	0.2342	0.7657	9.2816	3.2698
T1,+2.5B	785		2.55	0.422	0.16	0.047	0.371	1	0.1124	0.8875	2.6375	7.8936
T1,+2.5B	795		2.55	0.627	0.105	0.066	0.2	0.998	0.2481	0.7518	5.9714	3.0303
T1,+2.5B	805		2.55	0.562	0.105	0.055	0.278	1	0.1651	0.8348	5.3523	5.0545
T1,+2.5B	725	RECHEK	2.55	0.264	0.295	0.039	0.401	0.999	0.0886	0.9113	0.8949	10.282

AVERAGE:	0.4328	0.1879	0.0467	0.3316
STD. DEV.:	0.2151	0.1317	0.0257	0.1546

TABLE 23. MICROPROBE DATA FOR SAMPLE T1, +3.4

SAMPLE NUMBER	POSITION	NOTES	STRAT POSIT	Mn	Fe	Ca	Mg	TOTAL	Ca/ Ca+Mg	Mg/ Ca+Mg	Mn/ Fe	Mg/ Ca
T1,+3.4	805	TOP	3.4	0.53	0.076	0.04	0.354	1	0.1015	0.8984	6.9736	8.85
T1,+3.4	800		3.4	0.523	0.124	0.04	0.313	1	0.1133	0.8866	4.2177	7.825
T1,+3.4	800		3.4	0.524	0.123	0.04	0.313	1	0.1133	0.8866	4.2601	7.825
T1,+3.4	790		3.4	0.781	0.048	0.058	0.113	1	0.3391	0.6608	16.270	1.9482
T1,+3.4	780		3.4	0.724	0.065	0.05	0.16	0.999	0.2380	0.7619	11.138	3.2
T1,+3.4	770		3.4	0.656	0.109	0.047	0.187	0.999	0.2008	0.7991	6.0183	3.9787
T1,+3.4	760		3.4	0.37	0.357	0.048	0.223	0.998	0.1771	0.8228	1.0364	4.6458
T1,+3.4	750		3.4	0.879	0.014	0.073	0.033	0.999	0.6886	0.3113	62.785	0.4520
T1,+3.4	740		3.4	0.61	0.099	0.244	0.046	0.999	0.8413	0.1586	6.1616	0.1885
T1,+3.4	730		3.4	0.537	0.127	0.037	0.298	0.999	0.1104	0.8895	4.2283	8.0540
T1,+3.4	720		3.4	0.399	0.357	0.023	0.22	0.999	0.0946	0.9053	1.1176	9.5652
T1,+3.4	710		3.4	0.868	0.023	0.07	0.038	0.999	0.6481	0.3518	37.739	0.5428
T1,+3.4	700		3.4	0.535	0.139	0.031	0.293	0.998	0.0956	0.9043	3.8489	9.4516
T1,+3.4	690	AB SULF	3.4	0.492	0.134	0.032	0.341	0.999	0.0857	0.9142	3.6716	10.656
T1,+3.4	680	CARB IN S	3.4	0.806	0.041	0.067	0.086	1	0.4379	0.5620	19.658	1.2835
T1,+3.4	670		3.4	0.908	0.02	0.032	0.039	0.999	0.4507	0.5492	45.4	1.2187
T1,+3.4	660		3.4	0.82	0.07	0.046	0.062	0.998	0.4259	0.5740	11.714	1.3478
T1,+3.4	650		3.4	0.899	0.026	0.033	0.0411	0.9991	0.4453	0.5546	34.576	1.2454
T1,+3.4	640		3.4	0.77	0.047	0.057	0.125	0.999	0.3131	0.6868	16.382	2.1929
T1,+3.4	630		3.4	0.695	0.076	0.044	0.185	1	0.1921	0.8078	9.1447	4.2045
T1,+3.4	620		3.4	0.757	0.06	0.05	0.132	0.999	0.2747	0.7252	12.616	2.64
T1,+3.4	610		3.4	0.352	0.359	0.253	0.035	0.999	0.8784	0.1215	0.9805	0.1383
T1,+3.4	600		3.4	0.664	0.092	0.044	0.199	0.999	0.1810	0.8189	7.2173	4.5227
T1,+3.4	590		3.4	0.927	0.005	0.063	0.004	0.999	0.9402	0.0597	185.4	0.0634
T1,+3.4	580		3.4	0.444	0.282	0.242	0.032	1	0.8832	0.1167	1.5744	0.1322
T1,+3.4	570		3.4	0.764	0.058	0.123	0.055	1	0.6910	0.3089	13.172	0.4471
T1,+3.4	560		3.4	0.886	0.014	0.027	0.072	0.999	0.2727	0.7272	63.285	2.6666
T1,+3.4	550	W SULF	3.4	0.279	0.444	0.251	0.024	0.998	0.9127	0.0872	0.6283	0.0956
T1,+3.4	540		3.4	0.753	0.062	0.131	0.053	0.999	0.7119	0.2880	12.145	0.4045
T1,+3.4	530		3.4	0.769	0.062	0.048	0.121	1	0.2840	0.7159	12.403	2.5208
		AVERAGE:		0.6640	0.1171	0.0781	0.1399					
		STD. DEV.:		0.1831	0.1164	0.0704	0.1081					

TABLE 24. MICROPROBE DATA FOR SAMPLE T1, +5.9

SAMPLE NUMBER	POSITION	NOTES	STRAT POSIT	Mn	Fe	Ca	Mg	TOTAL	Ca/ Ca+Mg	Mg/ Ca+Mg	Mn/ Fe	Mg/ Ca
T1,+5.9	540	TOP	5.9	0.819	0.026	0.115	0.039	0.999	0.2532	0.7467	31.5	2.9487
T1,+5.9	590		5.9	0.721	0.039	0.098	0.141	0.999	0.5899	0.4100	18.487	0.6950
T1,+5.9	630		5.9	0.7	0.108	0.077	0.114	0.999	0.5968	0.4031	6.4814	0.6754
T1,+5.9	680		5.9	0.865	0.007	0.11	0.017	0.999	0.1338	0.8661	123.57	6.4705
T1,+5.9	730		5.9	0.789	0.022	0.12	0.069	1	0.3650	0.6349	35.863	1.7391
T1,+5.9	780		5.9	0.814	0.005	0.148	0.032	0.999	0.1777	0.8222	162.8	4.625
T1,+5.9	820	BASE	5.9	0.785	0.005	0.175	0.034	0.999	0.1626	0.8373	157	5.1470
			AVERAGE:	0.7847	0.0302	0.1204	0.0637	0.9991				
			STD. DEV.:	0.0530	0.0338	0.0299	0.0434					

TABLE 25. MICROPROBE DATA FOR SAMPLE T1, +8.5

SAMPLE NUMBER	POSITION	NOTES	STRAT POSIT	Mn	Fe	Ca	Mg	TOTAL	Ca/ Ca+Mg	Mg/ Ca+Mg	Mn/ Fe	Mg/ Ca
T1,+8.5	547	TOP	8.5	0.65	0.005	0.322	0.022	0.999	0.0639	0.9360	130	14.636
T1,+8.5	597		8.5	0.829	0.006	0.149	0.015	0.999	0.0914	0.9085	138.16	9.9333
T1,+8.5	647		8.5	0.666	0.038	0.186	0.109	0.999	0.3694	0.6305	17.526	1.7064
T1,+8.5	697		8.5	0.583	0.01	0.369	0.037	0.999	0.0911	0.9088	58.3	9.9729
T1,+8.5	747		8.5	0.679	0.005	0.294	0.021	0.999	0.0666	0.9333	135.8	14
T1,+8.5	797		8.5	0.496	0.008	0.46	0.035	0.999	0.0707	0.9292	62	13.142
T1,+8.5	815	BASE	8.5	0.749	0.053	0.161	0.037	1	0.1868	0.8131	14.132	4.3513
			AVERAGE:	0.6645	0.0178	0.2772	0.0394	0.9991				
			STD. DEV.:	0.0997	0.0180	0.1084	0.0295					

TABLE 26. MICROPROBE DATA FOR SAMPLE T1, +9.8

SAMPLE NUMBER	POSITION	NOTES	STRAT POSIT	Mn	Fe	Ca	Mg	TOTAL	Ca/ Ca+Mg	Mg/ Ca+Mg	Mn/ Fe	Mg/ Ca
T1,+9.8	560	TOP	9.8	0.178	0	0.816	0.005	0.999	0.0060	0.9939		163.2
T1,+9.8	570		9.8	0.2	0	0.794	0.006	1	0.0075	0.9925		132.33
T1,+9.8	580		9.8	0.135	0.012	0.847	0.005	0.999	0.0058	0.9941	11.25	169.4
T1,+9.8	590		9.8	0.169	0.009	0.803	0.019	1	0.0231	0.9768	18.777	42.263
T1,+9.8	600		9.8	0.118	0.008	0.864	0.009	0.999	0.0103	0.9896	14.75	96
T1,+9.8	610		9.8	0.124	0.006	0.866	0.003	0.999	0.0034	0.9965	20.666	288.66
T1,+9.8	620		9.8	0.121	0.005	0.788	0.085	0.999	0.0973	0.9026	24.2	9.2705
T1,+9.8	630		9.8	0.118	0.006	0.871	0.004	0.999	0.0045	0.9954	19.666	217.75
T1,+9.8	640		9.8	0.136	0.008	0.85	0.005	0.999	0.0058	0.9941	17	170
T1,+9.8	650		9.8	0.143	0.005	0.845	0.006	0.999	0.0070	0.9929	28.6	140.83
T1,+9.8	660		9.8	0.129	0	0.862	0.008	0.999	0.0091	0.9908		107.75
T1,+9.8	670		9.8	0.121	0.006	0.869	0.004	1	0.0045	0.9954	20.166	217.25
T1,+9.8	680		9.8	0.119	0.012	0.86	0.008	0.999	0.0092	0.9907	9.9166	107.5
T1,+9.8	690		9.8	0.201	0.006	0.769	0.023	0.999	0.0290	0.9709	33.5	33.434
T1,+9.8	700		9.8	0.13	0.009	0.851	0.01	1	0.0116	0.9883	14.444	85.1
T1,+9.8	710		9.8	0.133	0.009	0.846	0.012	1	0.0139	0.9860	14.777	70.5
T1,+9.8	720		9.8	0.15	0.007	0.825	0.017	0.999	0.0201	0.9798	21.428	48.529
T1,+9.8	MISC PT1		9.8	0.117	0.006	0.849	0.027	0.999	0.0308	0.9691	19.5	31.444
T1,+9.8	MISC PT2		9.8	0.121	0.006	0.777	0.095	0.999	0.1089	0.8910	20.166	8.1789
T1,+9.8	MISC PT3	HOMO GR	9.8	0.121	0.003	0.871	0.004	0.999	0.0045	0.9954	40.333	217.75
		AVERAGE:		0.1392	0.0061	0.8361	0.0177	0.9992				
		STD. DEV.:		0.0261	0.0033	0.0324	0.0250					

TABLE 27. MICROPROBE DATA FOR SAMPLE T1, +12.5

SAMPLE NUMBER	POSITION	NOTES	STRAT POSIT	Mn	Fe	Ca	Mg	TOTAL	Ca/ Ca+Mg	Mg/ Ca+Mg	Mn/ Fe	Mg/ Ca
T1,+12.5	786	TOP	12.5	0.248	0.066	0.667	0.018	0.999	0.0262	0.9737	3.7575	37.055
T1,+12.5	736		12.5	0.357	0.052	0.547	0.042	0.998	0.0713	0.9286	6.8653	13.023
T1,+12.5	686		12.5	0.344	0.056	0.554	0.045	0.999	0.0751	0.9248	6.1428	12.311
T1,+12.5	636		12.5	0.399	0.052	0.509	0.039	0.999	0.0711	0.9288	7.6730	13.051
T1,+12.5	586		12.5	0.218	0.03	0.73	0.021	0.999	0.0279	0.9720	7.2666	34.761
T1,+12.5	542	BASE	12.5	0.278	0.015	0.67	0.036	0.999	0.0509	0.9490	18.533	18.611
		AVERAGE:		0.3073	0.0451	0.6128	0.0335	0.9988				
		STD. DEV.:		0.0639	0.0172	0.0801	0.0103					

TABLE 28. MICROPROBE DATA FOR SAMPLE T1, +15.7

SAMPLE NUMBER	POSITION	NOTES	STRAT POSIT	Mn	Fe	Ca	Mg	TOTAL	Ca/ Ca+Mg	Mg/ Ca+Mg	Mn/ Fe	Mg/ Ca
T1,+15.7	536	TOP?	15.7	0.33	0	0.639	0.031	1	0.0462	0.9537		20.612
T1,+15.7	566		15.7	0.249	0.006	0.708	0.037	1	0.0496	0.9503	41.5	19.135
T1,+15.7	586		15.7	0.22	0.006	0.742	0.032	1	0.0413	0.9586	36.666	23.187
T1,+15.7	637		15.7	0.342	0.008	0.606	0.043	0.999	0.0662	0.9337	42.75	14.093
T1,+15.7	662		15.7	0.16	0.004	0.826	0.008	0.998	0.0095	0.9904	40	103.25
T1,+15.7	687		15.7	0.103	0.085	0.785	0.025	0.998	0.0308	0.9691	1.2117	31.4
T1,+15.7	737		15.7	0.233	0.038	0.689	0.04	1	0.0548	0.9451	6.1315	17.225
T1,+15.7	787		15.7	0.288	0.019	0.656	0.036	0.999	0.0520	0.9479	15.157	18.222
T1,+15.7	827	END	15.7	0.208	0.009	0.749	0.033	0.999	0.0421	0.9578	23.111	22.696
		AVERAGE:		0.237	0.0194	0.7111	0.0316	0.9992				
		STD. DEV.:		0.0726	0.0255	0.0673	0.0097					

TABLE 29. MICROPROBE DATA FOR SAMPLE T1, +19.0

SAMPLE NUMBER	POSITION NOTES	STRAT POSIT	Mn	Fe	Ca	Mg	TOTAL	Ca/ Ca+Mg	Mg/ Ca+Mg	Mn/ Fe	Mg/ Ca
T1,+19.0	NONE	19	0.332	0.019	0.609	0.039	0.999	0.0601	0.9398	17.473	15.615
T1,+19.0		19	0.332	0.012	0.618	0.038	1	0.0579	0.9420	27.666	16.263
T1,+19.0		19	0.305	0.003	0.658	0.003	0.969	0.0045	0.9954	101.66	219.33
T1,+19.0		19	0.252	0.001	0.708	0.038	0.999	0.0509	0.9490	252	18.631
T1,+19.0		19	0.237	0.063	0.665	0.035	1	0.05	0.95	3.7619	19
T1,+19.0		19	0.003	0.988	0.003	0.004	0.998	0.5714	0.4285	0.0030	0.75
T1,+19.0		19	0.441	0.016	0.503	0.038	0.998	0.0702	0.9297	27.562	13.236
T1,+19.0		19	0.433	0.01	0.522	0.034	0.999	0.0611	0.9388	43.3	15.352
T1,+19.0		19	0.39	0	0.546	0.063	0.999	0.1034	0.8965		8.6666
T1,+19.0		19	0.258	0.047	0.658	0.036	0.999	0.0518	0.9481	5.4893	18.277
T1,+19.0		19	0.136	0.006	0.85	0.008	1	0.0093	0.9906	22.666	106.25
T1,+19.0		19	0.342	0	0.621	0.035	0.998	0.0533	0.9466		17.742
T1,+19.0		19	0.004	0.986	0.004	0.006	1	0.6	0.4	0.0040	0.6666
T1,+19.0		19	0.465	0.013	0.492	0.03	1	0.0574	0.9425	35.769	16.4
T1,+19.0		19	0.425	0.008	0.533	0.033	0.999	0.0583	0.9416	53.125	16.151
T1,+19.0		19	0.445	0.018	0.502	0.033	0.998	0.0616	0.9383	24.722	15.212
T1,+19.0		19	0.076	0.64	0.271	0.012	0.999	0.0424	0.9575	0.1187	22.583
T1,+19.0		19	0.001	0.989	0.003	0.006	0.999	0.6666	0.3333	0.0010	0.5
T1,+19.0		19	0.054	0.826	0.108	0.011	0.999	0.0924	0.9075	0.0653	9.8181
T1,+19.0		19	0.064	0.737	0.186	0.013	1	0.0653	0.9346	0.0868	14.307
T1,+19.0	LATHE FAB	19	0.032	0.006	0.939	0.022	0.999	0.0228	0.9771	5.3333	42.681
T1,+19.0		19	0.231	0.014	0.729	0.024	0.998	0.0318	0.9681	16.5	30.375
	AVERAGE:		0.239	0.2455	0.4876	0.0255	0.9976				
	STD. DEV.:		0.1616	0.3839	0.2674	0.0153					

TABLE 30. MICROPROBE DATA FOR SAMPLE T1, +26.7

SAMPLE NUMBER	POSITION NOTES	STRAT POSIT	Mn	Fe	Ca	Mg	TOTAL	Ca/ Ca+Mg	Mg/ Ca+Mg	Mn/ Fe	Mg/ Ca
T1, +26.7	OOID	26.7	0.19	0	0.774	0.035	0.999	0.9567	0.0432		0.0452
T1, +26.7	PELLOID	26.7	0.144	0	0.819	0.037	1	0.9567	0.0432		0.0451
T1, +26.7	OOID	26.7	0.158	0	0.803	0.038	0.999	0.9548	0.0451		0.0473
T1, +26.7	PELLOID	26.7	0.201	0	0.763	0.034	0.998	0.9573	0.0426		0.0445
T1, +26.7	OOID CTR	26.7	0.203	0.014	0.731	0.051	0.999	0.9347	0.0652	14.5	0.0697
T1, +26.7	OOID CTR	26.7	0.13	0.124	0.711	0.035	1	0.9530	0.0469	1.0483	0.0492
T1, +26.7	OOID RIM	26.7	0.171	0.001	0.791	0.036	0.999	0.9564	0.0435	171	0.0455
T1, +26.7	MATRIX	26.7	0.188	0	0.771	0.041	1	0.9495	0.0504		0.0531
	AVERAGE:		0.1731	0.0173	0.7703	0.0383	0.9992				
	STD. DEV.:		0.0252	0.0405	0.0335	0.0051					

TABLE 31. MICROPROBE DATA FOR SAMPLE T1, +35.4

SAMPLE NUMBER	POSITION	NOTES	STRAT POSIT	Mn	Fe	Ca	Mg	TOTAL	Ca/ Ca+Mg	Mg/ Ca+Mg	Mn/ Fe	Mg/ Ca
T1, +35.4			35.4	0.217	0.005	0.7337	0.04	0.9957	0.9483	0.0516	43.4	0.0545
T1, +35.4			35.4	0.182	0.008	0.769	0.04	0.999	0.9505	0.0494	22.75	0.0520
T1, +35.4		NR PY	35.4	0.169	0.006	0.794	0.029	0.998	0.9647	0.0352	28.166	0.0365
		AVERAGE:		0.1893	0.0063	0.7655	0.0363					
		STD. DEV.:		0.0202	0.0012	0.0247	0.0051					

TABLE 32. MICROPROBE DATA FOR SAMPLE T1, +45.3

SAMPLE NUMBER	POSITION	NOTES	STRAT POSIT	Mn	Fe	Ca	Mg	TOTAL	Ca/ Ca+Mg	Mg/ Ca+Mg	Mn/ Fe	Mg/ Ca
T1, +45.3	828	TOP	45.3	0.021	0	0.946	0.032	1	0.9672	0.0327		0.0338
T1, +45.3	800	MATRIX	45.3	0.016	0	0.961	0.022	1	0.9776	0.0223		0.0228
T1, +45.3	775		45.3	0.022	0.001	0.957	0.019	1	0.9805	0.0194	22	0.0198
T1, +45.3	750	NR SHELL	45.3	0.016	0	0.954	0.029	0.999	0.9704	0.0295		0.0303
T1, +45.3	725	MATRIX	45.3	0.012	0	0.953	0.033	0.998	0.9665	0.0334		0.0346
T1, +45.3	707	NR SHELL	45.3	0.021	0	0.956	0.022	0.999	0.9775	0.0224		0.0230
T1, +45.3		INT SPAR	45.3	0.065	0	0.926	0.007	0.998	0.9924	0.0075		0.0075
T1, +45.3		SH WALL	45.3	0.085	0	0.902	0.011	0.998	0.9879	0.0120		0.0121
T1, +45.3		DISAR SH	45.3	0.021	0	0.952	0.027	1	0.9724	0.0275		0.0283
T1, +45.3		DISAR SH	45.3	0.025	0	0.954	0.02	0.999	0.9794	0.0205		0.0209
T1, +45.3		MATRIX	45.3	0.059	0.001	0.915	0.024	0.999	0.9744	0.0255	59	0.0262
		AVERAGE:		0.033	0.0001	0.9432	0.0223					
		STD. DEV.:		0.0234	0.0003	0.0187	0.0077					

TABLE 33. MICROPROBE DATA FOR SAMPLE T1, +47.9

SAMPLE NUMBER	POSITION NOTES	STRAT POSIT	Mn	Fe	Ca	Mg	TOTAL	Ca/ Ca+Mg	Mg/ Ca+Mg	Mn/ Fe	Mg/ Ca
T1, +47.9		47.9	0.108	0.142	0.566	0.183	0.999	0.7556	0.2443	0.7605	0.3233
T1, +47.9		47.9	0.093	0.008	0.885	0.014	1	0.9844	0.0155	11.625	0.0158
T1, +47.9		47.9	0.141	0.011	0.815	0.032	0.999	0.9622	0.0377	12.818	0.0392
T1, +47.9	PELLOID	47.9	0.168	0	0.794	0.037	0.999	0.9554	0.0445		0.0465
T1, +47.9	MATRIX	47.9	0.086	0.007	0.891	0.015	0.999	0.9834	0.0165	12.285	0.0168
T1, +47.9	MATRIX	47.9	0.141	0.011	0.813	0.035	1	0.9587	0.0412	12.818	0.0430
T1, +47.9	SHELL	47.9	0.096	0	0.861	0.042	1	0.9534	0.0465		0.0487
T1, +47.9	CEMENT	47.9	0.046	0.004	0.92	0.029	0.999	0.9694	0.0305	11.5	0.0315
	AVERAGE:		0.1098	0.0228	0.8181	0.0483					
	STD. DEV.:		0.0361	0.0452	0.1037	0.0517					

TABLE 34. MICROPROBE DATA FOR SAMPLE T1, +78.1

SAMPLE NUMBER	POSITION	NOTES	STRAT POSIT	Mn	Fe	Ca	Mg	TOTAL	Ca/ Ca+Mg	Mg/ Ca+Mg	Mn/ Fe	Mg/ Ca
T1, +78.1		GRAIN	78.1	0.021	0.002	0.974	0.001	1	0.9989	0.0010	10.5	0.0010
T1, +78.1		MATRIX	78.1	0.018	0.005	0.963	0.013	0.999	0.9866	0.0133	3.6	0.0134
T1, +78.1		MATRIX	78.1	0.04	0.003	0.94	0.017	1	0.9822	0.0177	13.333	0.0180
T1, +78.1		GRAIN	78.1	0.039	0.016	0.938	0.006	0.999	0.9936	0.0063	2.4375	0.0063
T1, +78.1		GRAIN	78.1	0.019	0.002	0.972	0.006	0.999	0.9938	0.0061	9.5	0.0061
		AVERAGE:		0.0274	0.0056	0.9574	0.0086	0.999				
		STD. DEV.:		0.0099	0.0053	0.0154	0.0056					

TABLE 35. MICROPROBE DATA FOR VEIN FILLING AND BRECCIA ASSOCIATED CARBONATES.

SAMPLE NUMBER	POSITION	NOTES	Mn	Fe	Ca	Mg	TOTAL	Ca/ Ca+Mg	Mg/ Ca+Mg	Mn/ Fe	Mg/ Ca
MISC#2	NONE		0.752	0.014	0.186	0.047	0.999	0.7982	0.2017	53.714	3.3571
MISC#2	NONE		0.794	0.006	0.157	0.041	0.998	0.7929	0.2070	132.33	6.8333
MISC#2	NONE		0.845	0.004	0.114	0.035	0.998	0.7651	0.2348	211.25	8.75
MISC#2	NONE		0.858	0	0.113	0.028	0.999	0.8014	0.1985		
MISC#2	NONE		0.84	0.006	0.126	0.027	0.999	0.8235	0.1764	140	4.5
MISC#2	NONE		0.866	0	0.103	0.031	1	0.7686	0.2313		
MISC#3	NONE		0.118	0.169	0.504	0.208	0.999	0.7078	0.2921	0.6982	1.2307
MISC#3	NONE		0.121	0.167	0.512	0.2	1	0.7191	0.2808	0.7245	1.1976
MISC#3	NONE		0.129	0.168	0.503	0.198	0.998	0.7175	0.2824	0.7678	1.1785
MISC#4	NONE	ZONED	0.053	0	0.921	0.025	0.999	0.9735	0.0264		
MISC#4	NONE	RHOMB	0.128	0	0.853	0.018	0.999	0.9793	0.0206		
MISC#4	NONE		0.127	0	0.86	0.012	0.999	0.9862	0.0137		
MISC#4	NONE		0.054	0	0.916	0.029	0.999	0.9693	0.0306		
MISC#4	NONE		0.048	0	0.931	0.021	1	0.9779	0.0220		
MISC#4	NONE		0.057	0	0.91	0.032	0.999	0.9660	0.0339		
MISC#5	NONE		0.376	0.332	0.046	0.245	0.999	0.1580	0.8419	1.1325	0.7379
MISC#5	NONE		0.38	0.331	0.058	0.229	0.998	0.2020	0.7979	1.1480	0.6918
MISC#5	NONE		0.439	0.282	0.064	0.213	0.998	0.2310	0.7689	1.5567	0.7553
MISC#5	NONE		0.377	0.325	0.05	0.248	1	0.1677	0.8322	1.16	0.7630
MISC#6	NONE		0.029	0	0.956	0.014	0.999	0.9855	0.0144		
MISC#6	NONE		0.026	0	0.96	0.013	0.999	0.9866	0.0133		
MISC#6	NONE		0.021	0	0.966	0.012	0.999	0.9877	0.0122		

APPENDIX C

TABLE OF X-RAY DIFFRACTION LINES FOR CALCITE-TYPE AND DOLOMITE-TYPE CARBONATE MINERALS

AND

X-RAY DIFFRACTION PATTERNS FOR SAMPLES FROM THIS STUDY

TABLE 36. LIST OF HKL VALUES AND THEIR d-SPACINGS FOR THE CARBONATE MINERALS CONSIDERED.

MINERAL	FILE NUMBER	003 *	101 *	012	104	006	015 *	110	113	021 *	202	107 *	022	024
CALCITE	24-027			3.852	3.03	2.834		2.495	2.284		2.094			1.926
MAGNESITE	08-479				2.742	2.503		2.318	2.102				1.939	1.769
SIDERITE	29-696			3.593	2.795	2.564		2.346	2.134					1.796
RHODOCHROSITE	07-268			3.66	2.84			2.39	2.172					1.829
Mn-CALCITE	02-714				2.95			2.4	2.24					
Mn-SIDERITE	27-248			3.62	2.822	2.575	2.455	2.364	2.148					1.805
DOLOMITE	11-078		4.03	3.69	2.886	2.67	2.54	2.405	2.192	2.066				1.848
ANKERITE	12-088			3.704	2.899	2.685	2.552	2.411	2.199	2.067				1.852
KUTNAHORITE	11-345		4.27	3.75	2.94	2.73	2.59	2.44	2.23	2.1				1.876
Ca-KUTNAHORITE	19-234		4.13	3.78	2.981	2.771	2.771	2.462	2.248	2.248				1.896
Mg-KUTNAHORITE	20-225	5.41		3.73	2.91	2.701	2.564	2.423	2.209					1.862

* = Superstructure reflections for dolomite type minerals reported from Graf, 1961; Howie and Broadhurst, 1958; Tsusue, 1967; and Gabrielson and Sundius, 1965.

MINERAL	FILE NUMBER	018	116	009 *	211	122	027 *	1010	212	214	208	028	119	
CALCITE	24-027	1.907	1.872		1.625	1.604		1.582		1.524				1.5061
MAGNESITE	08-479	1.7	1.7		1.51	1.488		1.406		1.406	1.371		1.371/1.354	
SIDERITE	29-696	1.738	1.731		1.529	1.506		1.439		1.426	1.396			1.3818
RHODOCHROSITE	07-268	1.77	1.763		1.556	1.533				1.452	1.423			
Mn-CALCITE	02-714	1.85	1.81			1.56				1.48				
Mn-SIDERITE	27-248	1.745			1.536	1.517		1.447		1.435	1.406			1.392
DOLOMITE	11-078	1.804	1.786	1.781	1.567	1.545		1.496		1.465		1.445		1.431
ANKERITE	12-088	1.812	1.792	1.792	1.569	1.548		1.591		1.468		1.449		1.436
KUTNAHORITE	11-345	1.837		1.814	1.588	1.566			1.54	1.486		1.469		1.465
Ca-KUTNAHORITE	19-234	1.869	1.84		1.601	1.578		1.578		1.501	1.487			1.478
Mg-KUTNAHORITE	20-225	1.823	1.804	1.8	1.578	1.556	1.556	1.512		1.477	1.457			1.445

MINERAL	FILE NUMBER	125	1011	030	300	0012	303 *	217	0210	2010	128	306	220
CALCITE	24-027				1.4405	1.4168			1.3361				
MAGNESITE	08-479				1.338	1.252		1.2386	1.2022		1.1798	1.1798	1.1583
SIDERITE	29-696				1.3548	1.2823		1.2593	1.2269		1.2002	1.1977	1.1737
RHODOCHROSITE	07-268			1.379		1.306			1.248		1.221		
Mn-CALCITE	02-714				1.4	1.37		SEE	NOTES				
Mn-SIDERITE	27-248				1.363	1.289			1.234		1.208		1.181
DOLOMITE	11-078	1.413		1.389		1.335		1.297	1.269		1.238		1.202
ANKERITE	12-088	1.416		1.391		1.341		1.3	1.273		1.241		1.205
KUTNAHORITE	11-345	1.409				1.363				1.294	1.258		
Ca-KUTNAHORITE	19-234	1.448	1.448		1.418	1.386		1.386	1.311		1.273		
Mg-KUTNAHORITE	20-225						1.398	1.309	1.2816				1.2071

MINERAL	FILE NUMBER	131	223	1112	312	2012	220	2011	2110	134	0114	039
CALCITE	24-027								1.1779	1.1536		
MAGNESITE	08-479			1.1011					1.0669	1.0669		
SIDERITE	29-696			1.1254	1.1154				1.0872	1.082		
RHODOCHROSITE	07-268			1.146						1.1014		
Mn-CALCITE	02-714											
Mn-SIDERITE	27-248	1.131		1.131		1.09						
DOLOMITE	11-078			1.168	1.144				1.123			
ANKERITE	12-088			1.171	1.144				1.126	1.112		
KUTNAHORITE	11-345							1.189	1.145/1	1.126		
Ca-KUTNAHORITE	19-234							1.229				
Mg-KUTNAHORITE	20-225		1.1799	1.1799	1.1524		1.2071	1.2071	1.1328	1.1176	1.1176	1.1043

MINERAL	FILE NUMBER	226	309	1211	0015	404	318	2014	1016	321	232	1115
CALCITE	24-027	1.1417				1.0471	1.044					
MAGNESITE	08-479	1.051		1.0145		0.9692	0.9573	0.9455				
SIDERITE	29-696	1.0671				0.9825	0.9724	0.9666	0.9358	0.9309	0.9256	
RHODOCHROSITE	07-268											
Mn-CALCITE	02-714											
Mn-SIDERITE	27-248	1.076										
DOLOMITE	11-078	1.096	1.096		1.068	1.008	1.001		0.973			
ANKERITE	12-088	1.099	1.099		1.066	1.01	1.003		0.976			
KUTNAHORITE	11-345				1.089			1.022				0.9763
Ca-KUTNAHORITE	19-234											
Mg-KUTNAHORITE	20-225											

MINERAL	FILE NUMBER	ADDITIONAL LINES
CALCITE	24-027	
MAGNESITE	08-479	TEN
SIDERITE	29-696	
RHODOCHROSITE	07-268	
Mn-CALCITE	02-714	13 UN-INDEXED PEAKS
Mn-SIDERITE	27-248	
DOLOMITE	11-078	TWELVE
ANKERITE	12-088	3012=0.966, 322=0.953
KUTNAHORITE	11-345	
Ca-KUTNAHORITE	19-234	
Mg-KUTNAHORITE	20-225	

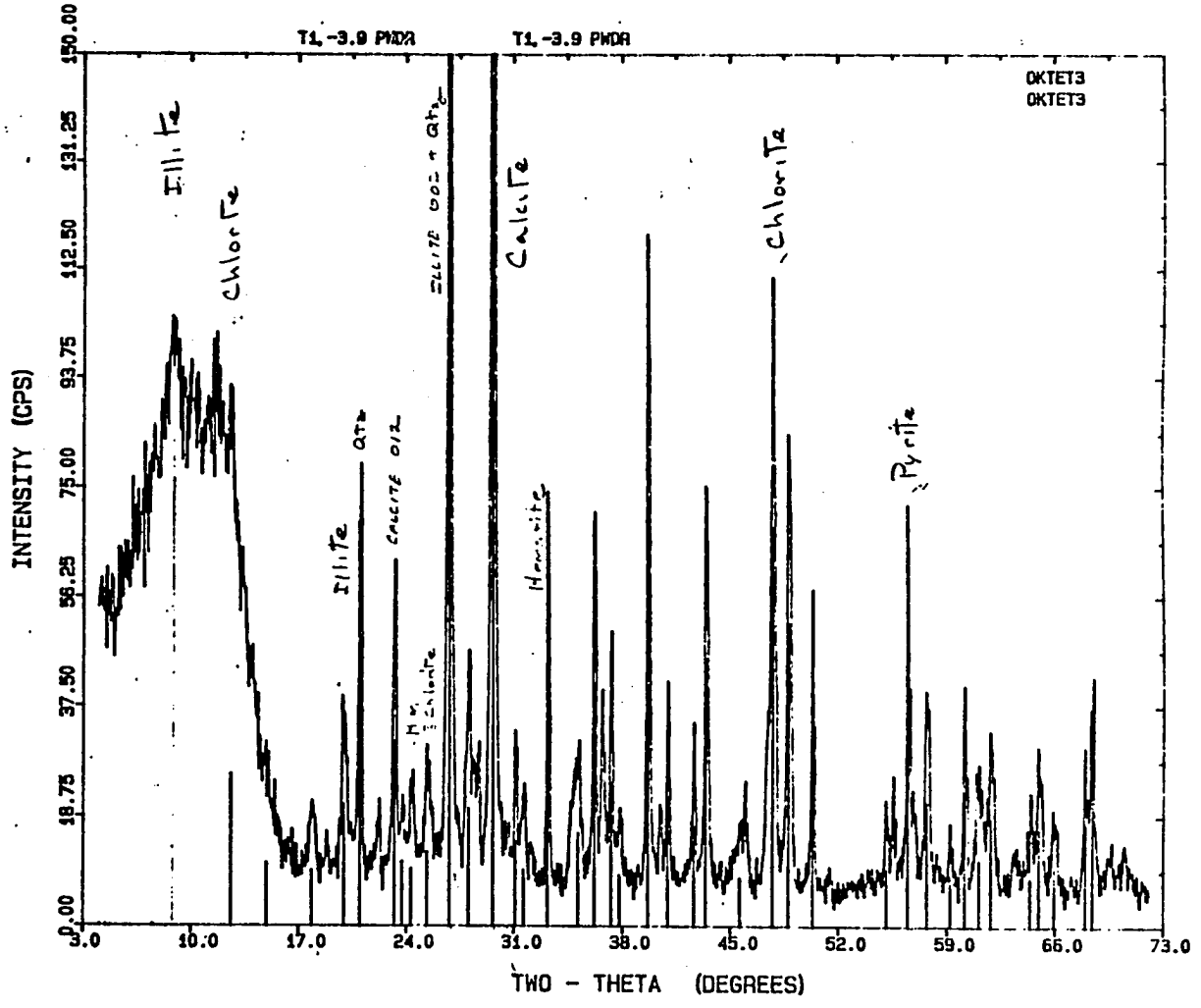

Figure 52. X-ray diffraction pattern for sample T1,-3.9.

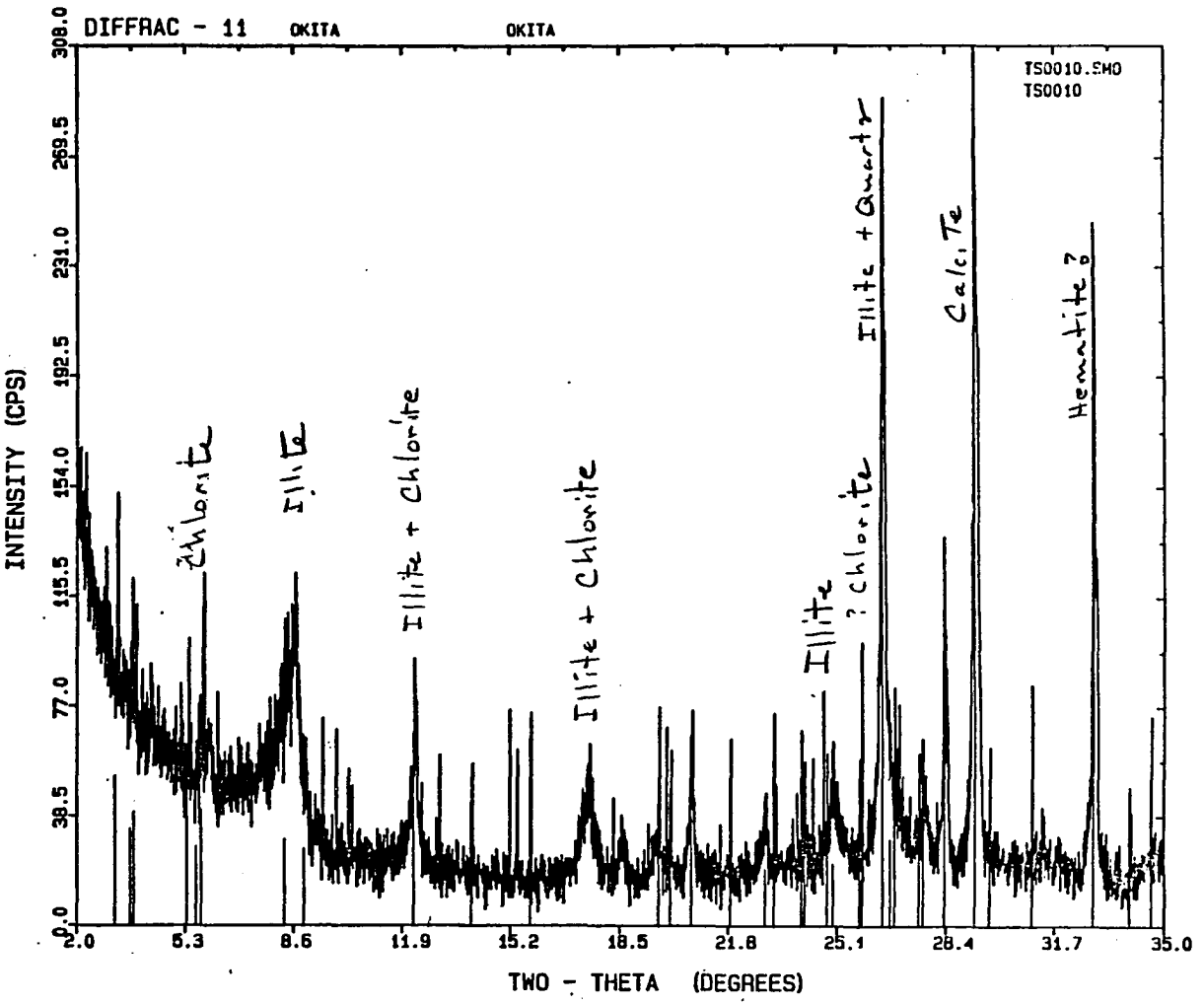

Figure 53. X-ray diffraction pattern for sample T1,-0.1.

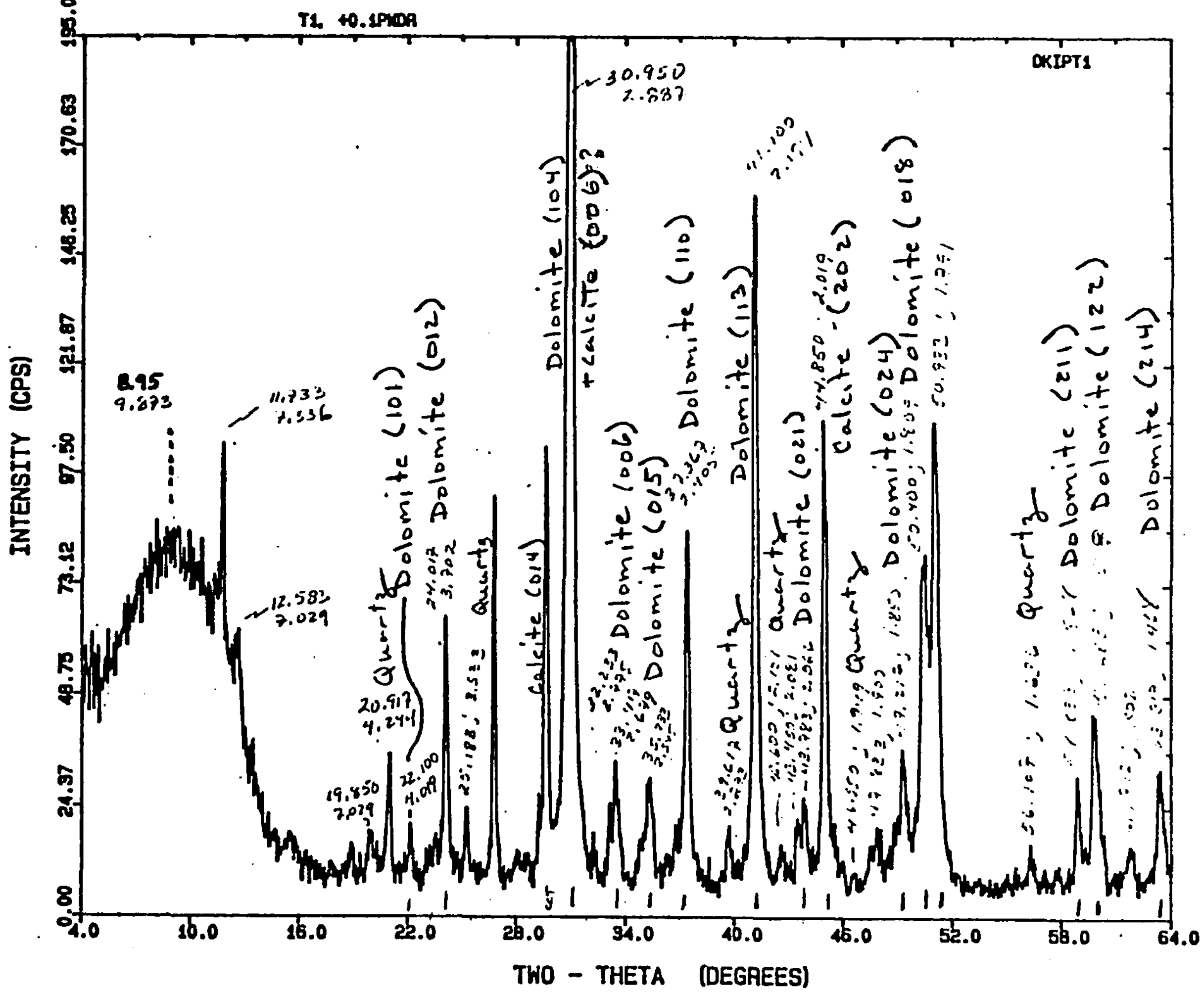

Figure 54 . X-ray diffraction pattern for sample T1,+0.1.

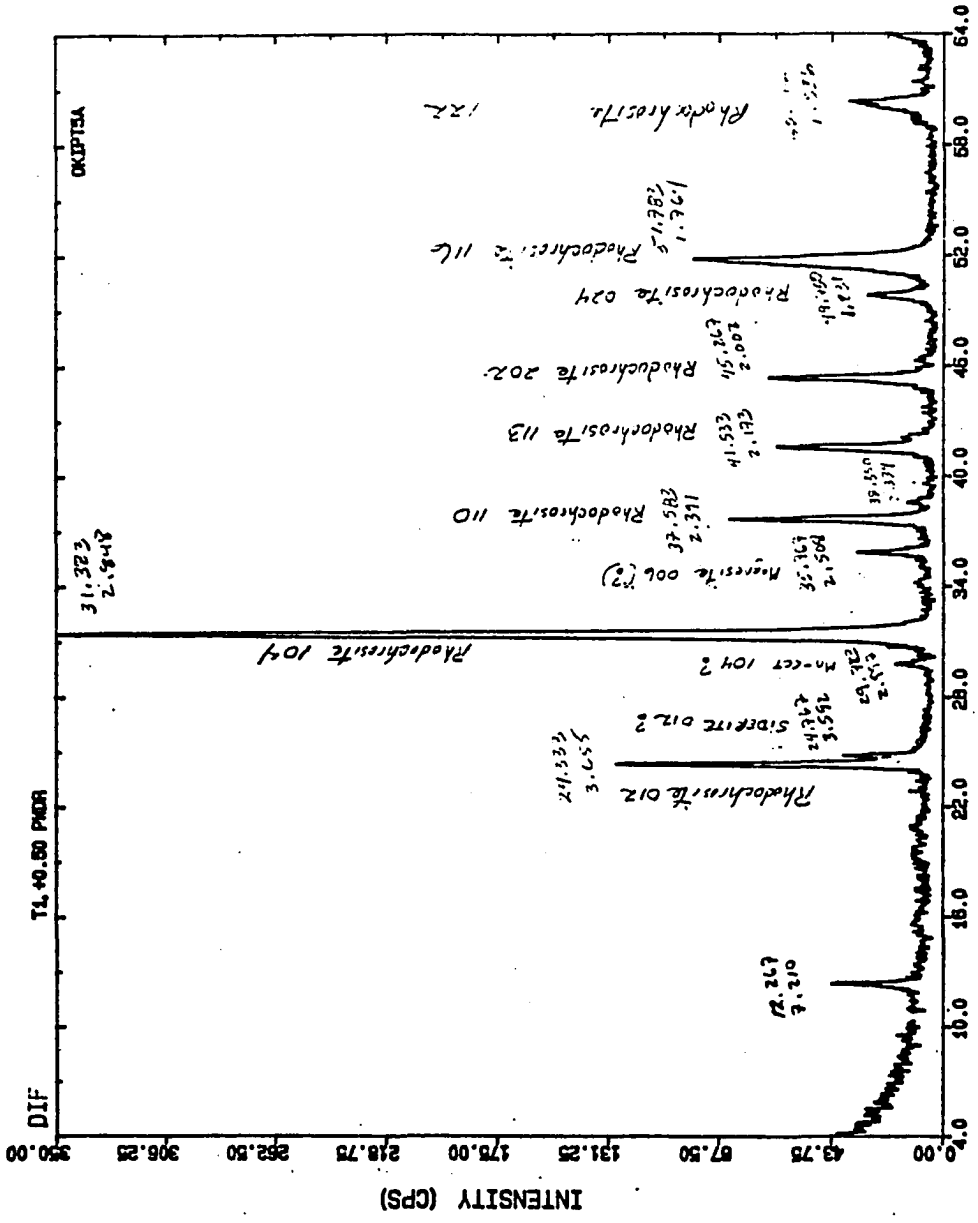

Figure 55. X-ray diffraction pattern for sample T1,+0.5.

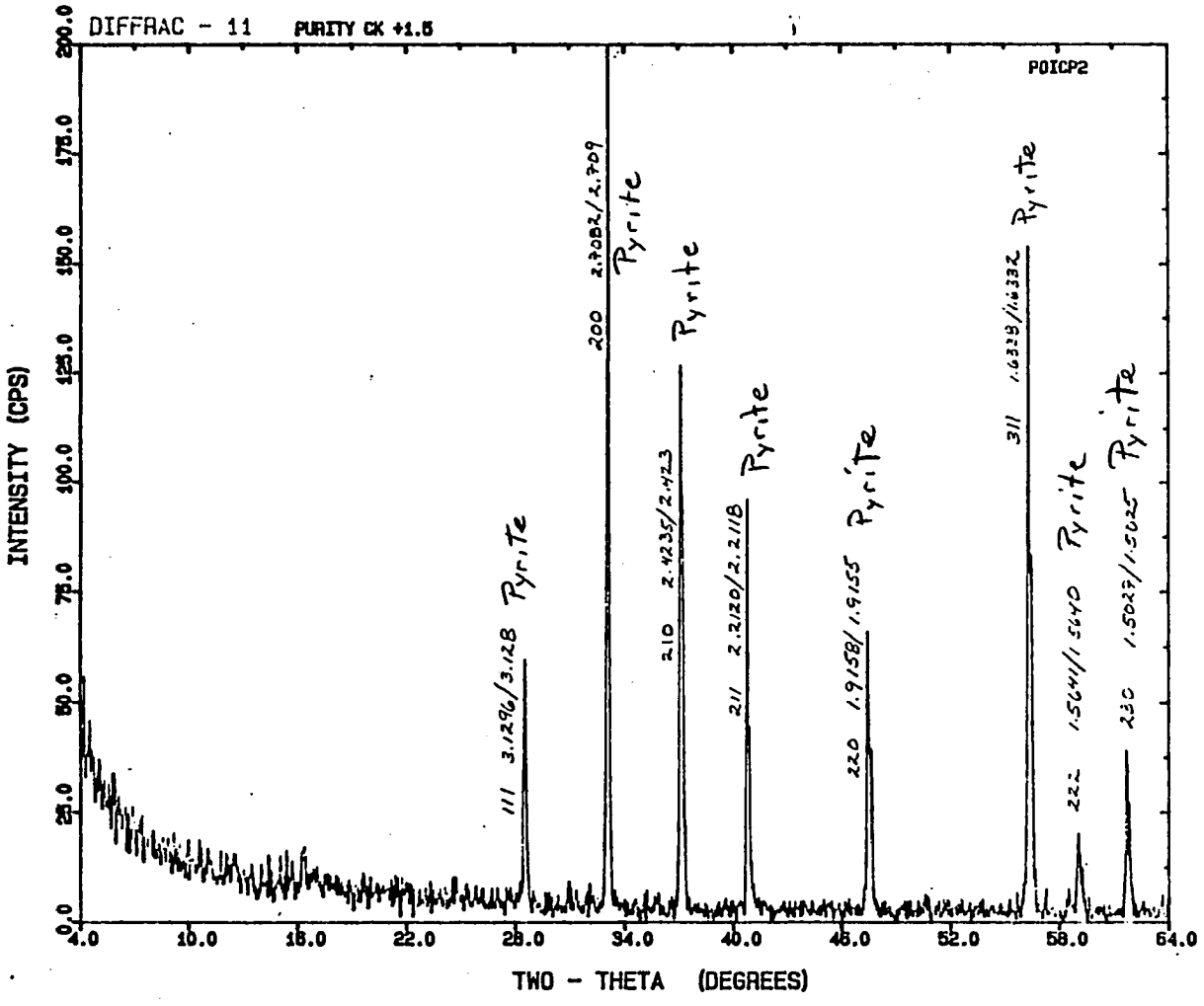

Figure 56 . X-ray diffraction pattern for sample T1,+1.5.

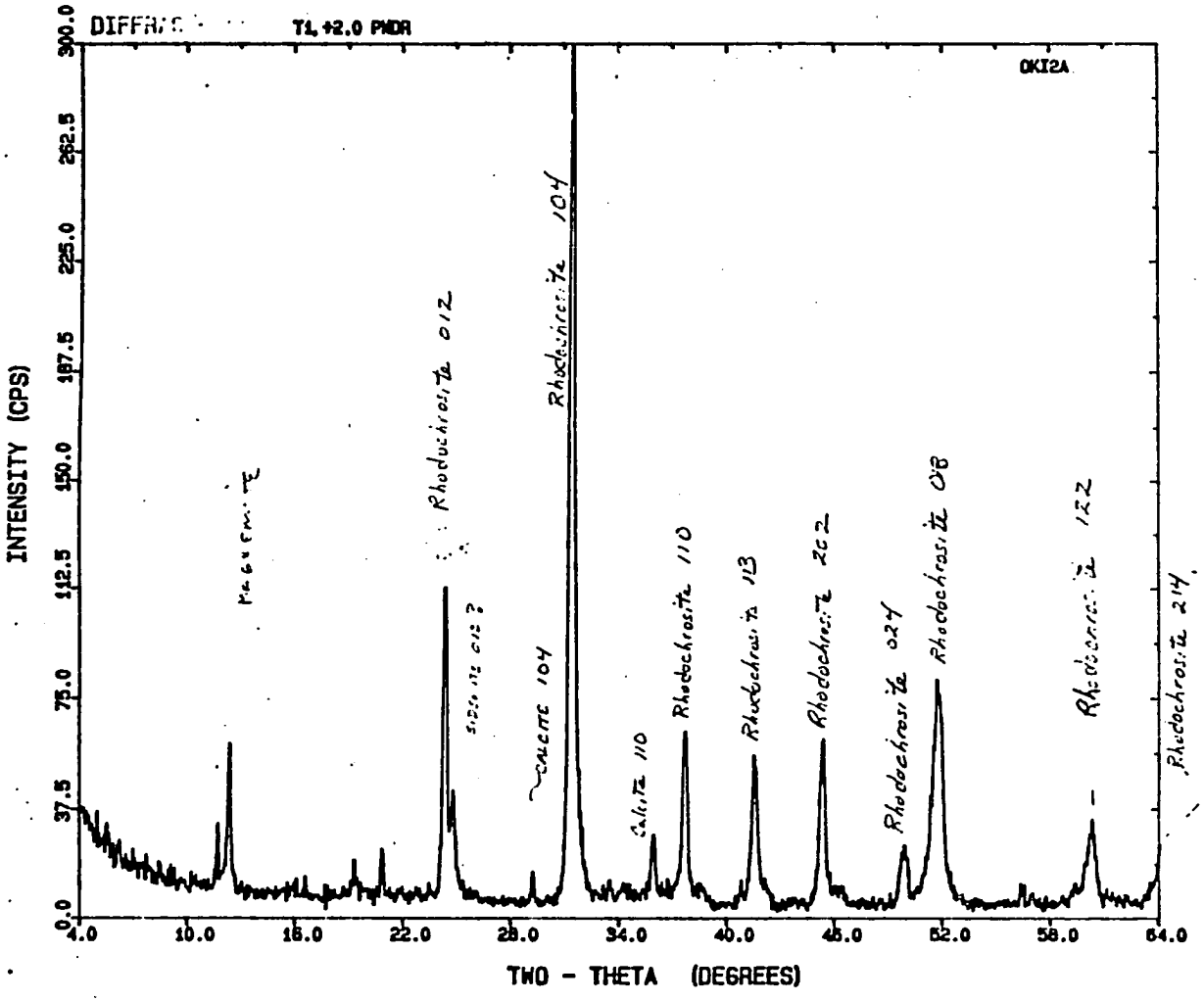

Figure 57. X-ray diffraction pattern for sample T1,+2.0.

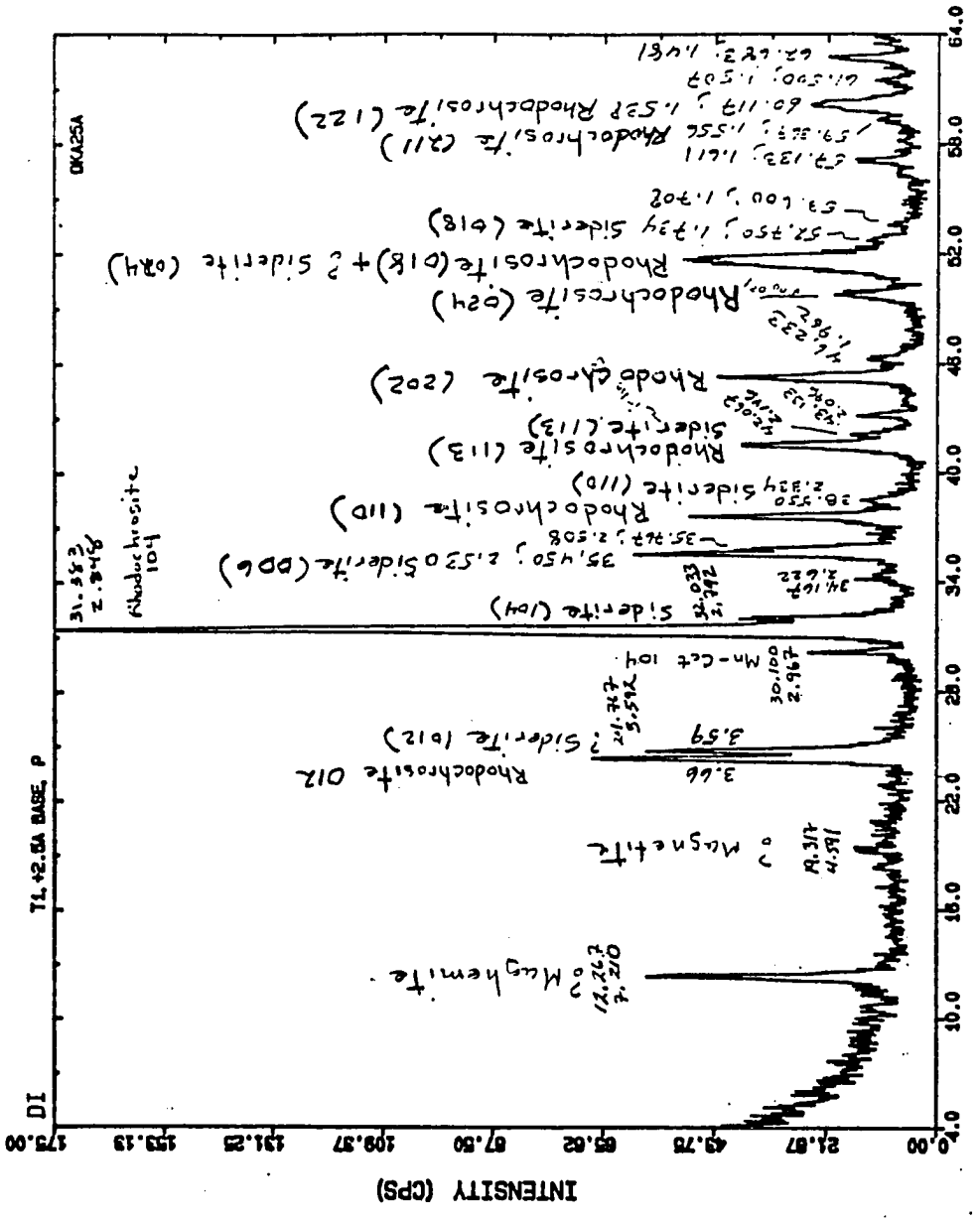

Figure 58. X-ray diffraction pattern for sample T1,+2.50.

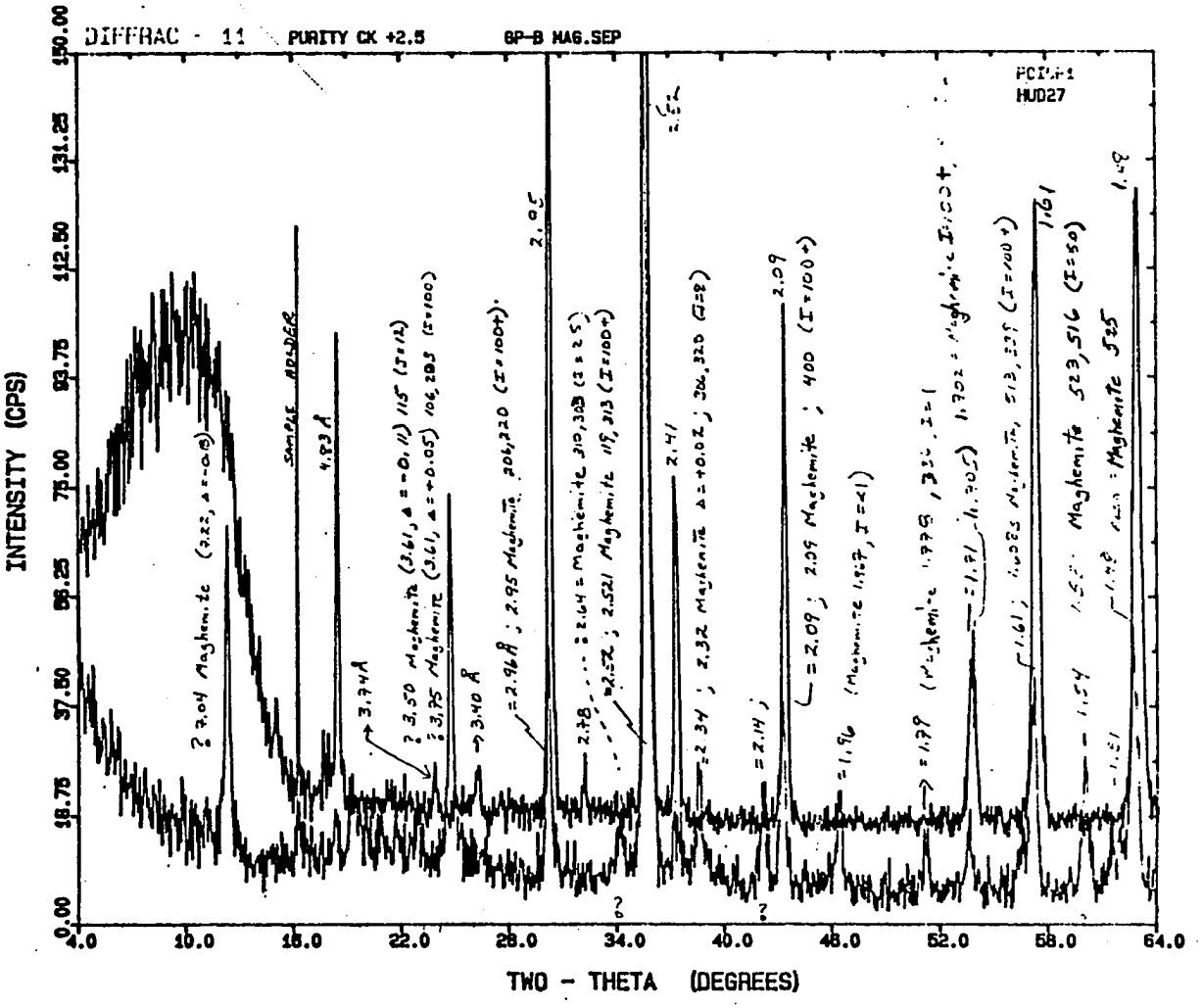

Figure 59. Comparison of X-ray diffraction patterns for the magnetic mineral seperate from sample T1,+2.50 (lower pattern) and a magnetite reference sample (upper pattern). Possible maghemite peaks are indexed.

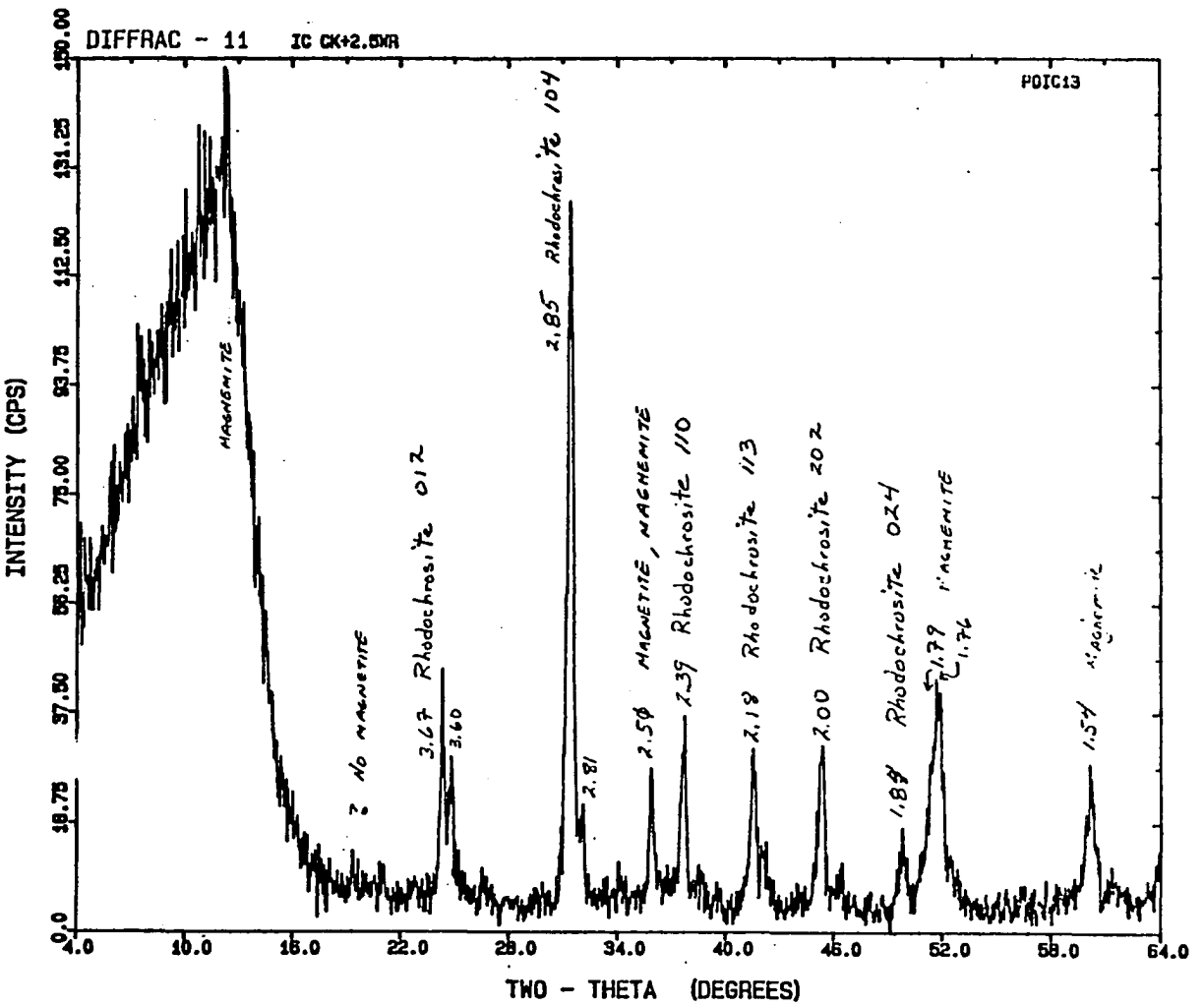

Figure 60 . X-ray diffraction pattern for sample T1,+2.55.

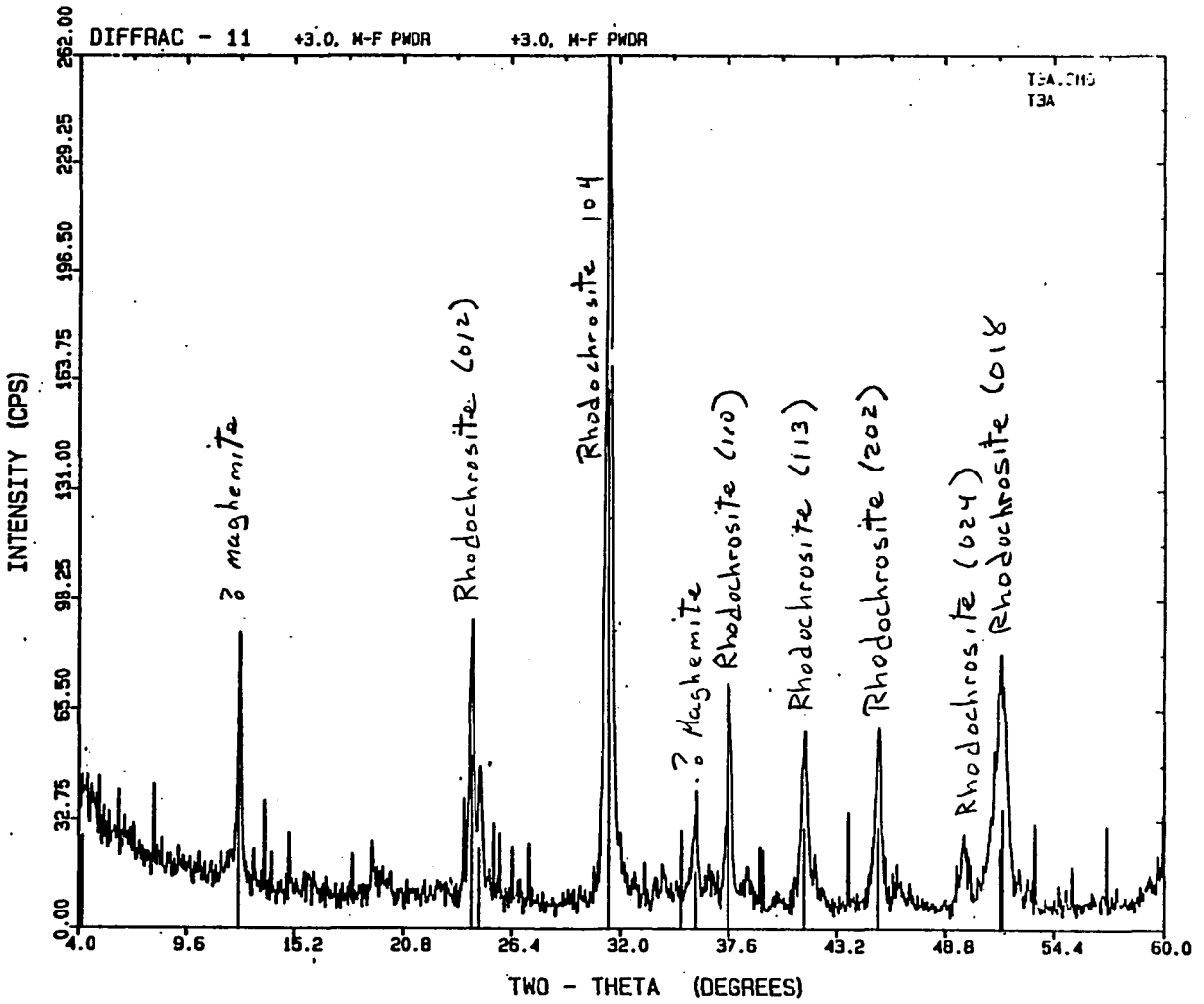

Figure 61 . X-ray diffraction pattern for sample T1,+3.0.

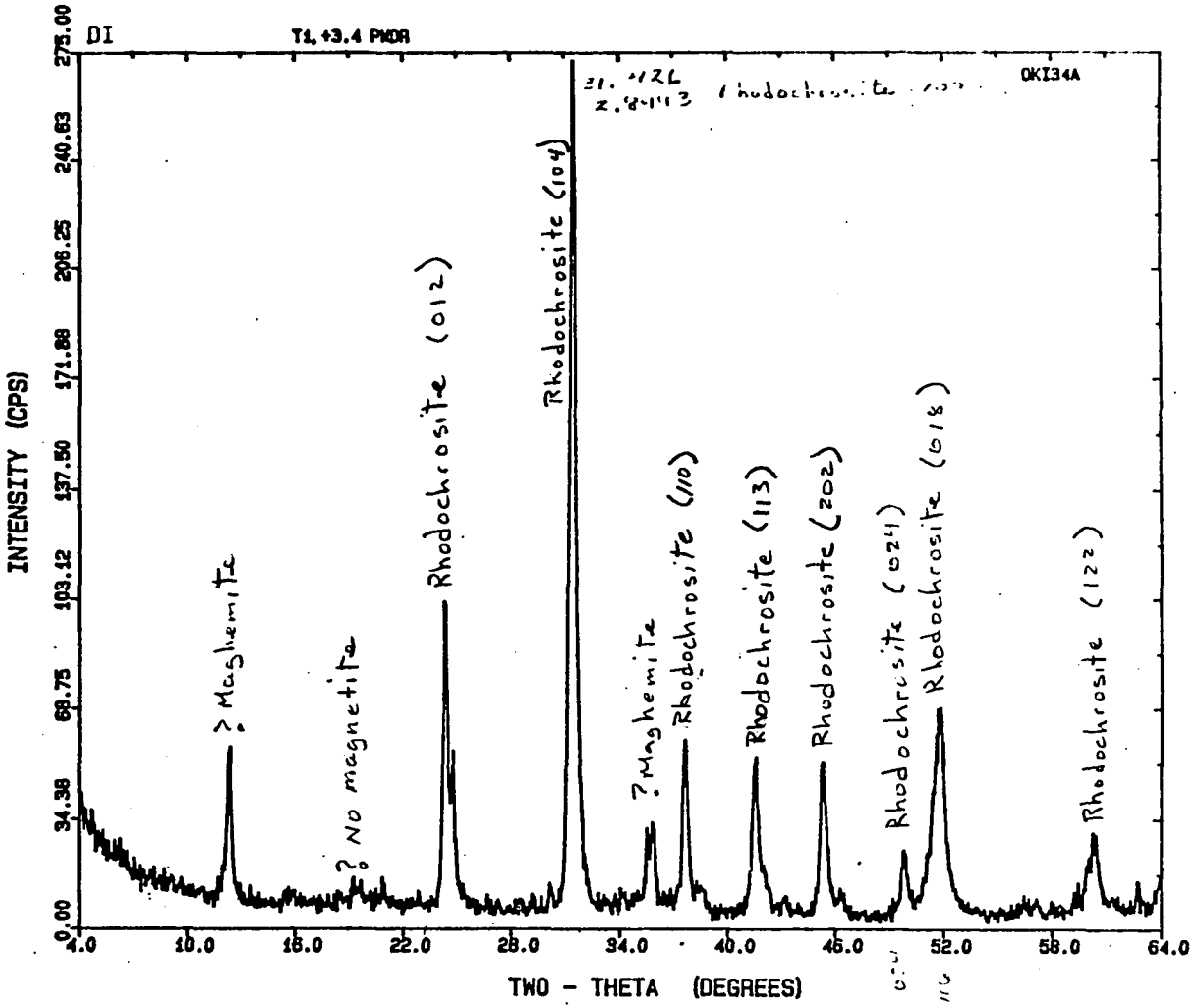

Figure 62. X-ray diffraction pattern for sample T1,+3.4.

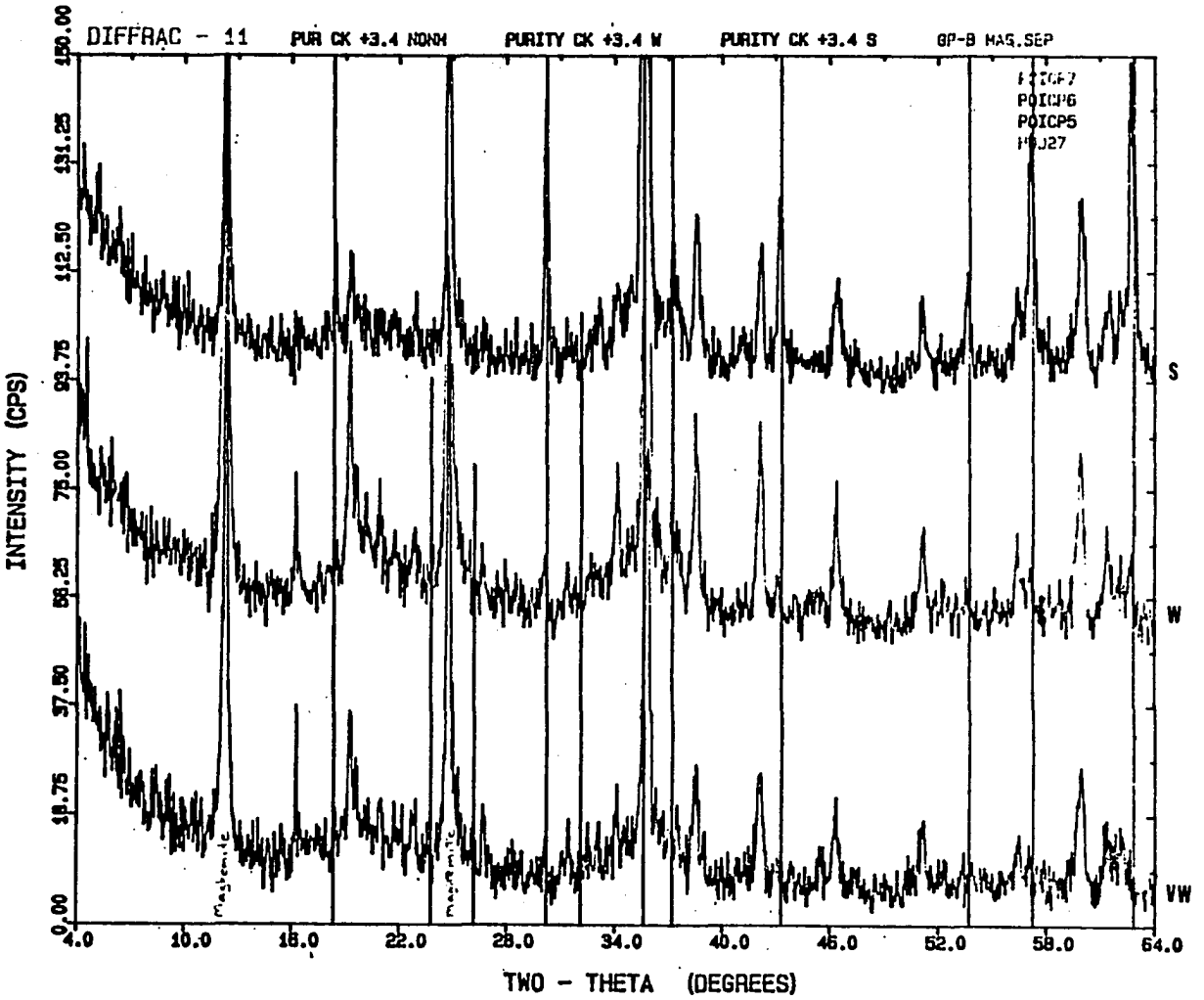

Figure 63 . Comparisons of X-ray patterns for strongly (S), weakly (W), and very weakly (VW) magnetic seperates from sample T1,+3.4. Vertical lines mark the position of magnetite peaks.

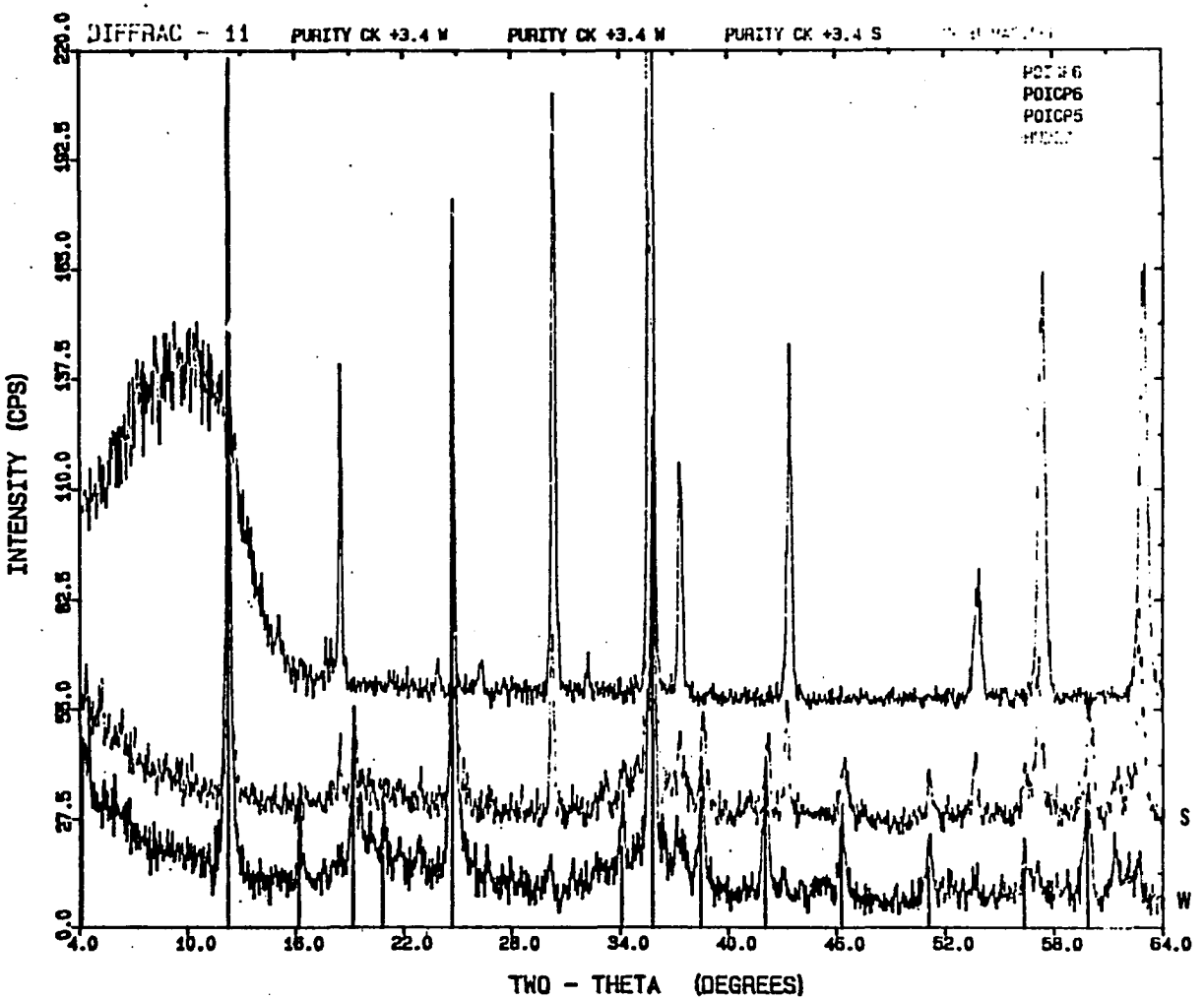

Figure 64. Comparisons of X-ray diffraction patterns for the strongly (S) and weakly (W) magnetic mineral seperates from sample T1,+3.4, with that of a magnetite reference standard (top pattern). Vertical lines mark the position of maghemite peaks.

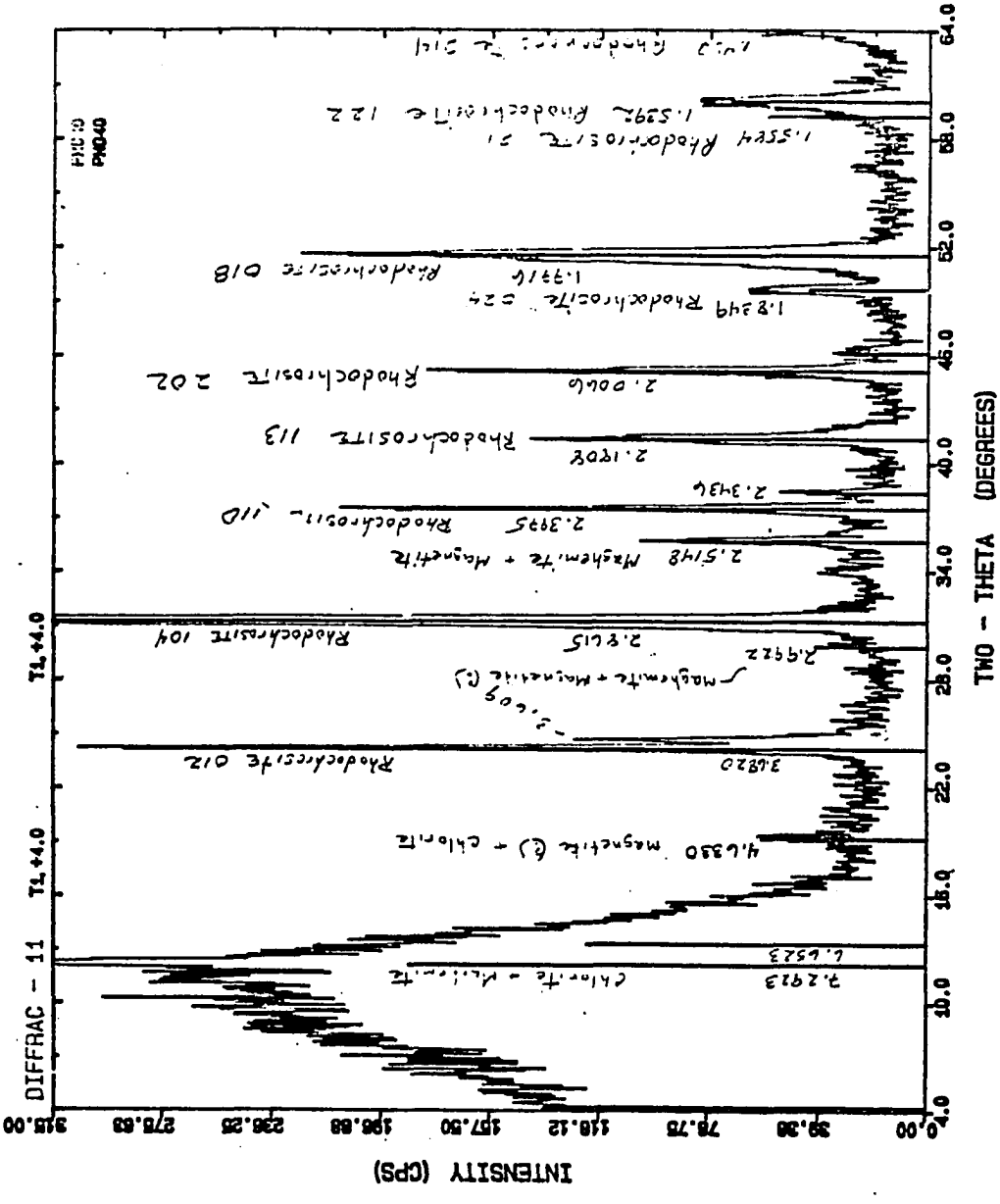

Figure 65. X-ray diffraction pattern for sample T1,+4.0.

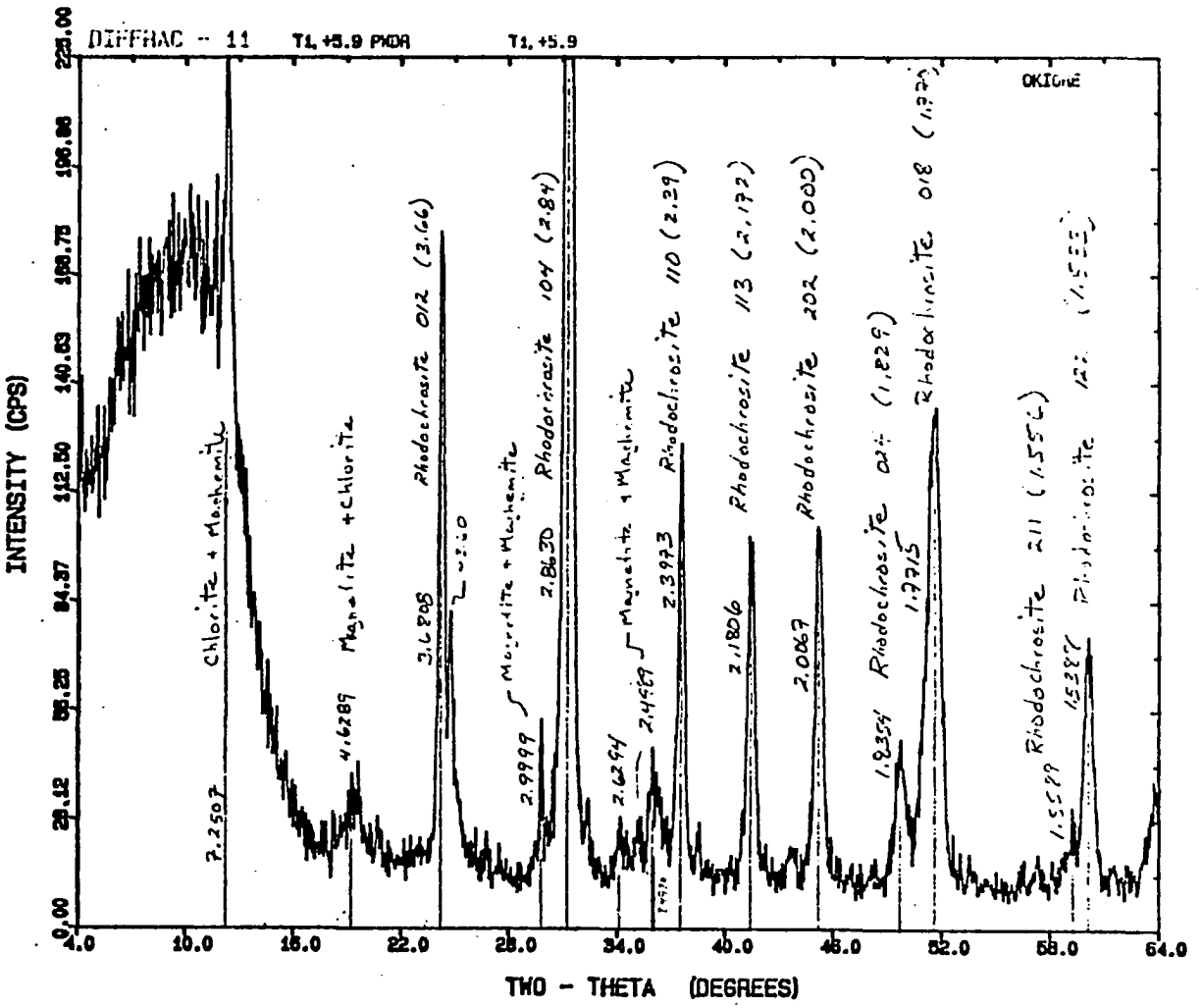

Figure 66. X-ray diffraction pattern for sample T1,+5.9.

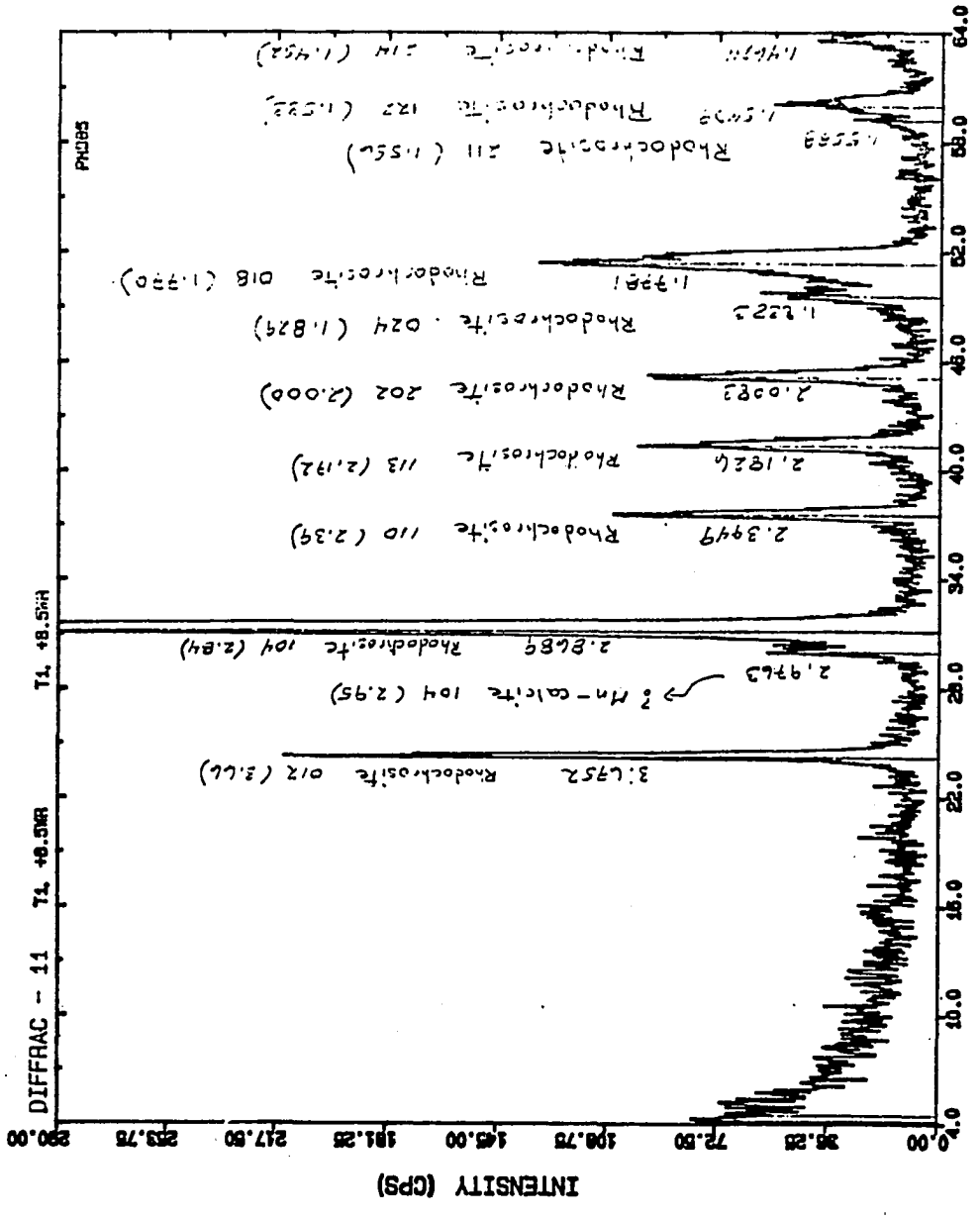

Figure 67. X-ray diffraction pattern for sample T1,+8.5.

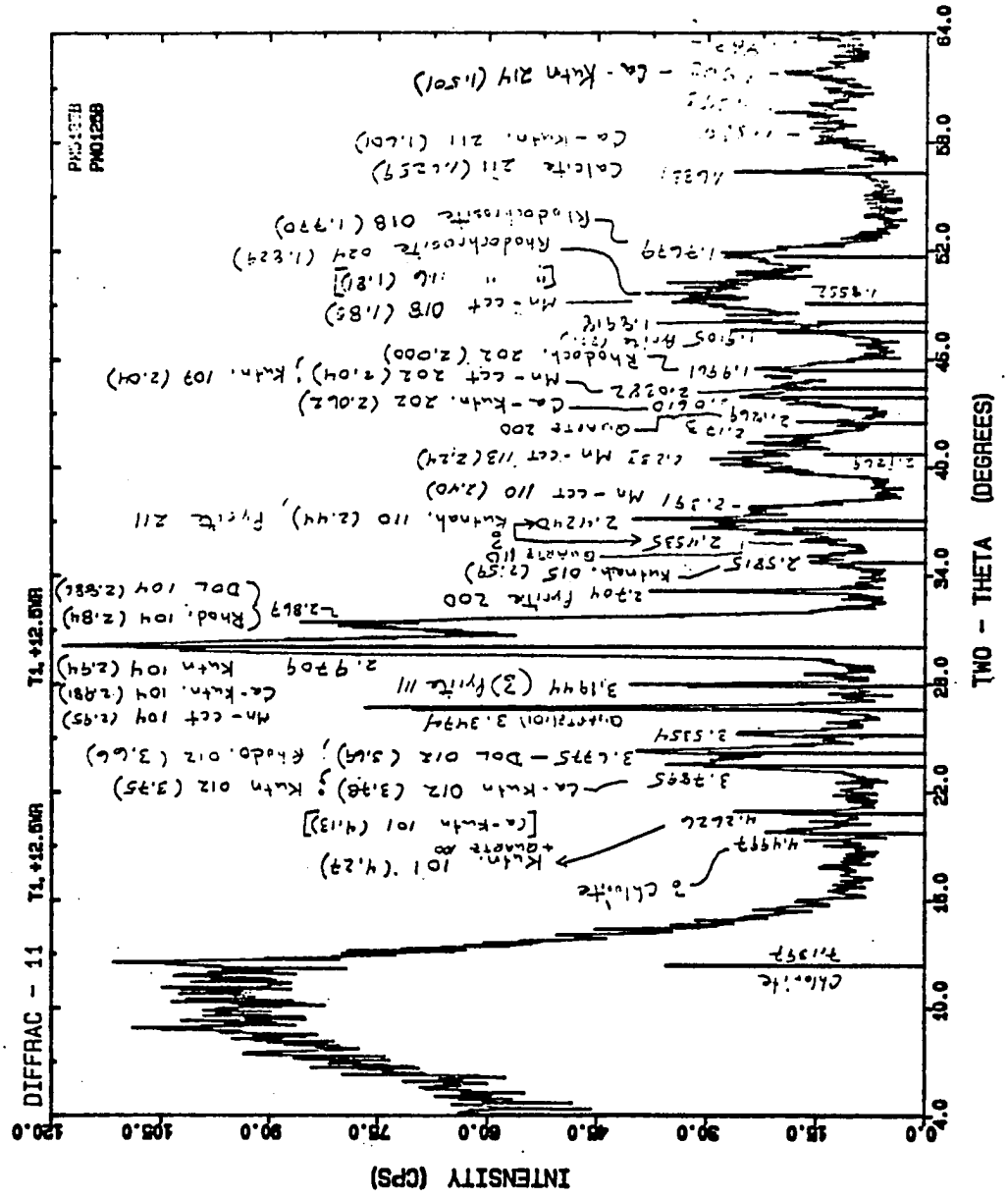

Figure 68. X-ray diffraction pattern for sample T1,+12.5.

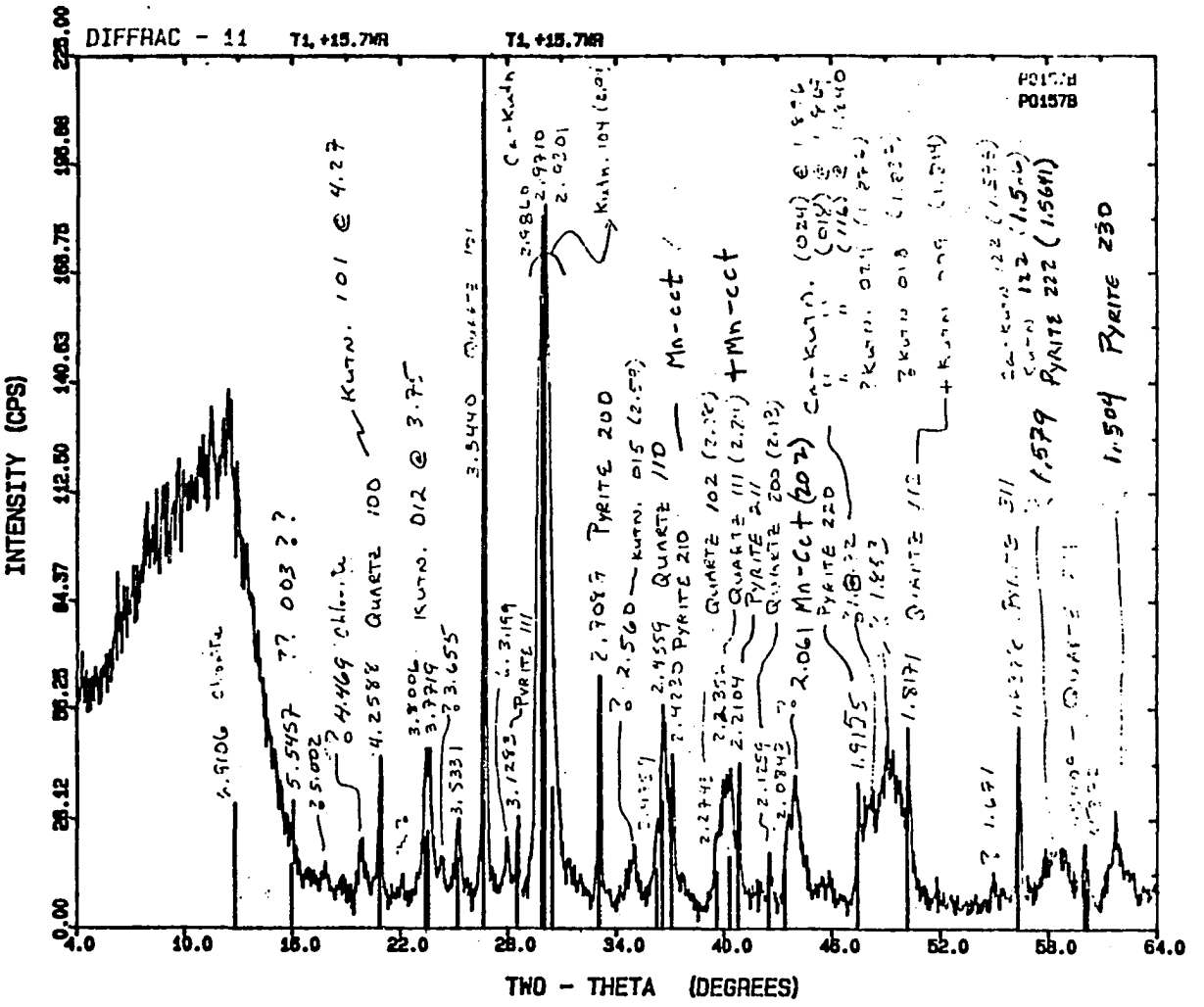

Figure 69. X-ray diffraction pattern for sample T1,+15.7.

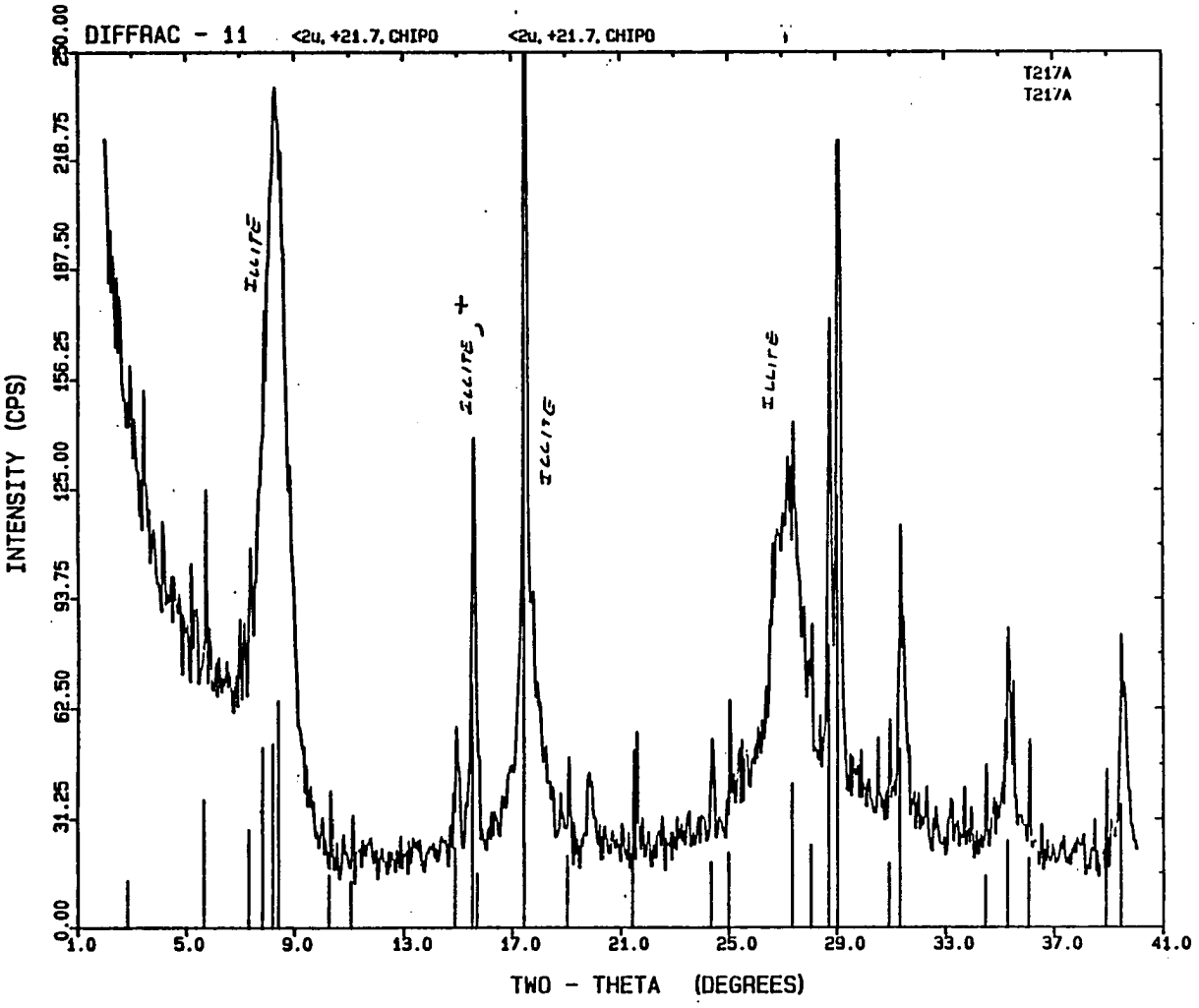

Figure 70. X-ray diffraction pattern for sample T1,+21.7.

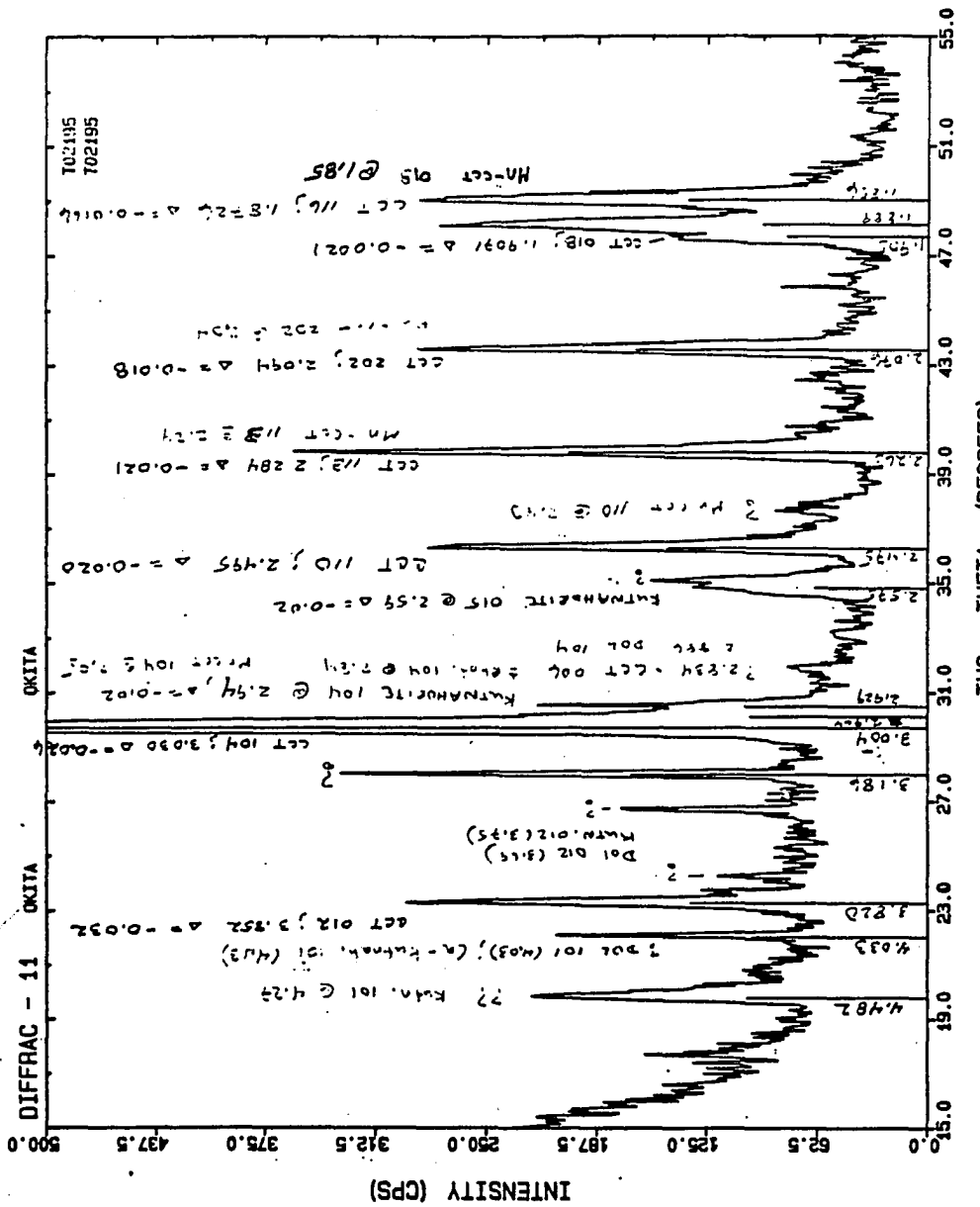

Figure 71. X-ray diffraction pattern for sample T1,+21.95.

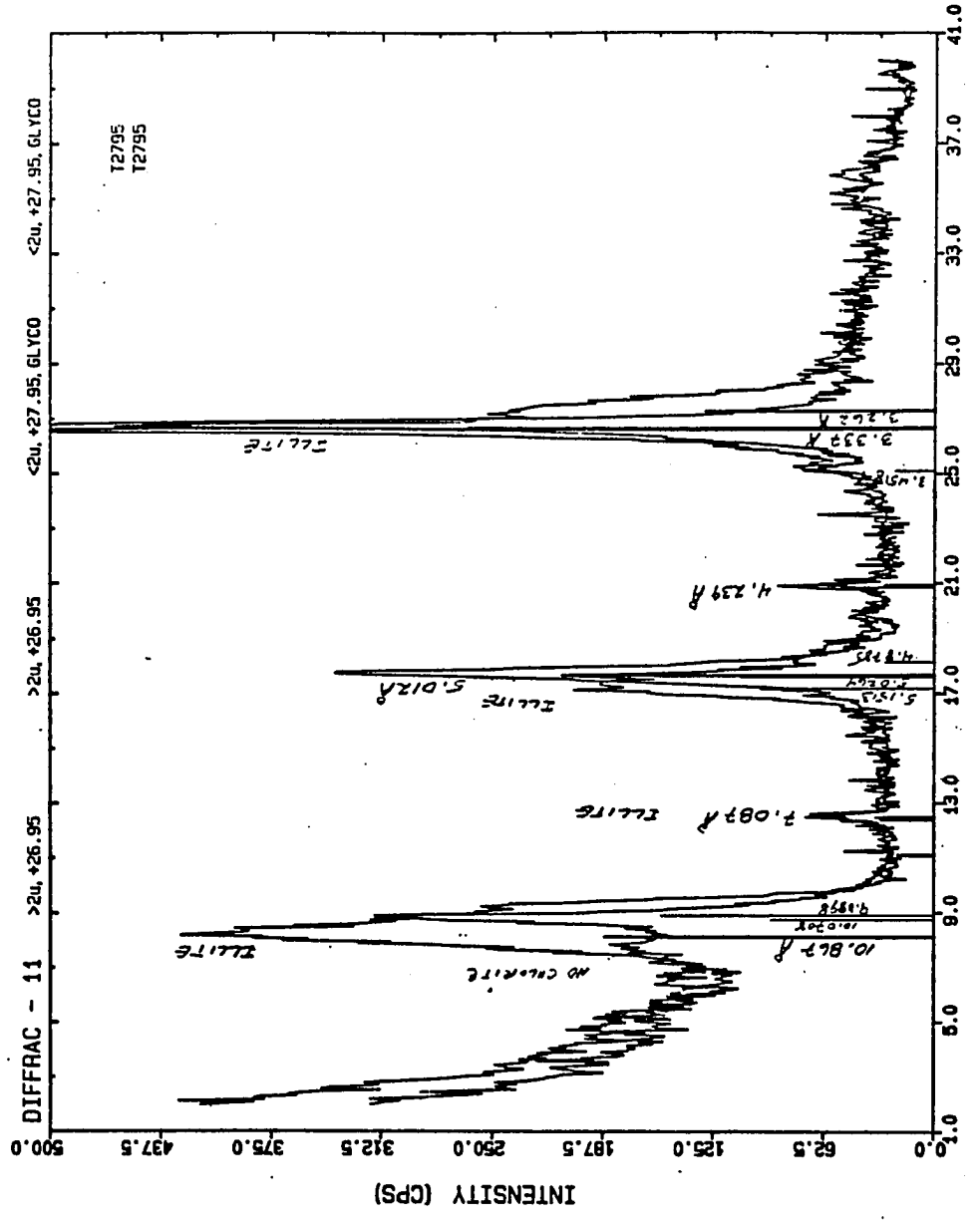

Figure 72. X-ray diffraction pattern for sample T1,+26.95.

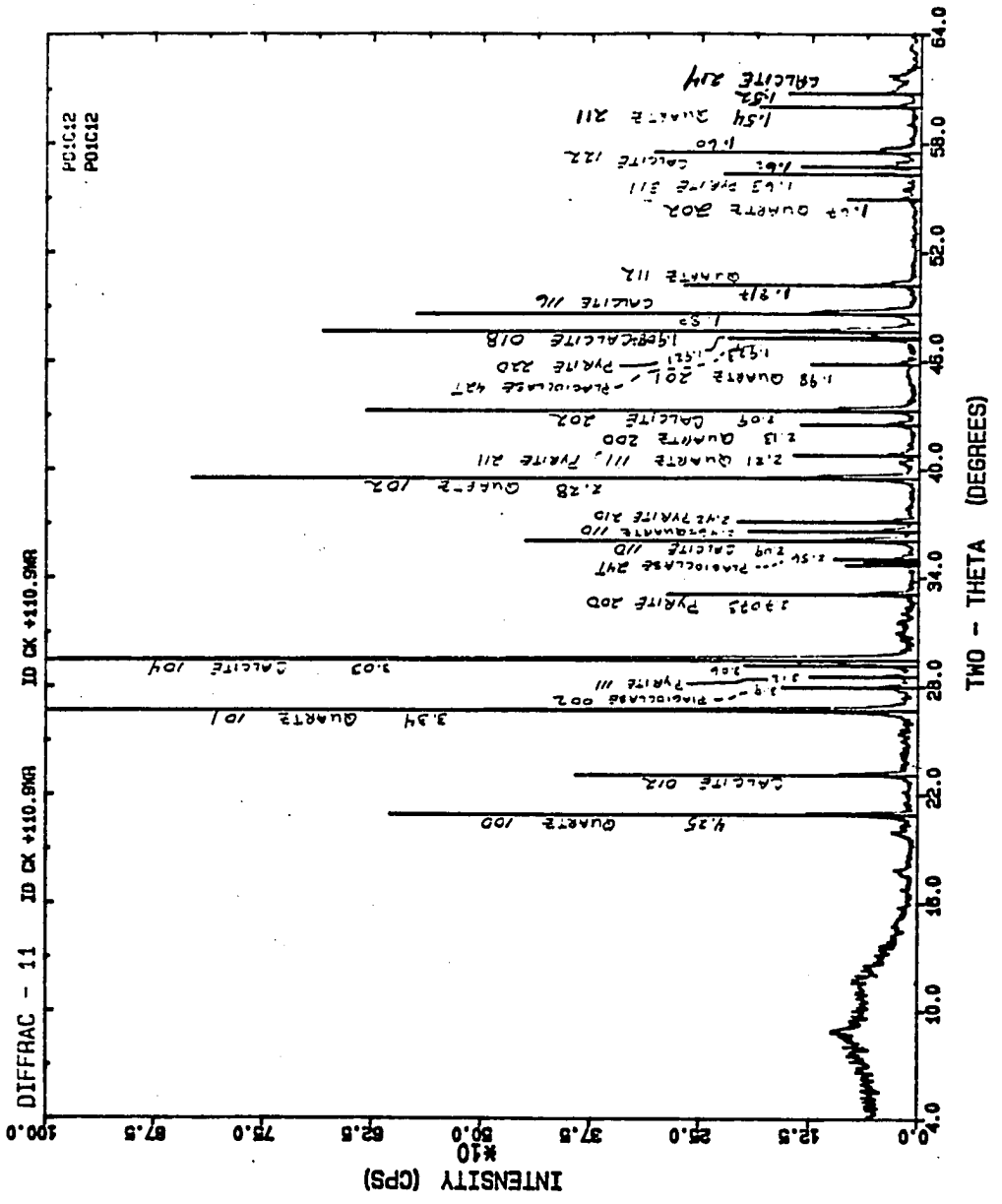

Figure 73. X-ray diffraction pattern for sample T1,+110.9.

APPENDIX D

GRAPHS OF COMPOSITIONAL VARIATION

IN INDIVIDUAL SAMPLES

Note: The spacing between analysis points for probe traverses is approximately 0.1 mm.

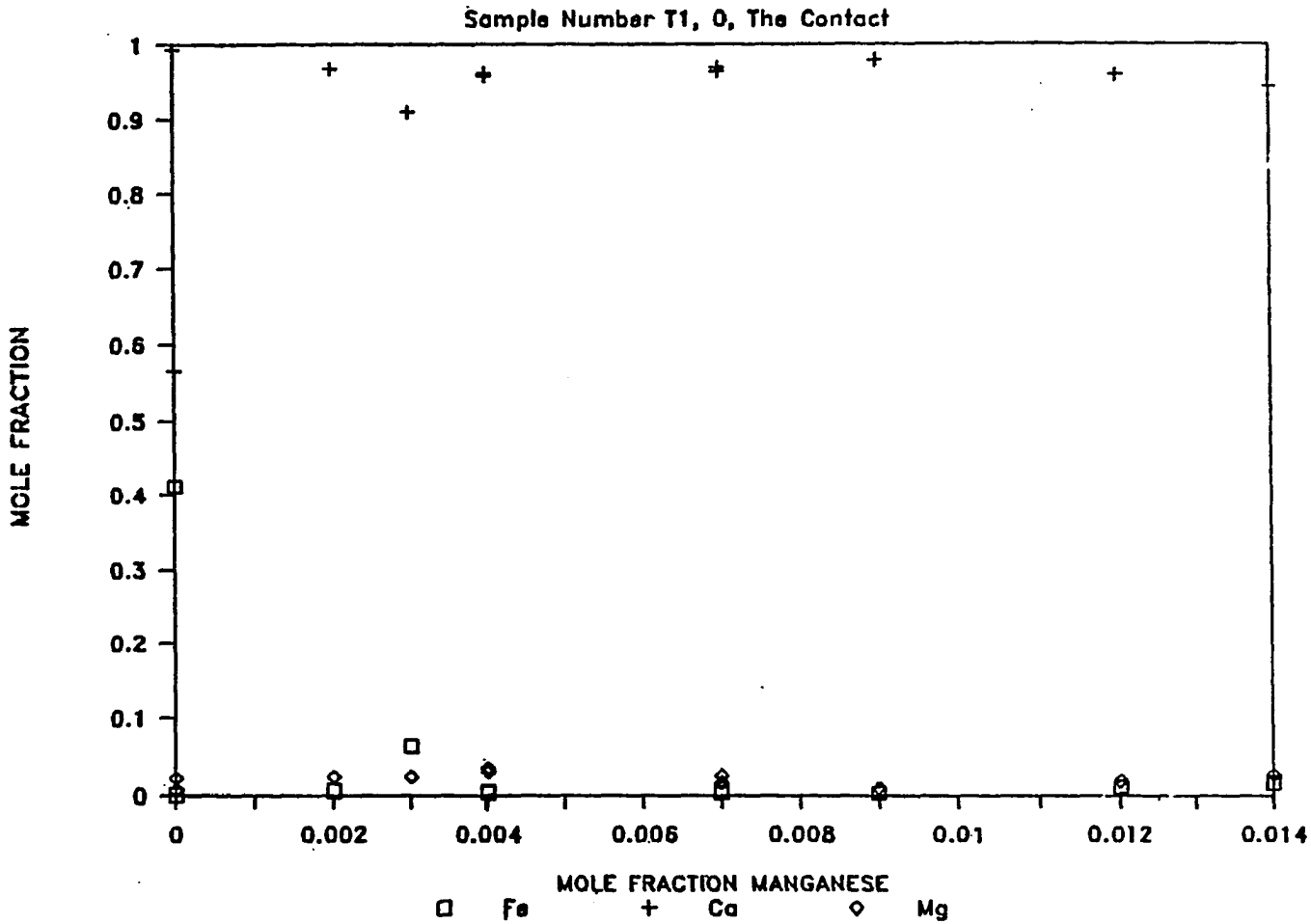

Figure 74. Graph of the mole fraction of Fe, Ca, and Mg plotted against the mole fraction of Mn in carbonate minerals from the sample noted at the top of the graph.

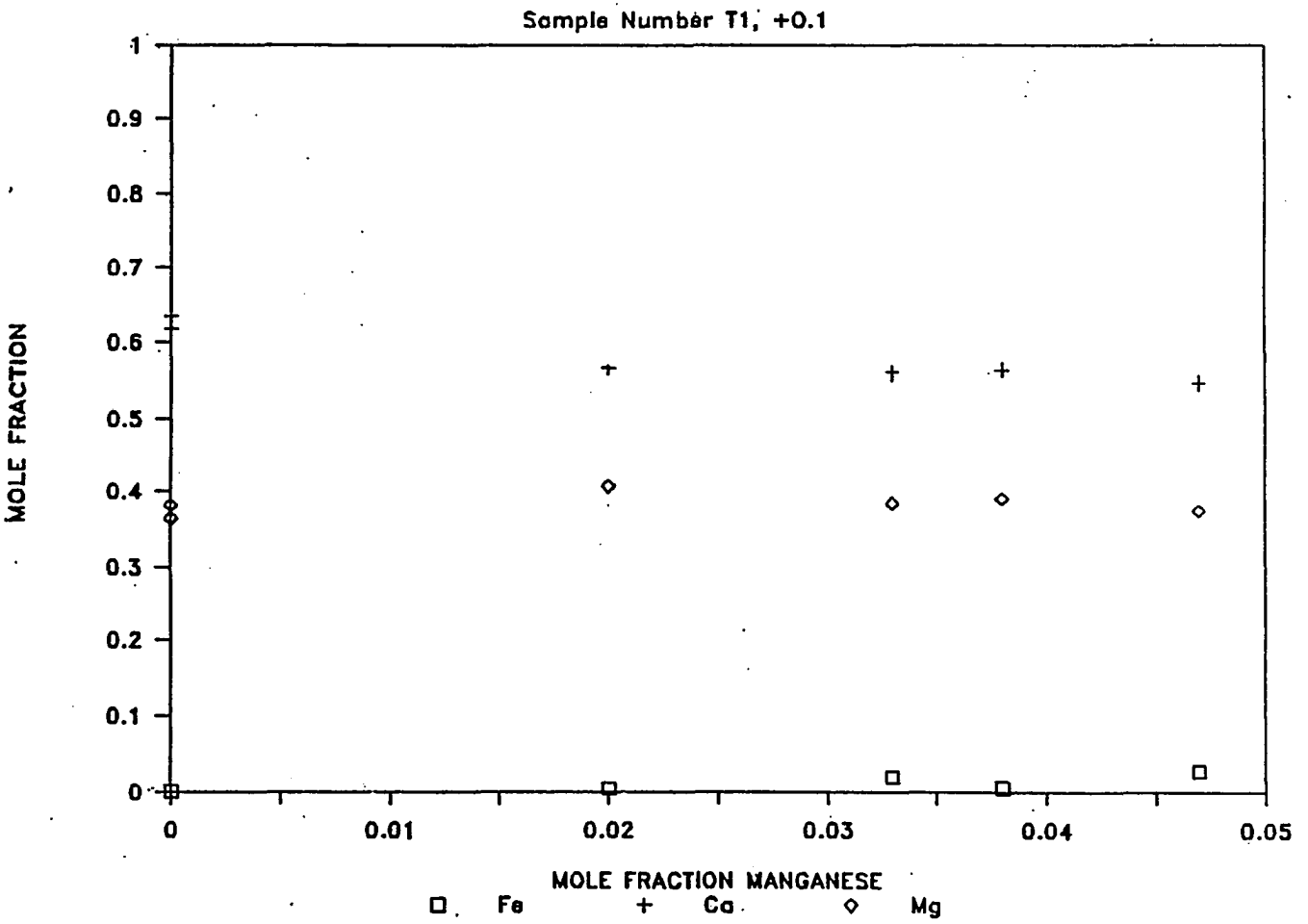

Figure 75. Graph of the mole fraction of Fe, Ca, and Mg plotted against the mole fraction of Mn in carbonate minerals from the sample noted at the top of the graph.

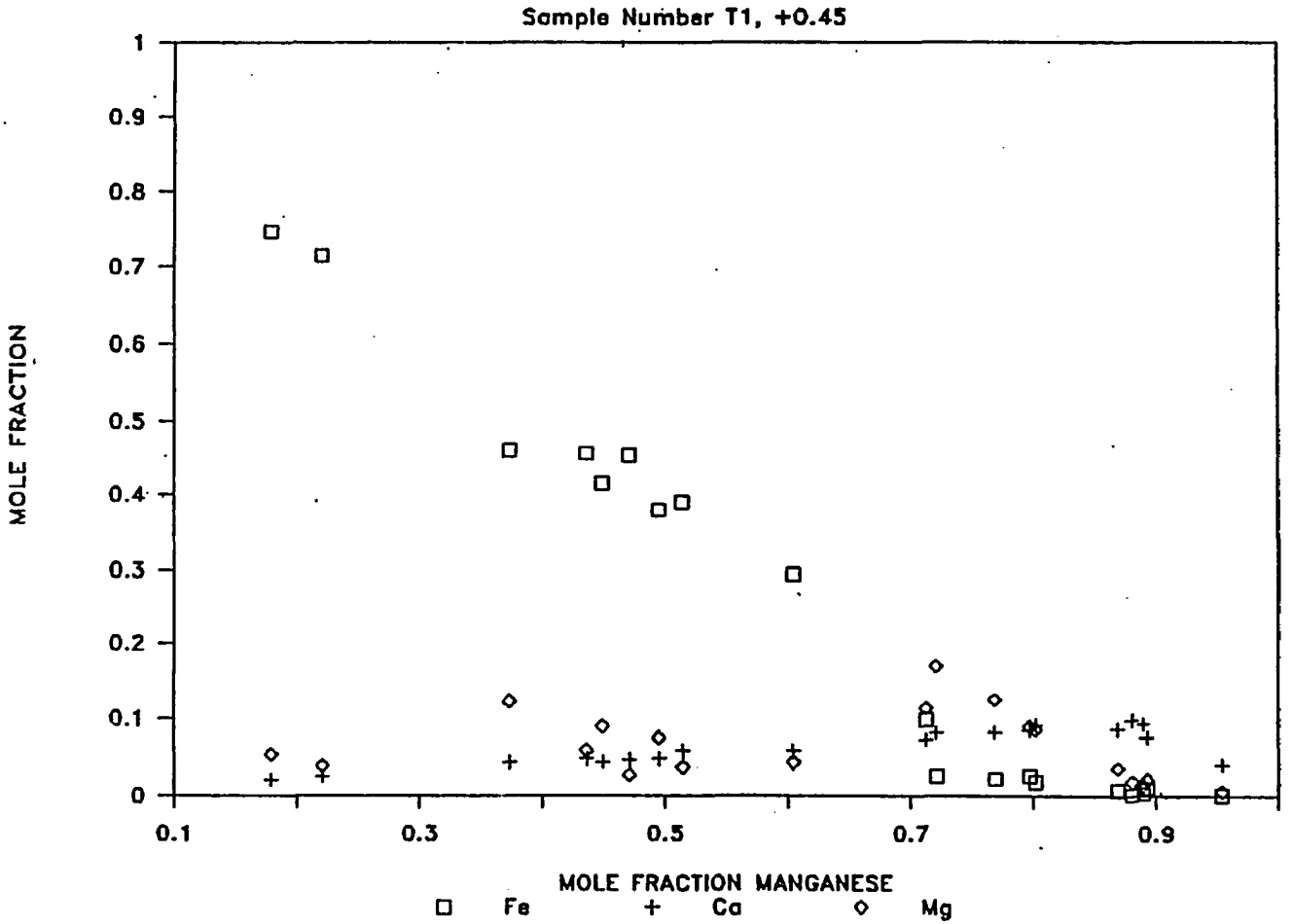

Figure 76. Graph of the mole fraction of Fe, Ca, and Mg plotted against the mole fraction of Mn in carbonate minerals from the sample noted at the top of the graph.

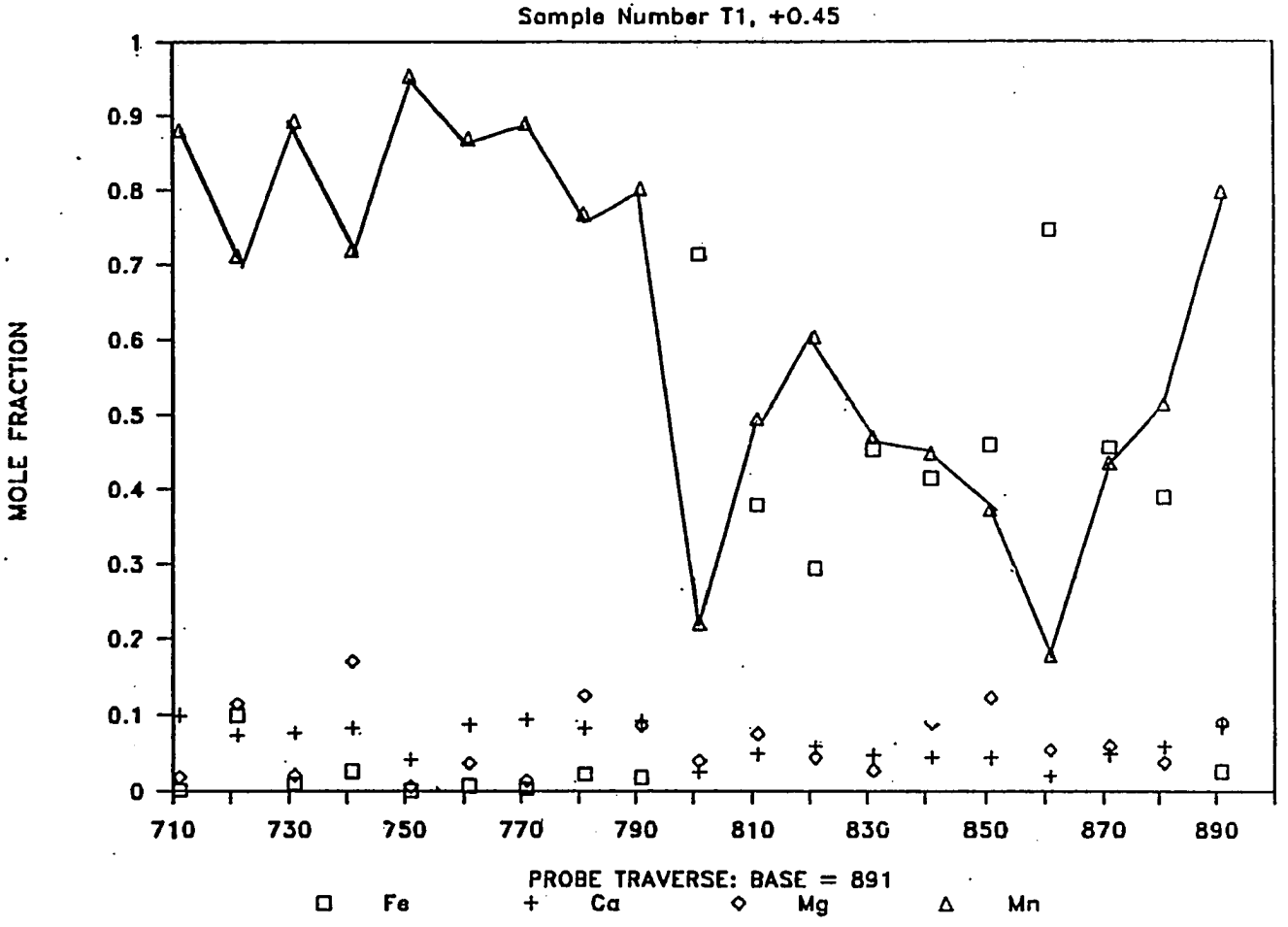

Figure 77. Probe traverse across bedding showing the variation in Mn, Mg, Fe, and Ca concentrations in carbonate minerals.

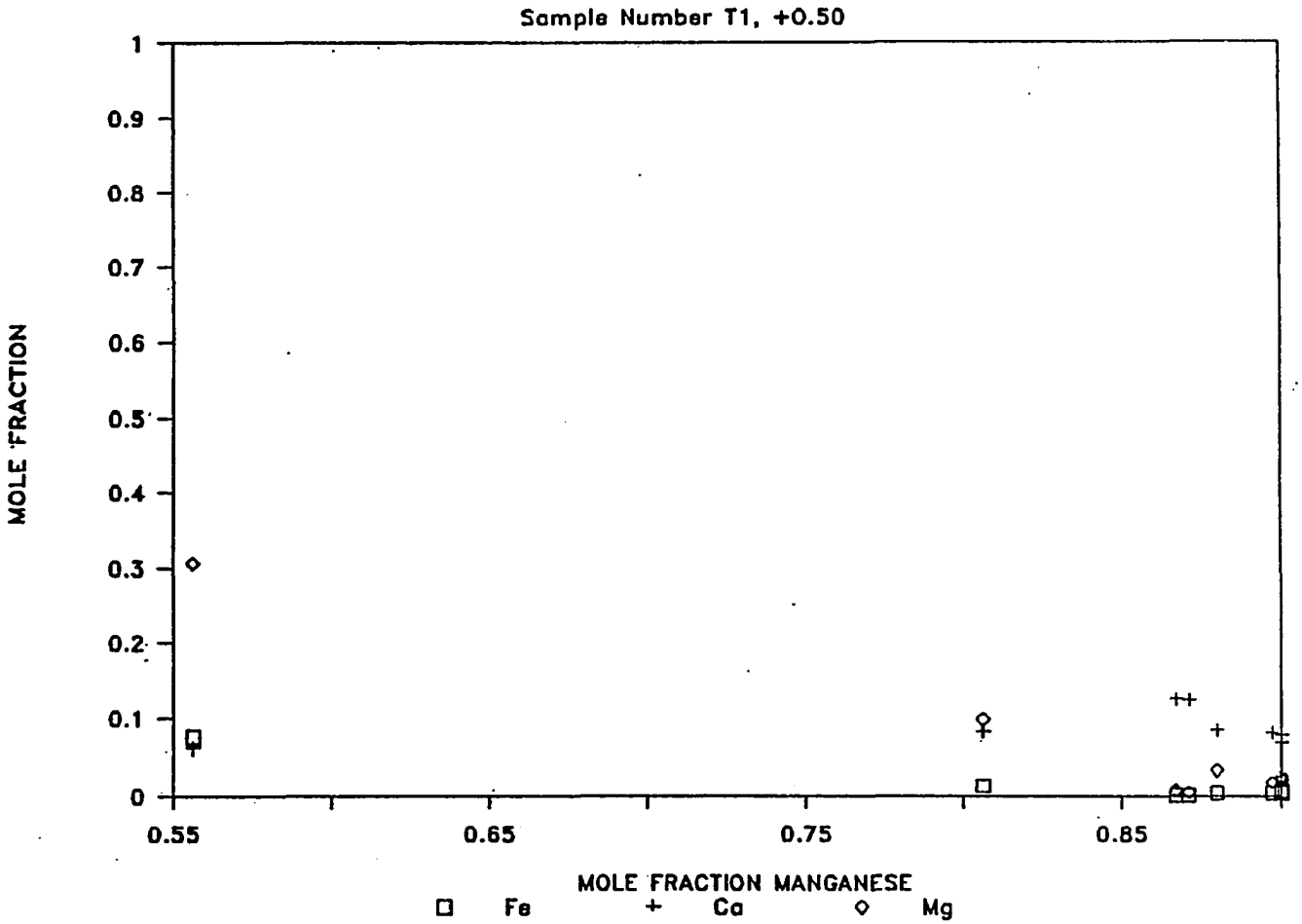

Figure 78. Graph of the mole fraction of Fe, Ca, and Mg plotted against the mole fraction of Mn in carbonate minerals from the sample noted at the top of the graph.

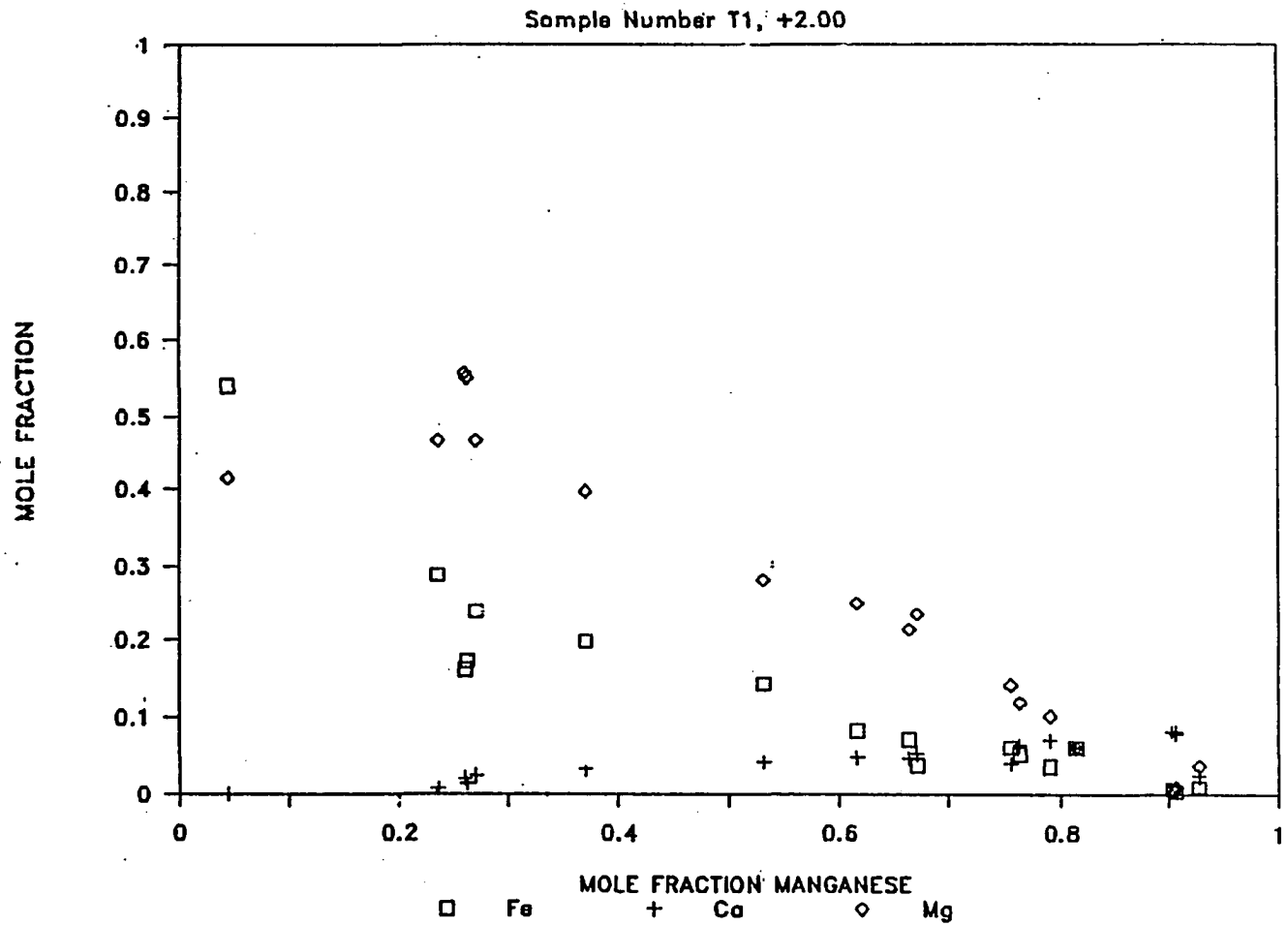

Figure 79 . Graph of the mole fraction of Fe, Ca, and Mg plotted against the mole fraction of Mn in carbonate minerals from the sample noted at the top of the graph.

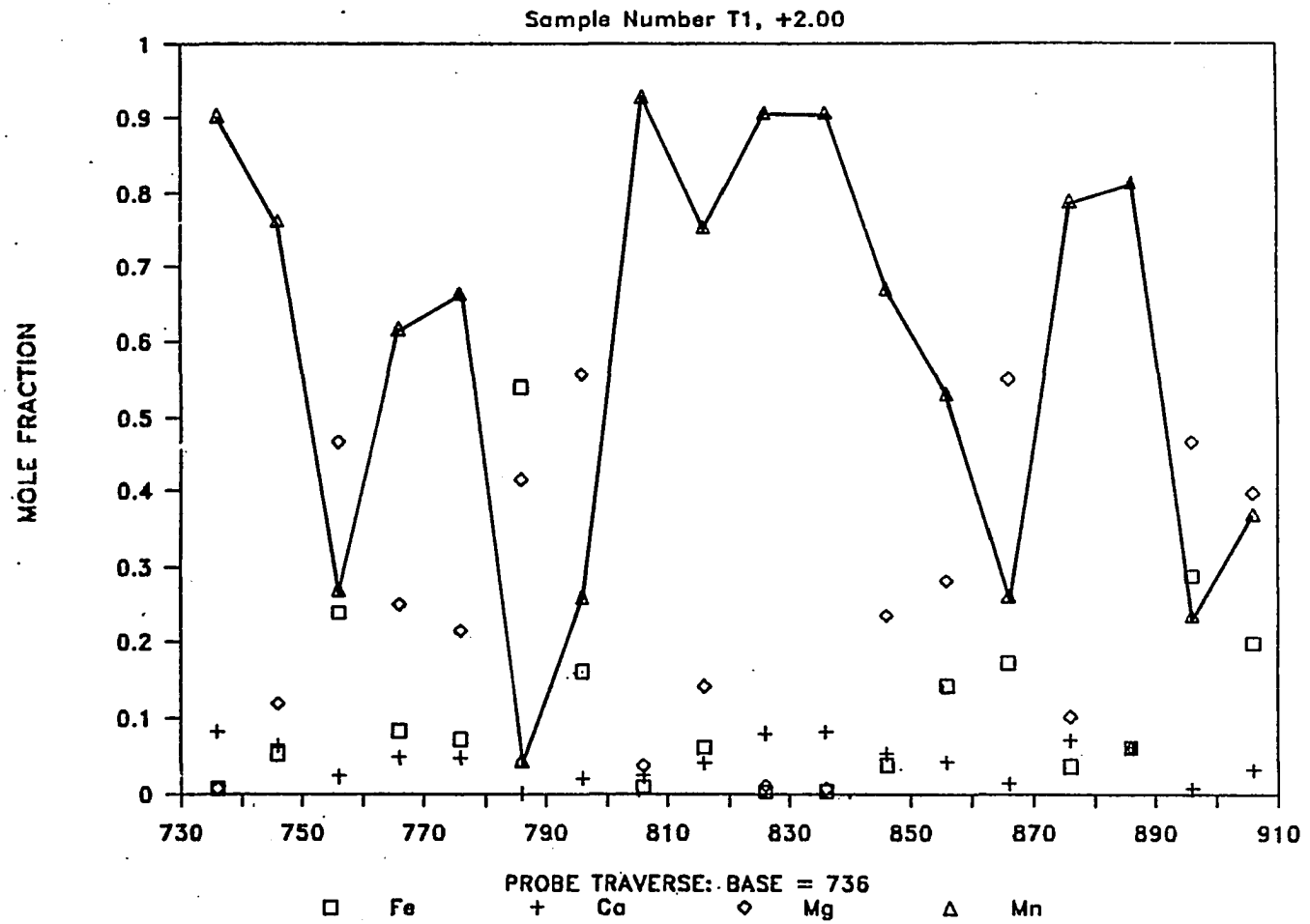

Figure 80 . Probe traverse across bedding showing the variation in Mn, Mg, Fe, and Ca concentrations in carbonate minerals.

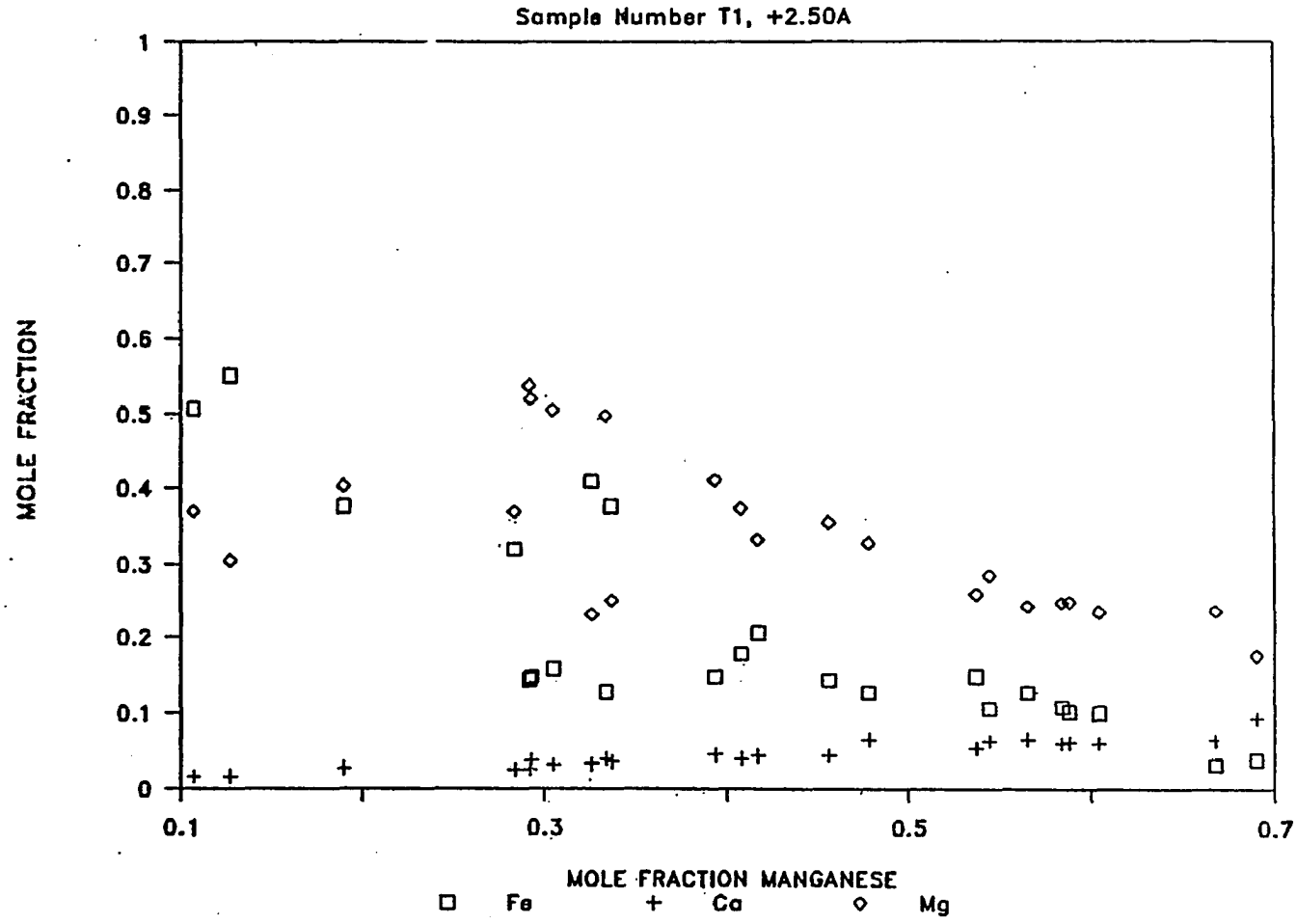

Figure 81. Graph of the mole fraction of Fe, Ca, and Mg plotted against the mole fraction of Mn in carbonate minerals from the sample noted at the top of the graph.

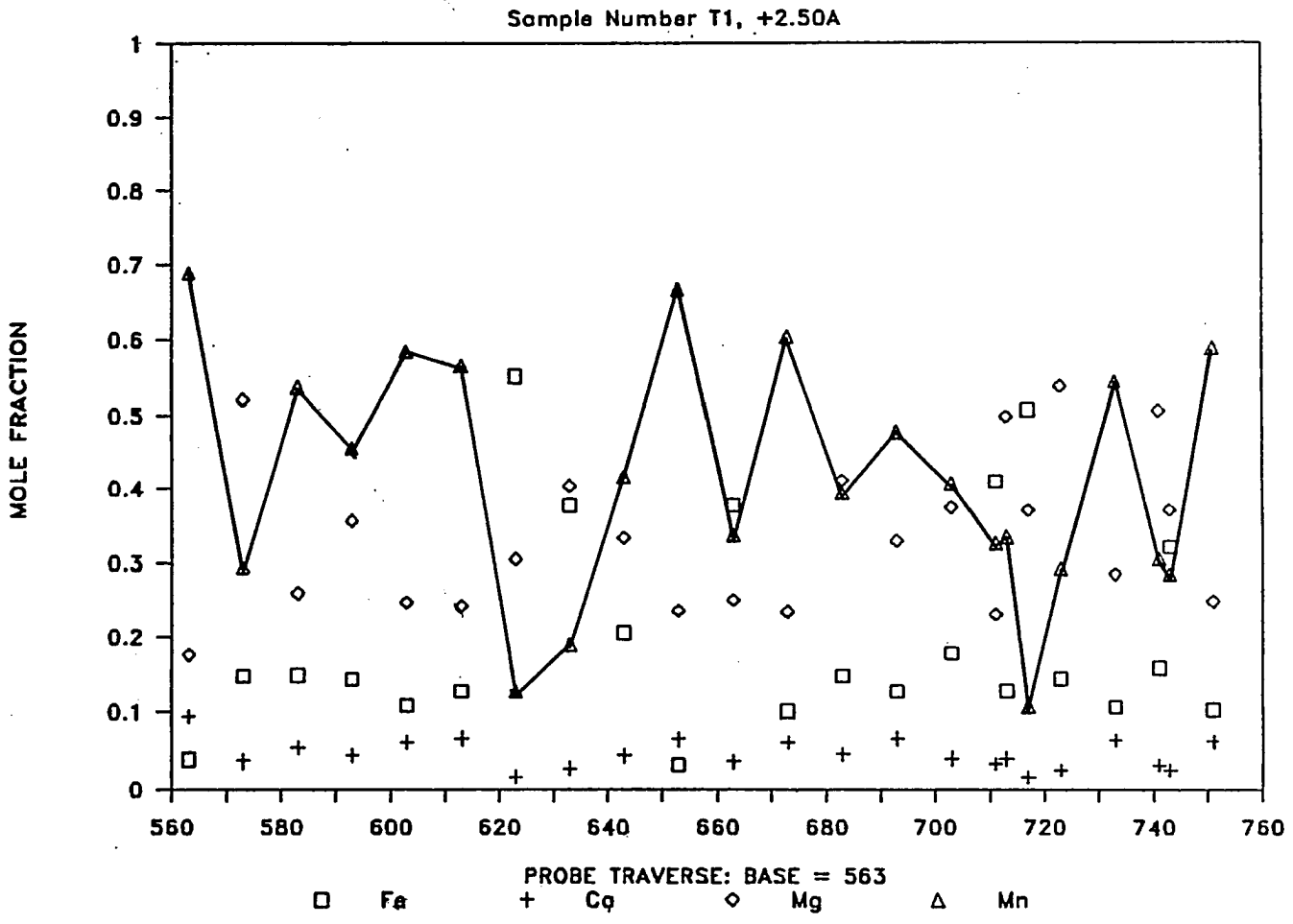

Figure 82. Probe traverse across bedding showing the variation in Mn, Mg, Fe, and Ca concentrations in carbonate minerals.

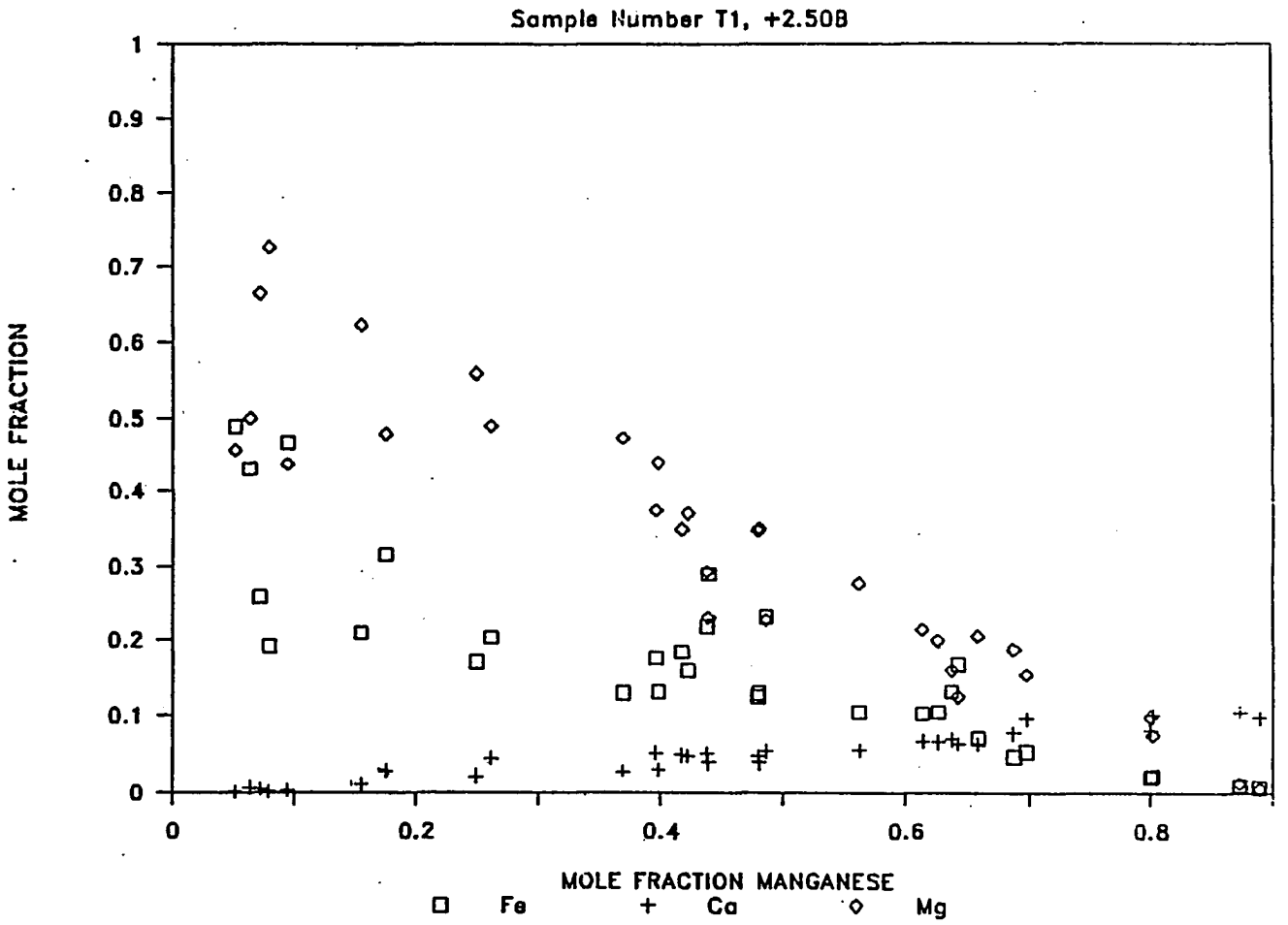

Figure 83. Graph of the mole fraction of Fe, Ca, and Mg plotted against the mole fraction of Mn in carbonate minerals from the sample noted at the top of the graph.

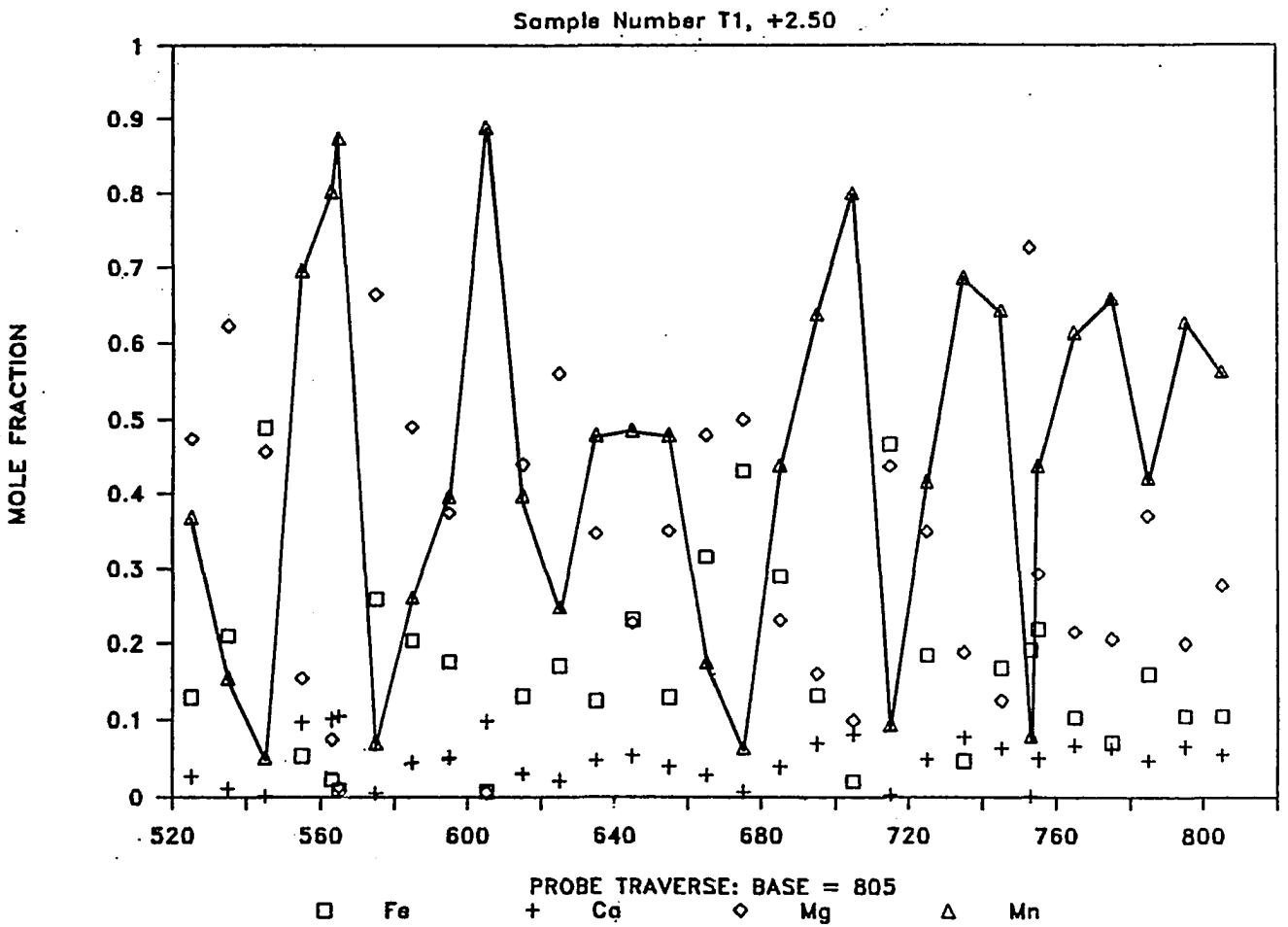

Figure 84. Probe traverse across bedding showing the variation in Mn, Mg, Fe, and Ca concentrations in carbonate minerals.

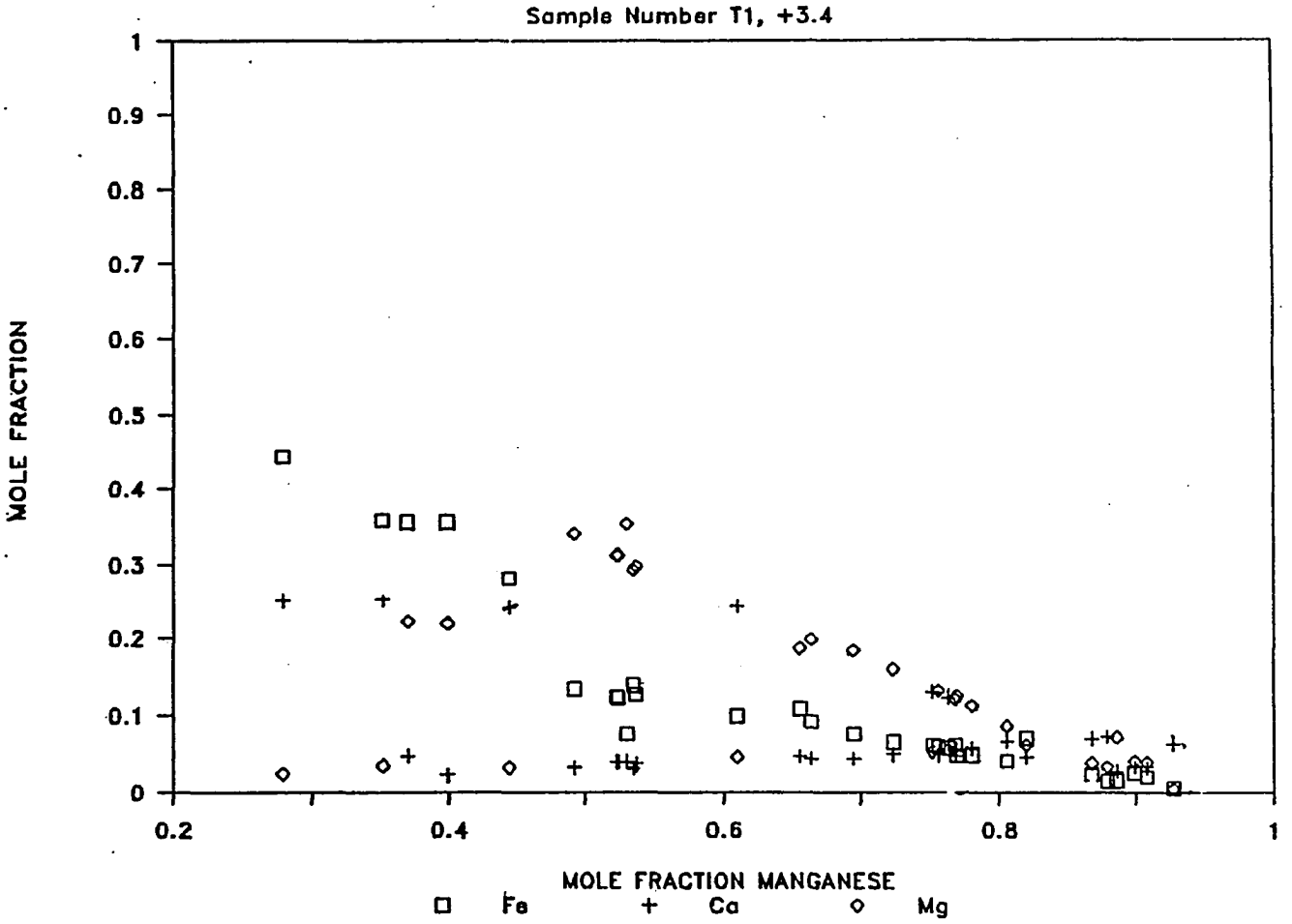

Figure 85. Graph of the mole fraction of Fe, Ca, and Mg plotted against the mole fraction of Mn in carbonate minerals from the sample noted at the top of the graph.

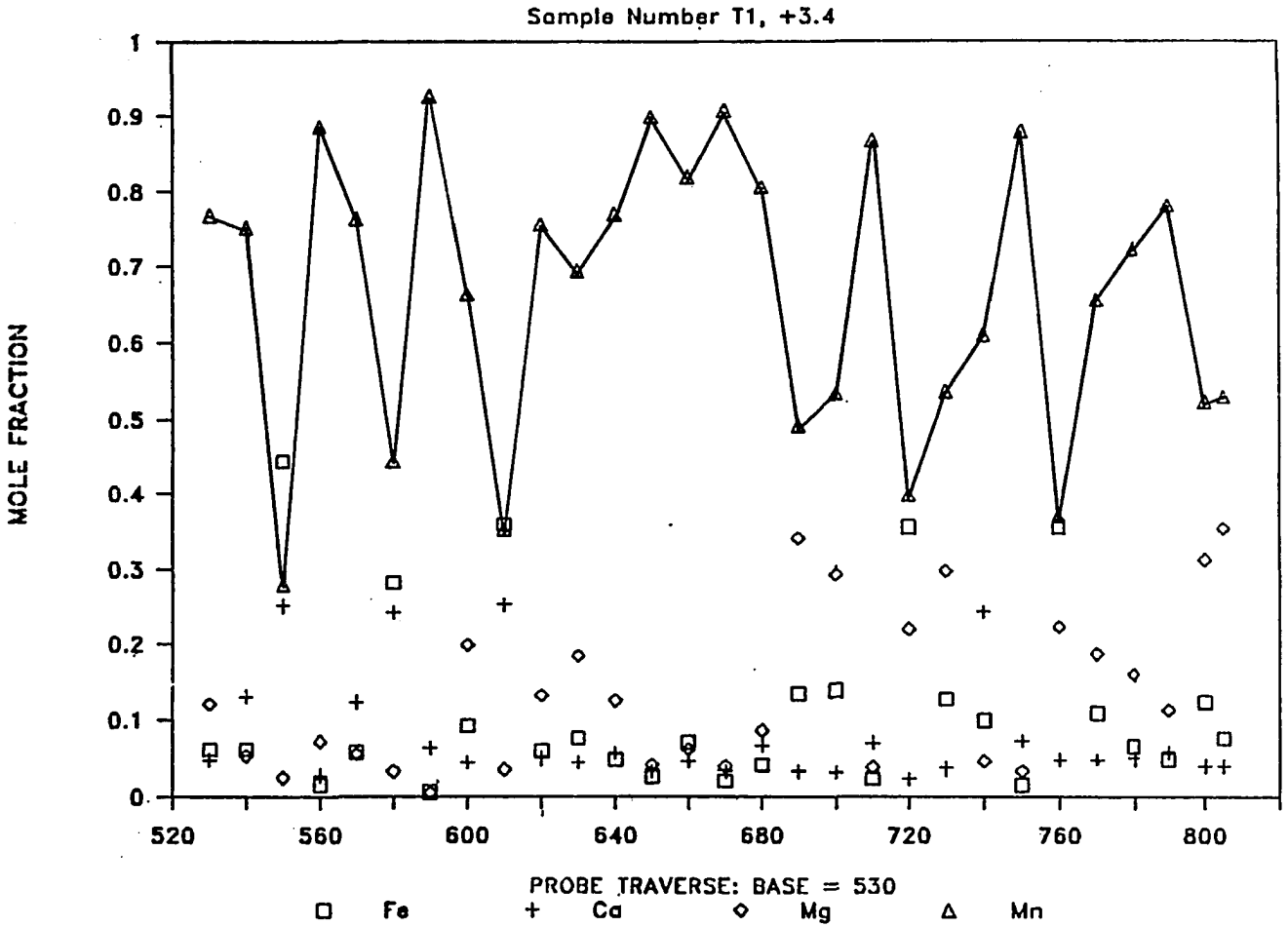

Figure 86. Probe traverse across bedding showing the variation in Mn, Mg, Fe, and Ca concentrations in carbonate minerals.

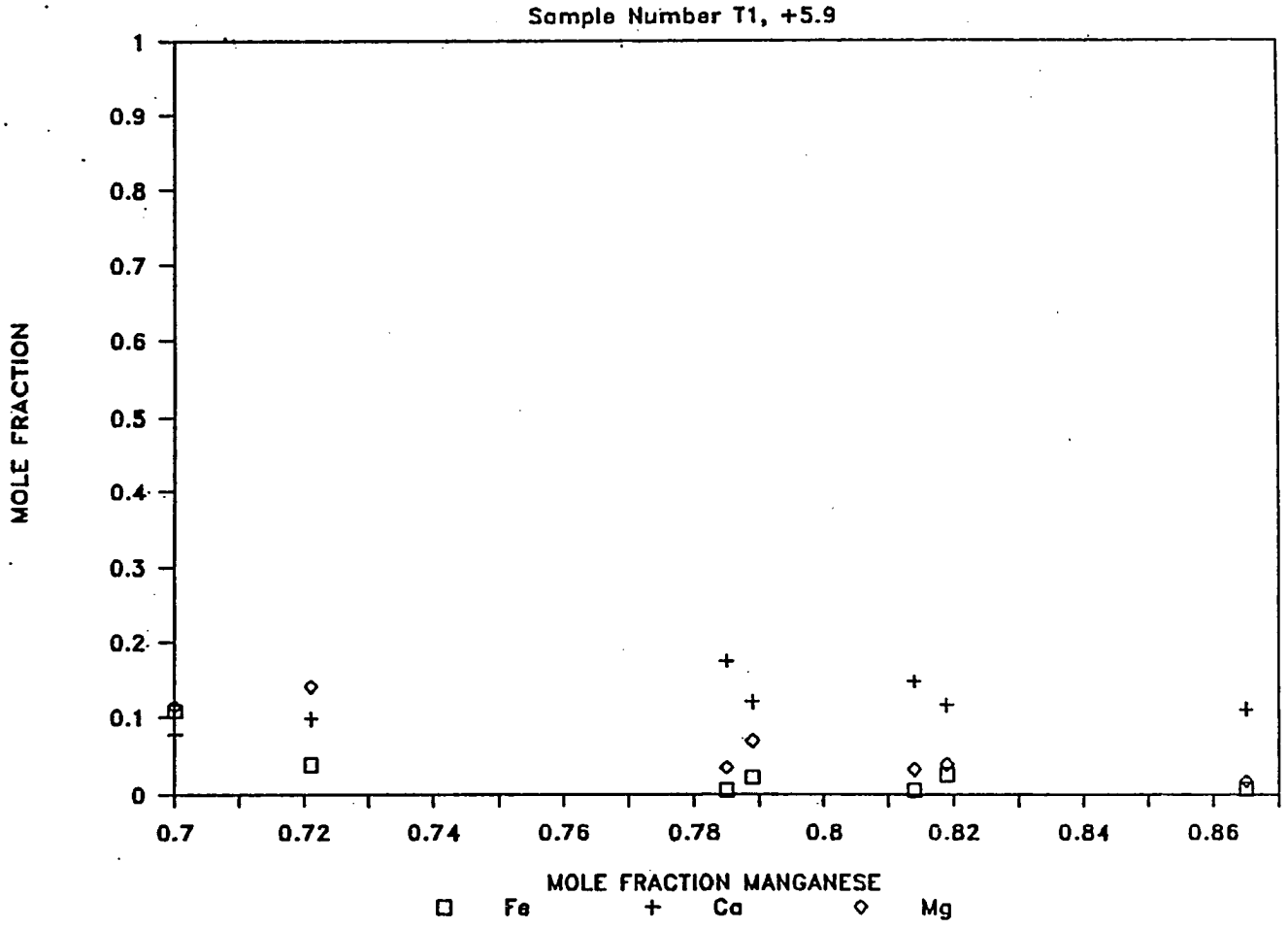

Figure 87. Graph of the mole fraction of Fe, Ca, and Mg plotted against the mole fraction of Mn in carbonate minerals from the sample noted at the top of the graph.

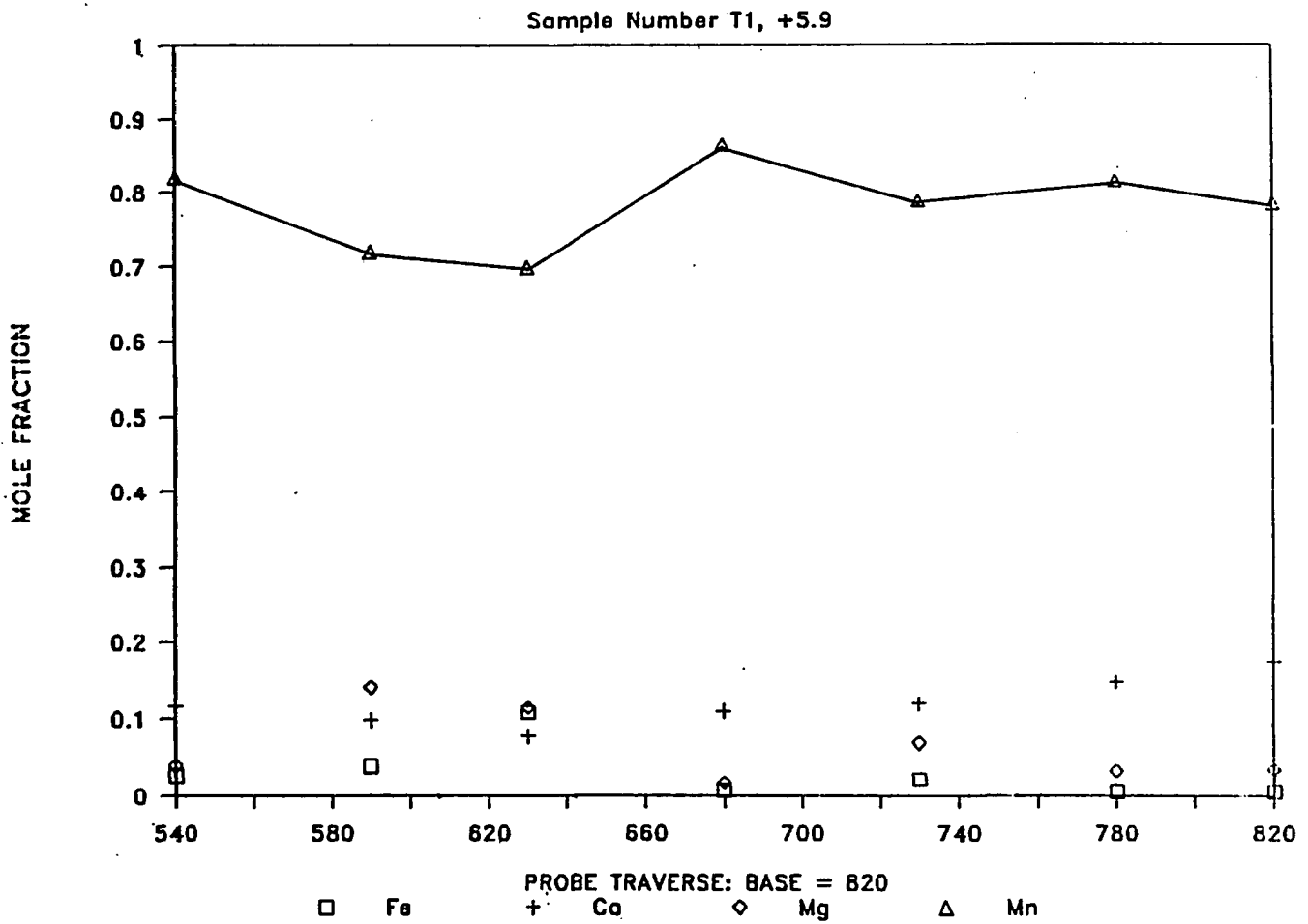

Figure 88. Probe traverse across bedding showing the variation in Mn, Mg, Fe, and Ca concentrations in carbonate minerals.

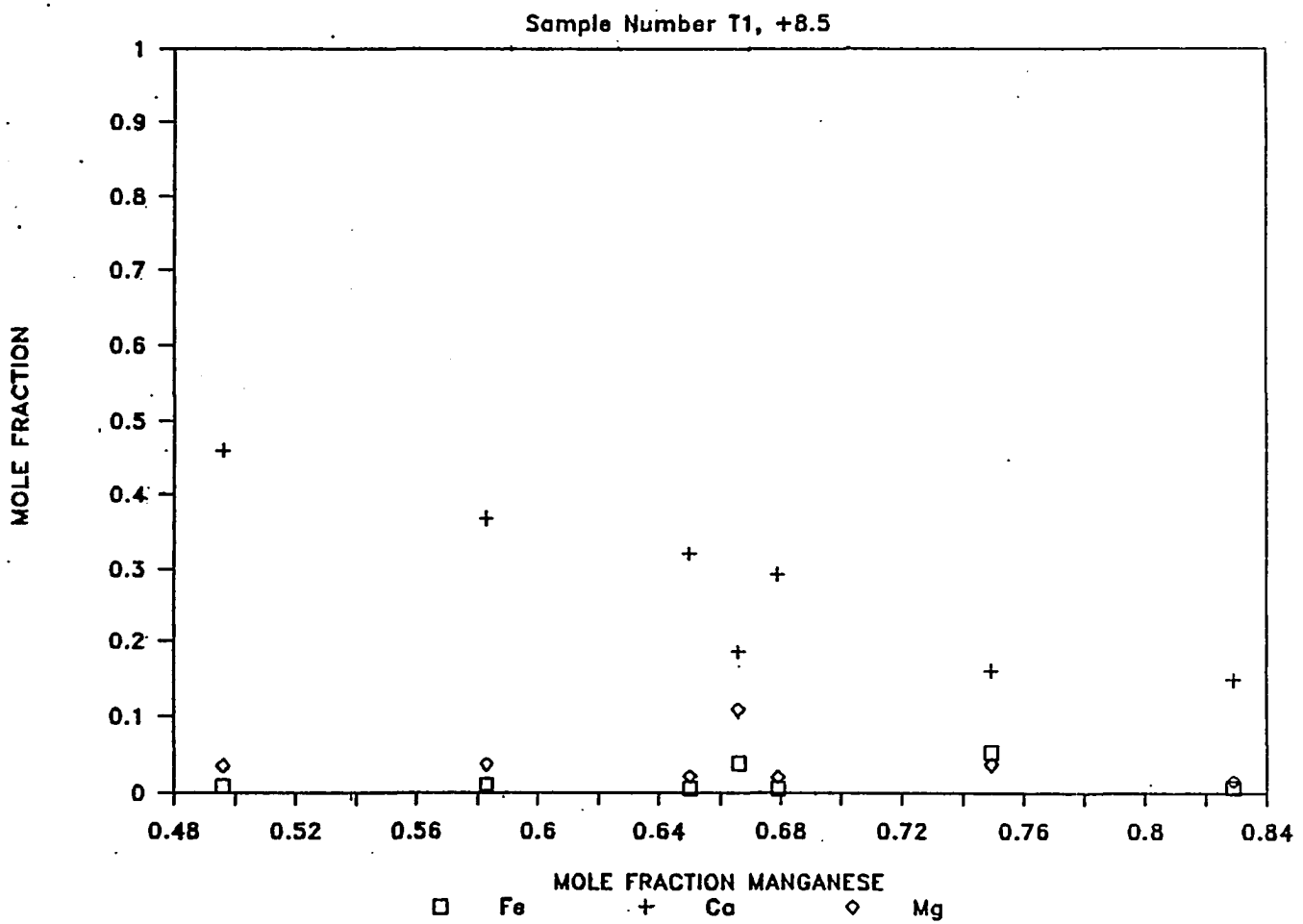

Figure 89. Graph of the mole fraction of Fe, Ca, and Mg plotted against the mole fraction of Mn in carbonate minerals from the sample noted at the top of the graph.

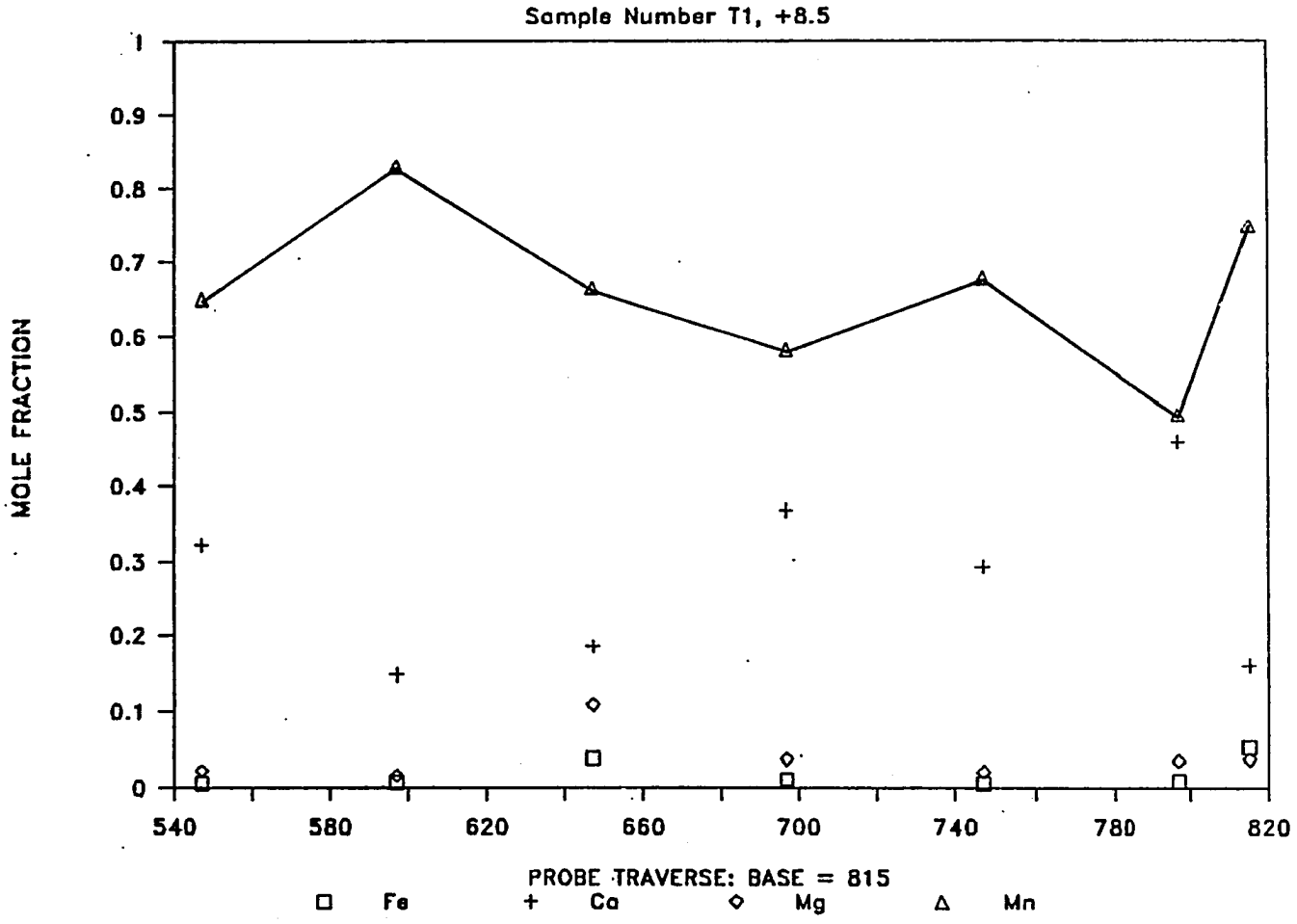

Figure 90. Probe traverse across bedding showing the variation in Mn, Mg, Fe, and Ca concentrations in carbonate minerals.

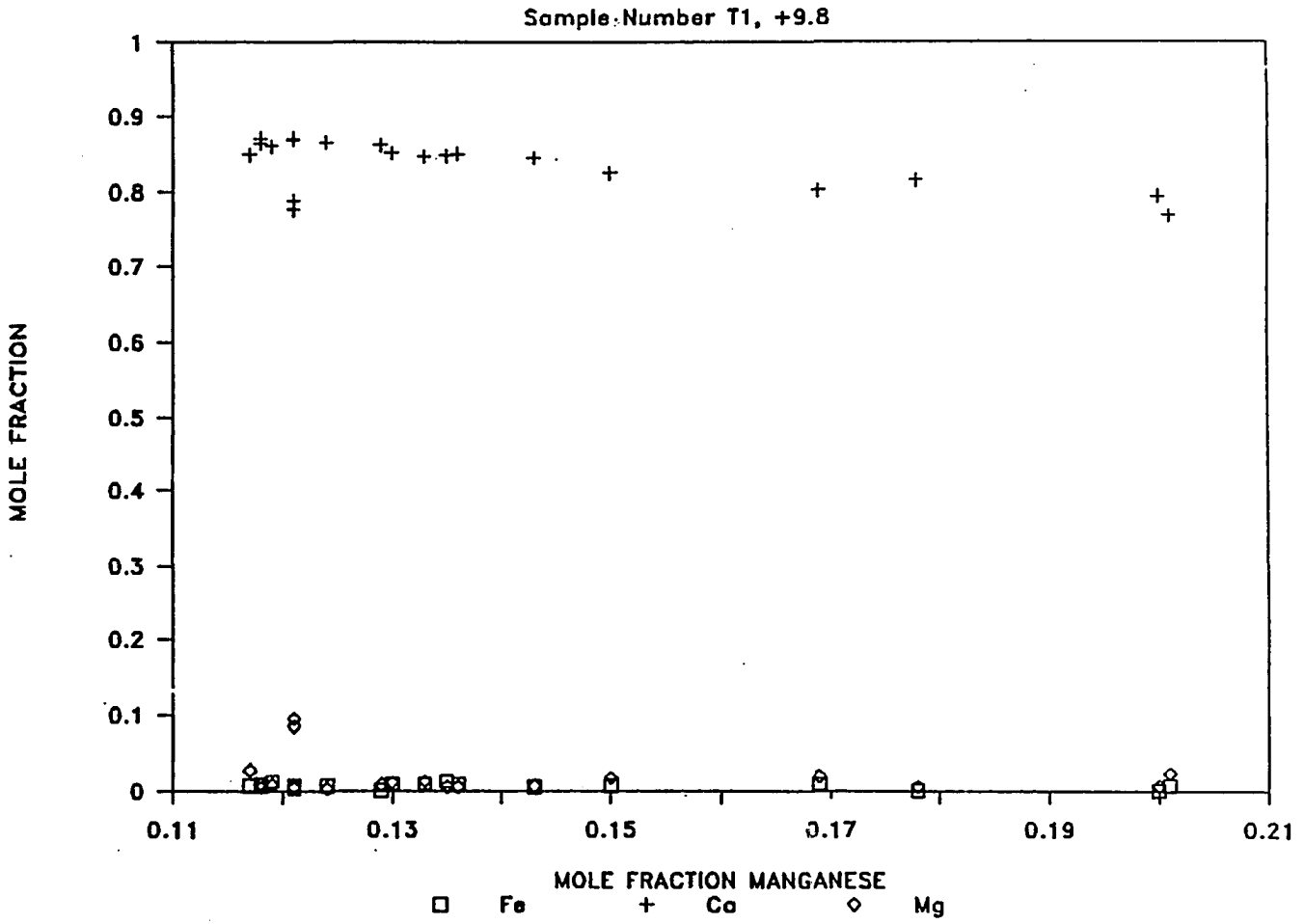

Figure 91. Graph of the mole fraction of Fe, Ca, and Mg plotted against the mole fraction of Mn in carbonate minerals from the sample noted at the top of the graph.

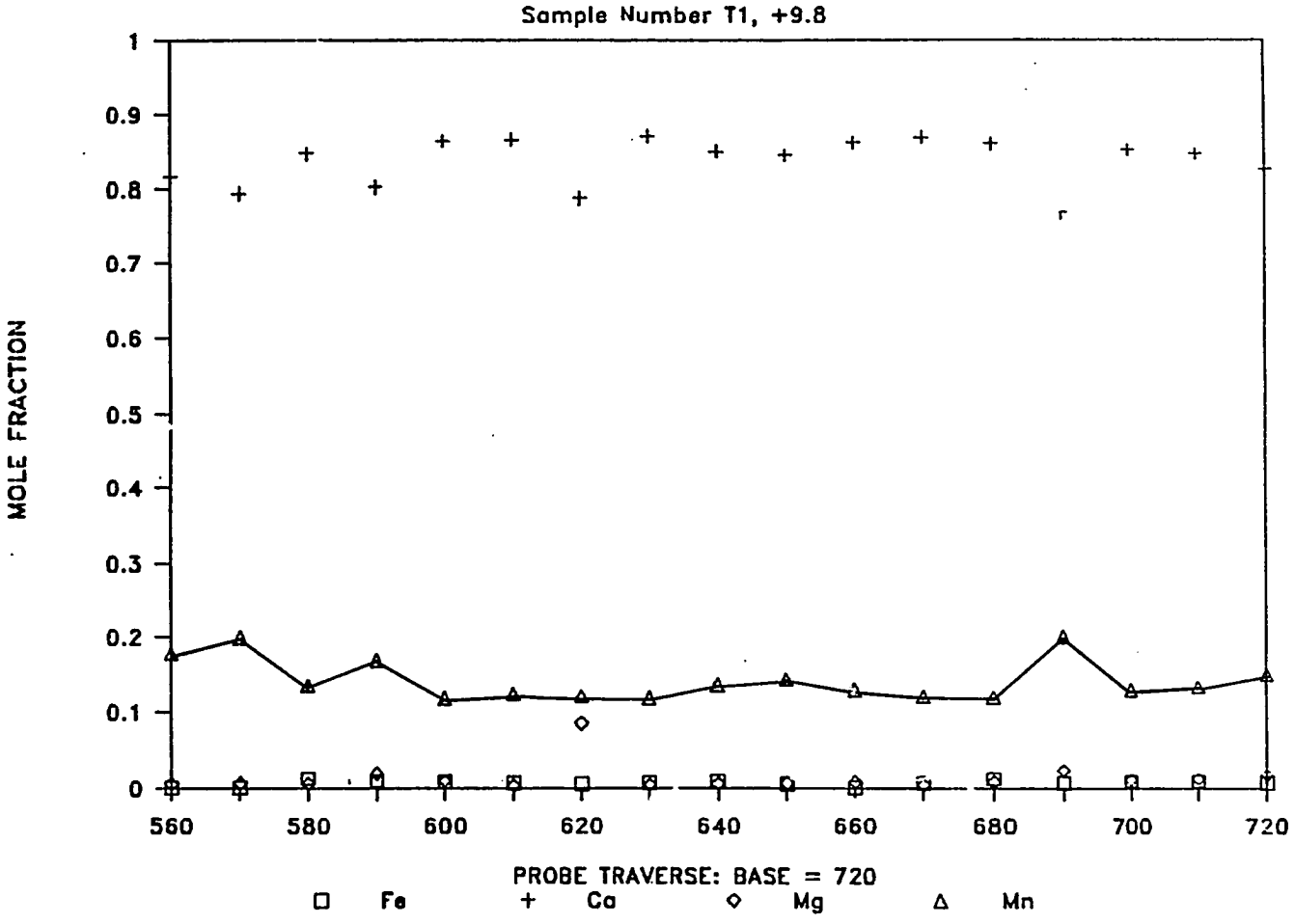

Figure 92. Probe traverse across bedding showing the variation in Mn, Mg, Fe, and Ca concentrations in carbonate minerals.

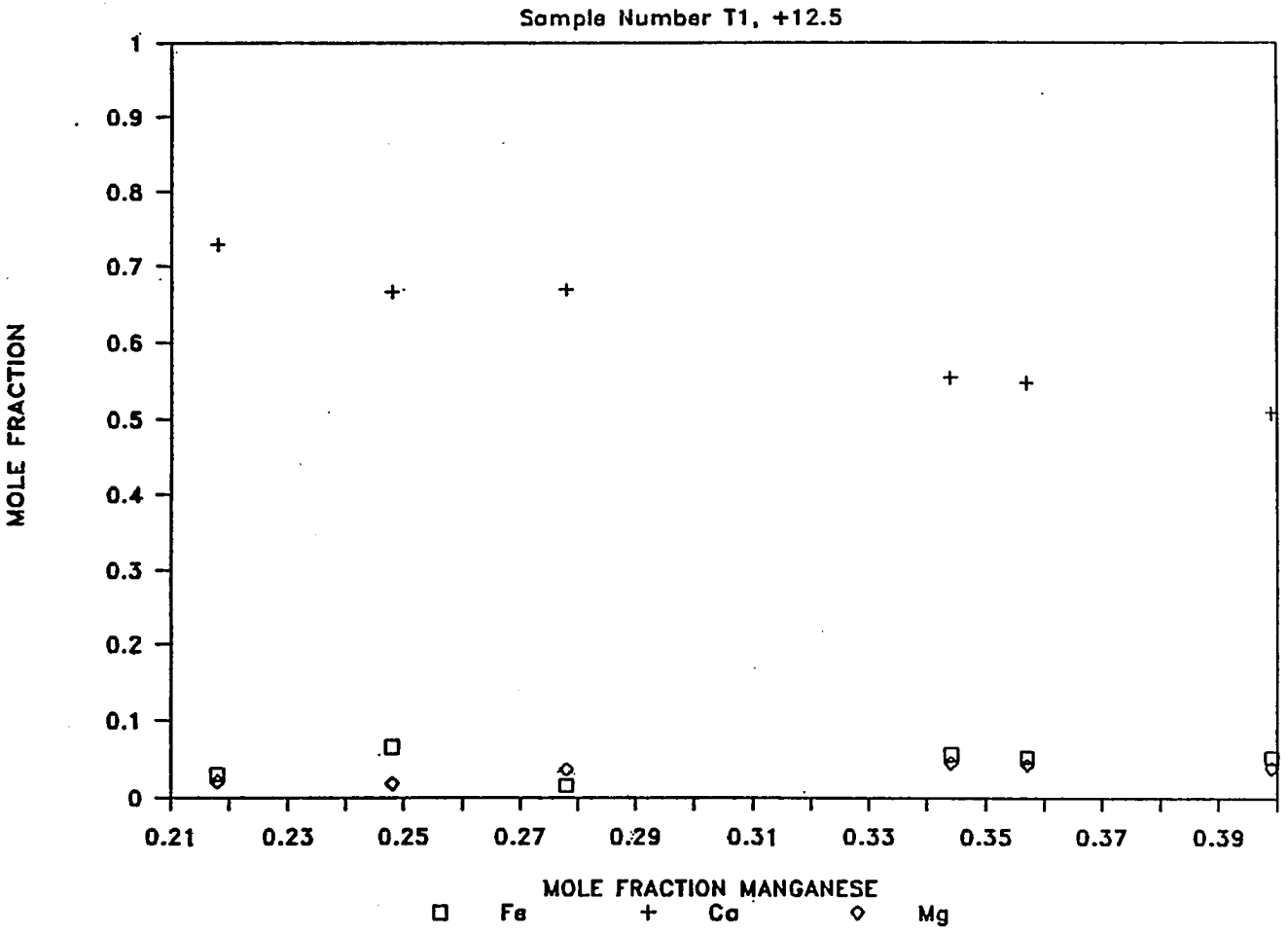

Figure 93. Graph of the mole fraction of Fe, Ca, and Mg plotted against the mole fraction of Mn in carbonate minerals from the sample noted at the top of the graph.

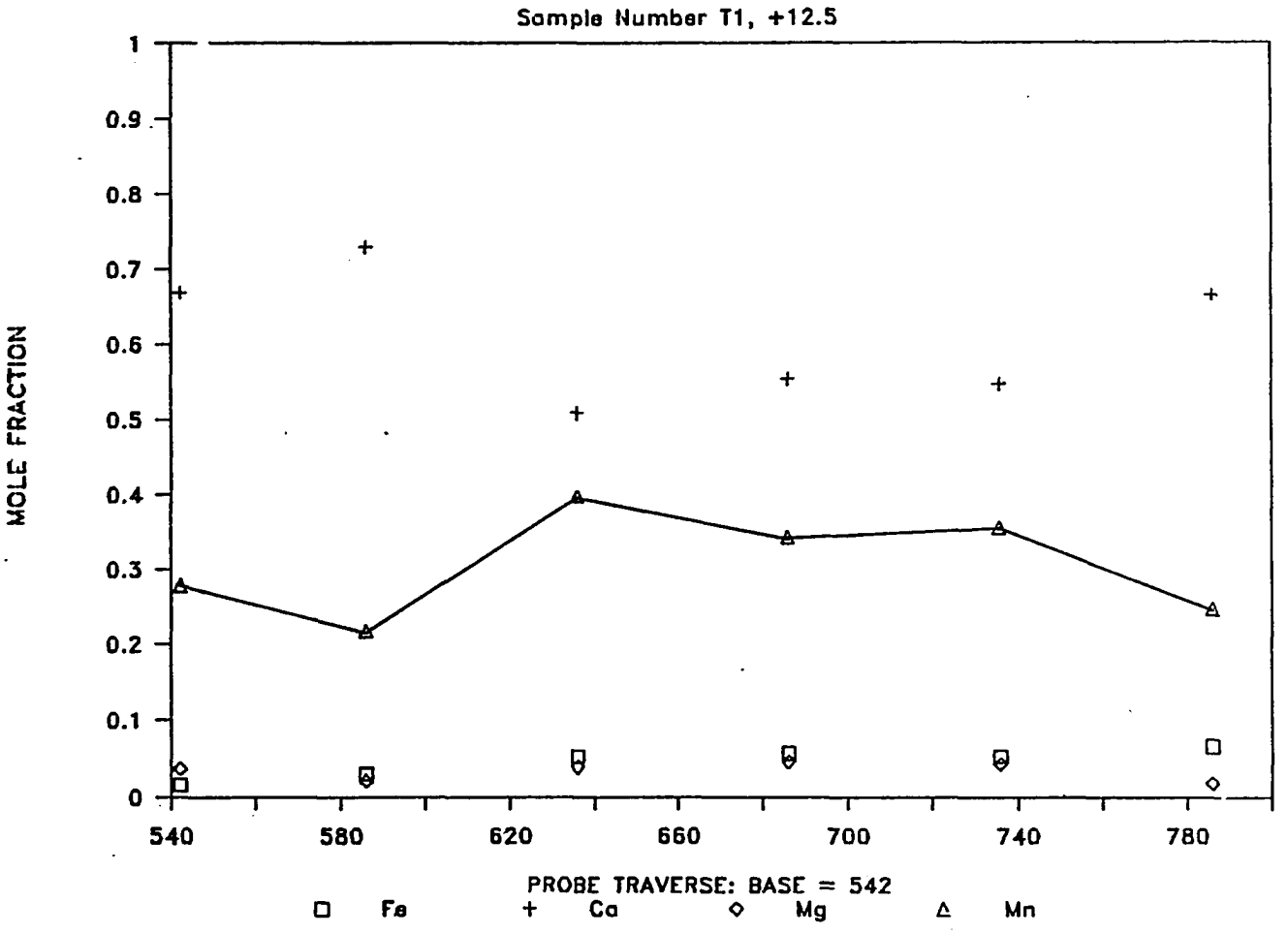

Figure 94. Probe traverse across bedding showing the variation in Mn, Mg, Fe, and Ca, concentrations in carbonate minerals.

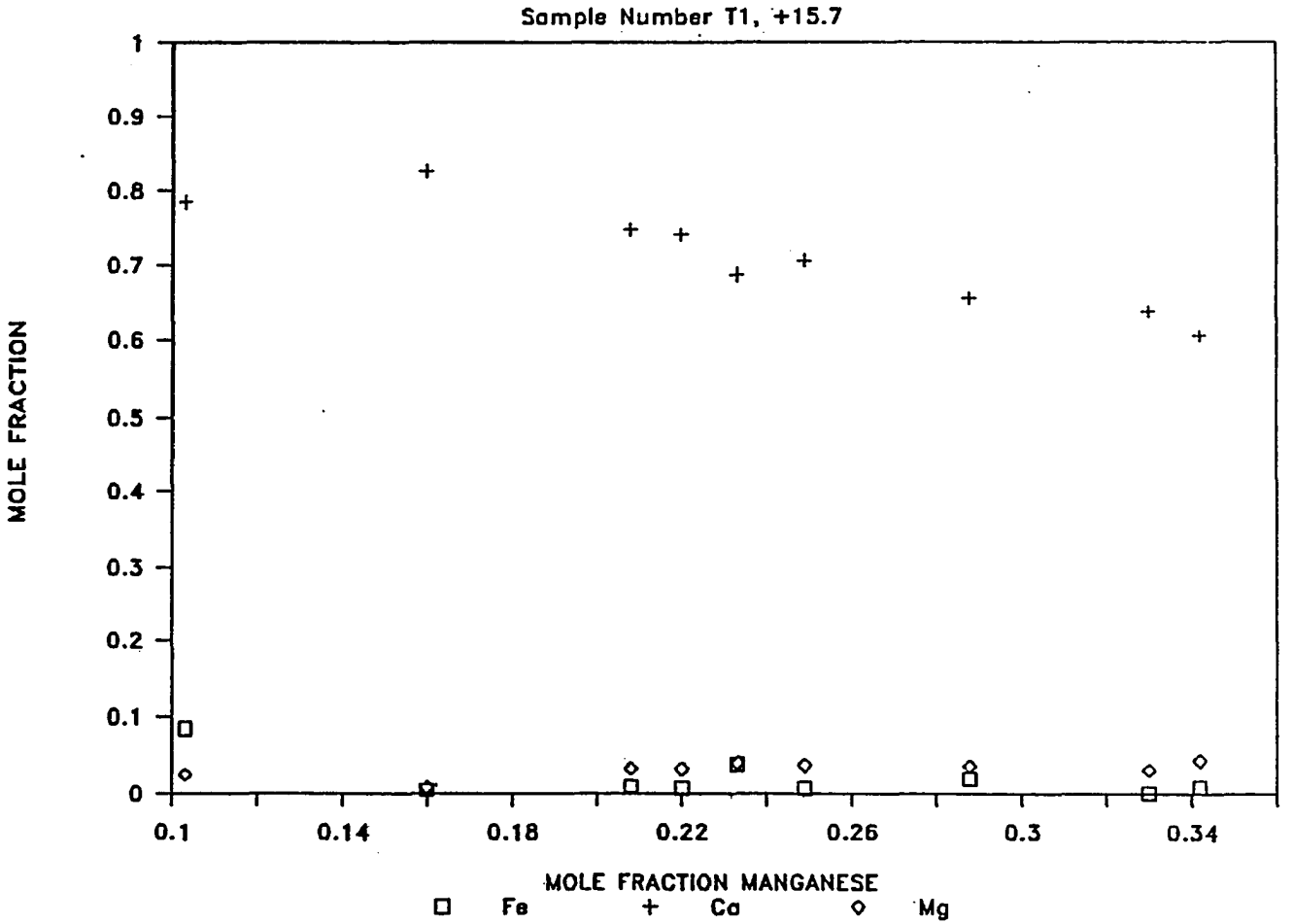

Figure 95. Graph of the mole fraction of Fe, Ca, and Mg plotted against the mole fraction of Mn in carbonate minerals from the sample noted at the top of the graph.

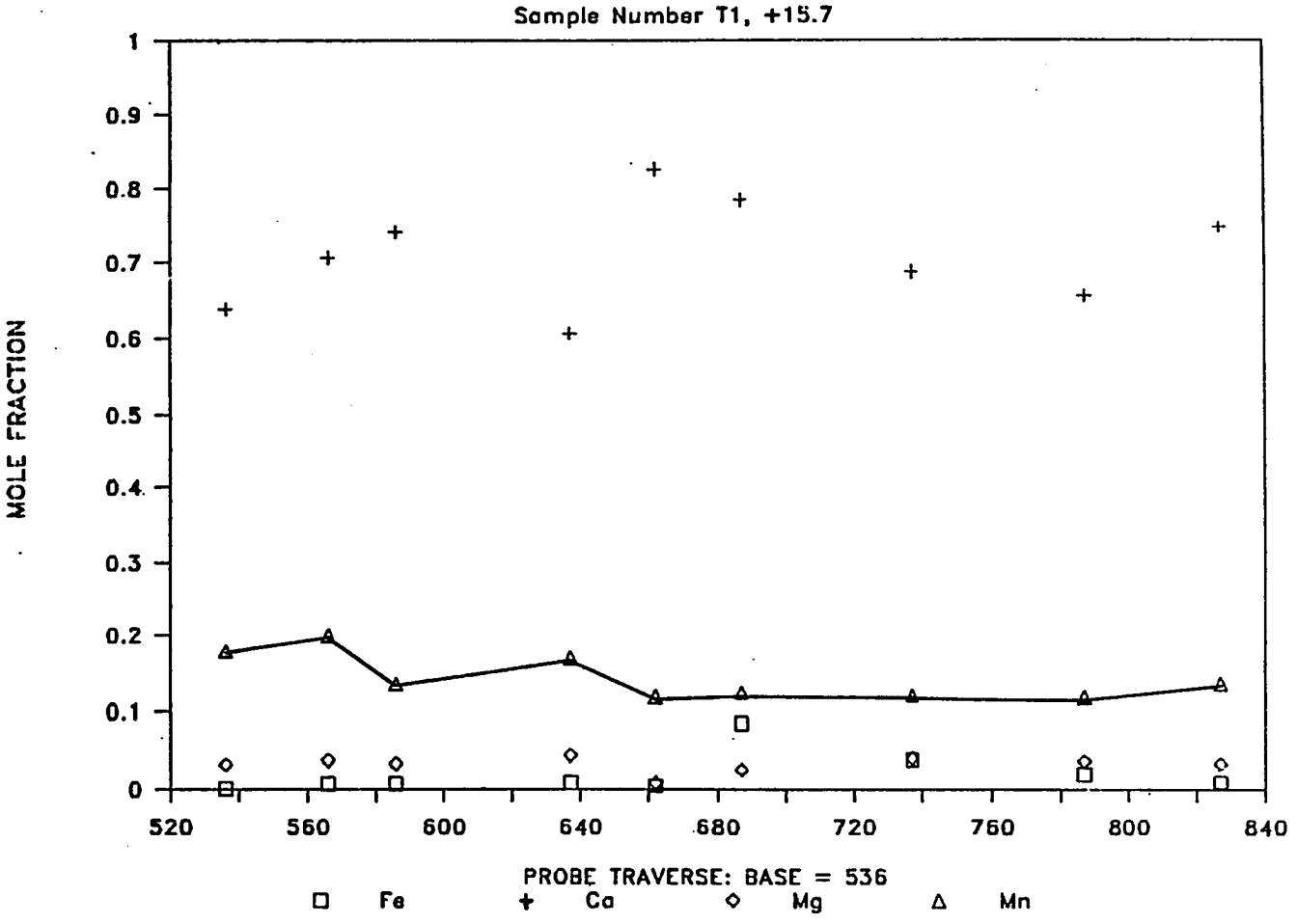

Figure 96. Probe traverse across bedding showing the variation in Mn, Mg, Fe, and Ca concentrations in carbonate minerals.

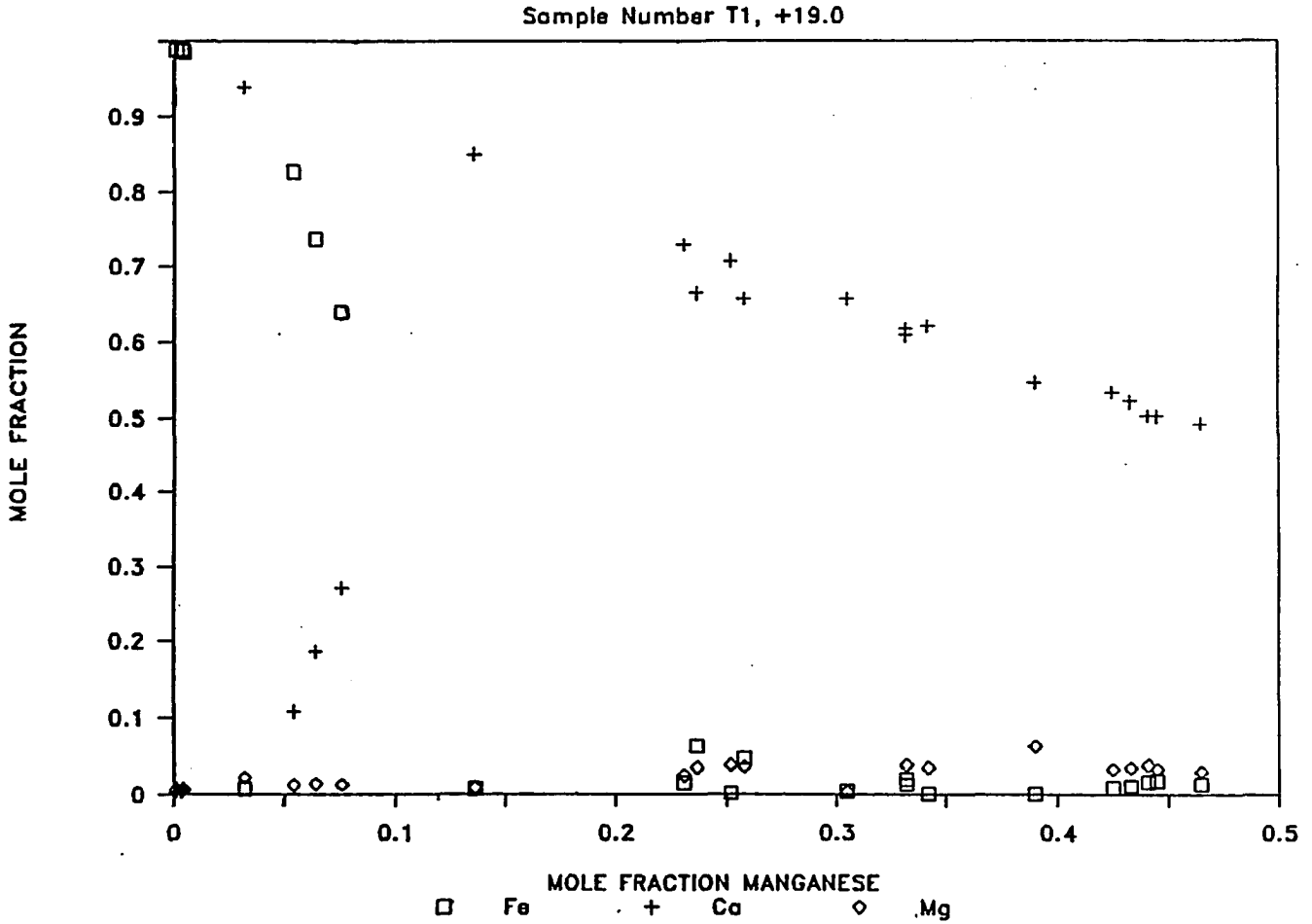

Figure 97. Graph of the mole fraction of Fe, Ca, and Mg plotted against the mole fraction of Mn in carbonate minerals from the sample noted at the top of the graph.

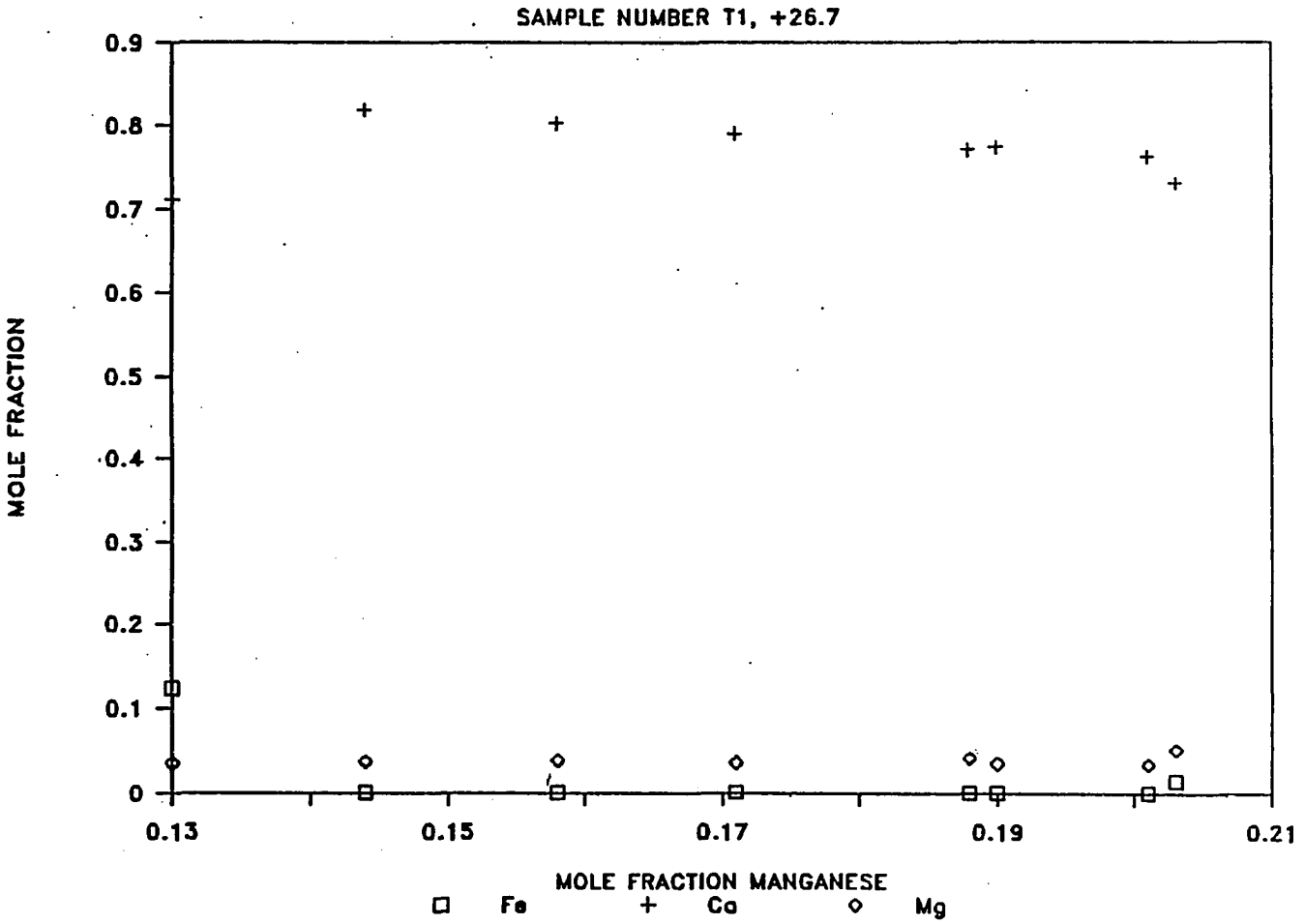

Figure 98. Graph of the mole fraction of Fe, Ca, and Mg plotted against the mole fraction of Mn in carbonate minerals from the sample noted at the top of the graph.

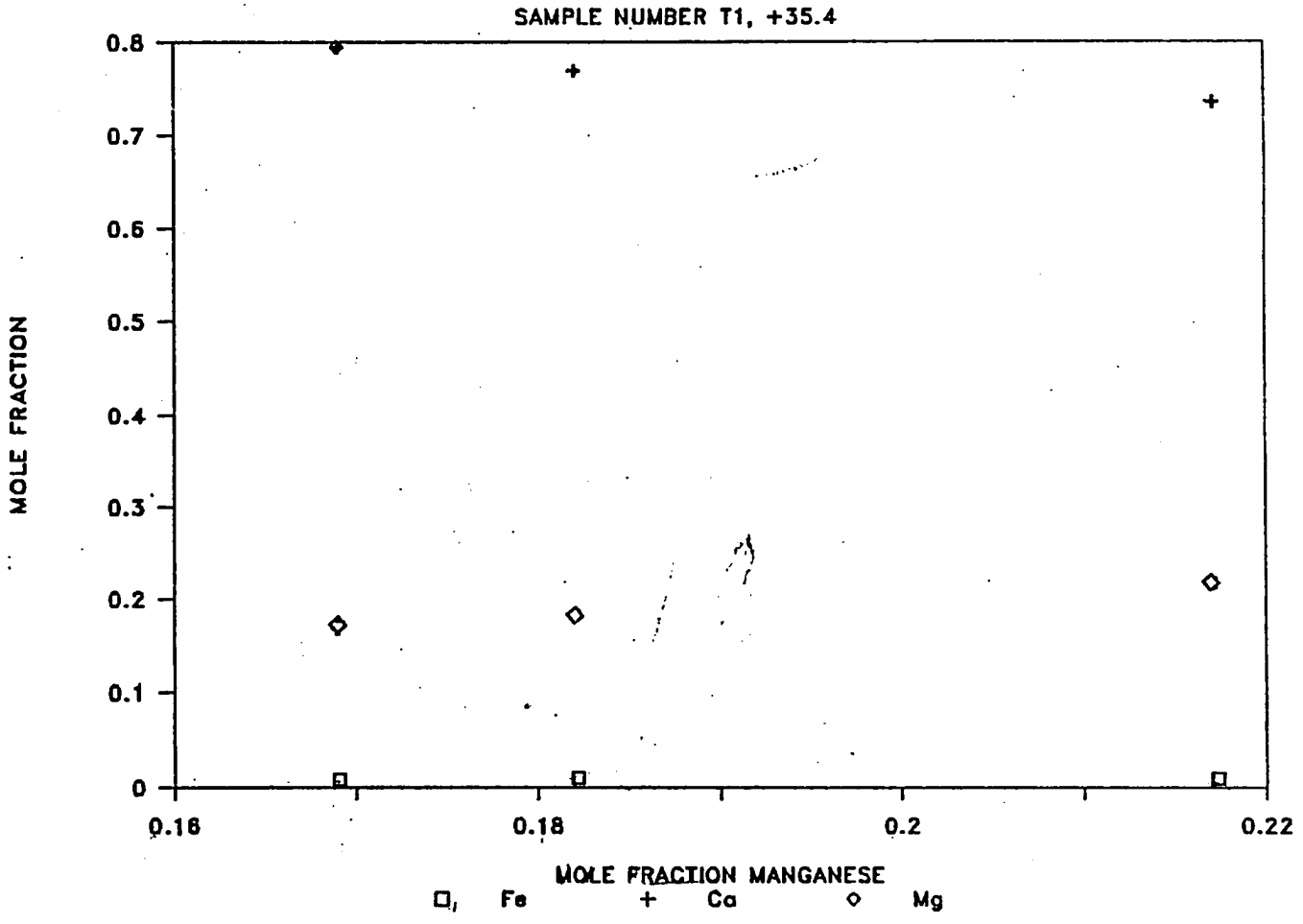

Figure 99. Graph of the mole fraction of Fe, Ca, and Mg plotted against the mole fraction of Mn in carbonate minerals from the sample noted at the top of the graph.

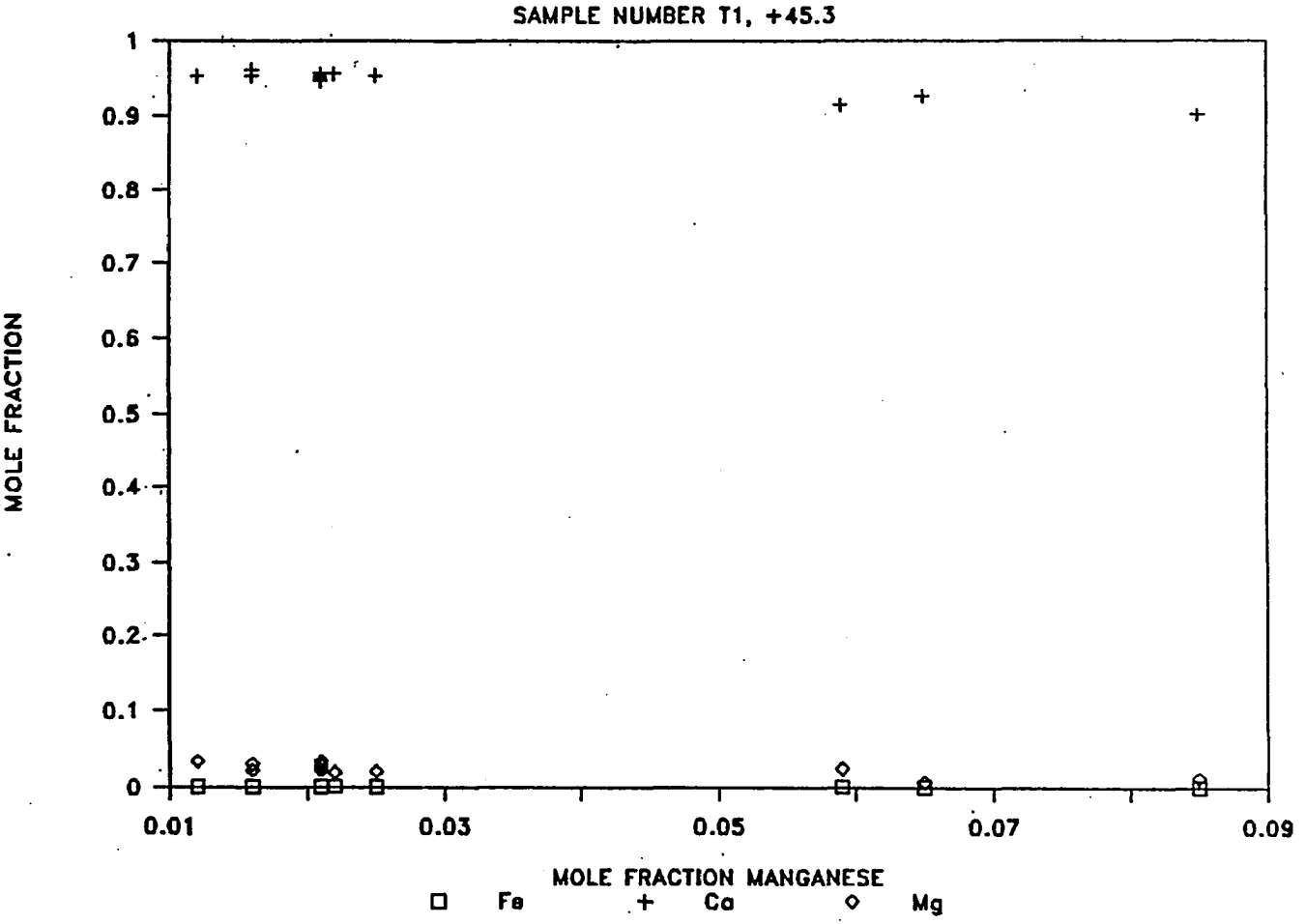

Figure 100. Graph of the mole fraction of Fe, Ca, and Mg plotted against the mole fraction of Mn in carbonate minerals from the sample noted at the top of the graph.

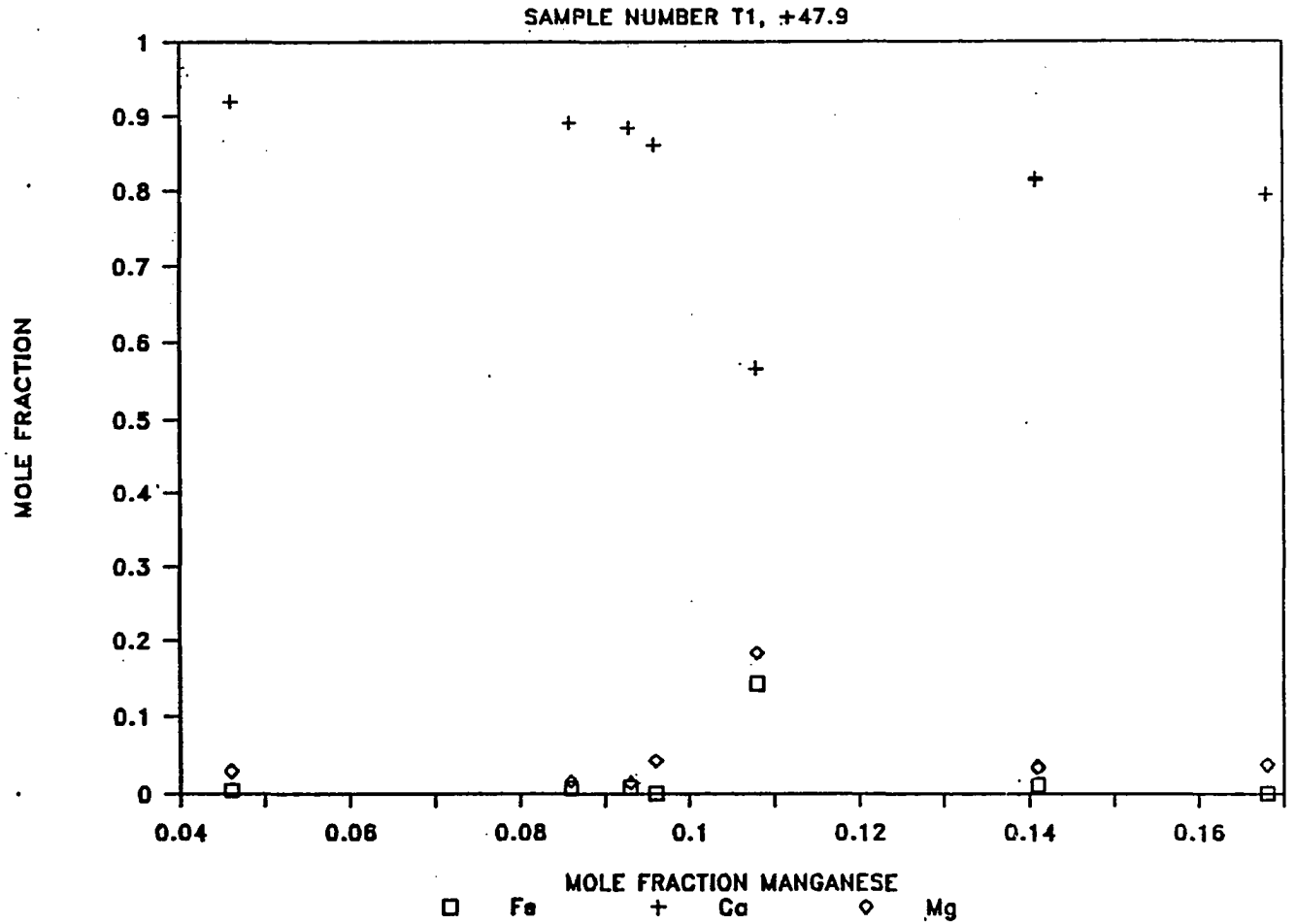

Figure 101. Graph of the mole fraction of Fe, Ca, and Mg plotted against the mole fraction of Mn in carbonate minerals from the sample noted at the top of the graph.

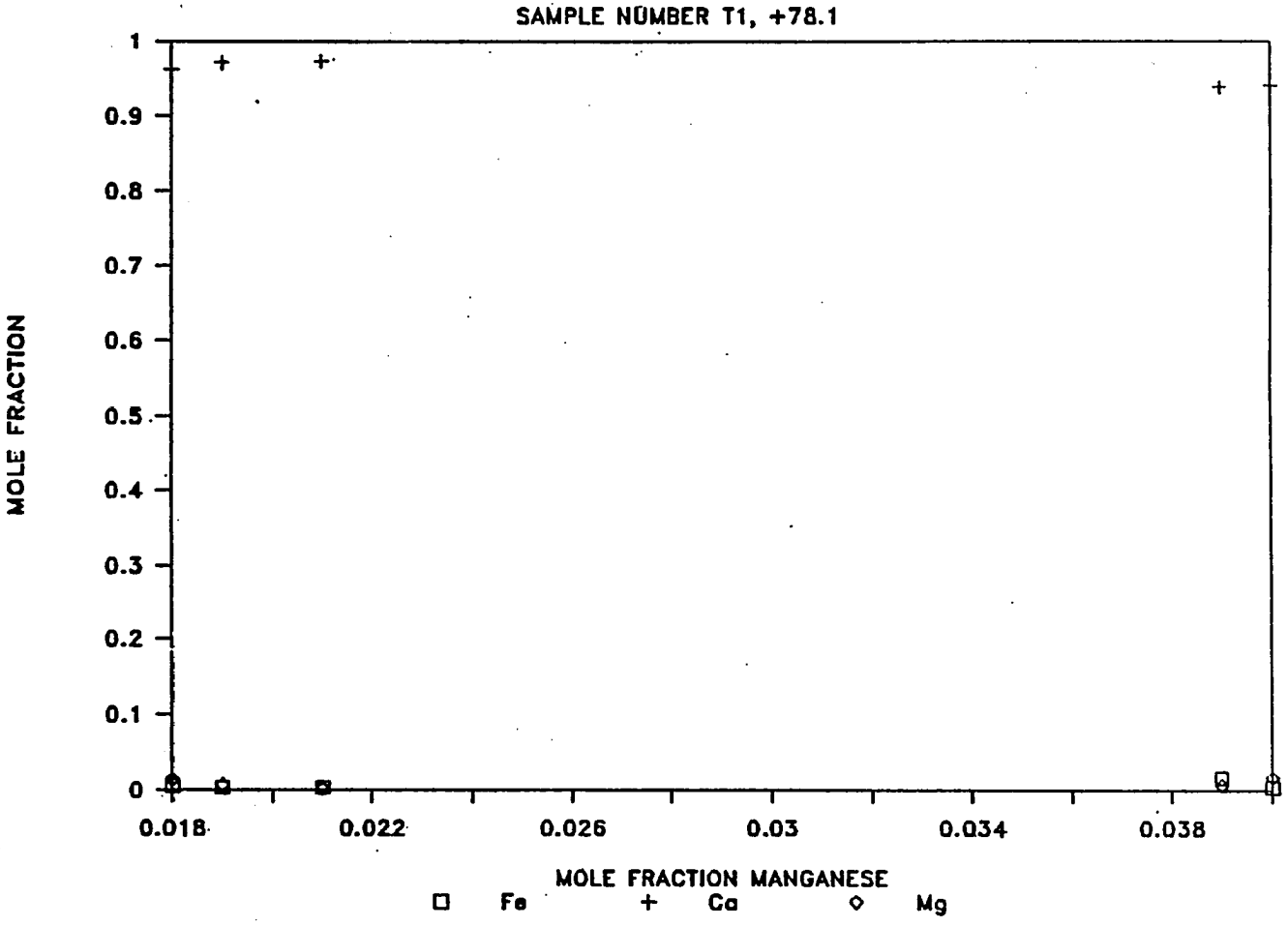

Figure 102. Graph of the mole fraction of Fe, Ca, and Mg plotted against the mole fraction of Mn in carbonate minerals from the sample noted at the top of the graph.

APPENDIX E

TRIANGULAR PLOTS OF COMPOSITIONAL DATA FOR INDIVIDUAL SAMPLES ANALYZED BY ELECTRON MICROPROBE

Nota Bene: Fe and Ca are added together in these plots. The notation used at the apex reflects the predominance of one of the cations. That is, "$FeCO_3$ + $CaCO_3$" indicates that the Fe component is greater than the Ca component, and vice versa. In addition, I have made note of the range of composition of the minor cation next to the apex label.

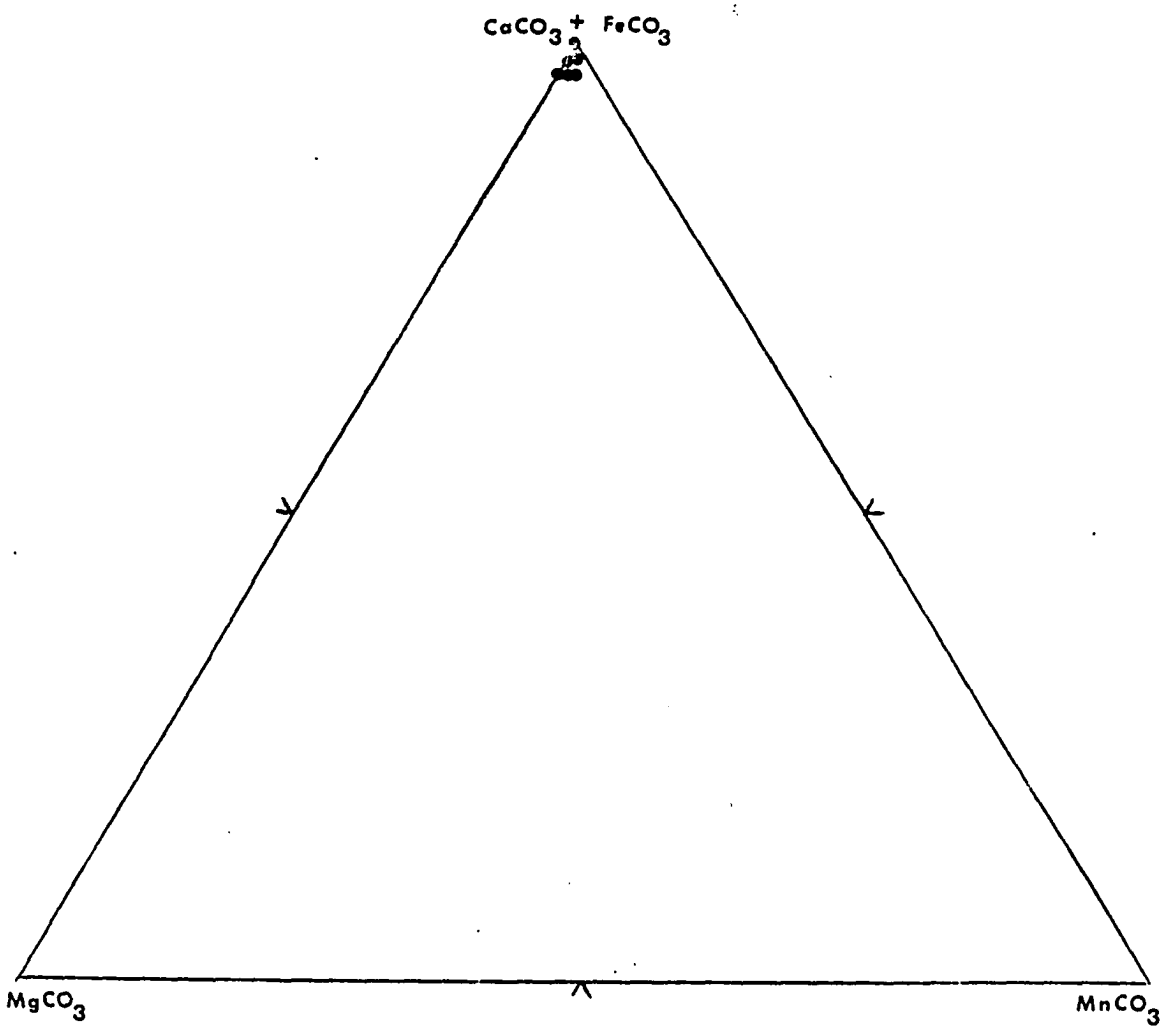

Figure 103. Compositional data for sample T1,0.
Fe: 0 - 0.007, 0.016, 0.063, 0.412.

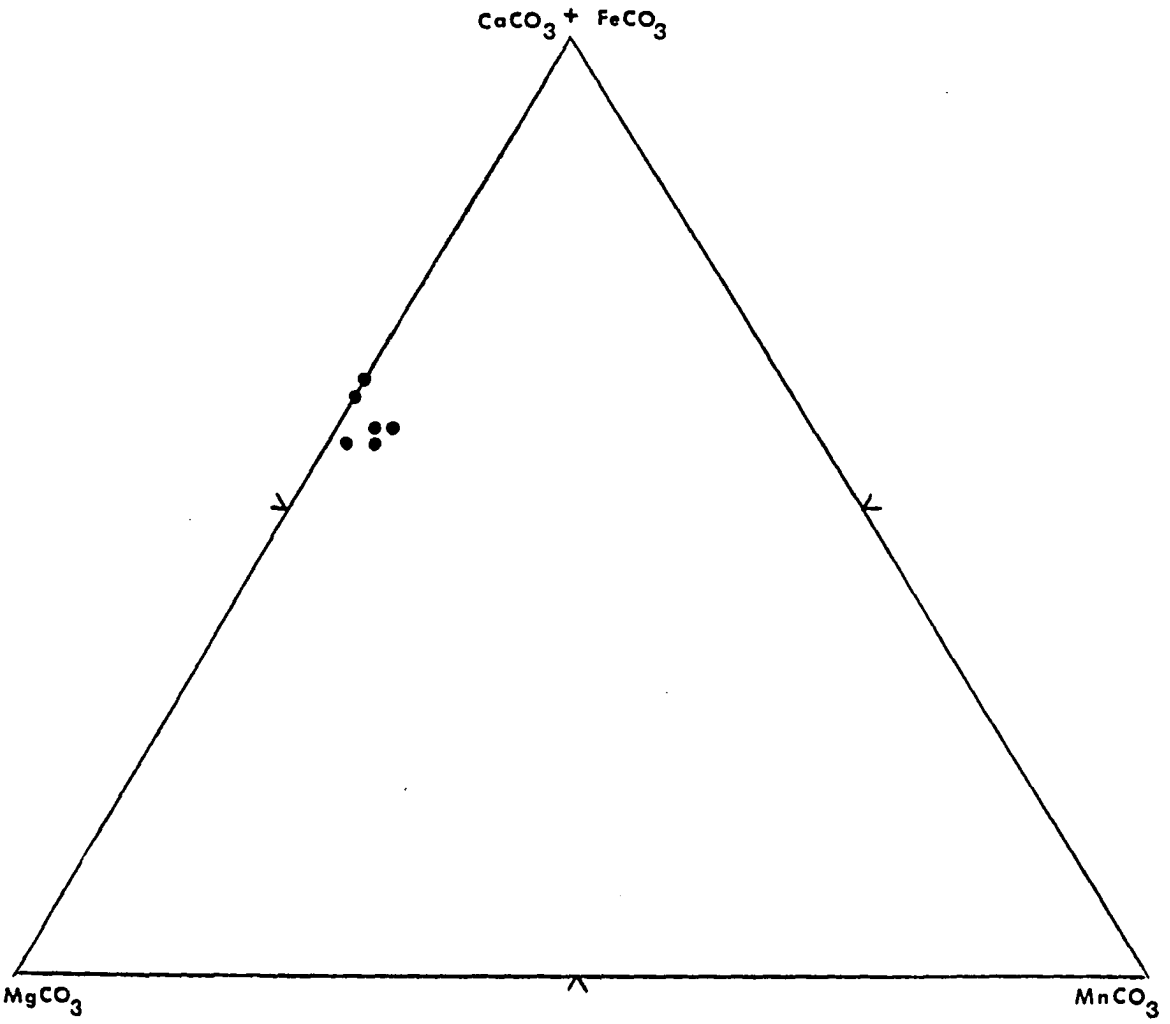

Figure 104. Compositional data for sample T1, +0.1.
Fe: 0 - 0.005, 0.028.

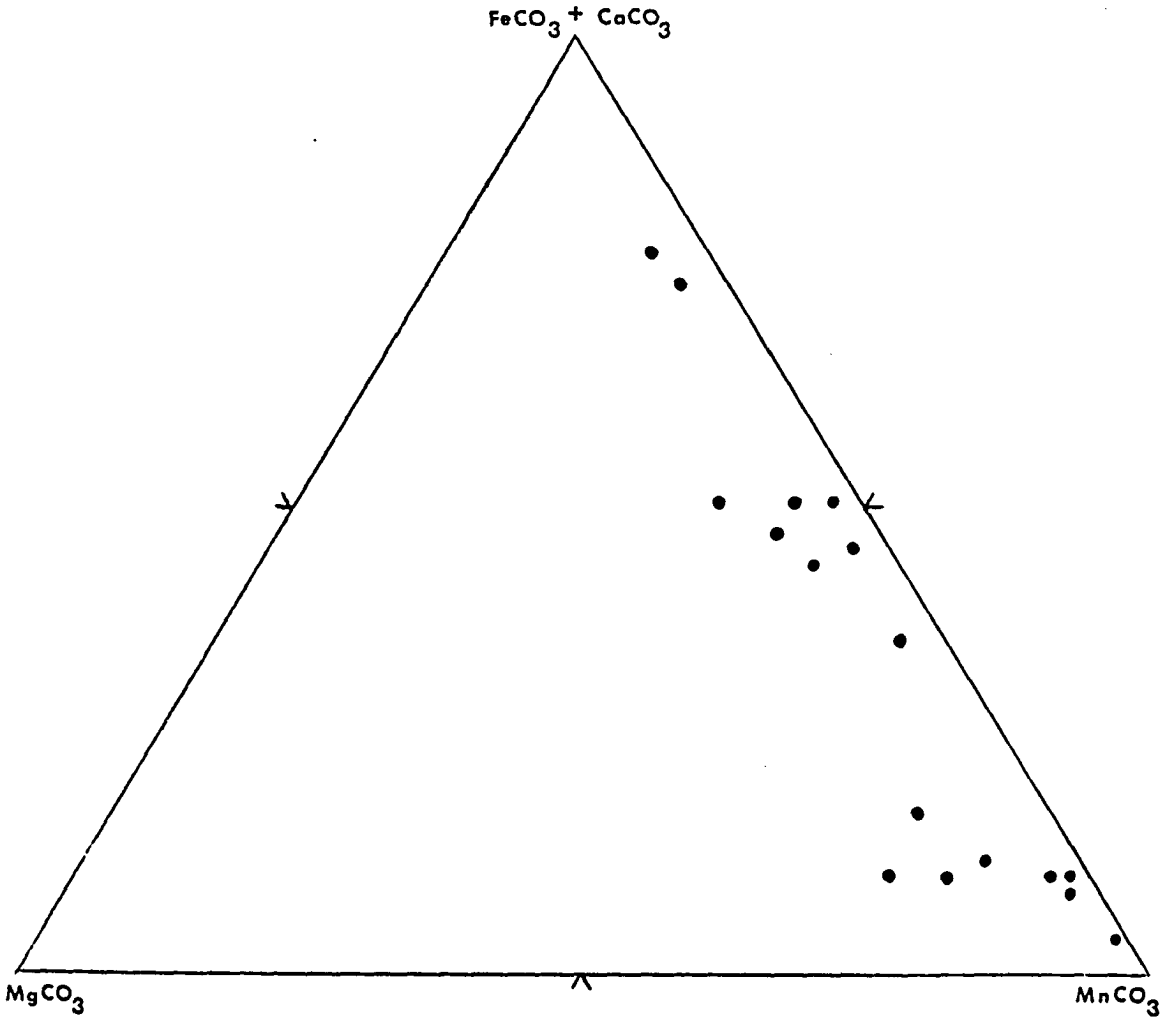

Figure 105. Compositional data for sample T1, +0.45.
Ca: 0.02 - 0.099.

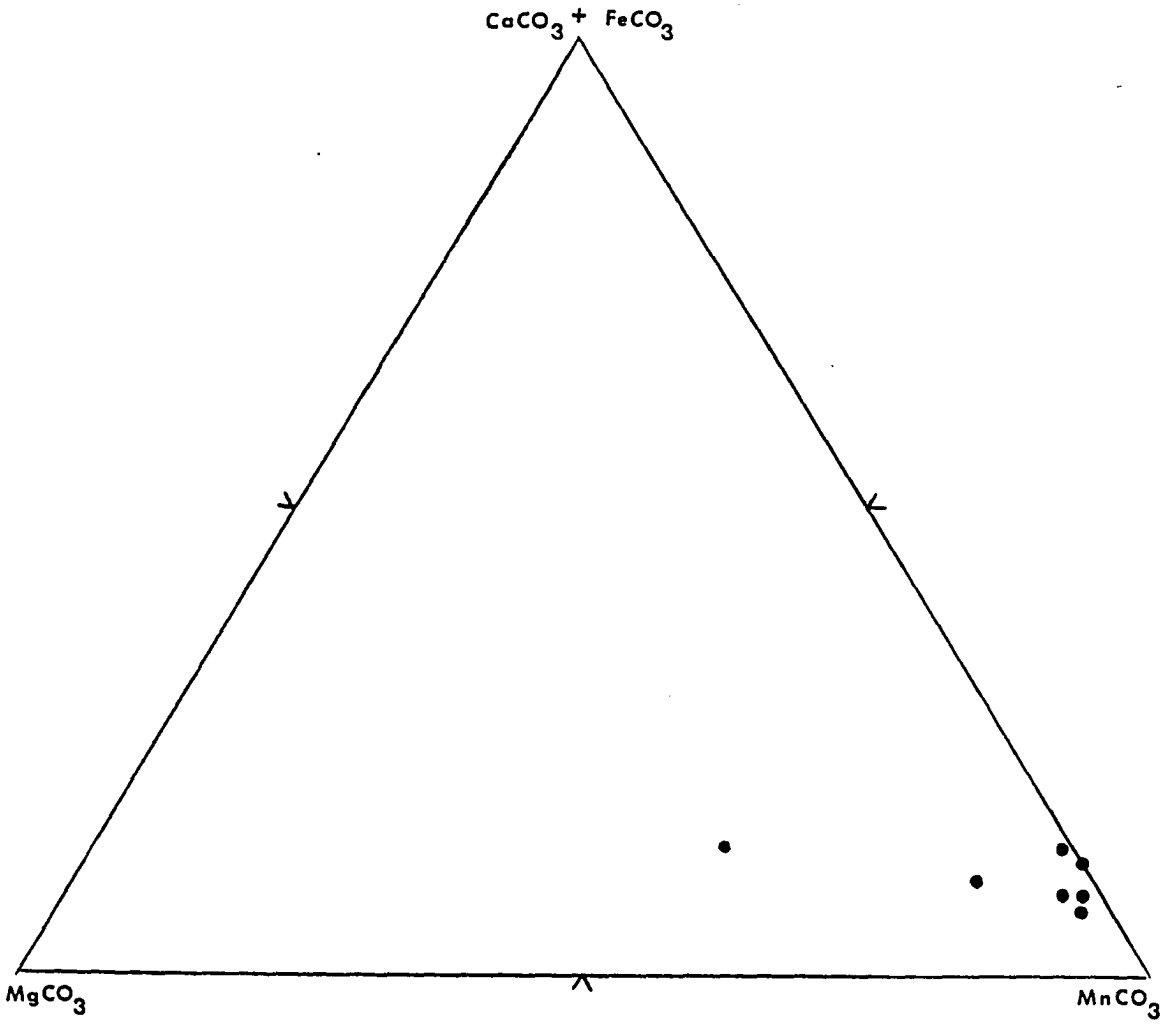

Figure 106. Compositional data for sample T1, +0.50.
Fe: 0 - 0.075.

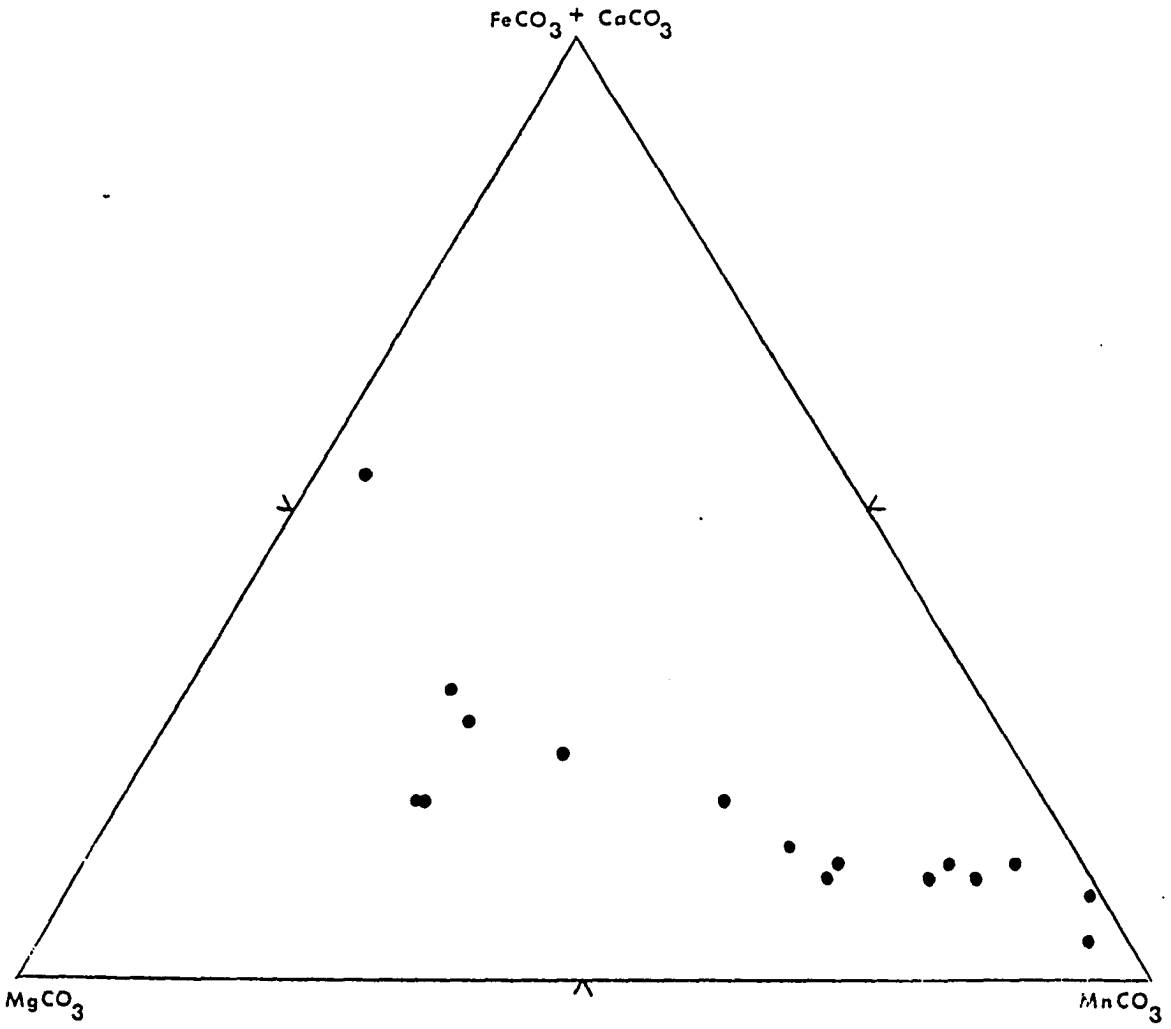

Figure 107. Compositional data for sample T1, +2.0.
Ca: 0 - 0.082.

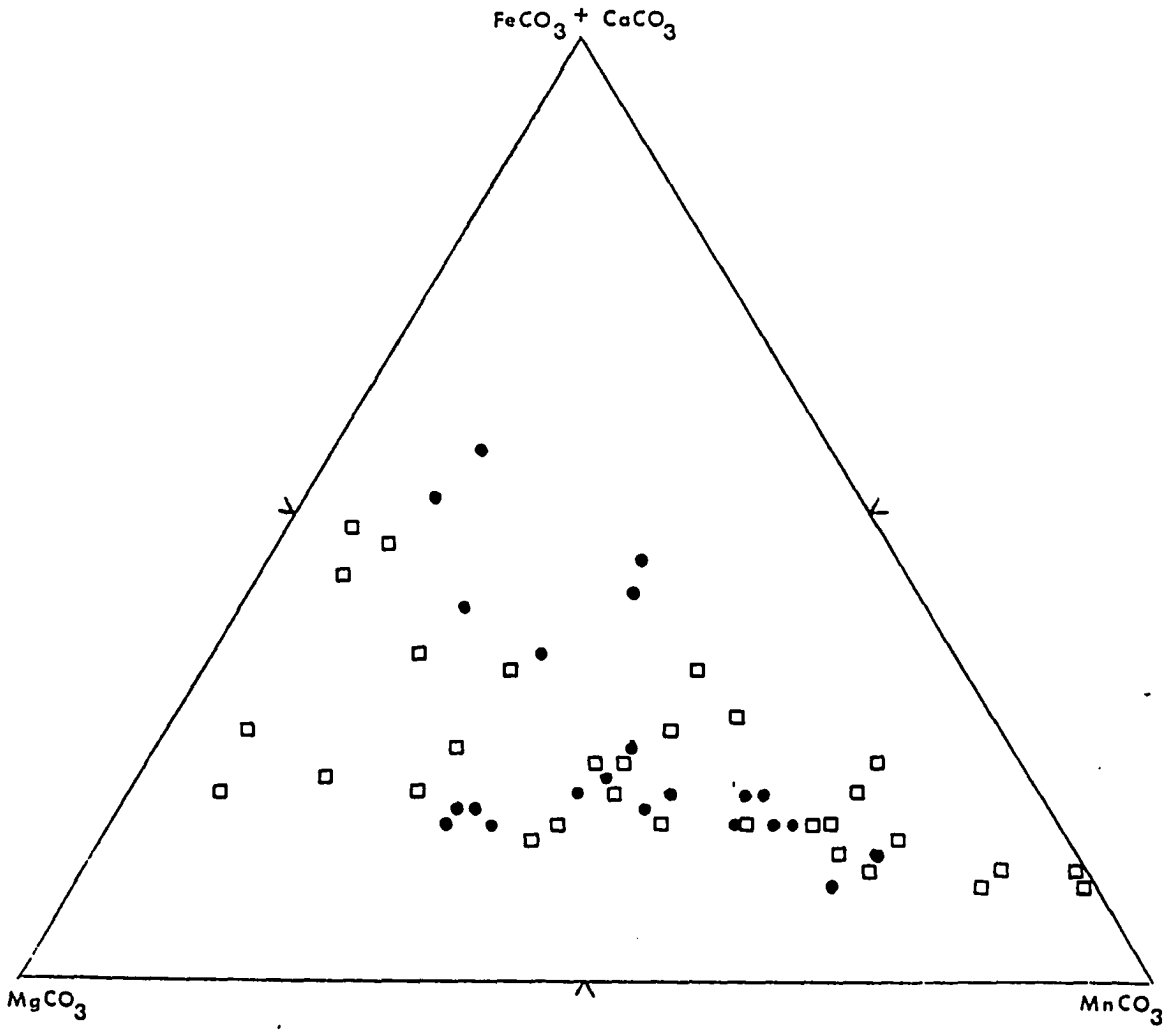

Figure 108. Compositional data for sample T1, +2.5 A and B.
Ca: 0.015 - 0.094 for A. ●
Ca: 0.001 - 0.105 for B. □

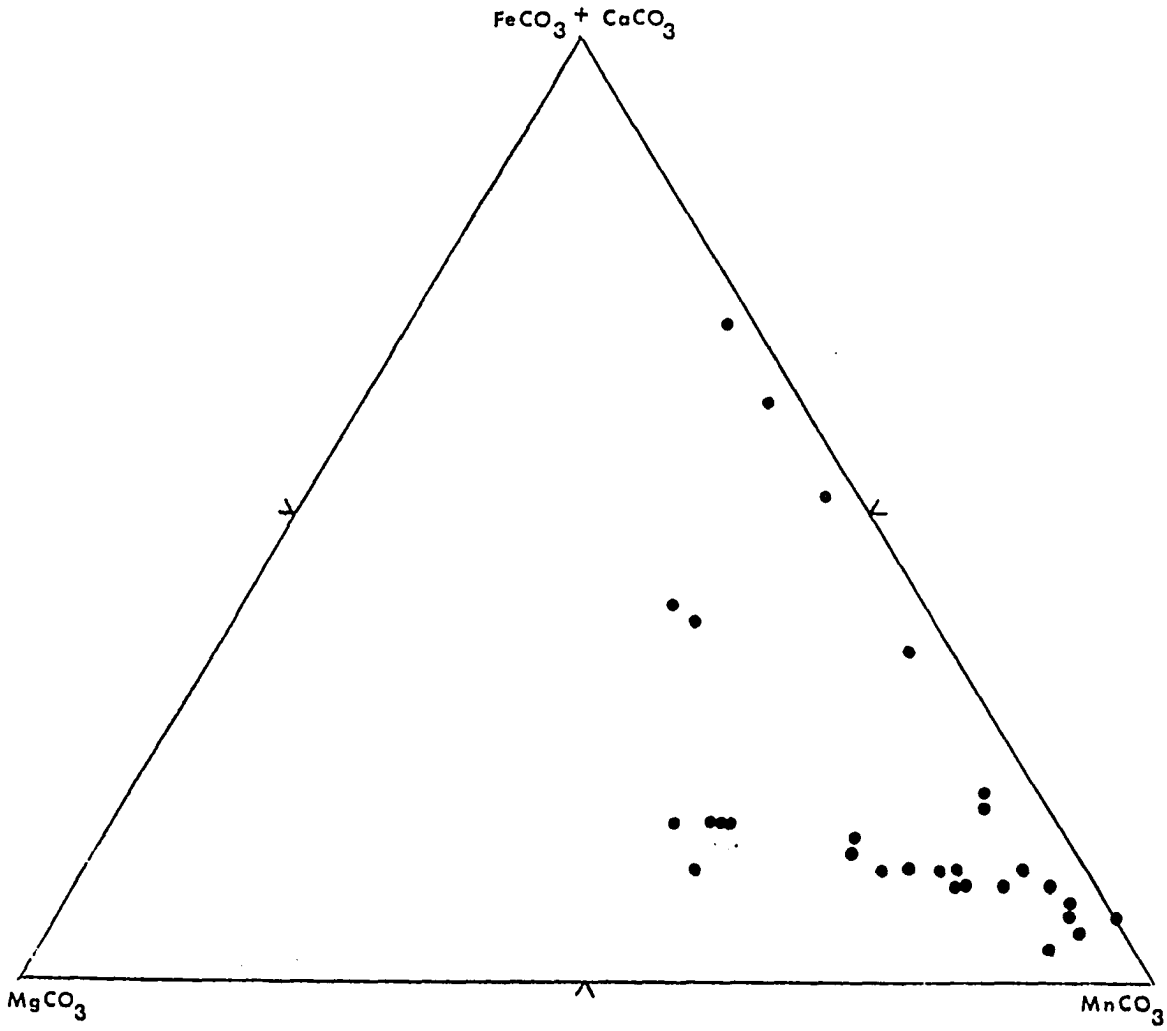

Figure 109. Compositional data for sample T1, +3.4.
Ca: 0.023 - 0.073; 0.115 - 0.253.

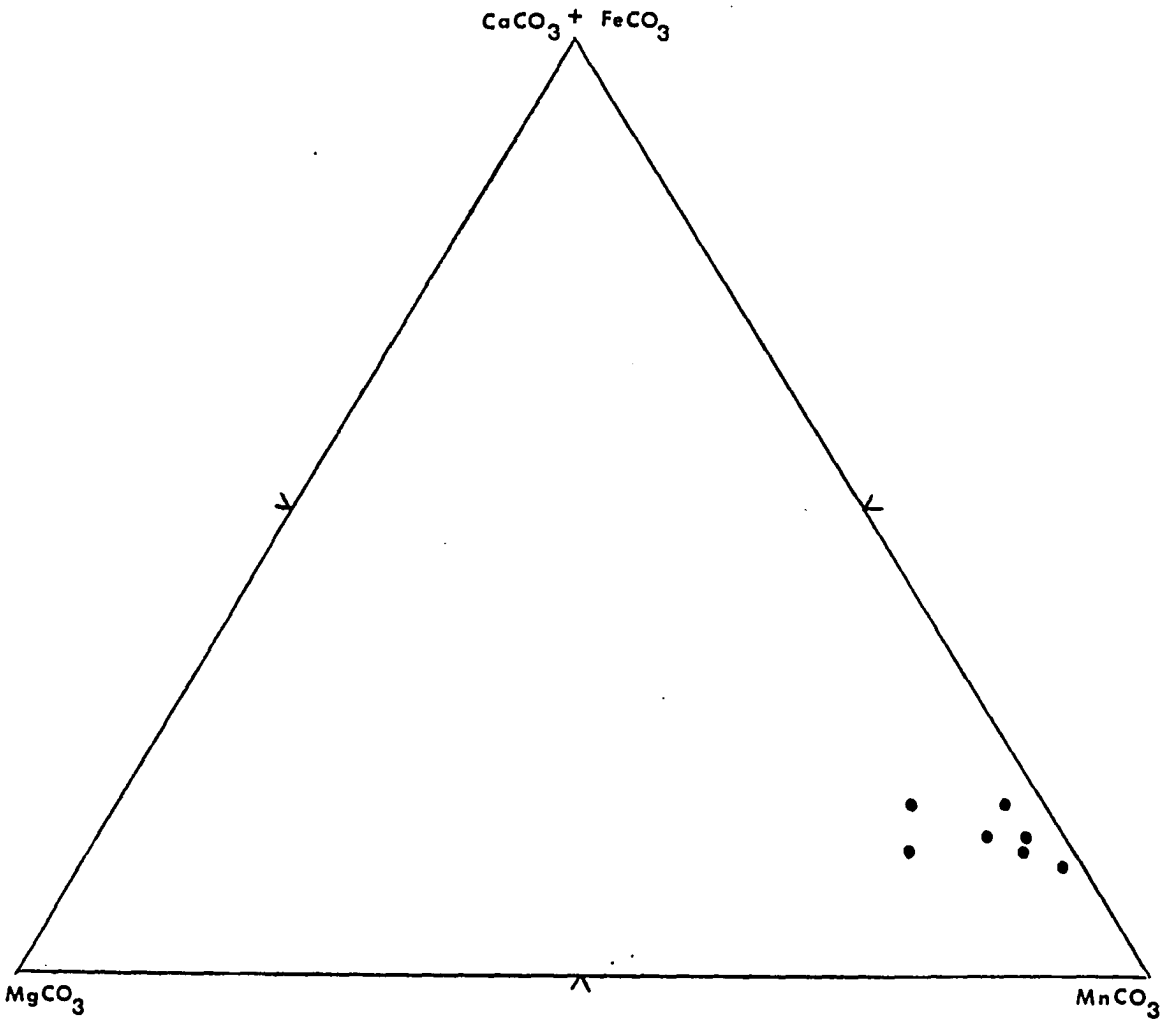

Figure 110. Compositional data for sample T1, +5.9.
Fe: 0.005 - 0.039; 0.108.

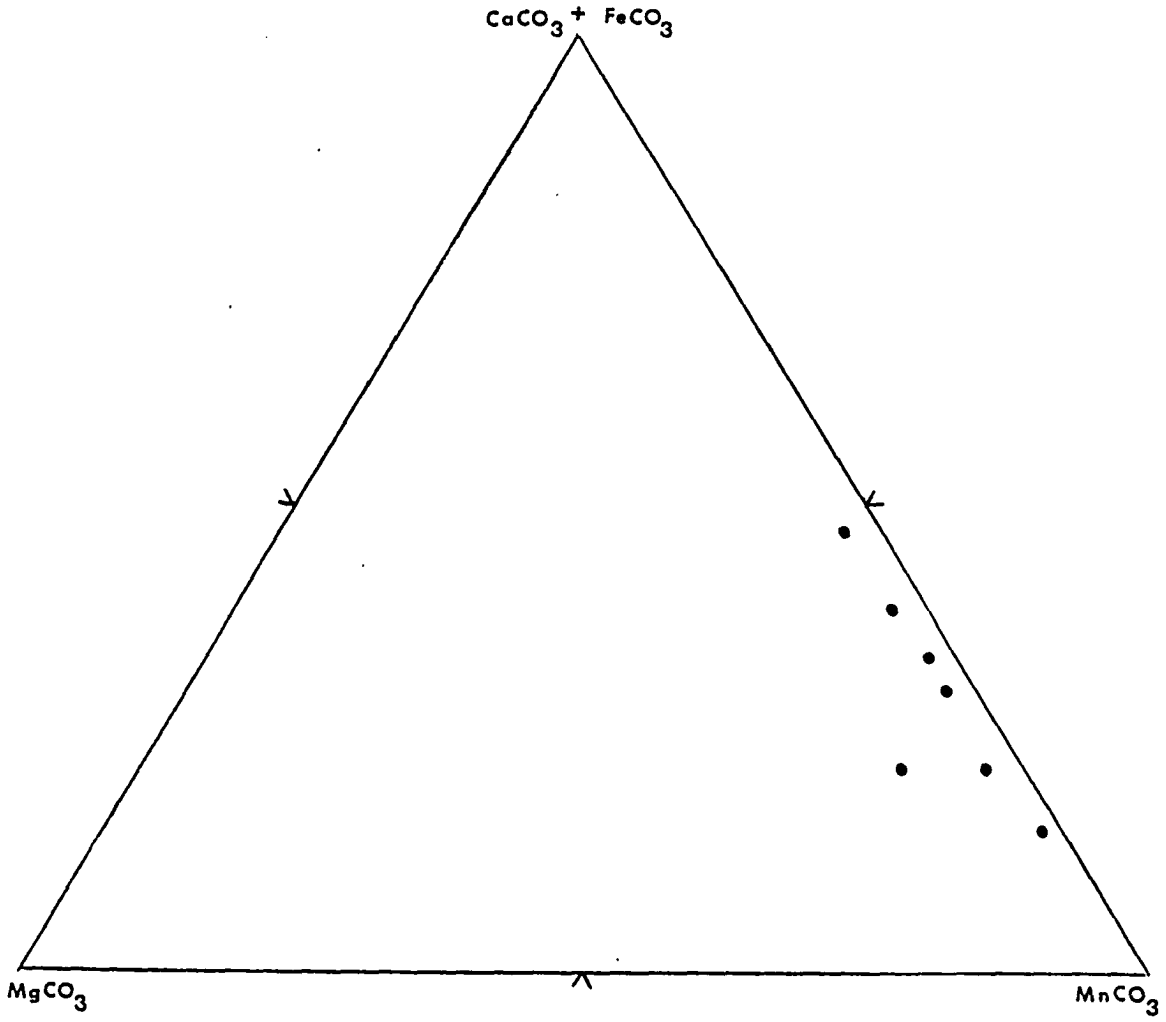

Figure 111. Compositional data for sample T1, +8.5.
Fe: 0.005 - 0.01; 0.038; 0.053.

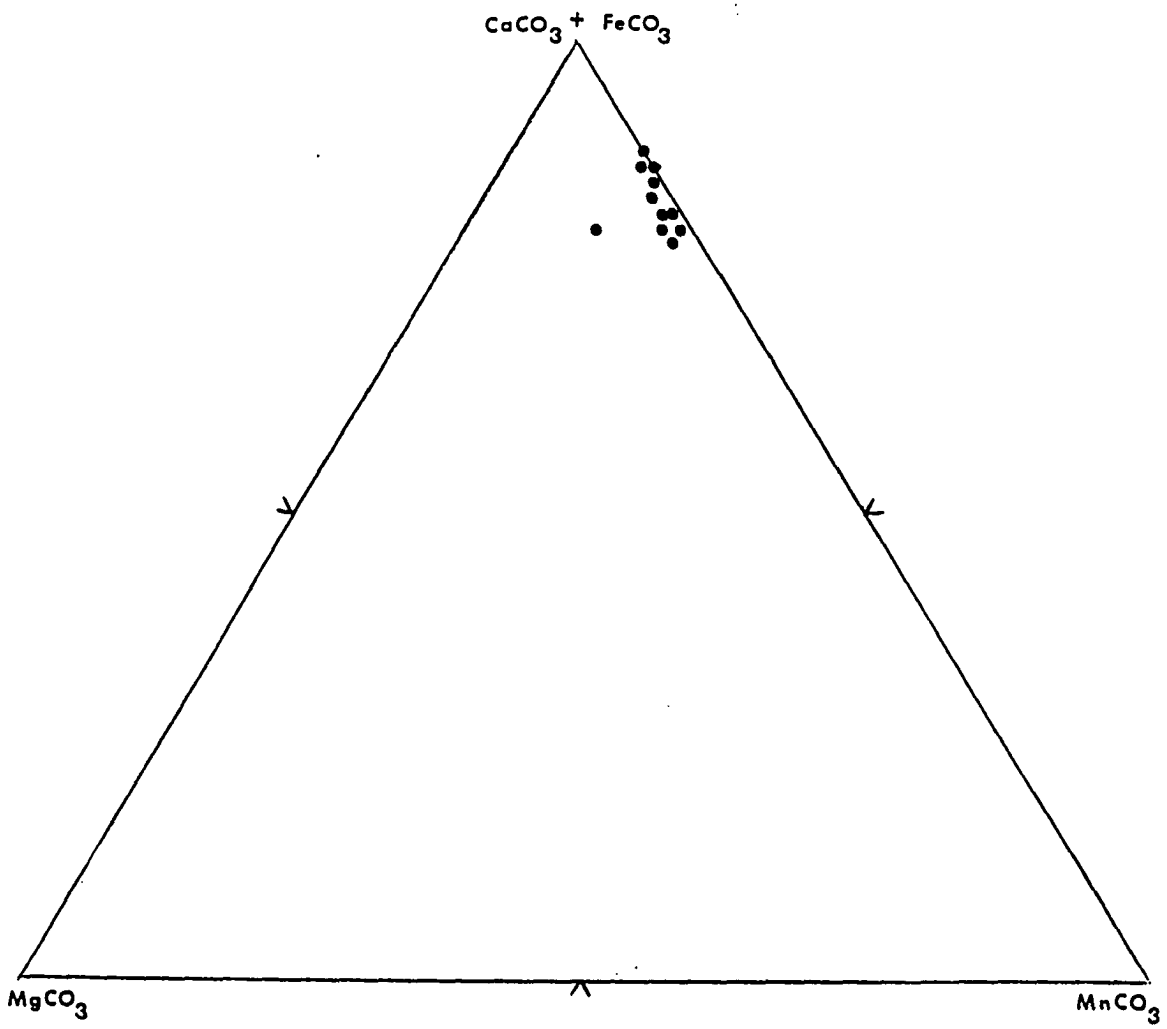

Figure 112. Compositional data for sample T1, +9.8.
Fe: 0 - 0.012.

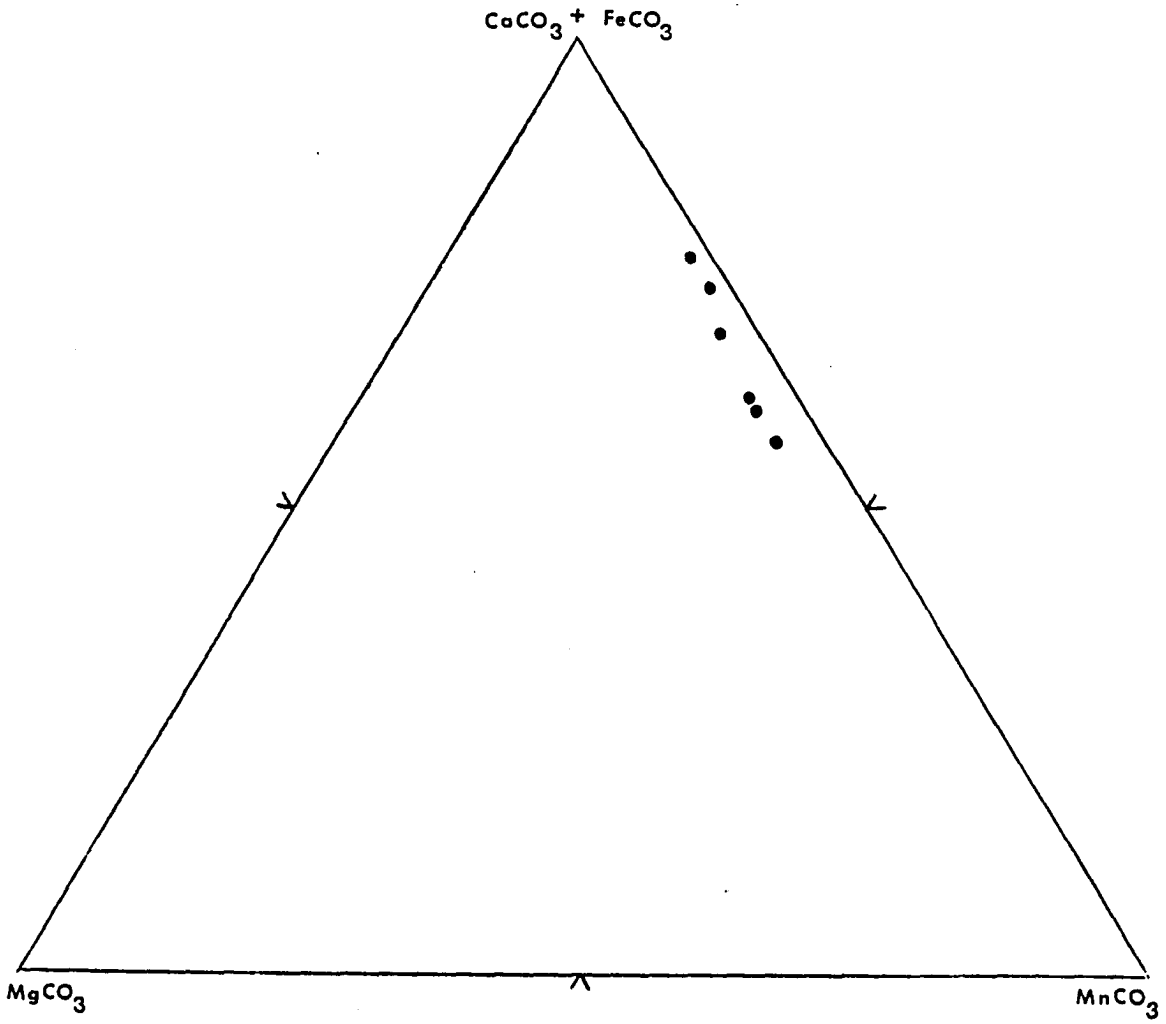

Figure 113. Compositional data for sample T1, +12.5.
Fe: 0.015 - 0.030; 0.052 - 0.066.

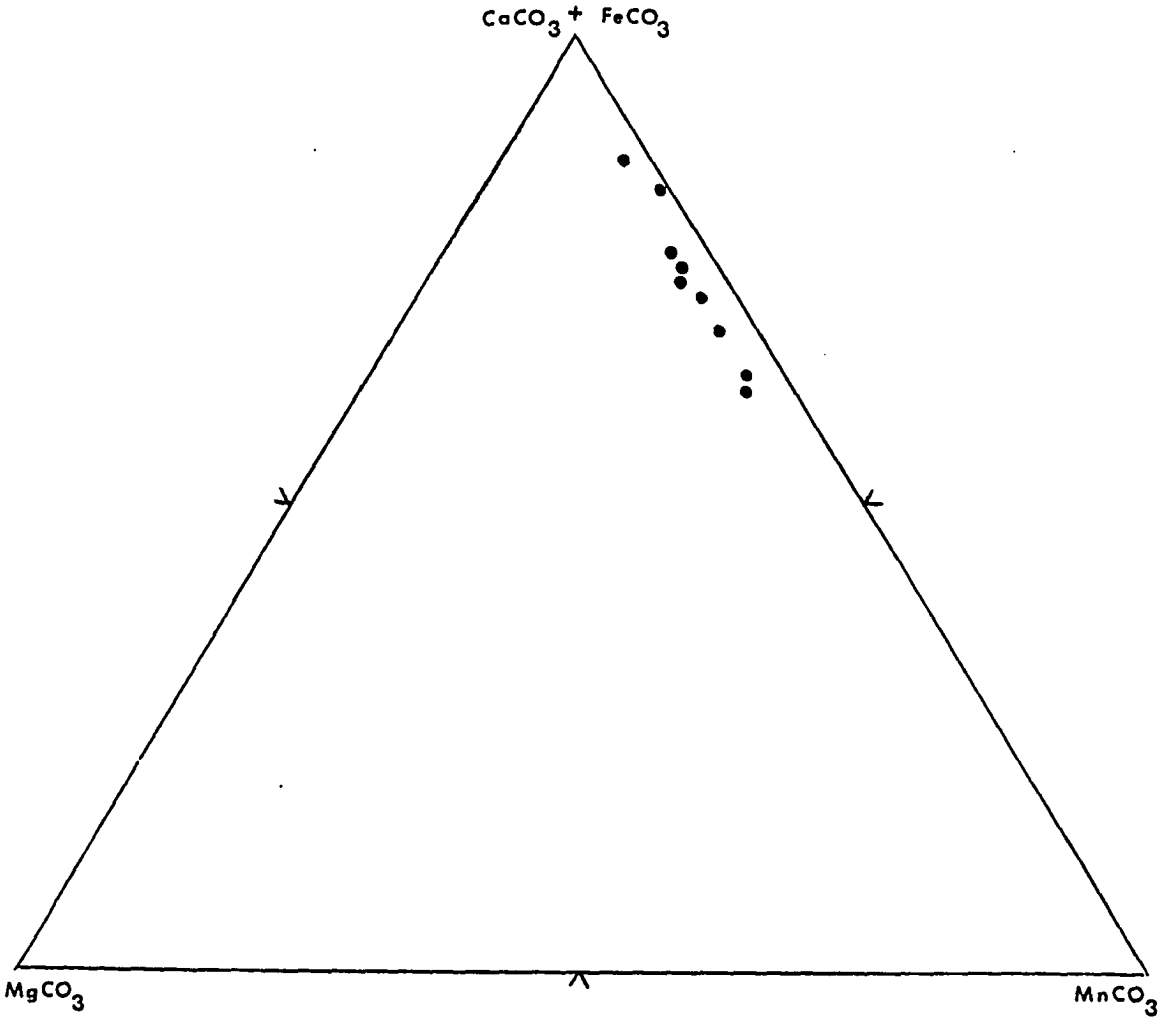

Figure 114. Compositional data for sample T1, +15.7.
Fe: 0 - 0.009; 0.019 - 0.085.

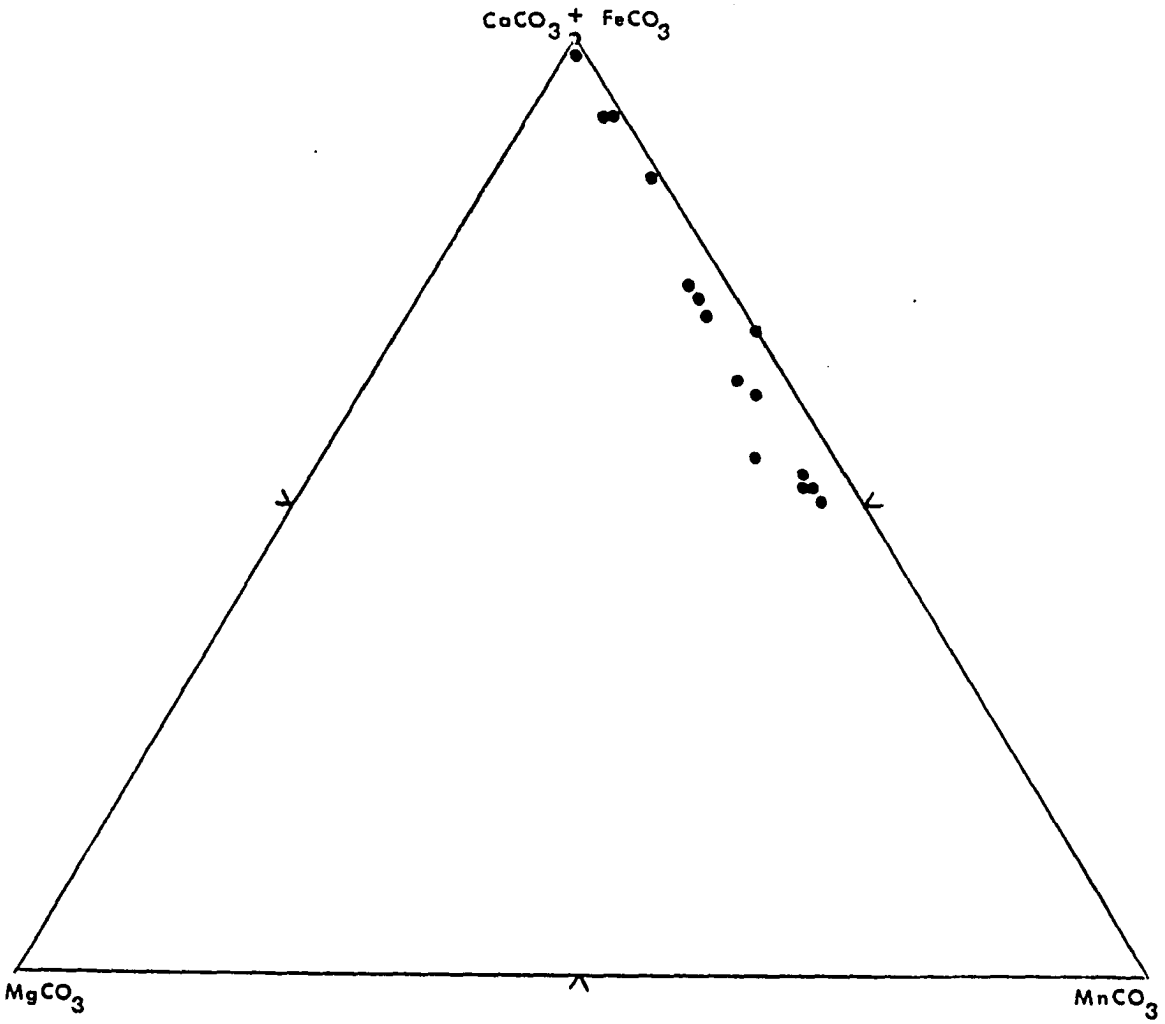

Figure 115. Compositional data for sample T1, +19.0.
Fe: 0 - 0.019; 0.047; 0.063; 0.737 - 0.988.

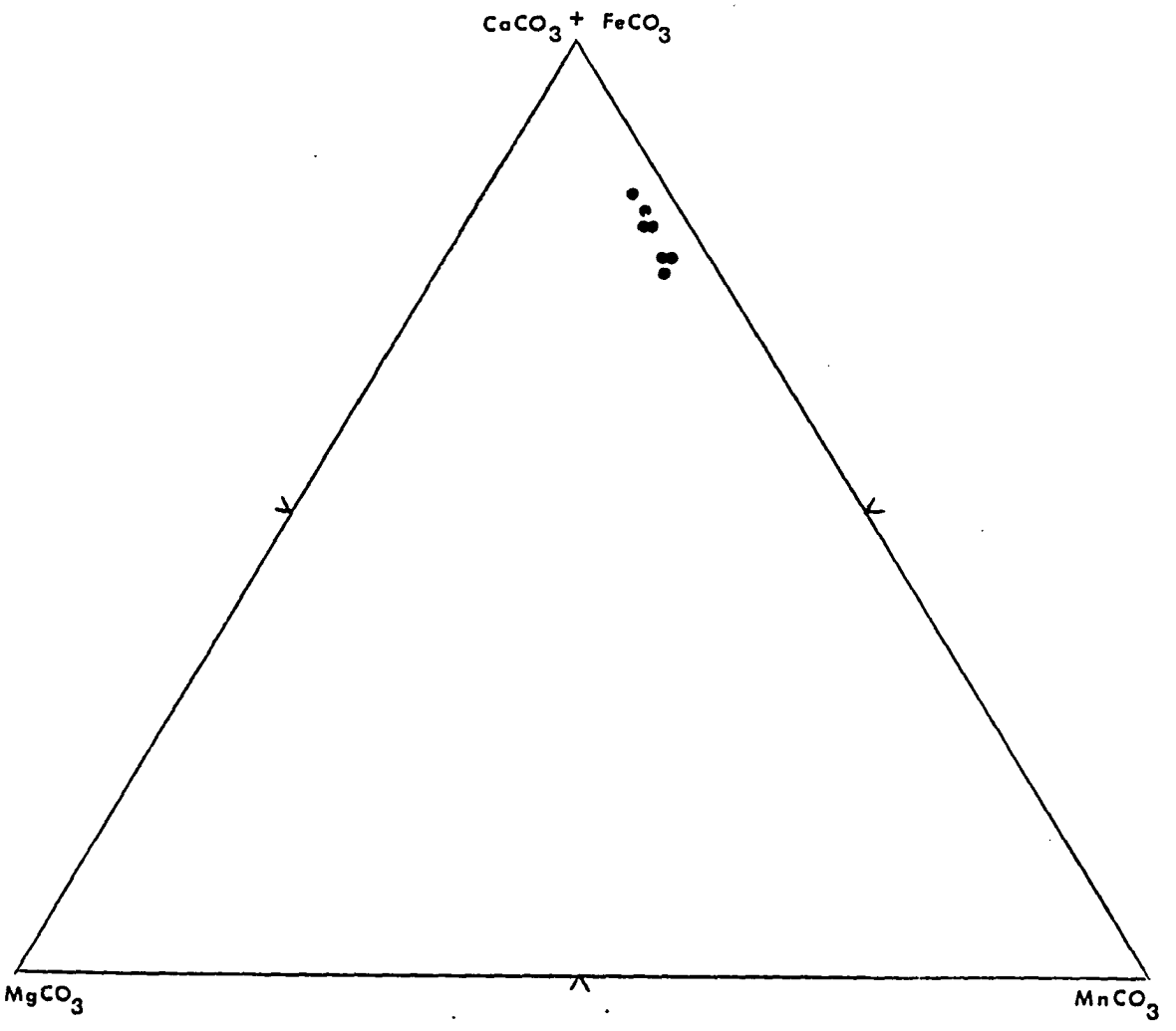

Figure 116. Compositional data for sample T1,+26.7.
Fe: 0 - 0.014, 0.124.

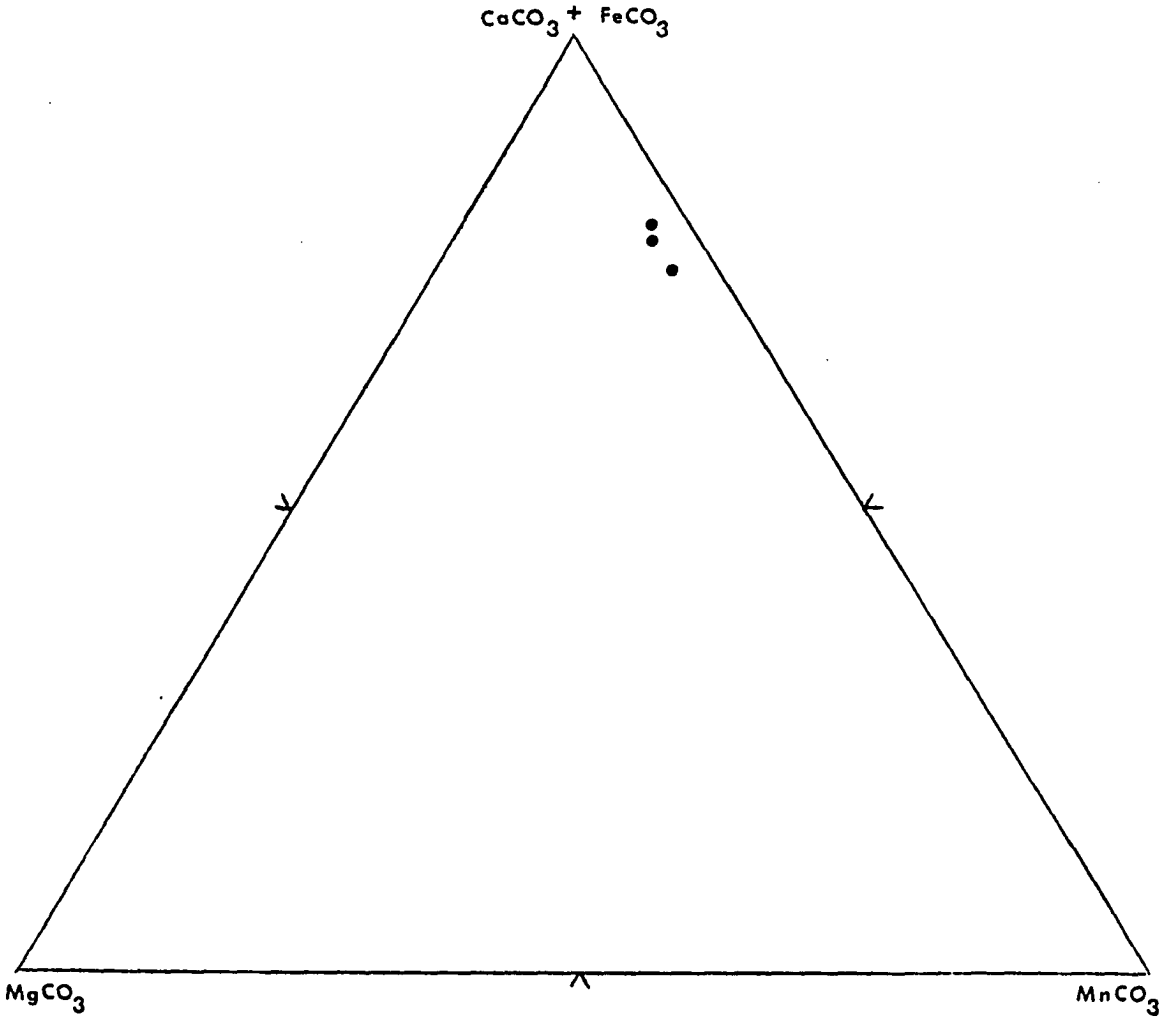

Figure 117. Compositional data for sample T1, +35.4. Fe: 0.005 - 0.008.

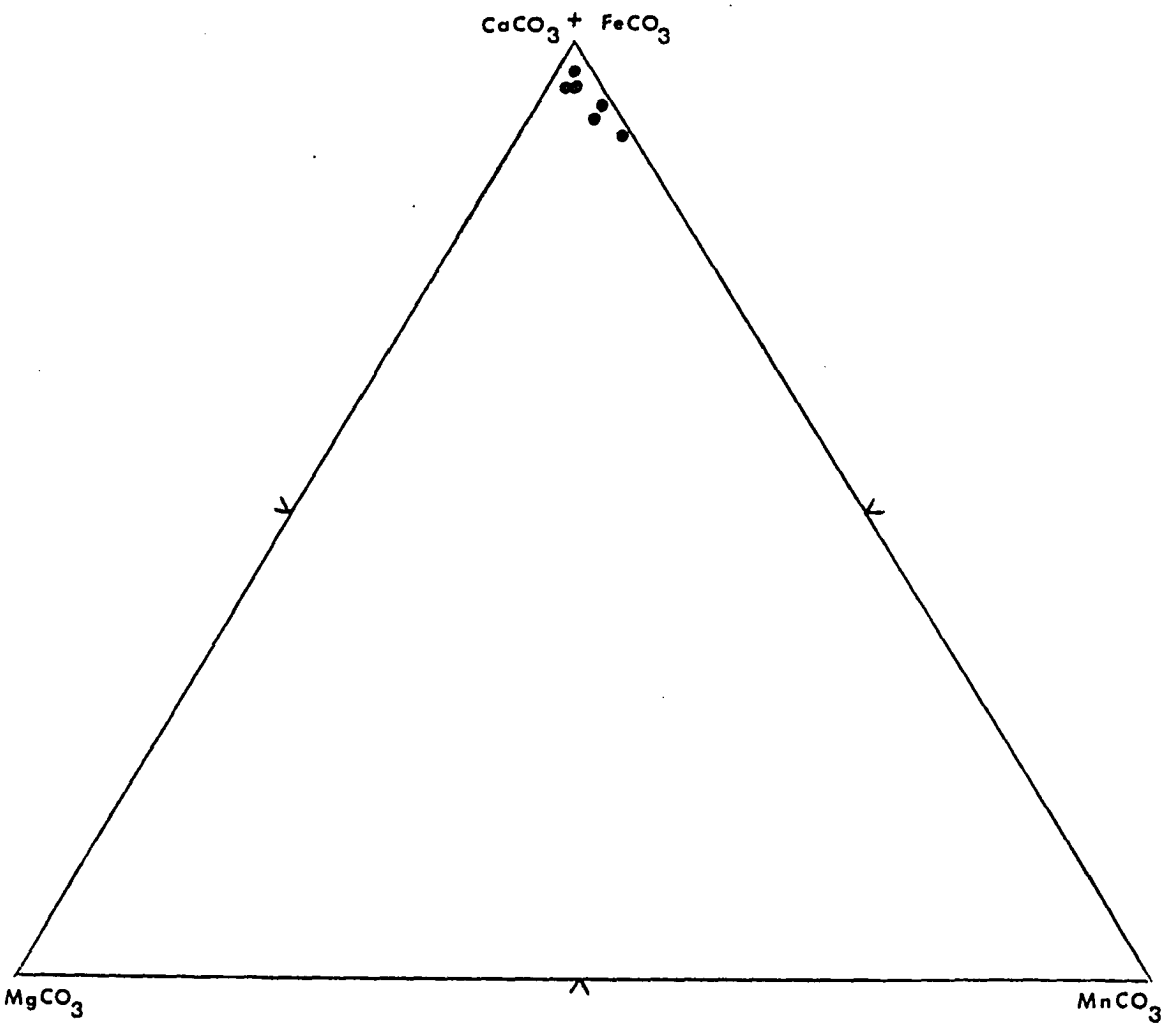

Figure 118. Compositional data for sample T1, +45.3.
Fe: 0 - 0.001.

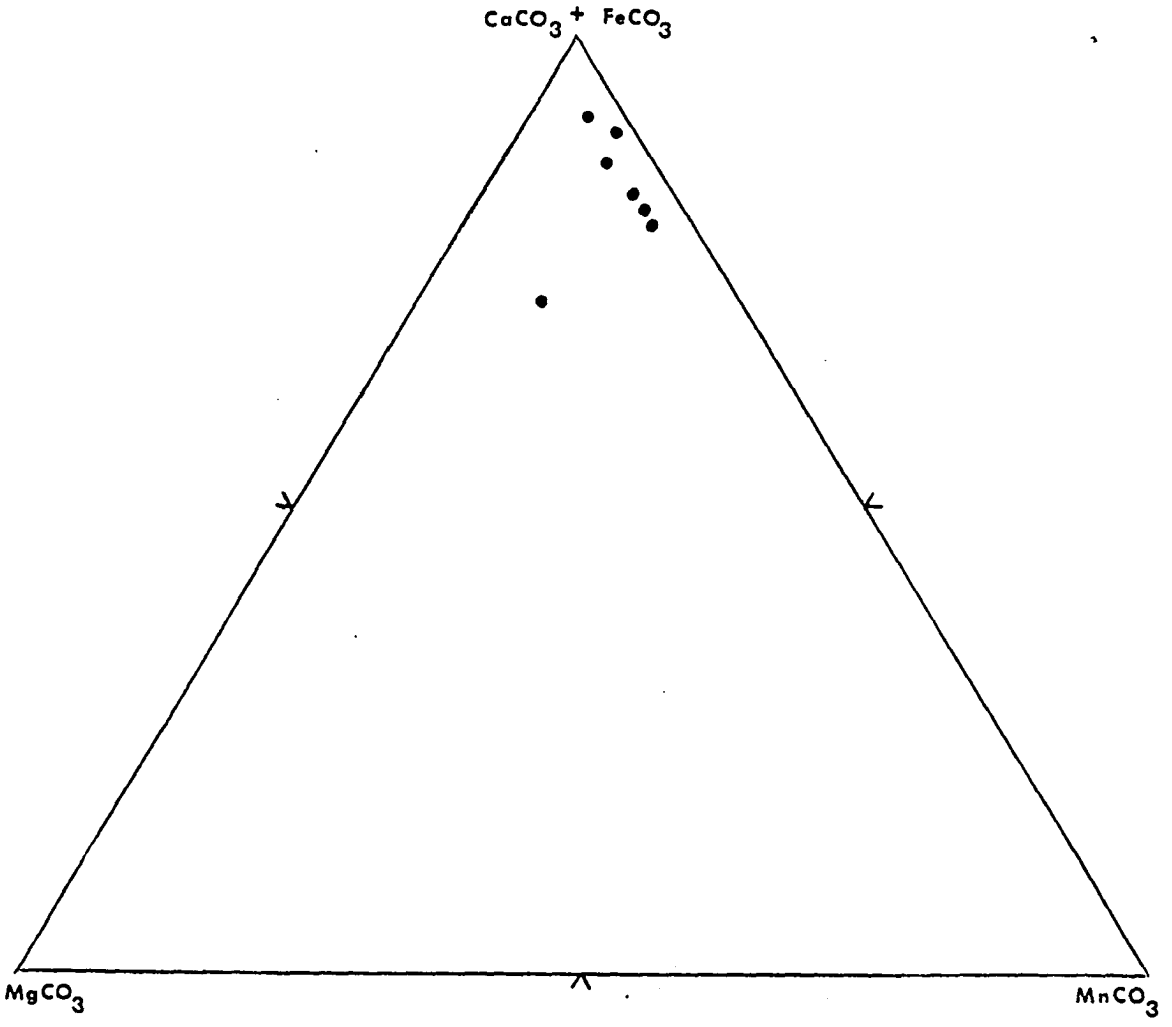

Figure 119. Compositional data for sample T1, +47.9.
Fe: 0 - 0.011; 0.142.

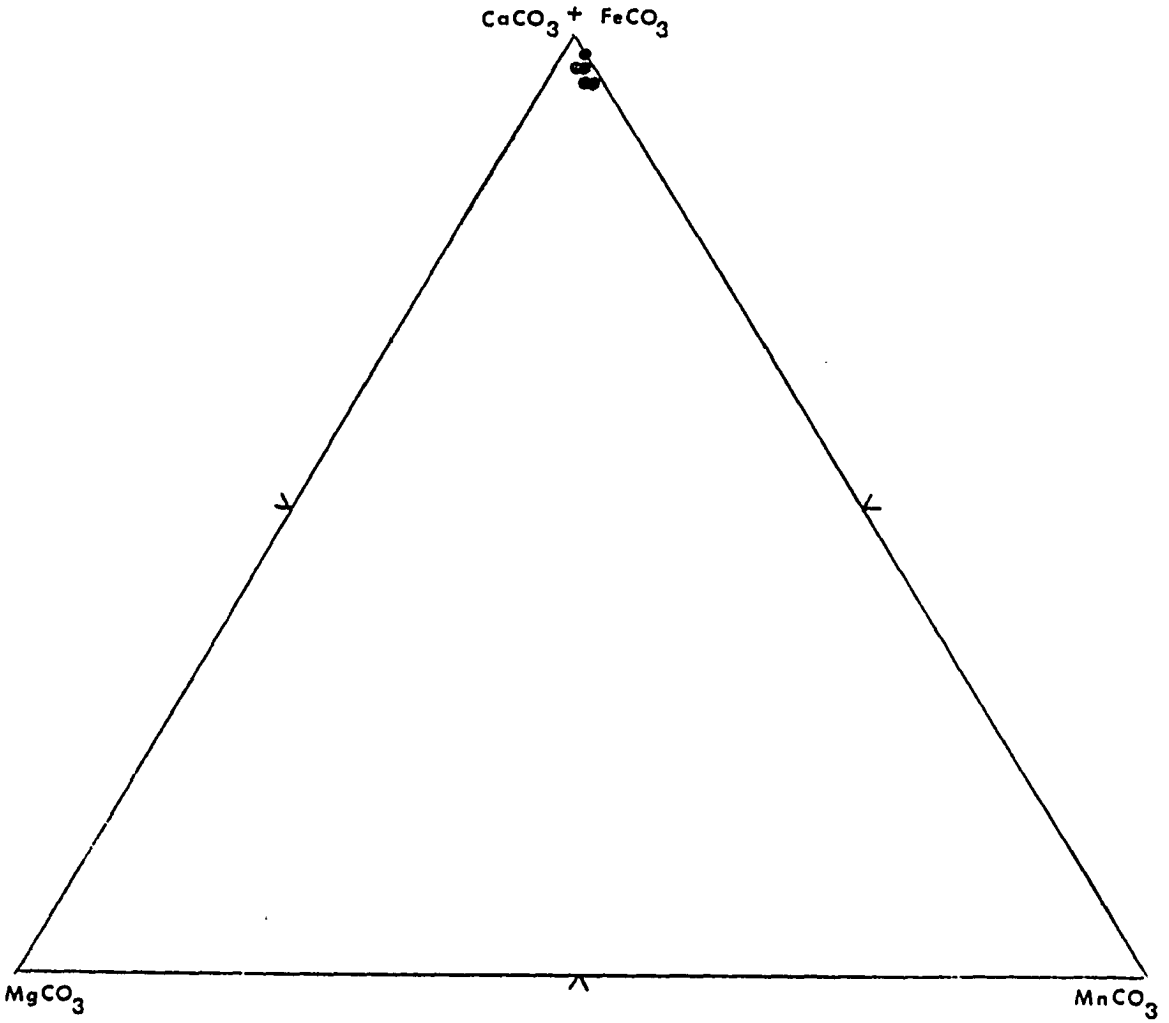

Figure 120. Compositional data for sample T1, +78.1.
Fe: 0.002 - 0.005; 0.016.

VITA

Patrick Masao Okita, was born in Governor's Island, New York on November 3, 1959. He received his grammar and high school education in western New York. In 1976 he graduated from John Marshall High School in Rochester, New York.

In the Fall of 1976 Pat enrolled in the University of Rochester and received the Bachelor of Science degree with honors and distinction in the fields of geology and biology in May, 1980. His bachelor thesis dealt with the stratigraphy and paleoecology of Devonian shales in western New York.

In June, 1980 he enrolled in the graduate program at the Louisiana State University and received the Master of Science degree in August, 1984. His thesis research was a study of the stratiform barite deposits of east-central Arkansas.

Patrick entered the Ph.D. program at the University of Cincinnati during the Fall of 1983. He was the Willis G. Meyer Fellow during 1985 and received the H. Sunderman Teaching Award.

At present he is a National Research Council Post-doctoral Research Associate in the Branch of Eastern Mineral Resources at the United States Geological Survey located in Reston, Virginia.